

DEVELOPMENT OF EPIDERMAL GROWTH FACTOR RECEPTOR (EGFR)
SPECIFIC NANOPROBES FOR SURFACE ENHANCED RAMAN SPECTROSCOPY
(SERS)

by

Leanne J. Lucas

Submitted in partial fulfilment of the requirements
for the degree of Master of Science

at

Dalhousie University
Halifax, Nova Scotia
July 2013

© Copyright by Leanne J. Lucas, 2013

DEDICATION PAGE

I would like to dedicate this thesis to my father, Leslie Harold Lucas (February 26, 1943 – September 21, 1999). I also dedicate this thesis to my mother, Colleen Lucas, who always encouraged my siblings and me to do the best we could and was there for us. My father told me I was smart and taught me that with discipline, a strong work ethic, honesty, and a lot of hard work, I could accomplish whatever I desired. I love and miss you. I would not be person I am today without you both.

TABLE OF CONTENTS

LIST OF TABLES	vii
LIST OF FIGURES	viii
ABSTRACT	xi
LIST OF ABBREVIATIONS AND SYMBOLS USED	xii
ACKNOWLEDGEMENTS	xv
CHAPTER 1: INTRODUCTION	1
1.1 Raman Spectroscopy and Surface Enhanced Raman Spectroscopy (SERS)	2
1.2 Properties of EGFR and EGF	5
1.3 Imaging EGFR Over-expression with Antibodies	10
1.4 Previous EGF to Nanoparticle Conjugation Methods	13
1.5 Our Approach	15
1.6 Significance	17
1.7 Thesis Outline	19
CHAPTER 2: EXPERIMENTAL METHODS	21
2.1 Nanoparticle Synthesis	22
2.2 Transmission Electron Microscopy (TEM)	24
2.3 Ultraviolet – Visible Spectrophotometry (UV-Vis)	25
2.4 Detection of EGF-linker Attachment by Mass Spectrometry (MS)	28
2.4.1. Time-of-Flight – Mass Spectrometry (TOF-MS)	28
2.4.2. In-Solution Tryptic Digestion for Determination of α -lipoic Acid Attachment Site	31
2.4.3. High Performance Liquid Chromatography (HPLC) for Determination of α -lipoic Acid Attachment Site	35
2.4.4. Linear Ion Trap – Mass Spectrometry (LTQ-MS) for Determination of α -lipoic Acid Attachment Site	38
2.5 Zeta Potential	40
2.6 Enzyme-linked Immunosorbent Assay (ELISA) for EGF	44
2.7 Cell Culture	46
2.8 Dark Field Microscopy	48
2.9 Raman Spectroscopy	50
2.9.1. Classical Raman Theory	50

2.9.2. T64000 Raman Spectrometer.....	52
2.9.3. High-Frequency Range Fibre Optic Raman Spectrometer	53
2.9.4. Renishaw Raman Spectrometer	54
2.10 Inductively Coupled Plasma – Mass Spectrometry (ICP-MS)	55
2.11 Summary of Methods.....	59
CHAPTER 3: APPROACHES AND RESULTS	60
3.1 EGF-linker Formation Through Carbodiimide Chemistry	60
3.2 EGF-linker Characterization	65
3.2.1 Time-of-Flight – Mass Spectrometry (TOF-MS)	66
3.2.2 Enzyme-linked Immunosorbent Assay (ELISA) of Human EGF Protein	76
3.2.3 Confirmation of EGF-linker Attachment Site with LTQ-MS.....	77
3.2.4 EGF-linker Characterization Summary	81
3.3 Characterization of Synthesized Nanoparticles	81
3.3.1 Transmission Electron Microscopy (TEM)	81
3.3.2 Ultraviolet-Visible Spectrophotometry (UV-Vis)	85
3.3.3 Characterization of Synthesized Nanoparticles Summary.....	86
3.4 Attachment and Stabilization of EGF-linker Bound Nanoparticles.....	86
3.4.1 Attachment of EGF-linker to Nanoparticles	86
3.4.2 Stabilization of Nanoparticles with α -lipoic Acid	87
3.4.3 Nanoparticle Purification	89
3.4.4 Summary of Attachment and Stabilization of EGF-linker Bound Nanoparticles	89
3.5 Characterization of EGF-linker Bound to Nanoparticles.....	89
3.5.1 Stability in Saline Solution	89
3.5.2 Transmission Electron Microscopy (TEM)	91
3.5.3 Transmission Electron Microscopy (TEM) of EGF-NPs with Uranyl Acetate (UA).....	91
3.5.4 Ultraviolet-Visible Spectrophotometry (UV-Vis) Time Course Study	97
3.5.5 Enzyme-linked Immunosorbent Assay (ELISA) for EGF of Human EGF Tagged Nanoparticles.....	99
3.5.6 Zeta Potential	102
3.5.7 Raman of EGF-linker or α -lipoic Acid Coated Nanoparticles.....	103

3.5.8 Summary of EGF-Nanoparticle Characterization Techniques	106
3.6 <i>In Vitro</i> Cell Imaging	107
3.6.1 Dark Field Microscopy of A431 Cells with α -lipoic Acid Control of EGF-linker Active Nanoprobes	107
3.6.2 SERS of A431 cells with Active EGF-linker or Control α -lipoic Acid Nanoprobes.....	110
3.6.3 <i>In Vitro</i> Cell Imaging Summary	113
3.7 <i>Ex Vivo</i> Biodistribution	114
3.7.1. Raman of Mouse Tissues	114
3.7.2. Inductively Coupled Plasma – Mass Spectrometry (ICP-MS) of Mouse Tissues.....	121
3.7.3. <i>Ex Vivo</i> Biodistribution Summary	124
3.8 Silver-Gold Core-Shell Nanoparticles	124
3.8.1 Synthesis of Ag-Au core-shell nanoparticles (AgAuNPs).....	125
3.8.2 Characterization of Gold Coated Silver Nanoparticles.....	128
3.8.3 Silver-Gold Core-Shell Nanoparticle Summary	135
3.9 Summary of Approaches and Results	135
CHAPTER 4: DISCUSSION.....	139
4.1 Au, Ag, & Ag-Au- α -lipoic Acid-EGF Synthesis and Characterization.....	139
4.2 <i>In Vitro</i> Cell Imaging	143
4.3 <i>Ex Vivo</i> Biodistribution	144
CHAPTER 5: CONCLUSIONS AND FUTURE WORK.....	146
5.1 Conclusions	146
5.2 Future Work	148
5.2.1 SERS Imaging and Photothermal Therapy Treatment.....	148
5.2.2 Core-Shell Silver-Gold Nanoparticles	148
5.2.3 LTQ-MS for Identification of α -lipoic acid to EGF Attachment Site	150
5.2.4 <i>In Vitro</i> and <i>Ex Vivo</i> Imaging	152
5.2.5 Raman Post-processing with Principle Components Analysis (PCA).....	153
BIBLIOGRAPHY.....	155
APPENDIX A Cell Culture	163
APPENDIX B LTQ-MS Data Output by Sequest.....	169

APPENDIX C	Cleaning Glassware with Aqua Regia.....	174
APPENDIX D	Copyright Permission Letters.....	177

LIST OF TABLES

Table 1.1	Comparison of Human and mouse EGF amino acid sequences.	8
Table 3.1	Human EGF to Human EGF-linker peak ratios from TOF-MS.	70
Table 3.2	Mouse EGF to mouse EGF-linker peak ratios from TOF-MS.....	73
Table 3.3	UV-Vis properties of as synthesized nanoparticles.	85
Table 3.4	Quantity of NPs, EGF, and α -lipoic acid for complete coverage of each NP type.....	88
Table 3.5	Zeta potentials of a variety of nanoparticle types.	103
Table 3.6	UV-Vis and TEM properties of synthesized Ag and AgAuNPs.....	129

LIST OF FIGURES

Figure 2.1 Nanoparticle synthesis apparatus – refluxing setup.....	23
Figure 2.2 Transmission Electron Microscope diagram and photo.....	25
Figure 2.3 Double beam Varian Cary Bio Ultraviolet-Visible spectrophotometer.....	26
Figure 2.4 Single beam Nanodrop Ultraviolet-Visible spectrophotometer.....	27
Figure 2.5 Time-of-Flight – mass spectrometer diagram and photo.....	30
Figure 2.6 In-Solution Tryptic Digestion schematic.....	34
Figure 2.7 High Performance Liquid Chromatography (HPLC) diagram.....	37
Figure 2.8 HPLC solvent gradient for peptide elution.....	38
Figure 2.9 Linear Ion Trap – mass spectrometer (LTQ-MS) diagram.....	39
Figure 2.10 Zeta potential diagram.....	43
Figure 2.11 Enzyme-linked Immunosorbent Assay (ELISA) diagram.....	45
Figure 2.12 Dark field microscope diagram.....	49
Figure 2.13 T64000 Raman spectrometer diagram.....	53
Figure 2.14 Tissue preparation for ICP-MS analysis.....	57
Figure 2.15 Inductively Coupled Plasma – mass spectrometer (ICP-MS) diagram.....	58
Figure 3.1 Amine groups (dashed arrows) on Human EGF protein.....	61
Figure 3.2 TOF-MS of Human EGF protein.....	67
Figure 3.3 TOF-MS of Human EGF-linker protein sample LLE49C.....	68
Figure 3.4 TOF-MS of Human EGF-linker sample LLE118A-3.....	69
Figure 3.5 TOF-MS of Human EGF-linker protein sample LLF23A-2.....	71
Figure 3.6 TOF-MS peak ratios of Human EGF-linker.....	72
Figure 3.7 TOF-MS spectrum of mouse EGF.....	74
Figure 3.8 TOF-MS spectrum of mouse EGF-linker.....	75
Figure 3.9 EGF-ELISA of EGF protein.....	77
Figure 3.10 LTQ-MS spectra of trypsin digested, α -lipoic acid conjugated Human EGF.....	80
Figure 3.11 TEM of Au and AgNPs.....	82
Figure 3.12 Au and Ag nanoparticle size distribution histograms from TEM.....	84
Figure 3.13 UV-Vis of Au and AgNPs.....	85
Figure 3.14 Stability test of gold and silver nanoparticles in 10 mM PBS buffer.....	90

Figure 3.15 Transmission electron microscope images of 18 nm AuNPs as synthesized with citrate (left) and α -lipoic acid/EGF-linker (right) attached.	91
Figure 3.16 TEM images of 5 or 18 nm diameter Au or 5 or 45 nm AgNPs stained with uranyl acetate (UA).	97
Figure 3.17 Time lapse UV-Vis absorption spectra of gold and silver nanoparticles with α -lipoic acid added at time zero.	98
Figure 3.18 The maximum absorbance wavelength (λ_{\max}) of silver nanoparticles following α -lipoic acid addition at $t = 0$	98
Figure 3.19 EGF-ELISA test of the total EGFR binding response for two concentrations of 18 nm Human EGF-linker and α -lipoic acid coated AuNPs.	100
Figure 3.20 EGF-ELISA determination of the total EGFR binding response for 18 nm Human EGF-linker and α -lipoic acid coated AuNPs.	101
Figure 3.21 EGF-ELISA test of the total EGFR binding response EGF-linker and 18 nm Au, 5 nm Ag, and 45 nm Ag nanoparticle samples coated with Human EGF-linker and α -lipoic acid.	102
Figure 3.22 Raman spectroscopy of 5 nm Au, 18 nm Au, 5 nm Ag, and 45 nm Ag nanoparticle samples coated with α -lipoic acid conjugated Human EGF (+) or α -lipoic acid (-) and aggregated with 100 mM MgSO_4 (Dalhousie).	104
Figure 3.23 Raman spectroscopy of 18 nm Au and 45 nm Ag nanoparticle samples coated with citrate, α -lipoic acid conjugated Human EGF, or α -lipoic acid and then aggregated with 100 mM MgSO_4 (Dalhousie).	105
Figure 3.24 Dark field microscopy of A431 (cancer) cells following 30 minute incubation with α -lipoic acid/EGF-linker coated Au- or Ag-based nanoprobe.	108
Figure 3.25 Dark field microscopy of A431 (cancer) cells following 30 minute incubation with 50 mM HEPES buffer or α -lipoic acid coated Au- or AgNP.	109
Figure 3.26 Raman of A431 cancer cell pellets following 30 minute incubation with α -lipoic acid/EGF-linker coated AgNPs (Stanford).	111
Figure 3.27 Raman of A431 cancer cell pellets following 30 minute incubation with α -lipoic acid/EGF-linker coated AgNPs (Dalhousie).	113
Figure 3.28 Raw Raman and fluorescence spectra of mouse kidneys, liver, and spleen.	117
Figure 3.29 Average Raman spectra of mouse kidneys, liver, and spleen.	120
Figure 3.30 ICP-MS of mouse organs containing 18 nm gold nanoparticles coated with α -lipoic acid or α -lipoic acid/EGF-linker.	122
Figure 3.31 ICP-MS of mouse organs containing 5 nm silver nanoparticles coated with α -lipoic acid or α -lipoic acid/EGF-linker.	123

Figure 3.32 Trisodium citrate dihydrate (left) and Polyvinyl pyrrolidone (PVP, right) nanoparticle reducing and capping agents.	128
Figure 3.33 UV-Vis of Ag and AgAuNPs.....	129
Figure 3.34 TEM images of Ag and AgAu nanoparticles.....	131
Figure 3.35 Stability test of core-shell silver-gold nanoparticles in 10 mM PBS buffer.....	132
Figure 3.36 Stability test of core-shell silver-gold nanoparticles at room temperature. .	133
Figure 3.37 EGF-ELISA test of silver-gold core-shell nanoparticles coated with EGF-linker.	134

ABSTRACT

Novel biocompatible nanoprobe for optical imaging of Epidermal Growth Factor receptor (EGFR) were created. 5 and 18 nm gold nanoparticles (AuNPs) and 5 and 45 nm diameter silver nanoparticles (AgNPs) were conjugated to EGF protein via α -lipoic acid. AgNPs were not previously attached to EGF. TOF-MS confirms EGF-linker formation. ELISA verifies the linked-EGF activity alone and with EGF-NPs. Core-shell silver-gold nanoparticles (AgAuNPs) gave similar results. TEM staining with uranyl acetate exhibits a bright ring, smaller than EGF, around nanoparticles. Dark field microscopy shows localized, intense cytoplasmic scattering, possibly lipid droplets, in cancer cells incubated with or without nanoprobe. Following injection, mice organs were harvested for EGF-NP immune response determination. Sterilization likely inactivated EGF before ICP-MS. Intense surface enhanced Raman scattering (SERS, 632.8 nm) follows MgSO_4 induced EGF-AgNPs aggregation. Pelleted EGF-AgNP tagged cancer cells lack SERS indicative intensity contrast. AgAuNPs could provide increased stability, brighter SERS, and reduced silver biocompatibility concerns.

LIST OF ABBREVIATIONS AND SYMBOLS USED

ACN	Acetonitrile
ATP	Adenosine Triphosphate
ADP	Adenosine Diphosphate
aLA	α -lipoic Acid
α -lipo-NPs	α -lipoic Acid Coated Nanoparticles
ATCC	American Type Culture Collection
-C(=O)-NR ₂	Amide (R = Carbon or Hydrogen)
-NH ₃	Amine
NH ₄ HCO ₃	Ammonium Bicarbonate
A. U.	Arbitrary Units
R	Arginine
R	Arginine
BSA	Bovine Serum Albumin
-COOH	Carboxylic Acid
CT	Computed Tomography
AgAuNPs	Core-Shell Silver-Gold Nanoparticles
Ci	Curie
C	Cysteine
C-C	Cystine
DISP	Dalhousie Integrated Science Program
Da	Dalton or g/mol
κ	Debye length or thickness of electrical double layer
DMSO	Dimethyl Sulfoxide
-S-S-	Disulfide
-SH x 2	Dithiol
DTT	Dithiothreitol
ESI	Electrospray Ionization
EPR	Enhanced Permeability and Retention Effect
ELISA	Enzyme-linked Immunosorbent Assay
EGF	Epidermal Growth Factor, typically referring to Human EGF
EGF-NPs	Epidermal Growth Factor Coated Nanoparticles
EGFR	Epidermal Growth Factor Receptor
EDC	1-Ethyl-3-[3-Dimethylaminopropyl] Carbodiimide
FBS	Fetal Bovine Serum
FWHM	Full Width at Half Maximum
G	Growth Cell Cycle Phase
AuNPs	Gold Nanoparticles
$f(\kappa a)$	Henry's function
HOMO	Highest Occupied Molecular Orbital
HPLC	High Performance Liquid Chromatography
H	Histidine
HCl	Hydrochloric Acid
HEPES	4-(2-Hydroxyethyl)piperazine-1-ethanesulfonic acid

ICP-MS	Inductively Coupled Plasma – Mass Spectrometry
IAA	Iodoacetamide
pI	Isoelectric point
kDa	Kilodalton
LDA	Linear Discriminant Analysis
LTQ-MS	Linear Ion Trap – Mass Spectrometry
LWD	Long Working-Distance
LUMO	Lowest Unoccupied Molecular Orbital
K	Lysine
MRI	Magnetic Resonance Imaging
m/z	Mass to Charge Ratio
MS	Mass Spectrometry
MALDI	Matrix Assisted Laser Desorption Ionization
MeOH	Methanol
μ W	Microwatt
mW	Milliwatt
MEM	Minimum Essential Medium
MWCO	Molecular Weight Cutoff
MCR	Multivariate Curve Resolution
Sulfo-NHS	N-hydroxysulfosuccinimide
NP	Nanoparticle
N \equiv N	Nitrile
NMR	Nuclear Magnetic Resonance Spectroscopy
NA	Numerical Aperture
ppb	Part Per Billion
ppm	Part Per Million
PenStrep	Penicillin Streptomycin Antibiotics
α	Polarizability
PVP	Polyvinylpyrrolidone
KOH	Potassium Hydroxide
P	Proline
rcf	Relative Centrifugal Force
PO ₄ ³⁻	Phosphate
PBS	Phosphate Buffered Saline
PCA	Principal Components Analysis
RxnT	Reaction Time
M Ω cm	Resistivity (Mega Ohm Centimeters)
RT	Room Temperature
S	DNA Synthesis Cell Cycle Phase
S	Serine
AgNPs	Silver Nanoparticles
NaBH ₄	Sodium Borohydride
-SH	Sulfhydryl or Thiol
SERS	Surface Enhanced Raman Spectroscopy or Scattering
TOF-MS	Time-of-Flight – Mass Spectrometry
TEM	Transmission Electron Microscopy or Microscope

TFA	Trifluoroacetic Acid
UA	Uranyl Acetate
UV-Vis	Ultraviolet – Visible Spectrophotometry
η	Viscosity

ACKNOWLEDGEMENTS

I wish to thank my mom, Colleen Lucas, her boyfriend, Alan Cleveland, my sister, Deanna Lucas, and my brothers, Stewart and Shawn Lucas, for their support. I also thank the members of my committee, Dr. Laurent Kreplak, and especially my supervisor, Dr. Kevin Hewitt, for their support and guidance. I acknowledge the following individuals for aid with specific project aspects: Dr. Peng Zhang and group (nanoparticle synthesis), Dr. Adil Kassam (discussion of EGF-linking reaction), Dr. Mladen Korbelik, Dr. Haishan Zeng, Dr. Michael Short, and Wei Zhang at the British Columbia Cancer Agency – Cancer Research Centre (BCCA-CRC), Drs. Sanjiv Gambhir, Adam Cole, and Jesse Jokerst at Stanford (Raman and zeta potential), and Dalhousie Integrated Science Program (DISP) students Joe Loung and Stefan Juckes (AgAuNPs). Thanks to Deanna Lucas and Markus Karahka for extra help with editing this thesis document.

I wish to acknowledge the financial support of NSERC Canada (2010-2011 PGS-M scholarship), the Nova Scotia Health Research Foundation through REDI (MED-RED-11-7612 and -7282) research grants, and the Alpha Gamma Delta Foundation (2011-2012 Foundation Scholarship). I also thank collaborators for assistance with the following lab equipment: Dr. Laurent Kreplak (dark field microscope and Nanodrop UV-Vis); Dr. Patrice Côté (cell culture facility); Dr. Peng Zhang (UV-Vis); Drs. Haishan Zeng and Mladen Korbelik (lab space in BC); Dr. Alan Doucette and Dennis Orton (trypsin digest and LTQ-MS); Dr. Jeff Dahn (nanopure water); Dr. Robbie Sanderson (shipping); Dr. Wan Lam (EMax microplate reader in BC); Dr. Thomas MacRae and Louise Tunnah (SpectraMax Plus 384 microplate reader at Dalhousie); and Dr. Neil Burford (glove box). I appreciate the efforts of Xiao Feng who helped guide use of the Time-of-Flight – mass spectrometer from the Facilities for Materials Characterization. I acknowledge Dr. Ping Lee, director of the Scientific Imaging Suite of the Department of Biology at Dalhousie, for aid in the operation of the Transmission Electron Microscope. I also appreciate the efforts of Dan Chevalier of the Minerals Engineering Centre, and Heather Daurie of the Centre for Water Resource Studies, both at Dalhousie University, for performing the Inductively Coupled Plasma – mass spectrometry measurements.

CHAPTER 1: INTRODUCTION

Molecular imaging, the identification and quantification of the molecular markers of disease in living subjects, is regarded as the future of medical imaging. Conventional imaging relies on the detection of end products of the molecular alterations attributed to diseases [1], whereas molecular imaging allows one to image disease at an earlier stage, so long as the particular Molecular Imaging probe is highly specific and can be imaged with high sensitivity. Three elements are necessary for Molecular Imaging: cellular and sub-cellular markers for the disease under study, biocompatible molecular probes of these markers, and a molecular specific imaging modality with great sensitivity as well as spatial and temporal resolution. The molecular imaging probe must exhibit the following characteristics to be of use: possess a unique affinity for the molecular and biological marker, gain access to the marker efficiently, cause low non-specific uptake or retention to allow low target-to-background ratios, and have a sufficiently long half-life to be detectable and functional at trace concentrations. Efficient marker access may be the result of two effects: increased blood flow to the periphery of large tumours, as well as the enhanced permeability and retention (EPR) effect which is the result of leaky, newly formed blood vessels feeding a tumour [2].

We use over-expression of the Epidermal Growth Factor receptor (EGFR) as our cancer marker of choice. The natural ligand for this receptor, Epidermal Growth Factor (EGF) protein, serves as the imaging probe when bound to gold and silver nanoparticles through a linking molecule. Raman spectroscopy acts as our molecular specific imaging tool. In this chapter we discuss Raman spectroscopy and surface enhanced Raman spectroscopy (SERS), properties of EGFR and EGF, other methods of imaging EGFR over-expression, previous methods of attaching EGF to nanoparticles, our approach for EGF to nanoparticle conjugation, the significance of the work, and end with an outline of the thesis.

1.1 RAMAN SPECTROSCOPY AND SURFACE ENHANCED RAMAN SPECTROSCOPY (SERS)

We wish to use a molecular specific tool, Raman spectroscopy, to detect cancer markers – cells over-expressing the Epidermal Growth Factor receptor. Metal nanoparticles used in close proximity to the markers enhance the Raman scattering signal in a process referred to as surface enhanced Raman spectroscopy. If successful, SERS imaging of EGF coated nanoparticles could be used as an early detection tool for EGFR over-expression on certain cancer cells, where EGF is specific for the EGFR marker. In our cases, the imaging probe is the combination of EGF attached to the molecule α -lipoic acid, an excess of α -lipoic acid for complete nanoparticle coverage, both sequentially attached to gold or silver nanoparticles. Treatment could be initiated at higher incident laser power because of heat generation in the metal nanoparticles transferred to the EGFR saturated tumour tissues. These imaging probes would therefore have both *therapeutic* and *diagnostic (theranostic)* value.

It is instructive to compare Raman spectroscopy, an inelastic light scattering technique, to other light absorption or scattering techniques, for example: Infrared spectroscopy (result of an absorption process), fluorescence microscopy (result from inelastic scattering processes), and white light microscopy (result from elastic scattering processes). The molecular information gained from Raman is complementary to Infrared spectroscopy; however, Raman is better suited for imaging of biological samples *in vitro* and *in vivo*. The intense and abundant IR vibrations of water interfere with the IR signal, but are confined to a narrow spectral range in a Raman spectrum.

Raman signals in biological samples are inherently weak, and suffer from issues with light penetration into the tissue. To overcome the weak aspect, metal nanostructures placed within the tissues enhance the Raman signals in the process of surface enhanced Raman spectroscopy (SERS). Two independent phenomena give rise to this enhancement – the electromagnetic and chemical effect. *Electromagnetic enhancement* affects the Raman scattering power for SERS. Four factors influence the Raman scattering power and thus increase the Raman signal intensity: the incident laser light intensity, the number of molecules in the sample volume, the specific polarizability of each molecule adsorbed

on the nanoparticle surface and thus the Raman cross section, as well as enhancement factors for the laser excitation and scattered fields [3]. The interaction and subsequent excitation of the plasmon resonance frequency of the metal nanoparticles, or rather the conduction electrons in the metal nanoparticles, with light produces the laser excitation effect. Molecules near and adsorbed onto the nanoparticle surface experience an enhancement in excitation intensity. This is due to electric fields oscillating electrons around the nanoparticle, which creates a dipole. Since the intensity (I) is related to the electric field (E) as,

$$I = E^2, \quad (1)$$

the intensity falls off at a rate of $1/r^6$, where r is the particle radius, as the distance from the nanoparticle surface increases. As the wavelength of light is much larger than the nanoparticle diameter, light will penetrate the entire nanoparticle volume. When the plasmon resonance frequency matches that of the incident field, the reradiated field will be largest. The larger fields enhance the intensity of the characteristic Raman vibrations of the molecules immediately adjacent to the nanoparticle, or on the nanoparticle surface. Not all metal nanoparticles can create this SERS effect – it is possible with noble metal nanoparticles like gold and silver.

Chemical enhancement depends on the proximity of the molecules around the nanoparticle as well as of the molecular excitation energy to the incident laser wavelength. Chemical enhancement occurs from charge-transfer effects inherent to molecules adsorbed on the nanoparticle surface. In an energy diagram depicting Raman scattering, electrons in a molecule under study are raised to a virtual state from the ground state. The observed Raman signal is increased when this virtual state is nearer to a real electronic transition state. This is the case up to the electronic transition energy, as Fluorescence occurs as above the electronic transition state. When molecules bind to a metal, as with a metal nanoparticle, the molecular orbital energies change and electrons redistribute to obtain the lowest orbital energy possible. The highest occupied molecular orbital (HOMO) of the molecule-nanoparticle complex is below the previous ground state energy, or Fermi energy, of the uncomplexed molecule. Unoccupied molecular orbitals

above this Fermi energy are referred to as lowest unoccupied molecular orbital (LUMO). Chemical enhancement is also affected by the lowering of the energy of the HOMO to allow a larger energy gap between the HOMO and the virtual transition state. The greater energy gap influences the Raman signal intensity; the observed Raman signal is enhanced as the laser wavelength is nearer the orbital energy of the molecule-nanoparticle complex.

More intense SERS spectra of a molecule of interest can be obtained by shining laser light on metallic nanoparticles near the plasmon resonance frequency than can be obtained without metal nanoparticles using Raman alone, however, it is necessary to understand whether the nanoparticles are toxic before use with animals or Humans. Gold nanoparticles are inert and have been used since the 1920s as an arthritis treatment with no apparent harmful side effects [4]. They are effective in reducing joint swelling and inflammation in arthritic rats [5]. Small gold nanoparticles of less than 3 nm in diameter are cytotoxic, stimulating cell death from both apoptosis and necrosis pathways [6]. Silver nanoparticles, while brighter for SERS, are known to activate cytotoxic side effects. This was true for higher nanoparticle concentrations and long incubation times. 25 nm diameter silver nanoparticles did not show significant toxicity to two cell lines when incubated for 24 hours in concentrations up to 250 $\mu\text{g/mL}$. When the dose was more than doubled to 512 $\mu\text{g/mL}$, toxic effects were observed [7]. Toxicity of commercially available 20, 50, and 80 nm diameter uncoated and 25 and 35 nm carbon coated silver nanoparticles was assessed [8]. It is unclear whether these uncoated silver nanoparticles, tested both as received (unwashed) as well as after washing, were stabilized by a molecule adsorbed onto the surface. The unwashed nanoparticles contained 5.55 mg/mL of cytotoxic formaldehyde and methanol (see MSDS for side effects). The unwashed and uncoated, washed and uncoated, and carbon coated silver nanoparticles were applied to pig skin daily over two weeks or to cells for 24 hours. Chronic exposure to all silver nanoparticle types showed small scale skin inflammation and edema, but no large scale irritation. Both washed and carbon coated AgNPs were not toxic to cells in any concentration up to 42.5 $\mu\text{g/mL}$, however, formaldehyde and methanol contaminants caused a toxic cellular response in the presence of the unwashed and uncoated AgNPs. Gold nanoparticles were not toxic to cells so long as they were larger than 3 nm diameter. 25 nm diameter silver nanoparticles were safe to use with

cells. A broader-scale study showed 20 to 80 nm diameter silver nanoparticles were only toxic to cells when residual organic contaminants remained in solution.

Biocompatible gold and silver nanoparticles can be used for SERS imaging, although the imaging depth may limit the types of cancers which can be assessed. SERS imaging to tissue depths of 10 mm is possible using biocompatible 25 nm gold nanoparticles in mice [9]. This depth may be reduced in Humans depending on the thickness of skin through which the imaging occurs, as mice have thinner skin. Solutions to overcome the limit could be to use SERS for imaging cancers close to the surface of the skin, or for imaging cancers endoscopically in the lung or digestive tract near the surface of the tissue.

In the next section, we discuss the physical properties of the EGFR and EGF, as well as the interaction that occurs to produce the signal cascade characteristic of cancers in which EGFR over-expression takes place.

1.2 PROPERTIES OF EGFR AND EGF

Epidermal Growth Factor receptor (EGFR) facilitates cell growth, proliferation, and differentiation in multiple tissues, where proliferation hints to the ability of the cells to spread. EGFR is also known as HER1, or Human Epidermal Growth Factor receptor, or ErbB1, named for homology to the Erythroblastic Leukemia Viral Oncogene. We target this receptor in our studies with its natural ligand, Epidermal Growth Factor (EGF), by producing EGF conjugated nanoparticles for cancer imaging and treatment. In addition to HER1, the over-expression of HER2, HER3, and HER4 receptors, also known as ErbB2, ErbB3, and ErbB4, are characteristic of a variety of cancers. HER2 over-expression is common in breast cancer [10]. HER2 is unique as it is always in the open conformation and does not need a bound ligand, like EGF, for activation.

DNA, the building blocks of life, contains all information necessary to replicate cells. DNA codes for and allows the synthesis of proteins through RNA. Proteins put cellular functions into action, they direct all actions based on their concentrations and location in the cell. The transmembrane protein EGFR weighs 170 kDa and contains

1186 amino acids [11]. The approximately 40 kDa extracellular domain consists of 621 amino acids residues and includes the active site for EGF, of which 171 amino acids, residues 310-481, are essential for EGF binding and activation [12]. The EGFR and EGF binding is also visible from K. M. Ferguson et al., ID# 1NQL in the Protein Data Bank [13]. Binding of ligands, like EGF and anti-EGFR antibodies, to the extracellular domain of the receptor allows a conformation change to take place and facilitates the activation of downstream cellular signaling processes.

The intracellular domain on EGFR, located within the cell membrane, consists of 542 amino acids [11]. This portion of EGFR is necessary for tyrosine kinase function. EGFR is a tyrosine kinase, kinases are enzymes, and enzymes are proteins that catalyze a reaction. After binding of EGF, or similar ligands, to EGFR activates and changes the receptor shape to a more open conformation. The activated EGFR forms a complex, or dimerizes, with an additional activated HER receptor – another EGFR or one of the three other HER receptors. Specifically, this shape change triggers the EGFR tyrosine kinase to catalyze the transfer of phosphate (PO_4^{3-}) from adenosine triphosphate (ATP) to tyrosine residues in polypeptides, with the consequence of ATP reduction to adenosine diphosphate (ADP). Phosphorylation, which amplifies a signal about 10 times, activates downstream signaling targets to ultimately achieve the cell growth response [14]. The downstream targets also use phosphorylation to further the signal response. Tyrosine kinases are sometimes targets for cancer therapy [15].

After being engulfed into a cell, the EGF-EGFR complex is either degraded in endosomes or recycled to the cell surface. One aspect that makes cancer cells grow uncontrollably is the presence of more of these EGFR or other HER receptors on the cell surface than usual from too many recycled receptors [16]. Another aspect is dysregulation of the cell cycle growth and DNA synthesis (G and S) phases, which prevents checks to ensure cells grow normally at a uniform pace and causes longer periods of EGFR signaling [17]. Cellular substrates called tumour suppressors reduce the signal amplification by degrading the internalized receptors in endosomes. Examples of tumour suppressors are Bif-1 and p53, which decrease the activities of EGFR specific breast cancers and EGFR mediated cancers [18]. These tumour suppressors are often turned off

by cellular mutations, which lead to an increased cancer risk from uncontrollable cell growth.

EGFR is over-produced on the cell surface of certain cancers and is targeted through the EGFR extracellular domain in a lock and key mechanism, where the keys are ligands such as EGF protein or anti-EGFR antibodies. Human EGF protein contains 53 amino acids and is approximately 6.2 kDa [19] [20]. It contains three intermolecular disulfide bonds, made up of 6 cysteine (C) amino acids, to allow folding into its native conformation. The isoelectric point, pI, is the pH at which a protein is neutral – the charges of all the acidic and basic amino acids balance. Knowledge of the isoelectric point is necessary to understand the solubility and ionizability of a protein at a certain pH. Prediction of the pI involves a simple calculation based on the amino acid sequence. One sums all charges in a protein at a certain pH, where the amino (+ or neutral) and carboxy (- or neutral) termini, as well as all amino acid side chains have +, -, or neutral charges based on the solution pH. The pI achieved is when all contributing groups are either neutral, in other words the acids and bases balance to give a net neutral charge to the protein. Some portions of the protein would retain a + or - charge; however, the intact protein would have a zero net charge. The pI must not be identical to the pH of the solution, as these proteins have a net neutral charge and are not soluble in a polar solution when this is the case. Using the Human EGF sequence in Table 1.1 and the knowledge of side chain group charges from the amino acid sequence, the pI of Human EGF is 4.78 [21]. When replicated from RNA, EGF starts out as pro-EGF, which is 1185 amino acids long and weighs 131 kDa [22]. Pro-EGF is cleaved in the body to form the 6.2 kDa active form of EGF. The protein we use in the experiments is not pro-EGF, but the active recombinant EGF, as replicated by *E. coli* bacteria (PHG0313, Lot# 456035B, Life Technologies/Invitrogen, Grand Island, USA).

Table 1.1 Comparison of Human and mouse EGF amino acid sequences. Positives are amino acids which retain the charge, while identities are identical, and gaps are missing sequence areas. The two lysine (K) amino acids were not conserved in mice, but were replaced by serine (S) and arginine (R), which do not have a primary amine to react. The cysteine (C) amino acids were conserved, as should the protein tertiary structure.

Human	NSDSECPLSHDGYCLHDGVCMYIEALDKYACNCVVGYIGERCQYRDLKWWELR
Mouse	NSYPGCPSSYDGYCLNGGVCMHIESLDSYTCNCVIGYSGDRCQTRDLRWWELR
Comparison	NS__CP_S+DGYCL+_GVCM+IE+LD_Y_CNCV+GY_G+RCQ_RDL+WWELR
Identities = 37/53 (70%), Positives (+) = 44/53 (83%), Gaps = 0/53 (0%)	

To understand the response of the body to foreign agents, we seek to determine whether one can avoid an immune response to our probe by coating the nanoparticles with the ligand that is naturally produced. To do so in mice models requires the use of mouse EGF. The mouse EGF protein weighs 6.0 kDa and contains 53 amino acids [23]. The mouse EGF sequence shown in Table 1.1 and knowledge of the side chain amino acid sequence charges gives a protein pI of 4.89 [21]. The mouse EGF was replicated by *E. coli* bacteria (PMG8041, Lot# 790229B and 10918864, Life Technologies/Invitrogen, Grand Island, USA). The protein sequence is important as we use specific amino acids, the amino terminus and lysine (K) amino acids, to attach a molecule to EGF. This molecule, α -lipoic acid, forms a bridge between the EGF and the nanoparticle. Mouse EGF has approximately 70% sequence convergence with the Human EGF sequence, the BLAST program from the NIH was used for the comparison (Table 1.1) [20] [23] [24]. 83% of the amino acids in the Human and mouse sequences shared a similar charge. The tertiary structure should be conserved between the Human and mouse sequences, as all cysteine (C) amino acids remain. It is important to note that the mouse EGF lost both lysine amino acids which were present in the Human protein – lysine is replaced with serine (S) and arginine (R) in mouse EGF. Mouse EGF would only have 1 potential binding site for α -lipoic acid.

Over-production of EGFR is characteristic of many cancers and pre-cancers, including those of the breast, lung, bladder, skin, mouth, brain, and neck [25] [26] [27] [28] [29] [30] [31] [32] [33] [34]. Therapies that target this family of HER receptors have

shown promise. Breast cancers over-expressing the HER2 receptor have been treated with a monoclonal antibody with the trade name Herceptin, or Trastuzumab, as there are no known natural ligands to target this receptor [35] [36]. However, toxic side effects including cardiac arrest can be associated with the treatment [10] [37]. Antibodies for EGFR tagged with fluorescent probes [38] [39] and gold nanoparticles have been used for imaging EGFR over-expression as contrast agents [40] [41], but with at most a 10:1 intensity contrast. Raman imaging of cells and animals can be achieved through the EGFR with a Raman reporter molecule attached to gold nanoparticles [9], imaging of both the EGFR and HER2 can also take place [42].

A nanoprobe we previously developed, using antibodies for the EGFR (anti-EGFR), provided an order of magnitude improvement with respect to the signal intensity contrast [43]. The 632.8 nm laser wavelength excites the surface plasmon of aggregated metal nanoparticles, which leads to surface enhanced Raman spectroscopy. A point mapping scheme with a 0.3 to 1 μm step size was used for the Raman spectroscopy measurements of live cells to observe the nanoparticle, and thus, the EGFR distribution. These maps, or hyperspectral images, allow for the measurement of the Raman spectrum at a point, and an x-y stage allows for movement to collect spectra in a pre-determined area. Confocal objectives allow for focusing within 1-2 μm in the z-direction. As EGFR is engulfed through endocytosis, we expect to visualize the aggregated nanoprobe in endosomes and lysosomes when using a confocal microscope for white light and Raman imaging. Signal to noise ratios of 850:1 at 1583 cm^{-1} and 7 orders of magnitude enhancement were demonstrated from the surface plasmon of 30 nm AuNPs tagged with anti-EGFR antibody aggregated within EGFR over-expressing A431 cancer cells.

Techniques involving fluorescence and white light microscopy have been used by other researchers to image EGFR over-expression in cancerous cells, as compared to normal cells. Imaging with these techniques has been facilitated by both fluorescent proteins for image contrast and anti-EGFR antibodies for specificity to the receptor of interest, through attachment to the particles of interest. We present the fluorescent and white light microscopy techniques in the next section.

1.3 IMAGING EGFR OVER-EXPRESSION WITH ANTIBODIES

Traditionally, fluorescence and white light microscopy have been the methods of choice for imaging EGFR over-expression with a variety of anti-EGFR antibody coated probes. On the surface of normal cells, or cells which do not over-express EGFR, about 100 000 EGF receptors are present. The quantity and type of over-expressed receptors can vary depending on the specific cancer. On A431 Human epidermoid carcinoma cells (a cell line derived from an 85 yr old female [44]), there are about 2 million EGFRs per cell [45]. There are therefore at least 10 times more EGFRs on the surface of A431 cervical cancer cells than normal cells. At low (picomolar) concentrations EGF promotes cell growth of A431 cells whereas at higher (nanomolar) concentrations it inhibits growth by causing the cells to terminally differentiate.

J. Aaron et al. (2007) used elastic light scattering, or confocal dark field microscopy, to image SiHa cervical cancer (obtained from a 55 year old Asian female [46]) cells tagged with anti-EGFR coated 25 nm gold nanoparticles and showed bright yellow spots on the cells from the clusters of nanoparticles on the cell membrane [41]. Normal cells only showed a few less intense green spots from inherent light scattering within the cell. Point UV-Visible spectrophotometry of the bright yellow spots on the cancer cells showed a 120 nm shift in the plasmon absorbance wavelength from gold nanoparticles in solution at 530 nm to nanoparticles on the cancer cell surface at 650 nm. The red-shift in the plasmon absorbance is indicative of the laser frequency at which the nanoparticles on EGFR over-expressing cancer cells would give the most SERS, and is caused by the close proximity of the assembled nanoparticles. The presence of the anti-EGFR labeled gold nanoparticles in the cancer cells was confirmed with scanning transmission electron microscopy. The nanoparticles could be seen as bright white globules dimerized in the cells, as expected to occur when two EGFRs bind their anti-EGFR ligands and start the cell growth and proliferation signal cascade.

E. Hsu et al. (2004) attached anti-EGFR antibodies to Alexa Fluor 660 streptavidin fluorescent probes to image the EGFR distribution on SqCC/Y1 mouth cancer and MDA-MB-435S breast cells with confocal microscopy [38]. The SqCC/Y1

cells were visible as false coloured red rings typically around the outer edge of the cells with the anti-EGFR tagged fluorescent probe, while the MDA-MB-435S cells do not over-express EGFR and were not visible. Confocal images of cancerous tissue biopsies were clearly distinguishable by the bright red fluorescence when labeled with the fluorescent anti-EGFR. The normal tissue biopsies gave no fluorescence; both the cancerous and normal biopsies were confirmed by H&E staining.

X. Qian et al. (2008) imaged EGFR over-expression through SERS. The signal enhancers were composed of pegylated 60 nm gold nanoparticles attached to ScFv B10 antibody, specific for EGFR, as well as malachite green isothiocyanate dye or diethylthiatricarbocyanine (DTTC) as reporter molecules for the characteristic Raman signatures [9]. EGFR over-expressing Tu686 tongue cancer cells and non-EGFR over-expressing NCI-H520 carcinoma cell lines were studied with a 785 nm laser excitation. Nanoparticle solutions tagged with non-specific antibodies or without any antibodies, as well as the ScFv tagged nanoparticles on NCI-H520 cells all gave minimal SERS. The Tu686 EGFR over-expressing cells and the pure ScFv tagged nanoprobe both gave similar, intense SERS spectra. Additionally, *in vivo* SERS studies with mice at a 785 nm laser excitation showed detection of the pure ScFv tagged nanoprobe signature, with a 1 second integration time, both near the surface of the skin and with deep tissue injections of nanoprobe up to 10 mm below the skin. Longer integration times, up to 21 seconds, were required for the deep tissue injections, as opposed to 3 seconds with the nanoprobe near the skin surface. Control spectra of the skin did not show spectra similar to the nanoprobe tags. Additional *in vivo* SERS imaging studies, with 785 nm laser light, of uptake into tumour tissues from nanoprobe injected into the tail vein of mice revealed specific targeting of the ScFv antibody tagged nanoparticles to the tumour tissues with little response from the liver. The antibody-less gold nanoparticles showed little tumour uptake, while slightly higher SERS response from the liver showed that the nanoparticles were being filtered out by the immune system.

Similarly to X. Qian et al. (2008), K. Maiti et al. (2010) used Raman spectroscopy to image both the HER2 and EGFR receptors [9] [42]. Both Raman reporter molecules, possessing a known spectrum, and antibodies, for receptor specificity, were bound to commercially obtained 60 nm gold nanoparticles through α -lipoic acid. The use of α -

lipoic acid as a cross-linking molecule, as well as the use of carbodiimide chemistry to form the linkage, is similar to our approach. The Supplementary data outlines the nanoprobe conjugation information. First, α -lipoic acid was attached to a variety of Raman reporter molecules through formation of an amide bond using carbodiimide chemistry. These Raman reporters were subsequently bound to the gold nanoparticles by the sulfhydryl group on the other end of α -lipoic acid. Second, antibodies were affixed to the gold nanoparticles using bifunctional PEG molecules. The bifunctional PEG contained a thiol group to bind to the nanoparticle, as well as a carboxylic acid for conjugation to the antibody through carbodiimide chemistry. An excess of thiol-PEG, with no carboxylic acid group, was used to protect the nanoparticles and render them non-reactive, or at least less reactive than if the carboxyl groups from the bifunctional PEG was the major component of the outer nanoparticle layer. Using a 633 nm laser, SERS was confirmed from both cell cultures and mice containing the antibody-nanoparticle conjugates. Four types of cell lines, those positive for EGFR, positive for HER2, or negative for either EGFR or HER2 were incubated with the antibody-nanoparticle conjugates, where the antibodies were specific for either the EGFR or HER2 receptors. SERS was observed in the EGFR or HER2 positive cells, while no features of the Raman reporter were seen with the EGFR or HER2 negative cells. These observations of the EGFR or HER2, positive or negative cells were confirmed with the use of fluorescence microscopy. SERS signals which correspond to that of the pure nanotag were found in injections just under the skin of mice. The spectra were different from the background spectra of the skin.

These methods of EGFR imaging by J. Aaron et al. (2007), E. Hsu et al. (2004), only offer contrast factors of 10 between the cancerous and normal tissue. The enhancement effects from SERS exploited by X. Qian et al. (2008), by K. Maiti et al. (2010), in our approach, and by others should give higher signal intensities between the cancerous and normal tissue. Up to 7 orders of magnitude of enhancement, or 12-14 orders of magnitude in special circumstances, should be achievable through the electromagnetic and chemical enhancements which are possible from SERS [47]. A contrast factor of $1:10^6$ should be possible from SERS, while fluorescence and elastic light scattering give a contrast factor on the order of 1:10. SERS also allows for

molecular imaging, and has the potential to detect changes earlier, as opposed to traditional imaging techniques which track physical changes (e.g. in density) resulting from these molecular alterations. The increased scattering cross section from SERS, which can reach $\log(-10) \text{ cm}^2$ or similar orders of magnitude as fluorescence and infrared spectroscopy, is a benefit to the technique.

EGF has been affixed to a variety of nanoparticle types through several different methods of attachment; we will discuss these approaches in the next section.

1.4 PREVIOUS EGF TO NANOPARTICLE CONJUGATION METHODS

The use of antibodies for specificity and additional reporter tags for detection by fluorescence, microscopy, and Raman techniques have been the focus for solid tumour targeted nanoprobes [38] [9] [48]. A variety of methods have been attempted to affix EGF to nanoparticles with inconsistent success [48] [49] [50] [51] [52], as summarized in this section. None use silver nanoparticles, which we found possible with our approach [53].

P. Diagaradjane et al. (2008) reduced the three inherent disulfide bridges, composed of cysteine amino acids, in EGF protein to allow binding of the freed sulfhydryl groups to 21 nm semiconductor CdSeTe/ZnS quantum dots [48]. The bond formed is through the thiol (-SH) of the protein to the maleimide group present on the particle. The reduced-EGF coated particles remained active, as confirmed by ELISA. *In vivo* fluorescence demonstrated stability and specificity of the tagged particles for cancerous regions in mice. These particles are not SERS active. As well, the particles are toxic as they contain cadmium which reduced their suitability for use in biological applications.

N. Ibaraki et al. (1996) analyzed cell passage number and EGFR expression in Human Lens Epithelial (HLE) cells [49]. EGF protein was adsorbed to the surface of 10 nm gold nanoparticles, the EGF-NPs were incubated with cells, and thin sections were imaged with TEM (transmission electron microscopy). A few nanoparticles were seen on

the surface and internalized, especially in the early passage cells. The adsorbed EGF-NP affinity is difficult to assess as particle uptake by the cells seemed sparse. The limited visualization of particles in the cells could represent nonspecific uptake of the EGF-NPs.

A biotin-avidin reaction was used to attach EGF to large (220 nm) gelatin nanoparticles by C-L. Tseng et al. (2007) [50]. Fluorescent tags conjugated to the nanoparticles, with or without EGF, were incubated with A549 lung cancer cells. Fluorescent EGF-NPs were observed in the cytoplasm more often than those lacking EGF. Uptake of fluorescent EGF-NPs in lysosomes, as visualized through co-localization staining, indicated activity and specificity of the EGF-NPs. In the *in vivo* mouse models, A549 cancer cells were injected into the lung and allowed to grow. *In vivo* imaging of normal and cancerous mouse lungs displayed the fluorescing EGF-gelatin nanoparticles, with the cancerous tissue yielding more fluorescence. The large nanoparticle size was diffusion limiting and decreased the ability of the nanoparticles to penetrate solid tumors following injection. These gelatin nanoparticles also lack SERS activity.

N. de Jonge et al. (2009), in a similar manner to C-L. Tseng et al. (2007), coupled EGF to 10 nm AuNPs through a biotin-streptavidin interaction [50] [51]. Nanoparticle stability was confirmed at physiological pH and salt content. A liquid scanning TEM (liquid STEM) setup was used to image EGF-AuNPs in COS7 African Green Monkey fibroblasts to determine whether improved resolution and data acquisition speed over other imaging methods was possible. Observation of both single and clusters of nanoparticles in intact cells were achieved with STEM, suggesting nanoparticle affinity towards EGFRs.

With reaction chemistry the most similar to ours, M. Creixell et al. (2010) [52] functionalized 13 nm iron oxide nanoparticles (IONPs, Fe_2O_3 , R-NH₂, R=alkyl chain) with carboxymethyldextran (CMDx, R-COOH, R=alkyl chain) through EDC (1-ethyl-3-[3-dimethylaminopropyl] carbodiimide) carbodiimide chemistry. EGF was then attached to the CMDx-IONPs with an additional carbodiimide reaction. Prior to imaging with fluorescence microscopy, green fluorescent protein (GFP) was affixed to the EGF-IONPs. Fluorescence and light microscopy techniques showed clear uptake of the GFP-EGF or EGF conjugated particles by the CaCo-2 colon cancer cells, while CMDx-IONPs without EGF were not. The iron oxide nanoparticles are not SERS active.

We briefly outline our EGF to α -lipoic acid attachment protocol in the next section.

1.5 OUR APPROACH

We wish to create and validate a SERS nanoprobe for optical imaging of the Epidermal Growth Factor receptor, as well as for thermal therapy of cancers and pre-cancers. Raman spectroscopy should aid in differentiating the signal of the cancerous and normal tissues. We synthesize gold and silver nanoparticles (Au or AgNPs) of various sizes and couple them to EGF via the carboxyl end of a short ligand, α -lipoic acid (206 g/mol). α -lipoic acid is a small molecule with antioxidant properties [54]. It is biocompatible, as it is the result of cellular processes – it is part of the TCA cycle and energy generation in mitochondria in cells [55]. α -lipoic acid is converted to dihydrolipoic acid upon reduction of the disulfide bond within cells [54]. Excess α -lipoic acid is thought to help mitigate free radical formation, however, sometimes the opposite may be the case because of prooxidant activity [54] [56]. Free radicals form from reactive oxygen or reactive nitric oxide species as a byproduct of cellular oxidation processes. Today, R/S-lipoic acid and R-lipoic acid are widely available as over-the-counter nutritional supplements in the United States in the form of capsules and tablets, and in hospitals as intravenous liquids. The commercially available racemic mixture of α -lipoic acid appears as a powder of fine yellow crystals. α -lipoic acid is a weak acid. The structure of α -lipoic acid, a chain of 8 carbon atoms with a carboxylic acid on one end and a disulfide bond between carbons 6 and 8 at the other, means that the molecule is not directly soluble in water, but requires methanol or ethanol to dissolve. At physiological pH, α -lipoic acid converts to its conjugate base lipoate. In the body, α -lipoic acid works in both fat and water based tissues, thus it can pass the blood-brain barrier. Medically, α -lipoic acid is approved to treat some liver diseases and peripheral neuropathy in Germany [56]. It also lowers blood sugar levels. Additionally, α -lipoic acid is thought to reduce inflammation, cardiovascular disease and atherosclerosis, cancer, aging, as well as to increase chronic wound healing while reducing oxidative stress [56] [54]. Some of the

effects noticed in the studies were conducted with mice or other animals, and have not been confirmed to occur in Humans. Additional studies are ongoing or do not conclusively support or deny the benefits of oral α -lipoic acid with regards to diabetes and with brain function for stroke or dementia treatment.

Carbodiimide chemistry adjoins an amine group on EGF to the carboxylic acid group on α -lipoic acid. We outline the carbodiimide attachment in detail in Section 3.1. α -lipoic acid binds strongly to both gold and silver nanoparticles by its disulfide group [57]. Dougan et al. (2007) showed that α -lipoic acid, which consists of a disulfide (-S-S-) attached in the form of a ring, bound to oligonucleotides produced gold and silver nanoparticles which were more stable than those with a dithiol (-SH and -SH) or thiol (-SH) groups. Each type of sulfur groups attached to the oligonucleotide was allowed to attach to nanoparticles for 18 hours. The α -lipoic acid conjugated to gold nanoparticles showed half-lives almost 200 times longer than the dithiol and thiol coated nanoparticles when slowly mixed over 5 days with PBS and NaCl (final concentration 0.3M). The half-lives of α -lipoic acid conjugated to silver nanoparticles were 30 times longer than the dithiol and thiol coated nanoparticles. The half-lives of α -lipoic acid conjugated to silver nanoparticles were generally shorter than gold. A paper by Horovitz et al. (2009) explores the binding of α -lipoic acid to the surface of silver nanoparticles [58]. 7 μ L of silver nanoparticle solution were mixed with 0.5 μ L of α -lipoic acid dissolved in ethanol. Horovitz et al. (2009) found with TEM that when the nanoparticles became coated with α -lipoic acid, they remained into the lower polarity ethanol and aggregated. The use of α -lipoic acid as a linker increases the nanoparticle stability under biological conditions. When α -lipoic acid adds to gold or silver nanoparticles, the disulfide (-S-S-) group binds directly to the nanoparticle. Ag-S and Au-S bonds form stronger covalent bonds to replace the citrate and borohydride groups weakly bound to the nanoparticle surface upon synthesis. M. Creixell et al. (2010) combined the protein and NPs by an alternate linker, in reverse order [52]. We attach the α -lipoic acid linker to the EGF protein, and then the conjugated protein to the nanoparticle. Our reaction sequence could increase the stability of the notoriously fragile nanoparticles by limiting the number of reactions performed on their surface, which is typically the approach used by V. M. Rotello.

Next, we discuss the significance of a molecular imaging and treatment modality involving Raman spectroscopy.

1.6 SIGNIFICANCE

Cancers have not previously been imaged through SERS with Epidermal Growth Factor protein conjugated nanoparticles as signal enhancers. This method of molecular cancer imaging and treatment through thermal therapy would be significant as an additional tool to target cancers more effectively and directly than existing techniques. It could also reduce health care costs. Identifying sensitive and selective imaging and treatment methods for the early diagnosis of a disease, such as cancer, decreases the rates of such chronic diseases and the need for long term cancer care.

This approach of attaching EGF protein to gold or silver nanoparticles through α -lipoic acid could be deployed in conjunction with or as a replacement for some cancer detection and treatment modalities. The precise capacity in which these EGFR-specific nanoparticles, combined with Raman spectroscopy to give SERS, would be used is yet to be determined as the technique is still in the developing stage. Long-term research is necessary to evaluate the EGF-linker nanoprobe for tissue imaging, and to gauge the parameters of their use for thermal therapy. Care should be taken to ensure that the silver nanoparticles, which provide increased enhancement over gold nanoparticles, are used within safe concentration ranges to avoid toxicity.

An alternative use for the EGF protein attached to α -lipoic acid could be to affix the protein to radioactive gold nanoparticles. Dr. Rowan Thomson talked briefly about work completed by Dr. Mohamed Kahn, now at the BC Cancer Agency, and colleagues. They used antibody coated radioactive gold nanoparticles, $\{^{198}\text{Au}^0\}$, for targeted dose delivery in radiation therapy [59]. As noted in the paper, the large cross section of stable $\{^{197}\text{Au}^0\}$ allows for efficient proton conversion and neutron capture, for transformation into unstable $\{^{198}\text{Au}^0\}$. $\{^{198}\text{Au}^0\}$ then emits the majority of radiation as beta-minus rays (electrons) of 0.96 MeV to conserve charge and releases the remaining 0.98% of radiation as gamma rays of 1.1 MeV. The $\{^{198}\text{Au}^0\}$ decays with a half-life of 2.69 days to

form ^{198}Hg . $\{^{197}\text{Au}^0\}$ nanoparticles were irradiated in polypropylene tubes for a variety of times, from 1 minute up to 3 hours, in a nuclear reactor to produce the $\{^{198}\text{Au}^0\}$ nanoparticles. After 2 days, the particles were tested and used only if they gave a constant decay rate of 15000 second counts of gamma radiation. The radioactive gold nanoparticles of 10 to 29 nm diameters were studied *in vivo* with mice for therapeutic dose functionality with brachytherapy. Functionality of these probes for radiation therapy is dependent on radiation doses low enough that it does not cleave the antibodies or proteins, while doses high enough to provide the destruction of tumour cells is also necessary. In the study, the radioactive gold nanoprobles coated with antibodies provided 74 μCi and lead to 45% reduced tumour size over 8 days as compared to control mice with non-radioactive nanoparticles. Toxicity was not seen over the course of the study. These radioactive nanoprobles should also function with EGF protein attached to α -lipoic acid as the imaging probe, instead of an antibody, for detection and treatment of the marker EGFR in cancer cells.

Raman spectroscopy is by far a more cost effective (tens of thousands versus millions of dollars) imaging alternative to magnetic resonance imaging (MRI), ultrasound, computed tomography (CT) and radiography, notwithstanding the lack of tissue penetration with Raman that do not limit many of the other techniques. The advantages take into account the base instrumentation costs as well as reduced construction costs associated with the imaging and treatment facilities, as there is no need for thick concrete and lead shielding barriers, such as those which enclose the X-ray and radiation therapy suites. Laser thermal therapy may also be superior to radiation therapy and chemotherapy, and can be easily implemented with gold or silver nanoparticles.

Although rare, another advantage is the greatly decreased chance of health risks to the patient from radiation burns and poisoning as compared to X-ray, CT, and radiation therapy, since laser thermal therapy uses lower energy visible to near infrared laser light instead of higher energy ionizing radiation. Some risk of burns is still present when using lasers, however proper observation of the patient and determination of appropriate dose levels would exclude this possibility.

Using a laser based approach for diagnosis and treatment would allow access in developing countries, where non-communicable diseases are becoming more prevalent,

as well as in rural areas of Canada, where treatment access is not always readily available. Raman systems have also been miniaturized, allowing for portability and ease of use. A more portable system would remove one barrier to increase availability with respect to rural treatment access here in Canada. The scans can be performed non-invasively through the skin, decreasing pain associated with testing and treatment. Alternatively, an endoscopic fibre optic Raman system, to target lung cancers, is in Human trials at the BC Cancer Research Agency (Drs. Haishan Zeng, Mladen Korbelik, and Michael Short). This endoscopic system could also be employed for cancers of the digestive tract.

Small nanoparticles, on the order of 5 nm in diameter, should avoid detection by the immune system while retaining diffusion capabilities to accumulate and aggregate in tissues to give SERS [60]. If successful, the EGF conjugated nanoprobe would aid the development of a novel *in vivo* imaging modality for the early detection of cancer.

In the next section, we describe the layout of the thesis, and the steps taken to form and test the modified protein.

1.7 THESIS OUTLINE

The thesis focuses on four areas: 1) synthesis and characterization of Epidermal Growth Factor coated gold and silver nanoparticles (EGF-NPs), 2) Assessment of the SERS activity of the nanoprobe, 3) *in vitro* cellular imaging of the nanoprobe using SERS and dark field microscopy, and 4) assessment of the biodistribution of the nanoprobe *ex vivo* using mouse models.

The first objective (Sections 3.1, 3.2, 3.4, and 3.5) is to determine whether EGF affixes well to the nanoparticles through a covalently bonded linker, whether the nanoprobe is stable at physiological salt content and pH, and whether they retain specificity for EGFR following conjugation. We find the answers to these questions using Enzyme-linked Immunosorbent Assay (ELISA), Ultraviolet-Visible spectrophotometry (UV-Vis), transmission electron microscopy (TEM) with uranyl acetate (UA) stain, time-of-flight – mass spectrometry (TOF-MS), In-Solution Tryptic Digestion and high

performance liquid chromatography (HPLC) linear ion trap – mass spectrometry (LTQ-MS), zeta potential, and salt stability tests.

The second objective (Sections 3.5.7) is to determine if the EGF-NPs are SERS active in solution. We accomplish this with Raman spectroscopy measurements of the particle solutions.

The third objective (Sections 3.6) is to determine whether EGFR induced aggregation of the nanoprobes in cell structures produces SERS. To quantify these steps, we study the Raman spectra of A431 cells with active EGF-linker or control α -lipoic acid, gold or silver nanoparticles of a variety of sizes. In addition, we use dark field microscopy in an attempt to visualize the nanoprobes in the cultured cells.

The fourth objective (Sections 3.7) is to assess the immune response and biological fate of the EGF-NPs in mouse models. We complete the determination of whether small, 5 nm, EGF-NPs avoid an immune response through inductively coupled plasma – mass spectrometry (ICP-MS) analysis of the total metal content in three organs, the kidneys, liver, and spleen. Raman spectroscopy measurements of the tissues are present in Sections 3.6.2 and 3.7.1.

The identification of molecular targets of disease through Molecular Imaging is the next step in the field of medical imaging for both early diagnosis and treatment of cancers. In this opening chapter we described how the EGF protein can be used as part of our biocompatible molecular imaging probe, specific for the cancer marker EGFR; and how Raman spectroscopy can be used as the imaging modality. We described Raman spectroscopy and surface enhanced Raman spectroscopy; Epidermal Growth Factor receptor and EGF protein; previous ways to image EGFR over-expression with anti-EGFR antibodies; past methods to attach EGF to nanoparticles, as well as our own approach.

We discuss the variety of techniques used to complete the thesis research in the next chapter, the Experimental Methods chapter.

CHAPTER 2: EXPERIMENTAL METHODS

In Chapter 1, we outlined the three necessities for implementing molecular imaging: cellular and sub-cellular markers for the disease under study, biocompatible molecular probes of these markers, and a molecular specific imaging modality with great sensitivity as well as spatial and temporal resolution. The marker, EGFR was discussed in the previous chapter (Section 1.2).

We also addressed Raman spectroscopy as a molecular specific imaging modality in Section 1.1. We discuss the theory of and give experimental details regarding Raman spectroscopy in the current chapter (Section 2.9). Also, details regarding the preparation of nanoparticles and the characterization of both nanoparticles and the EGF protein coated nanoparticle imaging probes will be discussed. The characterization methods and corresponding measured properties are:

- (a) **NP size and morphology**: Transmission electron microscopy (TEM),
- (b) **Plasmon frequency, NP concentration**: Ultraviolet-Visible spectrophotometry (UV-Vis),
- (c) **Protein mass changes from reaction**: Time-of-flight – mass spectrometry (TOF-MS),
- (d) **Reduce protein size to find α -lipoic acid protein binding site**: In-Solution Tryptic Digestion,
- (e) **Clean and measure amount of protein**: High performance liquid chromatography (HPLC),
- (f) **Find α -lipoic acid binding site on protein**: Linear ion trap – mass spectrometry,
- (g) **Nanoprobe surface charge**: Zeta potential,
- (h) **Nanoprobe affinity for EGFR**: Enzyme-linked Immunosorbent Assay (ELISA),
- (i) **Nanoprobe affinity *in vitro***: Dark field microscopy,
- (j) **Molecular imaging**: Raman spectroscopy, and
- (k) **Au/Ag concentration in organs**: Inductively coupled plasma – mass spectrometry (ICP-MS).

2.1 NANOPARTICLE SYNTHESIS

Gold and silver nanoparticles were synthesized according to established methods. Hydrogen tetrachloroaurate(III) trihydrate (36400, 99.99% metal and min. 49.5% Au) was purchased from Alfa Aesar (Ward Hill, USA). Silver nitrate (209139, min. 99.9%), trisodium citrate dihydrate (S4641, min. 99.9%), and sodium borohydride (71321, min. 99%) were obtained from Sigma-Aldrich (St. Louis, USA). The sodium borohydride and hydrogen tetrachloroaurate(III) trihydrate were weighed in a glove box, as the gold salt is sensitive to moisture. Sodium borohydride is sensitive to both oxygen and moisture. Solutions were made with deionized distilled water from a Barnstead Nanopure system; the water was purified with a resistivity of 18.2 M Ω cm (Thermo Fisher Scientific, Waltham, USA). The final synthesized gold nanoparticle solutions appeared red to purple in color, while silver ones were shades of yellow.

18 nm AuNPs were formed using a version of the traditionally established methods of G. Frens (1973) and J. Turkevich et al. (1951), as modified by K. C. Grabar et al. (1995) to yield a more concentrated nanoparticle solution [61] [62] [63]. In a fume hood, 125 mL of a 0.04% by weight gold chlorate solution was stirred and heated to boiling in a clean round bottomed flask fitted with a refluxer (Figure 2.1). The flask was heated in a bath of silicon oil to ensure even heat distribution. 12.5 mL of 1% by weight sodium citrate was added all at once to reduce the gold salt with continued boiling. Heating of the nanoparticles solution continued for 10-15 minutes, until the solution colour stabilized. Cooled nanoparticles were stored at 4°C.

The large silver nanoparticles were created by using the method of P. C. Lee and D. Meisel (1982), again as modified by K. C. Grabar et al. (1995) [63] [64]. 100 mL of a 0.02% by weight silver nitrate solution was stirred and heated to boiling using the same setup as previously mentioned with the gold nanoparticles. A volume of 1% or 0.1% by weight sodium citrate was added. The amount of sodium citrate added to the stirring silver solution ultimately determined the final size of the silver nanoparticles, as smaller quantities of citrate produced larger particles. This is also true for the gold nanoparticles.

2 mL of 1% citrate solution gave a mean diameter of 45 nm, while 2 mL 0.1% yielded 69 nm mean diameter particles. The reducing agent was added all at once.

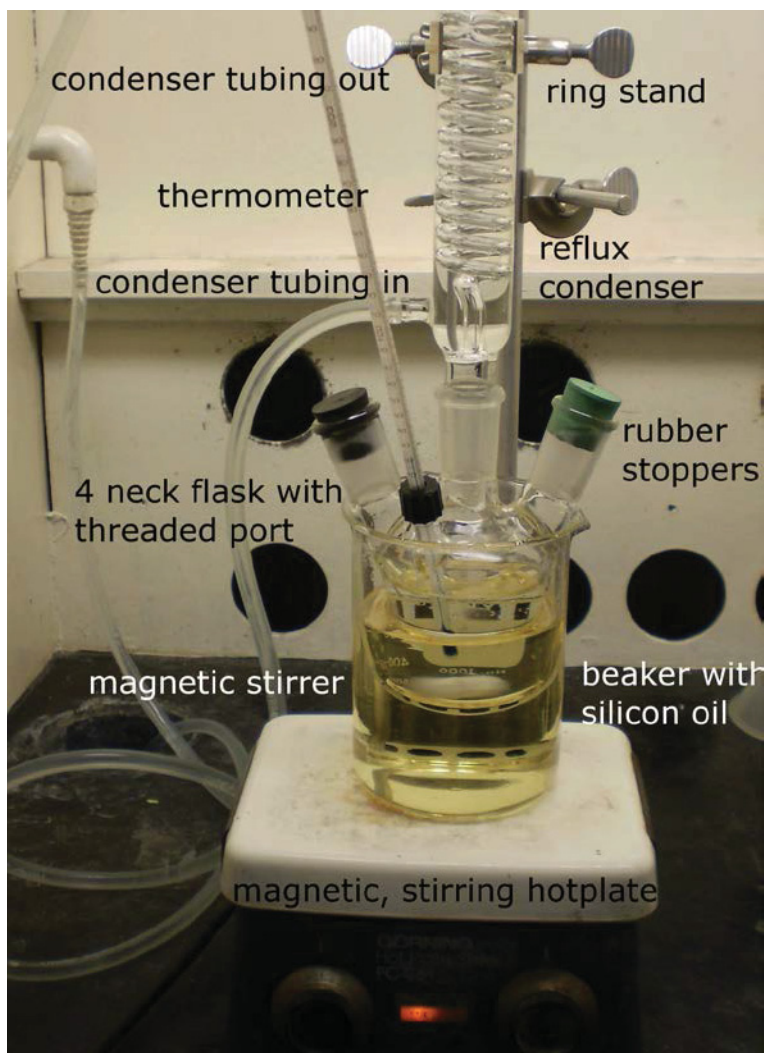


Figure 2.1 Nanoparticle synthesis apparatus – refluxing setup.

The glassware and equipment used to produce 18 nm Au and 45 nm AgNPs.

5 nm gold nanoparticles were synthesized according to the modified method of Noyong et al. (2007) [65]. 200 mL of 0.01% by weight gold chlorate solution was added to an Erlenmeyer flask and stirred at room temperature. 15 mg of NaBH_4 in 4 mL H_2O was then added all at once to the stirring gold salt solution. Stirring continued for 10 minutes or until the colour of the solution stabilized.

5 nm silver nanoparticles were prepared similarly to the gold particles with the procedure of K. C. Song et al. (2009) as modified by Ishrat Jalal [66] [67]. 15 mg of NaBH_4 in 12.5 mL H_2O was added to an Erlenmeyer flask. 12.5 mL of 0.01% by weight silver nitrate was added to the stirring sodium borohydride solution using a burette. The silver salt solution was introduced at a rate of 3-5 drops per second. The solution was stirred for 5 minutes after the silver solution was added.

We outlined the protocols to synthesize gold or silver nanoparticles of four sizes, 5 nm AuNPs, 5 nm AgNPs, 20 nm AuNPs, and 45 nm AgNPs. Next, we consider transmission electron microscopy imaging of nanoparticles for the determination of nanoparticle diameters.

2.2 TRANSMISSION ELECTRON MICROSCOPY (TEM)

A transmission electron microscope was used to image as-synthesized nanoparticle samples to confirm the particle diameters. Stained intact protein coated nanoparticles were also measured to determine the protein layer size.

TEM images were captured of samples blotted onto 300 mesh copper grids coated with carbon (CF300-Cu, Electron Microscopy Sciences, Hatfield, USA). A 20 μL drop of nanoparticles was spotted onto the grid and air dried overnight before imaging. The instrument (Tecnai 12, FEI, Hillsboro, USA) produced a beam of electrons at 80 keV, whose wavelength is 15.5 pm.

A low emissivity metal cathode filament, made of LaB_6 or W, produces the electron beam, which then focuses through magnetic lenses onto the sample grid (Figure 2.2). Nanoparticles absorb electrons and appear dark when the sample image projects onto a fluorescent screen. Alternately a CCD camera captures the image. Images were obtained using DigitalMicrograph software and a CCD camera, both from Gatan (Pleasanton, USA). A minimum of 100 particles were counted and analyzed with ImageJ software (NIH, Bethesda, USA) to obtain the average (mean) particle diameter and the standard deviation. Figure 2.2 also shows a photo of the TEM.

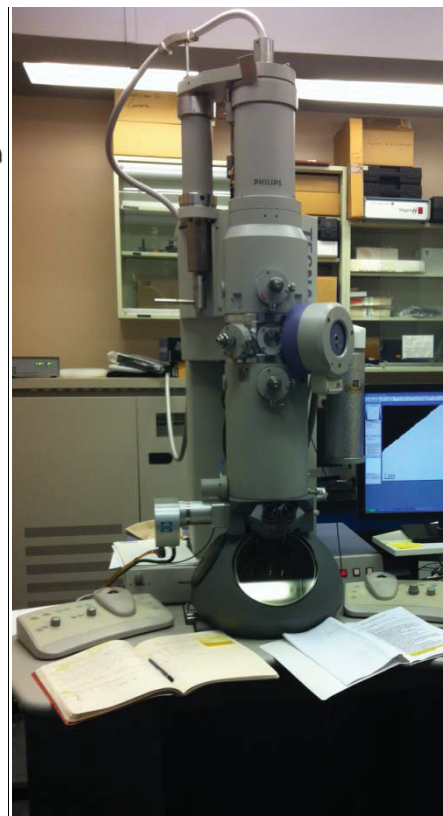
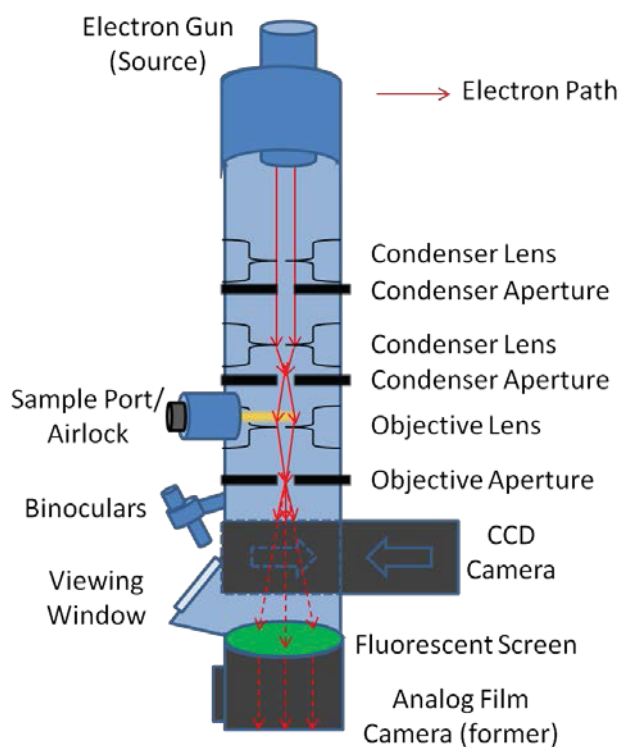


Figure 2.2 Transmission Electron Microscope diagram and photo.

Lenses focus a beam of electrons from the electron gun, or filament, onto a grid containing the sample. An image of the sample then projects onto a fluorescent screen for viewing or onto a CCD camera for capture.

Nanoparticle and protein layer sizes were measured using TEM. The nanoparticle size and its optical properties are intimately related, so we next describe the use of UV-Vis spectrophotometry for determination of the plasma oscillation frequency of the free electrons.

2.3 ULTRAVIOLET – VISIBLE SPECTROPHOTOMETRY (UV-VIS)

Ultraviolet – Visible spectrophotometry was necessary to determine the absorbance, or plasmon, wavelength of the nanoparticles. This wavelength is where the metal nanoparticle absorption peak is at a maximum.

UV-Vis spectrophotometry measurements were obtained with two devices. A Varian Cary Bio 100 (Agilent Technologies, Santa Clara, USA) measured the nanoparticle sample absorbance in the range of 200-800 nm. Samples were measured with 500 or 1000 μL quartz cuvettes with a 1 cm path length.

Measurement of a blank prior to all samples accounts for any light absorption from the medium. The optical components of the double beam setup, shown in Figure 2.3, consist of tungsten filament and deuterium arc lamp light sources to provide the visible and ultraviolet light, respectively. The light source component wavelengths are spatially separated by a monochromator, while the grating and mirror setup rotates to scan through the available wavelength range of the source. A beamsplitter divides the light into a sample and a reference beam. The sample beam shines onto a cuvette containing the sample. A chopper directs the sample and reference beams onto a detector, where the blue square in the diagram represents a mirror reflecting the sample beam, the white square represents a hole to allow the reference beam to pass, and the black squares represent a beam block to act as a zero light reference. Absorption by the sample is determined by comparing the reference and sample beam intensity at each wavelength.

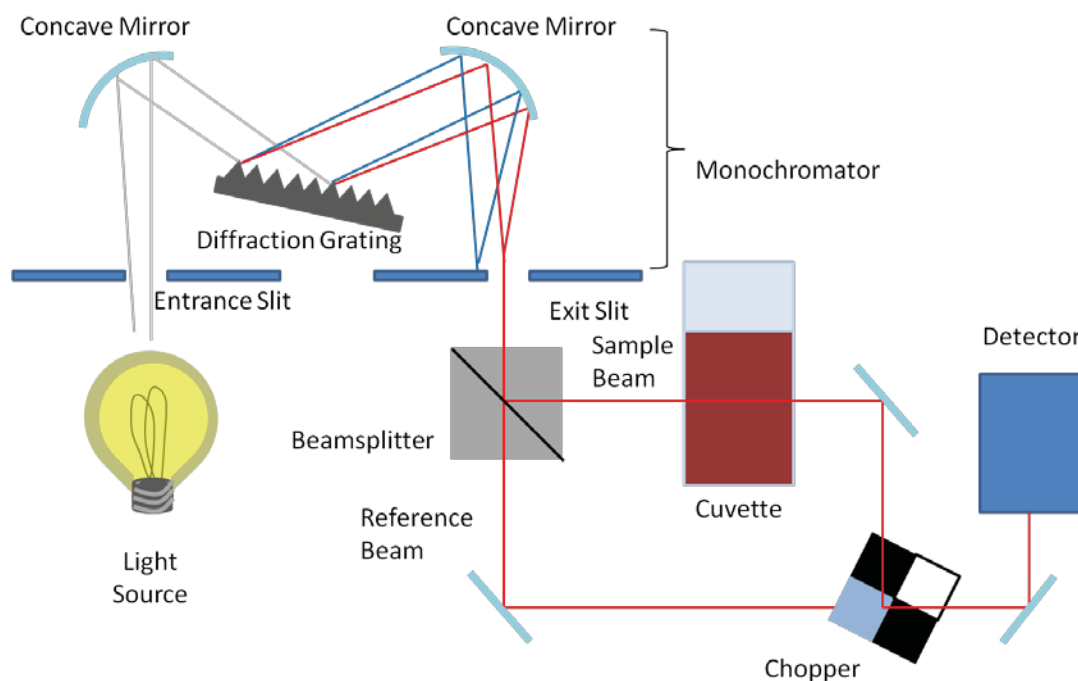


Figure 2.3 Double beam Varian Cary Bio Ultraviolet-Visible spectrophotometer.

A monochromator separates emissions from a light source to allow scanning through the component wavelengths. The light is split into two beams by a beamsplitter, a sample and a reference beam. The sample beam shines onto a cuvette containing the sample. The chopper alternates the reference and sample beams before they shine on the detector.

A ND-1000 UV-Vis from Nanodrop (Wilmington, USA) was also used. It reads the absorbance of a 5 μ L droplet of the sample in the spectral range 220-750 nm. The absorbance is automatically measured at path lengths of both 1 mm and 0.2 mm to ensure accuracy, and the 1 mm value is reported.

The optical path of the Nanodrop is similar to that of the Varian, although an alternate configuration allows collection of all light wavelengths simultaneously in a single beam configuration (Figure 2.4). A pulsed Xenon arc lamp provides light. Light shines on the quartz coated sample pedestal through a fibre optic cable. The light directs to a diffraction grating, and the spatially separated components are directed onto a multichannel CCD, which replaces the single channel photodiode/scanning monochromator pair.

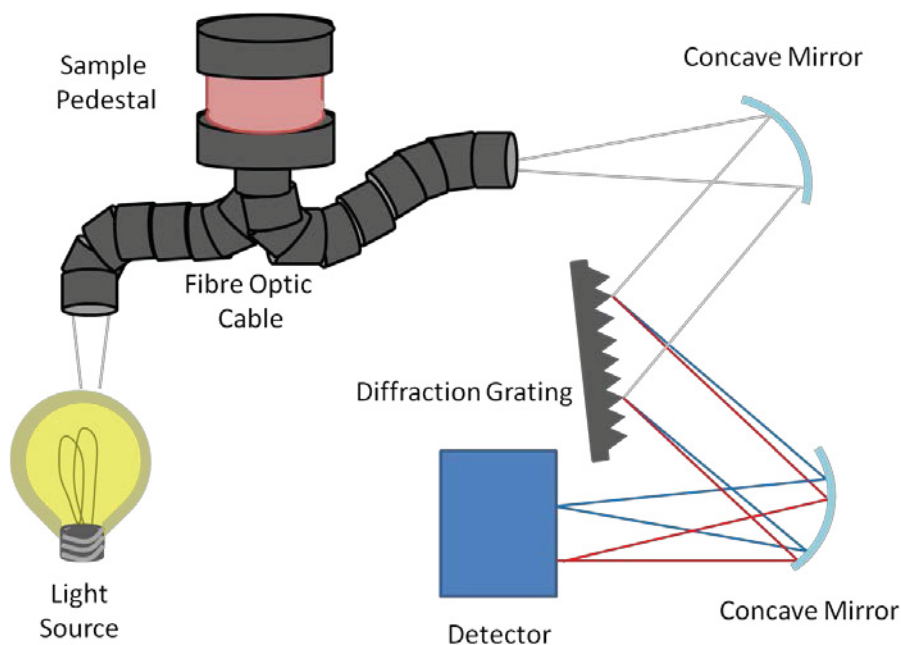


Figure 2.4 Single beam Nanodrop Ultraviolet-Visible spectrophotometer.

Light from the light source shines through fibre optic cables onto a pedestal containing a droplet of sample. The light then routes through fibre optic cables to a diffraction grating. A detector measures the individual wavelengths of light.

UV-Vis was used to measure the absorbance properties of nanoparticles and, as described later in Section 2.6, the efficacy of protein binding using a colourimetric assay - ELISA. In the course of building our nanoprobe, novel protein complexes need to be created. Two independent mass spectrometry techniques were used to determine whether the protein complexes were formed successfully, as described in the next sections.

2.4 DETECTION OF EGF-LINKER ATTACHMENT BY MASS SPECTROMETRY (MS)

Two separate methods involving mass spectrometry were utilized to determine whether α -lipoic acid was successfully attached to EGF. Time-of-Flight – mass spectrometry of the reaction product was used to detect whether there was a mass increase in EGF corresponding to the mass of the α -lipoic acid molecule. The second method required segmentation of the protein complex to determine where α -lipoic acid was bound. A protease, trypsin, was used to cleave at specific portions of the EGF-linker protein sequence, to produce smaller sequences known as peptides. These peptides were cleaned with high performance liquid chromatography (HPLC) and then analyzed with a Linear Ion Trap – mass spectrometer to see which of the three potential attachment sites on EGF, the amino terminus or one of two lysine amino acids, were tagged by α -lipoic acid.

2.4.1. Time-of-Flight – Mass Spectrometry (TOF-MS)

Time-of-Flight – mass spectrometry was used to confirm whether the α -lipoic acid attachment to the EGF protein occurred. This instrument could not distinguish which site

was targeted on EGF from the intact protein alone, Linear Ion Trap – mass spectrometry of trypsin digested EGF was later attempted to determine the attachment site and will be described in the sections following, Sections 2.4.2, 2.4.3, and 2.4.4.

Prior to mass spectrometry (MS) analysis, the intact protein samples were purified with 3 kDa centrifugal molecular weight cutoff (MWCO) filters, as smaller reaction byproducts and salts will depress the protein signal observed by the instrument. This procedure is outlined in Section 3.1. For the MS measurements, half of the recovered protein samples were diluted in 0.1% formic acid in a fume hood to 50 μL of 0.1 mg/mL protein. Deionized water, methanol (MeOH, A452-4, min. 99.9%, Fisher Scientific, Ottawa, Canada) and acetonitrile (ACN, 22927, min. 99.7%, Alfa Aesar, Ward Hill, USA) were added in a ratio of 50 H_2O : 30 ACN : 20 MeOH.

As mentioned previously, an ESI-qTOF (Electrospray Ionization quadrupole Time-of-Flight) from Bruker Daltonics (Billerica, USA) operated in positive ion mode $[\text{M}+\text{H}^+]$ was used for the measurements. A schematic and photo of the instrument are shown in Figure 2.5. The sample was introduced at a flow rate of 10-20 $\mu\text{L}/\text{min}$. The formic acid in the sample aids in ionization with ESI by increasing the conductivity. In the ESI inlet, the sample is also dried or heated to allow it to enter the gas phase. In this case, nitrogen gas heated to 180°C dried the sample at the ESI inlet. After the molecules are converted to gas phase ions, they are focused into the TOF by a quadrupole – a series of rods held at a potential which allows the ions to move in a single stream. In the TOF portion of the instrument, the sample (mass, m) is first accelerated by a voltage (V) when it leaves the quadrupole, travels down a flight tube at constant speed (v), and hits the detector. The ion mirror deflects the charged particles onto the detector, without introducing any new velocity or acceleration components. Conservation of energy requires,

$$V = \frac{1}{2}mv^2. \quad (2)$$

This relationship was rearranged to determine the mass of the sample (m), as we know V (the kick voltage), and v is the flight tube distance divided by the time to travel through the flight tube. The mass to charge ratio is a measure of the weight of the proteins or peptide fragments, but also gives extra information about the charge state of the ionized atom or molecule.

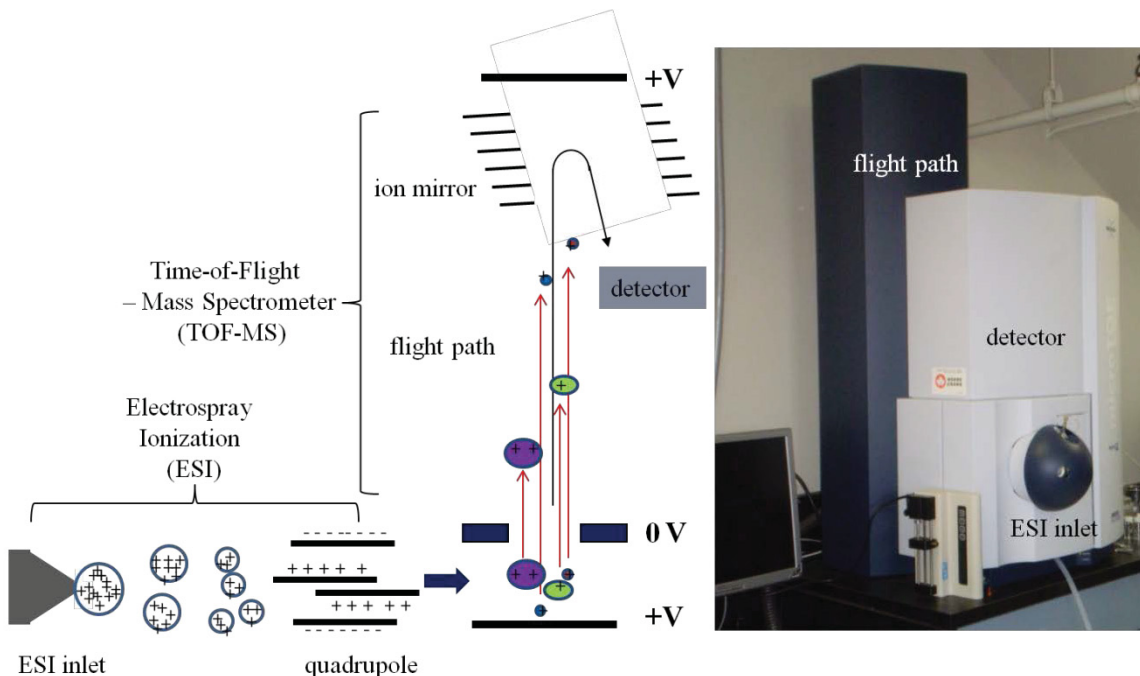


Figure 2.5 Time-of-Flight – mass spectrometer diagram and photo.

The setup consists of the Electro spray Ionization inlet, to introduce and ionize the sample; a quadrupole, to focus the ions; the flight path, to allow the ions to move at their own rate; an ion mirror, to reduce the instrument dimensions; and a detector, to measure when the ions arrive and then infer the m/z .

The instrument and data collection software were calibrated prior to the measurements for any changes in the flight tube length caused by changes to the ambient air temperature. The TOF-MS has a range of 20-20000 m/z [68]. The instrument resolution is high with a $M/\Delta M$ of 15000 FWHM, and a mass accuracy of 3-5 ppm. The m/z accuracy value varies from low to high m/z range. The accuracy in m/z is calculated from the m/z range value of interest multiplied by the accuracy in ppm and divided by

10^6 . Assuming low mass accuracy of 5 ppm, at 1200 m/z, the accuracy would be ± 0.006 m/z units.

The measurements described above tell us whether the linker, α -lipoic acid, was successfully attached to the intact EGF protein. The next three sub-sections explain an additional, yet entirely separate, method which also involves mass spectrometry in the determination of where the α -lipoic acid linking molecule was able to attach to EGF protein; i.e. to distinguish which of three amino acids on EGF are targeted for tagging.

2.4.2. In-Solution Tryptic Digestion for Determination of α -lipoic Acid Attachment Site

The Linear Ion Trap – mass spectrometry in conjunction with High Performance Liquid Chromatography (HPLC) was used to determine which of the three amino acids on the Human EGF protein the α -lipoic acid linker binds to; the amino terminus or one of two lysines. The protein was cleaved into peptides and the LTQ-MS selects fragments of those peptides for analysis. The protein samples were digested with a protease, cleaned offline with high performance liquid chromatography (HPLC), and then separated online with HPLC and measured for a size (mass) analysis with the LTQ-MS. We first discuss the method, known as In-Solution Tryptic Digestion, to selectively convert the intact protein into smaller peptides. This conversion occurs with the use of a digestive enzyme, trypsin.

Before using EGF in the digestion process, a “throwaway” protein-linker was synthesized with the protocol outlined in Section 3.1 to act as a sacrificial sample to ensure that the α -lipoic acid linking procedure could work with another cheap protein which also contains some lysines. Insulin (5.8 kDa, 91077C, Sigma-Aldrich, St. Louis, USA) was chosen as this throwaway protein. It is quite similar to EGF in its structural features. In addition to the lysine amino acids, insulin possesses 4 cysteine amino acids which make up 2 disulfide bonds [69]. A 2 g/L stock insulin sample was diluted and used at the same concentration as EGF to form the linker. The ratios of the reactants for the α -

lipoic acid linking reaction were those which seemed to give the best EGF-linker yields, 1 protein : 120 α -lipoic acid : 1300 EDC (1-ethyl-3-[3-dimethylaminopropyl] carbodiimide) : 3200 Sulfo-NHS (N-hydroxysulfosuccinimide). The same purification procedures as outlined at the end of Section 3.1, with the Amicon 3 kDa centrifugal filters, were also performed. An additional reason the insulin-linker sample was simultaneously run through the capping, trypsinization, HPLC purification, and LTQ-MS with the EGF-linker was to ensure that the protocols and instruments were functioning properly and ultimately prevent accidental losses of the EGF-linker sample.

The EGF and insulin protein unfolding occurs by capping the six cysteine amino acids which make up the three disulfide bridges with iodoacetamide to form carbamidomethyl groups. The following In-Solution Tryptic Digest protocol was obtained from the group of Alan Doucette in the Department of Chemistry at Dalhousie University and can be found in work completed by M. J. Wall et al. [70]. The protein of interest, ammonium bicarbonate (NH_4HCO_3 , A6141, min. 99.0%, Sigma-Aldrich, St. Louis, USA), dithiothreitol (DTT, 161-0611, Bio-Rad, Hercules, USA), iodoacetamide (IAA, I1149, min. 99%, Sigma-Aldrich, St. Louis, USA), trifluoroacetic acid (TFA, T6508, 99%, Sigma-Aldrich, St. Louis, USA), and trypsin (T8802, Sigma-Aldrich, St. Louis, USA) were required for the digest.

Solutions of proteins to be cleaved with a protease should not contain organic solvents, such as acetonitrile, as the organic solvent depresses the enzymatic abilities of the trypsin when in concentrations above 30% by volume [71]. Low concentrations of acetonitrile, nearer to 10% by volume, can boost the activity of trypsin. A pre-cleaning step with centrifugal filters, as outlined in Section 3.1, should take place prior to digestion of the protein. Alternately, drying the sample with a SpeedVac (Thermo Fisher Scientific, Waltham, USA), resuspending in an appropriate buffer, and then centrifuging for at least 5 minutes at 13 000 rcf would remove unwanted solvents. A SpeedVac, generally known as a centrifugal evaporator, uses a pump to create low pressure in the centrifugal chamber in order to evaporate solvents. The decrease in pressure lowers the solvent boiling point below the temperature in the centrifugal chamber, causing most solvents to evaporate without heating temperature sensitive proteins and peptides.

Ideal concentrations for protein solutions intended for digestion were between 0.1 to 1.0 g/L, otherwise the procedure requires adjustments to the amount of trypsin added. The protein was diluted to the ideal concentration in 50 mM NH_4HCO_3 , from a stock solution of 100 mM NH_4HCO_3 (4.75 mg NH_4HCO_3 per 600 μL deionized H_2O). The addition of the ammonium bicarbonate buffer adjusted the solution to a pH of 8, anywhere in the range of pH 7.5 and 8.5 was acceptable.

200 mM freshly prepared stock DTT solution (3.07 mg DTT per 100 μL deionized H_2O) was added to the protein solution in NH_4HCO_3 buffer to a final DTT concentration of 9.5 mM. 5 μL of DTT per 100 μL of sample gave the desired concentration of DTT. DTT cleaved the three intramolecular disulfide bonds to form 6 thiol groups per protein in addition to at least 2 more thiol groups per α -lipoic acid molecule attached to EGF. The protein and DTT solution was heated at 60°C for 20 minutes in an oven.

200 mM freshly prepared IAA (3.70 mg per 100 μL deionized H_2O) was then added to a final concentration of 19 mM, the solution was allowed to react in the dark for 20 minutes at room temperature. 9.5 μL of IAA solution per 100 μL of sample gave the final IAA concentration of 19 mM. The IAA capped the thiols to form the carbamidomethyl groups, which allowed the protein to unfold. This step also capped any thiols on the attached α -lipoic acid linker.

Stock trypsin solutions consisted of 10 μL aliquots at a concentration of 1 g/L made up in 0.1 mM hydrochloric acid (HCl, diluted from H-6100, ACP, Montreal, Canada) and stored frozen until use. An aliquot of stock trypsin was thawed and added to the unfolded protein in a 50 protein : 1 trypsin mass ratio, for a final trypsin concentration of 0.1 g/L. The protein solution was incubated at 37°C. 2 μL of the 1 g/L stock trypsin was added to achieve the 0.1 g/L final trypsin concentration. In our case, *our protein concentration was low to start at 10 μg per 500 μL solution, or 0.02 g/L*. This is significantly lower than the desired starting protein concentration of 0.1 to 1.0 g/L mentioned earlier. *This low level of target protein made it difficult to reach the 50 : 1 protein to trypsin ratio, the actual ratio was near 5 : 1. This increased the likelihood that trypsin would digest itself in solution.* In order to avoid missed cleavages of the EGF

protein by loss of trypsin from self digestion, a second 2 μ L portion of 1 g/L trypsin was added 4 hours after the first aliquot. The trypsin containing protein solution was incubated in a 37°C oven overnight. The trypsin, our protease and an enzyme, cleaved at the carboxyl side of certain amino acids in a protein sequence, lysine (K) and arginine (R), except when followed by the amino acid proline (P). This reduced the protein into smaller fragments. The trypsin cleavage reaction was halted the next day with the addition of 10% by volume of 10% TFA. A cartoon of the process is shown in Figure 2.6.

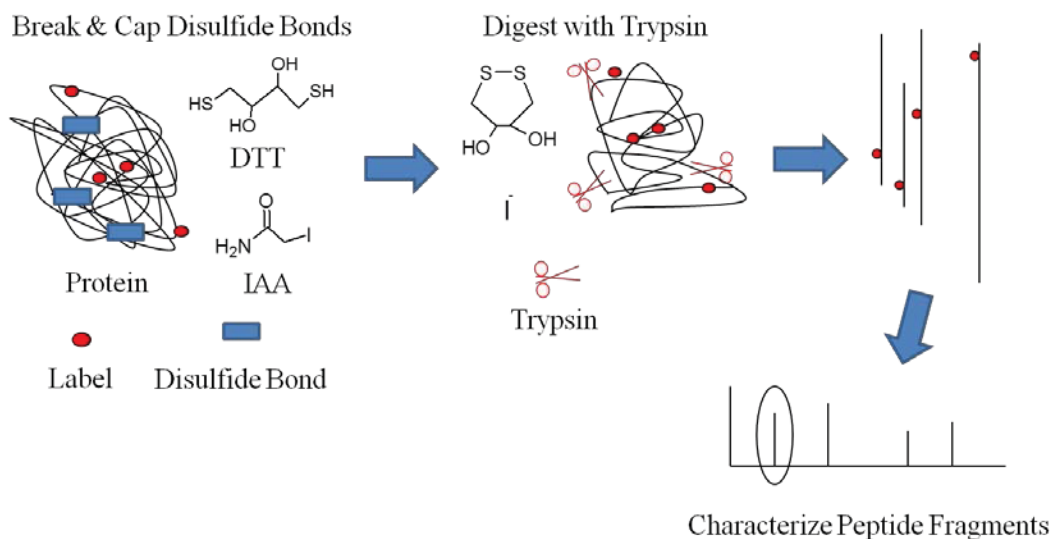


Figure 2.6 In-Solution Tryptic Digestion schematic.

The procedure consists of first unfolding the protein by breaking disulfide bonds with DTT (dithiothreitol) and IAA (iodoacetamide). Next the protein is converted to peptides with trypsin, a digestive enzyme. The peptide fragments can then be cleaned and analyzed.

We introduced and discussed In-Solution Tryptic Digestion, a protocol to cleave entire proteins into peptides with the use of the enzyme, trypsin. In-Solution Tryptic Digestion was the first of three steps to selectively fragment and analyze the peptides with Linear Ion Trap – mass spectrometry. This mass spectrometry method should tell whether α -lipoic acid was attached to EGF, as well as which of the three amino acids on Human EGF protein the α -lipoic acid linker was bound, the amino terminus or one of two lysines. In the next sub-section we address the second step, to clean unwanted reaction byproducts from the peptides with high performance liquid chromatography.

2.4.3. High Performance Liquid Chromatography (HPLC) for Determination of α -lipoic Acid Attachment Site

In the preceding sub-section, the EGF-linker and insulin-linker protein samples were digested with the protease, trypsin, to produce peptides by In-Solution Tryptic Digest. In the current sub-section, we describe how the peptides were cleaned offline with high performance liquid chromatography (HPLC) to prepare for future use with the Linear Ion Trap – mass spectrometer. LTQ-MS is able to detect a mass shift of each fragment, thereby indicating where α -lipoic acid attaches.

Peptides were concentrated for injection onto the HPLC column using a SpeedVac, which removes all solvents and brought the samples to dryness. The peptides were reconstituted up to a volume of 100 μ L with 0.1% TFA. Much pipetting up and down with a micropipettor allowed the resuspension all protein. Centrifugation at 13 000 rcf (relative centrifugal force) for 5 minutes was used to remove any undissolved peptides or reaction byproducts and prevent clogging of the column.

Ammonium bicarbonate buffer was used during the tryptic digestion to adjust the protein solution pH while introducing a minimum amount of salt, in the form of sodium and chlorine ions, to the sample. After the use of the SpeedVac, if all salt crystals were not able to redissolve and resuspend, then they could cause problems with the HPLC. Salts are detrimental to the HPLC, as excess salt can clog the column and cause sample losses.

The leftover dissolved trypsin, reaction byproducts, and buffers were cleaned from the peptides offline by HPLC with a reversed phase column. HPLC works by separating molecules by their retention time or elution time, as the beads packing the column trap molecules of a certain affinity. The HPLC was operated by Dennis Orton of the Doucette lab in the Department of Chemistry at Dalhousie University. Two HPLC solvents, *water and acetonitrile* which each contain 0.1% trifluoroacetic acid, were made up with fresh deionized water or acetonitrile. The solvents were first degassed, to prevent air bubbles from clogging the column, and then automatically mixed by the HPLC in the

desired ratios (Figure 2.7). 50 μL of the peptides were loaded into vials and sealed, while 2 aliquots of 20 μL each of the peptide samples were injected onto the column with the autosampler. Adjusting the relative proportion of water and acetonitrile solvents varies the polarity of the solution flowing through the reversed phase column, which was packed with somewhat non-polar beads. With mostly polar water as the solvent, the EGF peptide fragments and especially the non-polar amino acids, tended to remain stuck in the column because the fragments had low polarity. *The reverse phase column traps the more non-polar peptide components, while polar components wash through.* The polarity of the buffer mixture was then reduced by the addition of non-polar acetonitrile. The decrease in polarity allowed the trapped peptides to move out of the beads and back into the flowing solvent (mobile phase) and then to exit the column. *The peptides were removed from the column because the affinity of the peptide for the solvent increases as the polarity of the solution decreases.* Standard proteins or peptides allowed for calibration of the retention time so only the desired molecules were collected. Each injection run lasted 35 minutes. The starting buffer ratios (95% H_2O to 5% ACN) were rapidly altered to 15% H_2O and 85% ACN, remained constant (equilibrated) over 5 minutes, and then rapidly returned to the initial ratio, as seen in Figure 2.8. The sudden change in polarity allowed a pocket of peptides to be formed and collected over a short time. The peptides moved through the HPLC tubing and the amide bonds within the structure were detected by the UV-Vis at 214.40 nm with a zero reference signal at 350.25 nm. The automatic fraction collector then gathered the peptides, as the peptide elution time was preset to the time of the standard.

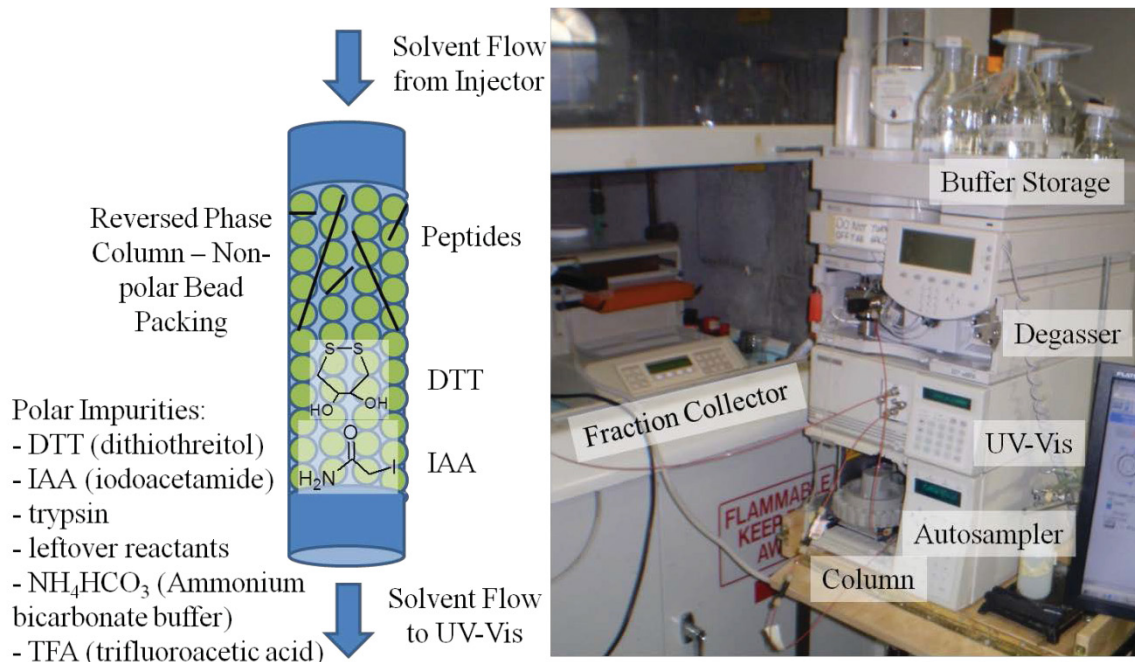


Figure 2.7 High Performance Liquid Chromatography (HPLC) diagram.

The column was flushed by polar H_2O with 0.1% TFA, and then the sample was injected onto the column. The buffers were degassed prior to mixing to prevent air bubbles. The polar impurities were washed away by the H_2O solvent, while the slightly non-polar protein sticks to column beads. The organic solvent concentration, ACN with 0.1% TFA, was increased to 85%, the peptides were released from beads and left the column. The peptides were visualized with the UV-Vis. An automatic fraction collection system – pre calibrated to protein elution time – collected the peptides.

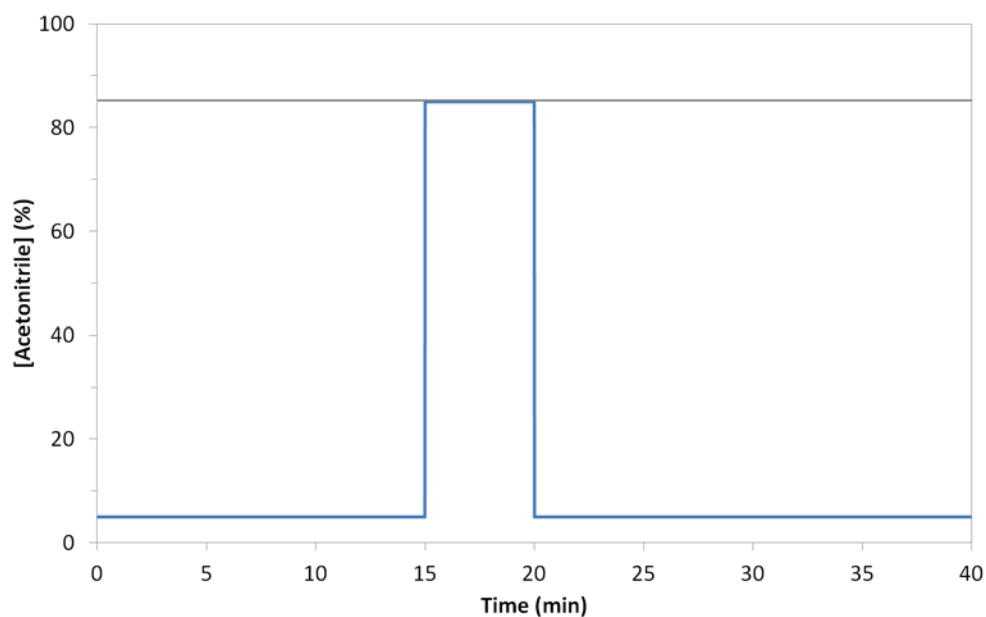


Figure 2.8 HPLC solvent gradient for peptide elution.

The concentrations of acetonitrile used to elute EGF peptides from a reversed phase column. The concentration of water is simply the percentage which remains required to reach 100%.

We have just described how the EGF-linker peptides were cleaned offline with HPLC. In the next sub-section we explain how the peptides were subsequently separated online with HPLC and analyzed by the Linear Ion Trap – mass spectrometer. LTQ-MS measures the peptides on the basis of size to infer where α -lipoic acid may have been added to EGF.

2.4.4. Linear Ion Trap – Mass Spectrometry (LTQ-MS) for Determination of α -lipoic Acid Attachment Site

In the previous two sub-sections, we discussed in-solution tryptic digestion to form smaller peptides from EGF protein, as well as using HPLC to remove reaction byproducts from the peptides. Here we describe the use of HPLC in conjunction with LTQ-MS to separate the peptides and measure their mass. We also describe the use of Sequest, a program for analysis and interpretation of the LTQ-MS data.

The LC-MS data collection was performed by Dennis Orton of the Doucette lab in the Department of Chemistry at Dalhousie University. After the HPLC cleaning, the peptide samples were dried down with the SpeedVac to remove any residual TFA. In preparation for MS, 3.5 μg of the dried peptide sample was diluted with 350 μL of a mixture of 95% H_2O and 5% ACN, each containing 0.1% formic acid to help with ionization, to give a peptide concentration of 0.1 $\mu\text{g}/\mu\text{L}$. As demonstrated in Figure 2.9, 10 μL of 0.1 $\mu\text{g}/\mu\text{L}$, or 0.1 μg , of the digested and cleaned EGF sample was injected onto another reversed phase HPLC column, to separate the peptides based on their retention time. Dual columns were used, where the column operations are alternated so as one column equilibrates, the other has sample injected onto it and is analyzed with the MS. Two blanks and four samples, 1 blank and a set of duplicate samples per column, were run. Each injected sample was run for 65 minutes, where the ACN ramped up from 5% to

85% slowly over 30 minutes. The HPLC was hooked up to the ESI-LTQ-MS (Finnigan/Thermo Fisher Scientific, Waltham, USA), which measures the mass to charge, or m/z , ratio of the peptides. The HPLC-ESI-LTQ-MS setup gave 2 dimensions of separation, retention time from HPLC and mass-to-charge from the mass spectrometer. The HPLC works in an identical manner as in Section 2.4.3. The separated peptides were funneled into the ESI inlet, which works the same way as the ESI in Section 2.4.1. Once ionized and in the gas phase, the sample sprays into the LTQ-MS. There are three sections on the LTQ, an entrance, an ion trap, and an exit. The LTQ works similarly to quadrupoles (Section 2.4.1), as it is held at a potential to analyze or fragment the ions, although the LTQ has the added ability of trapping ions to detect very low concentration samples. The ions then travel to a detector for quantification. The MS is calibrated to detect maximum signal intensities from 400 to 1200 m/z , but can see fragments from 350 m/z to 2000 m/z . We used the entire 350 m/z to 2000 m/z range for peptide detection.

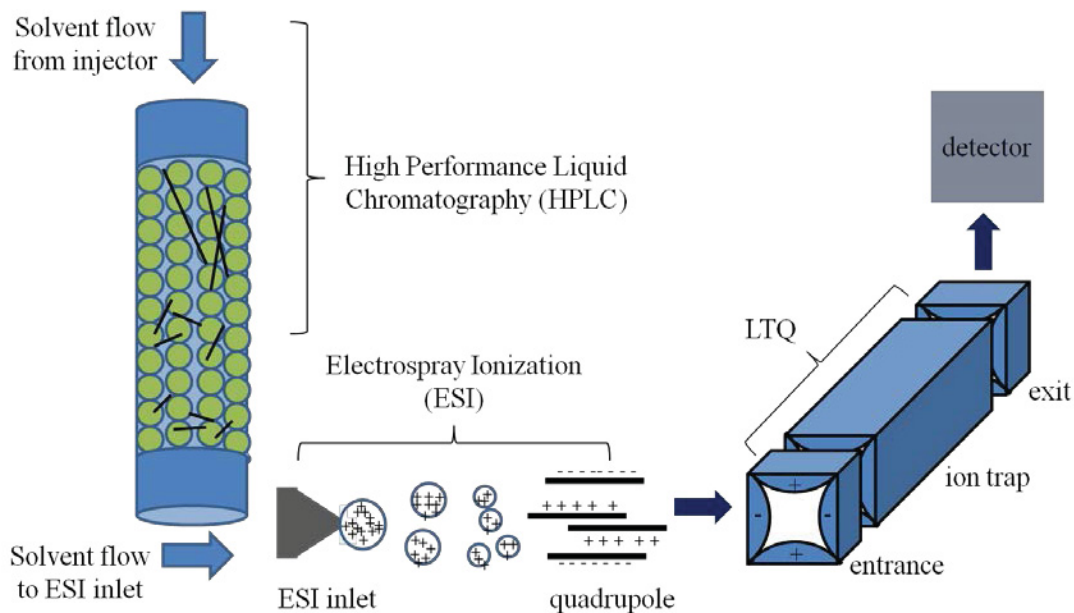


Figure 2.9 Linear Ion Trap – mass spectrometer (LTQ-MS) diagram.

Samples were injected onto one of two columns (second column not shown). The black lines in the column represent peptides, a gradient removed more polar peptides first. The peptides were then converted to gas phase ions in the ESI and were channeled into the LTQ. The ions were trapped in the LTQ until sufficient quantities were present, and then simultaneously sent to the detector.

The LTQ-MS data were processed with a program called, Sequest (Thermo Fisher Scientific, Waltham, USA). Sequest allows for a comparison between the known sequence of EGF and any modifications from the α -lipoic acid or post translational modifications while taking into account the digestion with trypsin. It calculates the mass to charge ratios of the modified peptides and compares these to the mass to charges found with LTQ-MS, while ranking the likelihood of the match. These fragments are then studied for the presence of the EGF-linker, as identified by the addition of a particular amount of mass to peptides containing the amino terminus, or lysine amino acids.

Two independent mass spectrometry methods, TOF-MS and LTQ-MS, were used to check that α -lipoic acid had attached to EGF protein. LTQ-MS was also used to identify which amino acids on EGF formed a bond to α -lipoic acid molecules. The TOF-MS experiments used the intact EGF-protein. More pre-processing was required for the additional method, wherein EGF protein was digested into peptide fragments with trypsin and then the digestion reaction byproducts were cleaned by HPLC from the solution. Finally, another HPLC separated the peptides based on their retention time and funneled the peptides directly into the LTQ-MS for size determination. Sequest software helped with interpretation of the LTQ-MS data.

One of the properties of any nanoprobe, in addition to its functionality, is its stability. A zeta potential measurement, as outlined in the next section, was used to quantify this property.

2.5 ZETA POTENTIAL

The zeta potential is a measure of the potential at the particle-solvent interface, and can be used to predict the stability of suspended particles. It was used to gauge the stability of uncoated, α -lipoic acid coated, or EGF-linker coated, gold or silver nanoparticles in solution. Moreover, it is important to know the sign of the surface charge because positively charged gold nanoparticles can penetrate deep into cell membranes,

whereas negatively charged particles do not enter the cell membrane (which is itself negatively charged) at all but instead prevents membrane degradation under certain conditions [72].

Zeta potentials are measures of stability from particulate colloidal suspensions, be they solids, liquids, or gases [73]. Instability of colloids results in flocculation (usually reversible) or coagulation (usually irreversible). The balance between the attractive and repulsive potential energies of the colloidal nanoparticles influences the stability of the solution the greatest. The repulsive potential energy (U_R) contains the zeta potential term,

$$U_R = 2\pi\epsilon a\zeta^2 e^{-kD}, \quad (3)$$

where ϵ is the dielectric constant, π is solvent permeability, a is the particle radius, k is the ionic composition, D is the particle separation, and ζ is the zeta potential. The repulsive potential energy is related to the electrophoretic mobility (U_E), or the particle speed in a unit electric field. An applied electric field causes the charged particles to move towards an electrode of opposing charge, while viscosity of a bulk solution opposes the charged particle movement. The particle speed becomes constant once the forces are at equilibrium. The electrophoretic mobility is defined as,

$$U_E = \frac{2\epsilon\zeta f(\kappa a)}{3\eta}, \quad (4)$$

where η is viscosity, $f(\kappa a)$ is Henry's function, and all the previous terms are the same. κ is known as the Debye length or electrical double layer thickness and has reciprocal units, while a is still the radius, so $f(\kappa a)$ is a measure of the ratio between the particle radius and the double layer thickness. The value of $f(\kappa a)$ is estimated at 1.5 for particles larger than 200 nm, and 1.0 for smaller particles. Rearranging the equation allows determination of the zeta potential.

The stability of the solution depends greatly on the groups around the surface of the nanoparticle, at the particle-solution interface, as these groups form a barrier to keep the particles intact while maintaining a repellent force to isolate the particles from one another and to prevent agglomeration. The overall charge imparted on a nanoparticle

comes from these surface groups, and generally result in a net positive or negative charge. The presence of nanoparticle stabilizing molecules containing many acidic groups will lead to net negative charges upon ionization of the acid in bulk solution. Conversely, basic stabilization groups will lead to net positive charges around the nanoparticle. The relative strength of the charge, positive or negative, depends on the ionic strength of the bonds of the stabilization groups as well as the pH of the bulk solution. In our case, the as synthesized gold and silver nanoparticles should be stabilized by citrate or borohydride groups, both of which contain acidic groups. The α -lipoic acid linker which binds to the nanoparticles also contains an acidic group. Our nanoparticles should give a net negative charge upon zeta potential analysis.

A negative or positive zeta potential, below -30 mV or above 30 mV, usually confirms particle stability. A neutral zeta potential denotes less particle stability, as there are less repellant forces. These nanoparticles would likely agglomerate shortly, especially upon addition to 0.9% salt concentration conditions used experimentally.

The zeta potential data were collected by Dr. Kevin Hewitt in collaboration with Dr. Jesse Jokerst at the lab of Dr. Sanjiv Gambhir at Stanford University in Palo Alto, California. A Zetasizer-90 (Malvern Instruments, Worcestershire, UK) was used for the measurements, as shown in Figure 2.10 [74]. The 633 nm laser light source was split into two beams by a beamsplitter. An attenuator adjusted the sample beam intensity to ensure that the signal intensities were not so strong as to fall outside of the measurable range. 1 mL of solution was loaded into a cuvette and measured using the sample beam. The reference beam recombined with scattered light from the sample beam with the use of a chopper, where the blue square reflects the reference beam onto the detector, the white square allows the scattered beam to pass through onto the detector, and the black squares block all light beams to give a zero reference. The signals were gathered with the detector and post processing of the data output the zeta potential. An electric field applied to the sample cell causes the particle to attain a constant speed in a viscous medium, which in turn causes a frequency change in the scattered light due to the Doppler effect. Equation 4 relates the speed to the zeta potential.

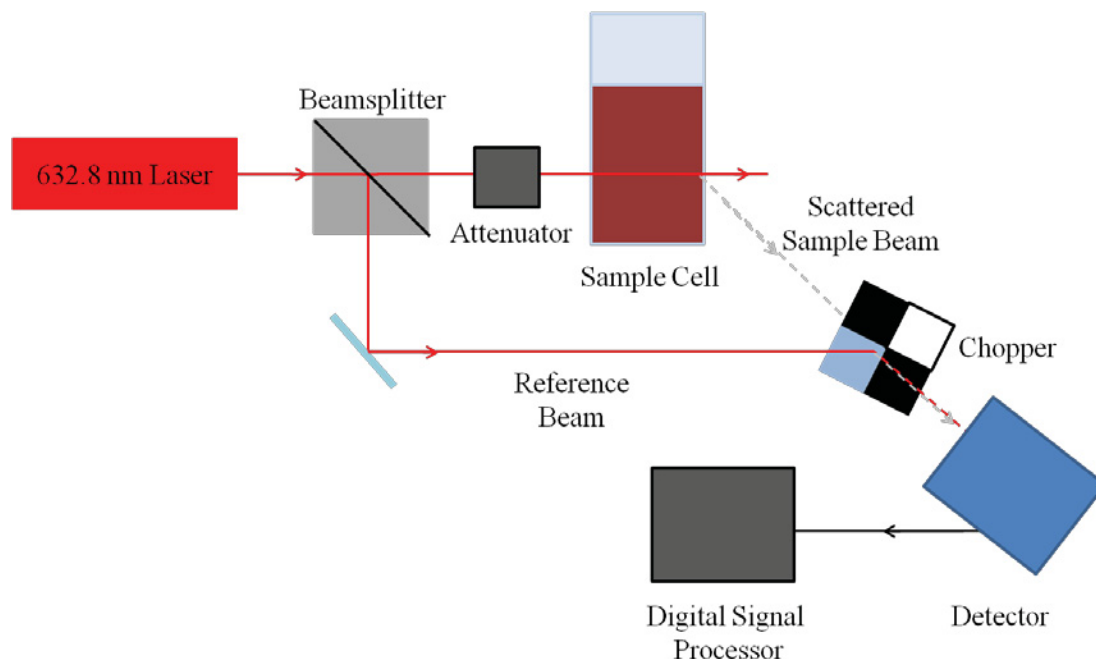


Figure 2.10 Zeta potential diagram.

The 633 nm laser light is shone on a beamsplitter to form a sample and a reference beam. The sample beam is attenuated to reduce oversaturation of the detector, and then shone through the sample. Scattered light from the sample is combined with the reference beam through a chopper. The light is detected and processed to find the zeta potential.

The solution pH and purity, the conductivity of adsorbed ions, and the particle concentration all affect the zeta potential. Reproducibility of the zeta potential data can be achieved by using sample preparation and measurement techniques suggested by nanoComposix [75]. We generally followed these protocols, and achieved reproducible data. The EGF coated active and α -lipoic acid coated control nanoparticles were purified by the method of S. Balasubramian et al. (2010) [76], which is further described in Section 3.4.3, to remove any residual nanoparticle synthesis reactants. The supernatant was replaced with 18.2 M Ω cm deionized water. The zeta potential measurements were analyzed multiple times for each sample, to ensure repeatability. The zeta potential measured the stability of nanoparticle solutions with a variety of coatings.

In the next section, we introduce ELISA, which was used to assess the activity of EGF-linker protein and EGF-linker tagged nanoparticles.

2.6 ENZYME-LINKED IMMUNOSORBENT ASSAY (ELISA) FOR EGF

ELISA allows one to determine whether the EGF-linker and also EGF-linker coated nanoparticles are specific for the EGFR. An ELISA kit from RayBiotech (Norcross, USA - purchased from Cedarlane Labs (Burlington, Canada), ELH-EGF-001) or purchased from Signosis (EA-0401, Sunnyvale, USA) was used to determine the EGF-linker activity as compared to unlinked EGF protein. The activity of the 5 & 18 nm AuNPs and 5 & 45 nm AgNPs fully-covered EGF-linker coated nanoparticles were tested. RayBiotech Technical Support stated that because there are wash steps, any EGF not bound to the capture antibody affixed to the well plate will be washed away and therefore the biotinylated detection antibody will only be able to access EGF bound to the capture antibody [77]. *Since they have not performed epitope mapping, it is not known exactly where on the EGF sequence the capture and biotinylated detection antibodies bind.* Also, as the kit has not been tested with nanoparticles, RayBiotech does not know exactly how nanoparticles would affect the assay.

ELISA well plates are coated with bound EGF antibodies. To this plate, protein samples diluted with the kit Assay Diluent B were added. The protein concentrations were 200, 80, 32, 12.8, 5.12, 2.05, and 0.82 pg/mL, with a 0 pg/mL blank of the Assay Diluent B. The Signosis ELISA kit protein concentrations were higher, they were 2000, 1000, 500, 250, 125, 62.5, and 31.25 pg/mL, with a 0 pg/mL blank of the 1X Diluent Buffer. Next, a series of reagents and antibodies were added stepwise to produce an enzyme-catalyzed colourimetric response (Figure 2.11). In particular, a biotinylated antibody was added which binds to any EGF bound to the well plate antibodies. Secondly, a Streptavidin-HRP (horseradish peroxidase) antibody was added; Streptavidin binds to Biotin on the biotinylated antibody while HRP will convert tetramethylbenzene (TMB) to provide the colourimetric response. Between each reagent addition, excess protein, antibodies, and substrate were removed with a series of wash steps. Next, TMB one-step substrate was added. Addition of 0.2 M sulfuric acid catalyzed the colour change from blue to yellow, which was observed through UV-Vis spectrophotometry.

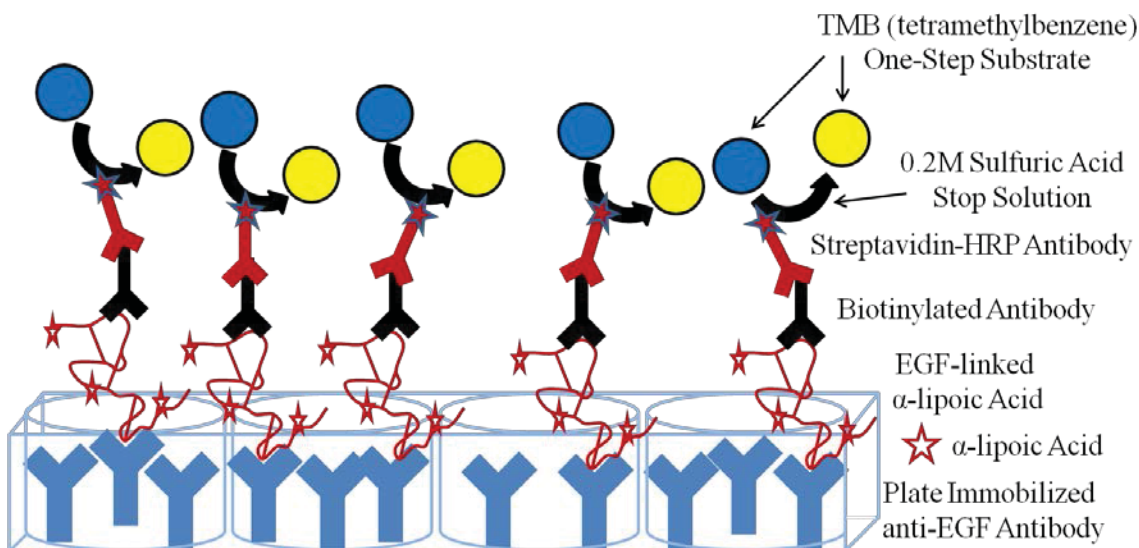


Figure 2.11 Enzyme-linked Immunosorbent Assay (ELISA) diagram.

The protein samples were added to the well plate coated with antibodies specific for EGF. Once attached, the excess protein was removed with a series of wash steps. Biotinylated antibody and then Streptavidin-HRP (horseradish peroxidase) were added to the wells stepwise, with wash steps in between to remove any residual antibodies. TMB one-step substrate was added to the sample wells, and the addition of 0.2 M sulfuric acid catalyzed the colour change from blue to yellow. The solutions were then measured with a UV-Vis at 450 nm.

We used the Nanodrop ND-1000 UV-Vis, read at 450 nm with a path length of 1 mm, to measure the absorbance of the ELISA solution colourimetric response. Additional details about the Nanodrop were presented in Section 2.3. Alternatively, an EMax microplate reader from Molecular Devices (path length = 1 cm, Sunnyvale, USA) was employed at the British Columbia Cancer Agency.

The ELISA response of the core-shell silver-gold nanoparticles synthesized by the Dalhousie Integrated Science Program (DISP) students, Joe Loung and Stefan Juckes, was measured with a SpectraMax Plus 384 microplate reader, also from Molecular Devices. Softmax pro software from Molecular Devices controlled the SpectraMax Plus 384 and automatically allowed the reader to shake the plate to mix the samples just prior to data collection. Louise Tunnah, from the lab of Dr. Thomas MacRae in Biology at Dalhousie University, helped us collect the DISP ELISA data.

Regardless of the measurement platform, each sample well from the test was measured in triplicate. The measurements were assessed with the Dixon's Q-test for outliers at the 95% confidence interval ($n=3$, $Q_{crit}=0.970$). All experimental values were below the critical Q value; none were rejected.

A Nanodrop UV-Vis or EMax microplate reader was used to perform the spectroscopic measurements on the ELISA plate. ELISA assesses the activity of proteins for a receptor through the use of an enzymatic assay. The next section discusses how the cancer cells were grown and prepared for imaging.

2.7 CELL CULTURE

We discuss the methods for cultivating EGFR over-expressing A431 cervical cancer cells (CRL-2592, American Type Culture Collection (ATCC), Manassas, USA), which were grown for the *in vitro* experiments.

The cell culturing protocols for starting and maintaining a cell culture, passing or subculturing cells, counting cells with a hemocytometer, and freezing cells are in Appendix A. The protocols were adapted from a work term report completed in August 2008. These protocols were obtained from the British Columbia Cancer Agency – Cancer Research Centre in Vancouver, BC (Soroush Merchant and Priscilla Fung in the lab of Dr. Mladen Korbelik).

Before using NPs with cells, the NPs should be sterile filtered. For sterilizing 1-20 mL nanoparticle volumes, Sterile Filters (0.22 μm pore, 10 mm diam., GVWP01300), Syringes (luer slip, 20 mL, XX1102012), and Swinnex Filter Holder (SX0001300), all from Millipore (Billerica, USA) are acceptable. Assemble the filters and filter holders before autoclaving and storing in a jar. In a biosafety cabinet, all necessary materials for the sterilization should be sprayed with 70% ethanol and moved into the hood. Fill a syringe with the nanoparticle solution to be filtered. Attach a sterile filter holder, containing a filter, to a syringe. Push the syringe plunger to filter the nanoparticle solution into a sterile, pre-labeled tube. The sample is now sterile. Repeat the filtering

process for all necessary samples. By accident, sterile filtering was not performed before the dark field microscope images were taken. ICP-MS NP samples were sterilized with 70% ethanol solutions, which likely caused problems for the protein linker activity. The Raman T64000 NP samples were sterilized with the filtering method prior to NP use.

A431 cells were incubated with 18 nm gold or 45 nm silver EGF-linker coated nanoparticles. To prepare the samples for imaging, about 500 000 cells were counted, dispensed, and allowed to attach to a glass bottom culture dish or a coverslip overnight. The cells were grown in MEM α cell culture medium (Minimal Essential Medium, 12571-063, Life Technologies/ Invitrogen, Grand Island, USA), which contained supplements of 10% FBS (Fetal Bovine Serum, F2442, Sigma-Aldrich, St. Louis, USA) and 1% PenStrep (penicillin streptomycin solution, 15140-122, Life Technologies/ Invitrogen, Grand Island, USA). Low passage number cells were used to ensure the cell properties were as expected [78] [79].

The next day, the cell medium was removed from each dish of cells, and the cells washed three times with sterile 50 mM HEPES (4-(2-Hydroxyethyl)piperazine-1-ethanesulfonic acid) buffer or MEM α medium. 100 μ L of 10.0 – 16.2 nmol fully covered EGF-linker coated active nanoparticles or α -lipoic acid coated positive control nanoparticles, as well as 500 μ L of sterile 50 mM HEPES buffer or MEM alpha medium, were added to a dish of cells. For negative control cells containing no nanoparticles, 500 μ L 50 mM HEPES buffer or MEM alpha medium were added to a Petri dish of cells. The nanoprobe solutions were pipetted out of the dishes, and the cells were washed two times with sterile 50 mM HEPES buffer or MEM alpha medium. The glass bottomed dishes of tagged cells were used as is, while the coverslips were transferred into glass bottomed dishes. In both cases, the dishes were filled with about 500 μ L of 50 mM HEPES buffer or MEM alpha medium for imaging.

Alternatively, if the cells were to be measured at Stanford University using the Renishaw Raman spectrometer (Section 2.9.4), the tagged cells were detached with trypsin just after tagging and frozen according to the protocol in Appendix A. The cells were shipped on dry ice to Stanford and unfrozen when ready for imaging. The cell

samples were not measured in glass bottomed dishes as described above, but the thawed cancer cell samples were transferred to centrifuge tubes and were spun at 600 rcf for 3 minutes to form a pellet of cells in the bottom of the tube. The cell samples were then ready for imaging. Some of the cells imaged at Dalhousie University also used this method, to obtain bulk measurement of the SERS activity of the nanoparticle tagged cells.

The protocol used to grow cells was presented above. The cells were used for *in vitro* dark field microscopy and Raman spectroscopy imaging, tagged with EGF-NPs or control NPs. The dark field microscope is discussed in the section which follows.

2.8 DARK FIELD MICROSCOPY

Imaging A431 cancer cells tagged with 18 nm gold or 45 nm silver, EGF-linker coated or control, nanoparticles was attempted with dark field microscopy. The samples were prepared for imaging using the protocol outlined in Section 2.7. A dark field microscope can be used to detect the light scattered by nanoparticles dispersed in the cells.

Dark field microscopy is the opposite of the brightfield technique, as samples appear bright while the field is darkened. The dark field setup consisted of an Olympus BH2-UMA inverted microscope outfitted with a dark field condenser and a Canon EOS Digital Rebel XSi 12.2 MP DSLR camera. A light source at the focus of a lens creates a collimated beam (Figure 2.12). A dark field patch stop blocks the centre of the light beam, allowing only a narrow ring of light to pass. The bright ring passes through the condenser and onto the sample. The large angle of the outer ring beam causes the objective aperture to block the direct beam. Light scattered from the sample impinges the microscope objective and forms an image. An image of the sample can be viewed with binoculars or photographed with a digital camera. Images were obtained with the 20X objective, and were captured 3-4 hours after the cells were finished incubating with the nanoprobles.

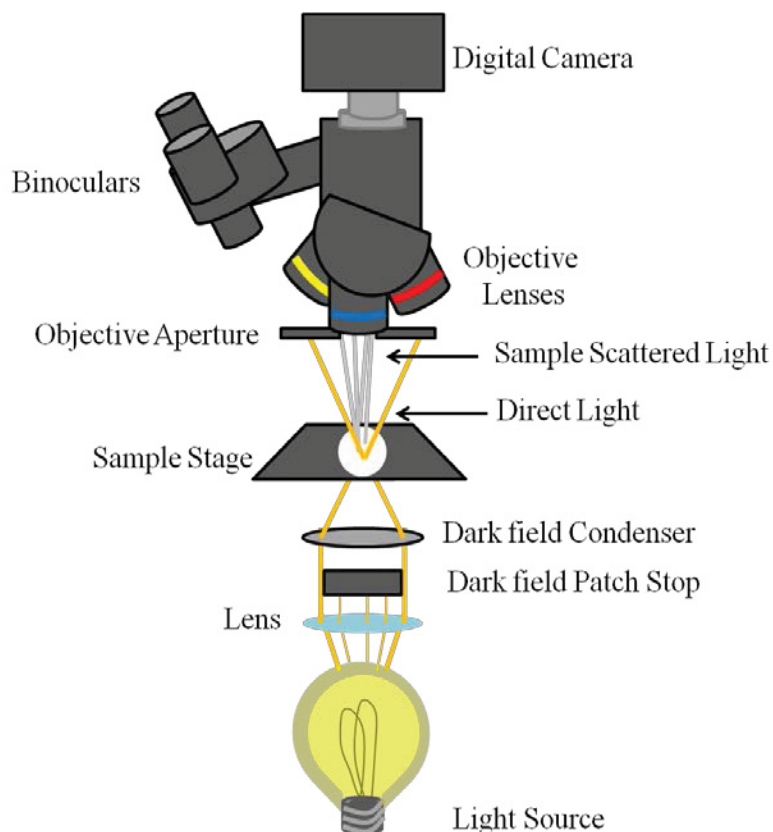


Figure 2.12 Dark field microscope diagram.

Light passes through a lens and onto the dark field patch stop, which blocks the interior of the light beam. The outer ring beam then shines through the condenser and onto the sample. Light scattered from the sample hits the microscope objective, while the objective aperture blocks the direct source light because of its extreme angle. The image formed from the sample scattered light then can be observed through binoculars or captured on a digital camera.

We have discussed how light scattered from a sample forms dark field microscopy images, which can be used to detect the light scattered from nanoparticles. The ultimate goal of our work is to use a spectroscopic technique, Raman spectroscopy, to detect the presence of the nanoparticles. Raman spectroscopy is therefore the subject of the next section.

2.9 RAMAN SPECTROSCOPY

In this section we discuss the theory behind Raman spectroscopy, introduce the T64000 Raman spectrometer at Dalhousie University, the Fibre Optic Raman system at BCCA Skin Care Centre, and the Renishaw Raman spectrometer at Stanford University. The latter was used for *ex vivo* Raman measurements of EGF-NPs injected *in vivo* through the tail vein of mice.

2.9.1. Classical Raman Theory

Raman spectroscopy, first discovered by Sir C. V. Raman in 1928, uses light scattering to gain molecular information from a sample by targeting differences in polarizability within the chemical structure. It is an inelastic light scattering technique where the incident laser light frequency and the scattered frequencies are different. Identical frequencies of both the incident and scattered light are Rayleigh scattering, or elastic light scattering.

In the classical theory of Raman scattering, the acceleration of electrons produces scattered radiation at characteristic frequencies from the interaction with atomic vibrations. The electrons accelerate by the force exerted by the electric field and the atomic vibrations modulate this interaction. Assume that light from a laser shines on a polarizable molecule at \mathbf{r} . The incident electric field, E , at \mathbf{r} is,

$$E = E_0 \cos(\omega_L t - \mathbf{k} \cdot \mathbf{r}), \quad (5)$$

with an angular frequency ω_L , wavevector \mathbf{k} , and amplitude E_0 . Atomic vibrations at a frequency, ω , will affect the polarizability of the molecule, α . To first order,

$$\alpha = \alpha_0 + \alpha_1 \cos(\omega t - \mathbf{q} \cdot \mathbf{r}) \quad (6)$$

represents the polarizability, where the static polarizability is α_0 and \mathbf{q} is the vibrational mode wavevector. Modification of the polarizability by the electric field produces an oscillating dipole moment, \mathbf{P} ,

$$\mathbf{P} = \alpha \mathbf{E}$$

$$P = E_0 \alpha_0 \cos(\omega_L t - \mathbf{k} \cdot \mathbf{r}) + E_0 \frac{\alpha_1}{2} \{ \cos[(\omega_L + \omega)t - (\mathbf{k} + \mathbf{q}) \cdot \mathbf{r}] + \cos[(\omega_L - \omega)t - (\mathbf{k} - \mathbf{q}) \cdot \mathbf{r}] \}. \quad (7)$$

The first term, $E_0 \alpha_0 \cos(\omega_L t - \mathbf{k} \cdot \mathbf{r})$, represents Rayleigh scattering. The second term, $E_0 \frac{\alpha_1}{2} \{ \cos[(\omega_L + \omega)t - (\mathbf{k} + \mathbf{q}) \cdot \mathbf{r}] + \cos[(\omega_L - \omega)t - (\mathbf{k} - \mathbf{q}) \cdot \mathbf{r}] \}$, is Raman scattering, where the light is emitted at a frequency that is shifted up ($\omega_L + \omega$) or down ($\omega_L - \omega$) by exactly the vibrational mode frequency. The up-shifted components are referred to as anti-Stokes and the down-shifted components Stokes scattering. The classical theory predicts that both components are equally favoured. However, in practice the Stokes components dominate because of quantum mechanical effects.

In a quantum mechanical interpretation, Stokes scattering occurs when the sample is in the ground state, excites to a higher virtual state, and then loses some – but not all – of the energy ($\hbar\omega$) and momentum ($\hbar\mathbf{q}$) to be left in a vibrational state above the ground state. This results in a shift to lower frequencies, or longer wavelengths, as compared to the incident light. In anti-Stokes scattering, the sample starts in an excited state, populated by thermal excitations. The sample gains energy to rise to a higher energy virtual intermediate state, and then loses more energy ($\hbar\omega$) and momentum ($\hbar\mathbf{q}$) than that which it gained to be left in the ground state. The frequency, $\omega_{AS} = \omega_L + \omega$, and momentum, $\mathbf{k}_{AS} = \mathbf{k} + \mathbf{q}$, of the scattered light increase in the anti-Stokes scattering process. It is exponentially more likely that the system is found in the ground state than an excited state. By Boltzmann statistics, Stokes scattering dominates at room temperature.

The Raman scattering power depends on several properties of the radiation field and medium but three quantities are of significant import, the intensity of the incident laser light, the number of molecules contained in the sample volume under study, as well

as the specific polarizability of each molecule, which relates to the Raman cross section [3].

2.9.2. T64000 Raman Spectrometer

The Raman system was used to measure reference spectra of potential markers which could be found near the nanoparticles and in the cells, as well as measurements of the nanoparticle solutions and maps of cells tagged with nanoparticles. Mapping of the EGFR receptors across a few cells could occur using a high magnification objective, or measurements of many cells with a low magnification objective would give bulk cell responses.

Located at Dalhousie University, Figure 2.13 shows a diagram of the T64000 Raman system configuration when using the single grating mode. A JDS Uniphase 632.8 nm HeNe laser with a power of 2.5 mW measured the samples. The laser shone through an interference filter, a mirror, and a 50X long working-distance (LWD) or a 100X objective lens and onto the sample. Bulk solutions and cell pellets were measured by focusing the laser just above the sample surface and performing manual spectral acquisitions, while individual cells were imaged with maps. The mapping scheme allowed up to 0.3 μm by 0.3 μm resolution, although 1.0 μm by 1.0 μm resolution was mainly used, as the sample stage moved across the x and y directions of the sample. Typically, two spectral acquisitions of 1 second each were performed at each point to account for cosmic rays. For individual spectrum collection, the acquisition times were often adjusted and increased to give more intense Raman spectral features. The Raman scattered light was collected by the objective, filtered, and separated into its component wavelengths by a grating. The separated wavelengths then shone on the detector.

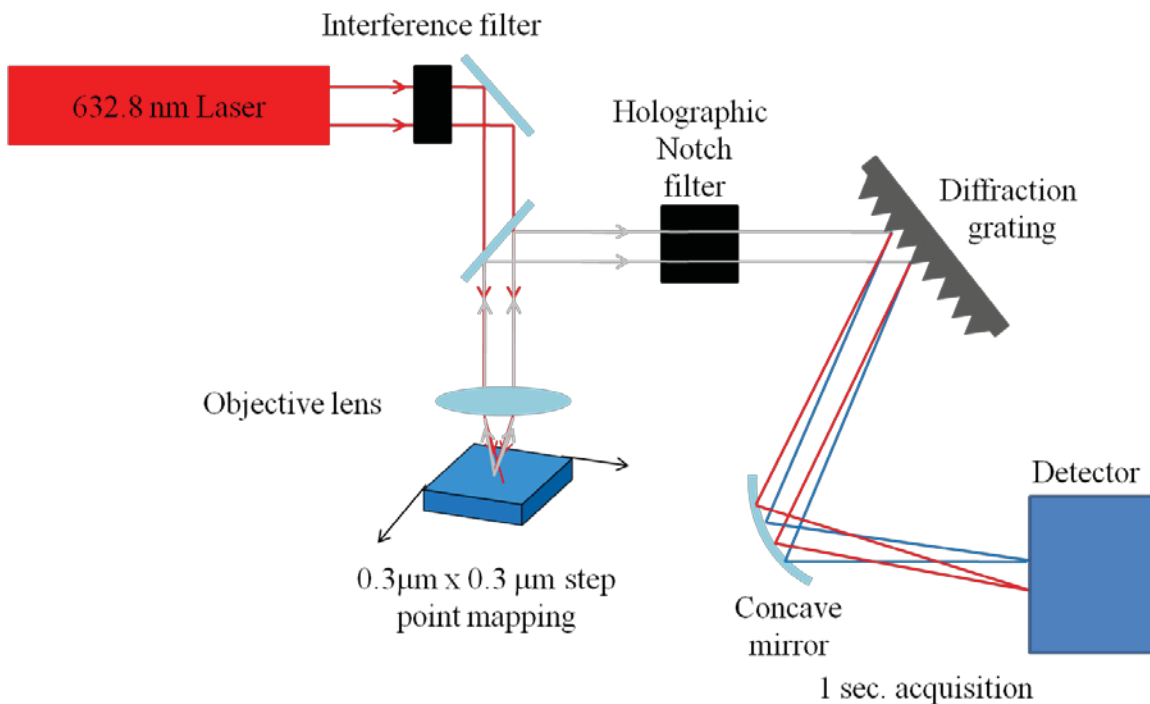


Figure 2.13 T64000 Raman spectrometer diagram.

The 633 nm laser light (2.5 mW power) shone through an interference filter, a 50X long working-distance (LWD) or 100X objective lens, and onto the sample. The stage can move in the x and y directions to map samples. The scattered light was collected by the objective, passed through a holographic notch filter, and bounced off of a diffraction grating. The grating separated the scattered light into the component wavelengths for detection.

Post-processing of the Raman data involved background subtraction of any fluorescence signals from single text files using a program called Vancouver Raman Algorithm, which we obtained from our colleague Haishan Zeng at the BC Cancer Agency [80] [81].

2.9.3. High-Frequency Range Fibre Optic Raman Spectrometer

SERS of mice was performed prior to analysis of the tissues by ICP-MS, as outlined in Section 2.10. *Ex vivo* Raman measurements were performed on the liver, kidney, and spleen tissues extracted from mice, which had been given *in vivo* injections of EGF-NPs or control NP solutions through the tail vein.

The tissues imaging took place with a high-frequency range fibre optic Raman system at the British Columbia Cancer Agency Research Centre. Wei Zhang explained the instrumentation and how to best perform the measurements. The general instrument setup was similar to that outlined in Figure 2.13, except the laser light was delivered through an endoscopic probe. The tissues were placed on aluminum foil, covered with a thin layer of plastic wrap to prevent any transfer onto the probe tip, and imaged with the fibre optic Raman system. The 785 nm laser line at a power of 130 mW was used, with a focal length of 9 mm. Three scans were averaged at an integration time of 0.1-1 seconds, depending on the fluorescence of the sample. Darker samples, like the spleen and especially the liver, fluoresced more. Tissue samples were kept on ice during imaging. As with the Raman data collected with the T64000 setup in Section 2.9.2, post-processing included the background subtraction of any fluorescence signals from the individual text files. The subtractions were performed with the Vancouver Raman Algorithm program [80] [81].

2.9.4. Renishaw Raman Spectrometer

A Renishaw Raman spectrometer at Stanford University was used to measure individual spectra of both nanoparticle solutions and cells tagged with nanoparticles. It functions much like the T64000 system, described in Section 2.9.2. A low magnification objective allowed for bulk cancer cell measurements to compare the SERS activity of pellets of cells previously treated with nanoparticles bearing the EGF protein (specific), or not as in the case of a non-specific probe. The Renishaw system used a 785 nm laser excitation.

The Renishaw Raman system was located in the lab of Dr. Sanjiv Gambhir. Measurements were performed with the help of Dr. Adam Cole or Dr. Jesse Jokerst. The instrumentation is similar to Figure 2.13, although this system has the option of using dual lasers for measurements. The laser shone through a 12X Raman optimized objective lens and onto the sample. 20 μ L of the cell pellet, formed as described in Section 2.7, was then pipetted onto a quartz coverslip, and the laser spot was focused on the cell droplet.

The stage can move in the x and y directions to form maps, this feature was not used. The data from the Raman measurements of cell pellets was not post-processed.

We discussed Raman spectroscopy theory and instrumentation, and its use to measure spectra of interest in solution, cells, and tissues. Next we introduce inductively coupled plasma – mass spectrometry for quantification of elemental metals, specifically gold and silver.

2.10 INDUCTIVELY COUPLED PLASMA – MASS SPECTROMETRY (ICP-MS)

ICP-MS was used to assess the biodistribution and toxicity of the EGF-linker coated 5 and 18 nm gold and 5 and 45 nm silver nanoparticles in mouse models. We studied three aspects of nanoprobe use with specific mouse organs to analyze where the nanoparticles travel, whether the particles seem to get stuck or cause an immune response, and to observe whether the mice seem ill following nanoparticle injection.

The EGF-linker/ α -lipoic acid coated nanoparticles were synthesized, as described in the forthcoming Approaches and Results section, to give a concentration of 9.94 nm² of nanoparticle surface area per EGF for near complete coverage. Any gaps on the protein were filled in with the α -lipoic acid [53]. The coated nanoparticles were purified using a three step method. These nanoparticles were not sterilized using filters, as outlined in Section 2.7. First, the samples were concentrated and the supernatant containing water was removed. Next, ethanol was added to the coated nanoparticles to make up a 70% solution. The nanoparticles then sat for 30 minutes to allow the sterilization to complete. The nanoparticles were centrifuged again to concentrate the particles and allow for the removal of the 70% ethanol. Third, the ethanol supernatant was exchanged for a 0.9% sterile saline solution in a biosafety cabinet. Note that at each of the three purification steps, the nanoparticle recovery was maximized and excess EGF-linker and α -lipoic acid removed by centrifuging the supernatant according to the method of S. Balasubramanian et al. (2010) [76]. The 18 nm gold nanoparticles were centrifuged at 7000 rcf, 45 nm silver at 5000 rcf, 5 nm silver at 10000 rcf, and the 5 nm gold at 14000

ref. The nanoparticles were centrifuged twice at each step for 20 minutes at 21°C. Specifically, the samples were centrifuged once to pellet, the supernatant was then spun to recover any additional nanoparticles, and the pellets of both spins were combined and diluted to 1 mL with the appropriate solvent. In a biosafety cabinet, the nanoparticles were diluted with the sterile saline solution to the desired concentration for injection.

Nine mice were tested in a preliminary study of the nanoparticles; 8 experimental and one control mouse. Figure 2.14 outlines the preparation protocol for ICP-MS. 90 µL of sterile coated nanoparticles or saline solution were injected into the tail vein of the mice. The injected nanoparticles contained 1000 pmoles of metal (gold or silver). The injection concentration was determined from P. Digaradjane et al. (2008) and X. Qian et al. (2008) [48] [9]. 24 hours later, the mice were sacrificed humanely with CO₂ gas. The required organs: liver, kidney, and spleen, were obtained and stored at 4°C in sterile 0.9% saline solution until use. It is at this point that the organs were measured with the fibre optic Raman instrument at the British Columbia Cancer Agency Research Centre outlined in Section 2.9.3.

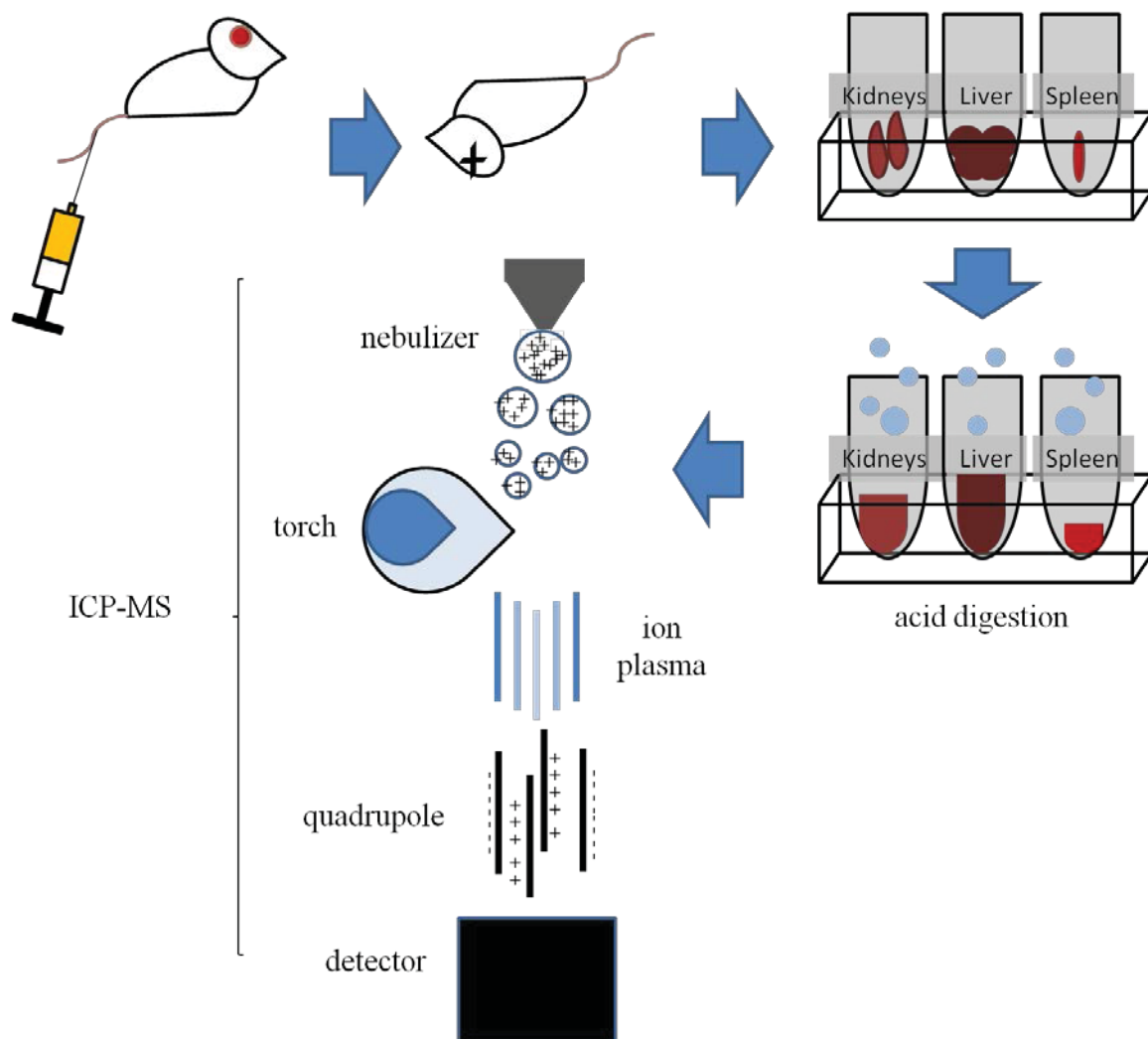


Figure 2.14 Tissue preparation for ICP-MS analysis.

The protocol involved 1) injection of gold or silver nanoparticles with α -lipoic acid or α -lipoic acid/EGF-linker coating, or sterile saline control, 2) humanely sacrificing the mice with CO_2 gas 24 hours after injection, 3) removing the organs of interest, the kidneys, liver, and spleen, from the mice for study, 4) Raman analysis of the intact organs, and then homogenization of the organs, 5) homogenization was carried out prior to acid digestion for subsequent ICP-MS analysis.

Next, the samples were then homogenized. In a fume hood, each sample was broken up using a homogenizer by two-15 second bursts separated by a 5 second pause to prevent overheating. More bursts were used for larger samples. The homogenizer was cleaned between samples to prevent cross contamination by dipping the moving blades in

distilled water and then dabbing the stationary blades with a kimwipe, ensuring the kimwipe did not get stuck in the blades. The samples were weighed, and stored at -20°C .

Digestion of the tissues was necessary before ICP-MS analysis. The Minerals Engineering Centre at Dalhousie University performed the aqua regia digestion. 30 mL of concentrated nitric acid and then 10 mL of concentrated hydrochloric acid was added to each of the homogenized organ samples, and heating overnight in a fume hood. The nitric acid was added first and mixed briefly to prevent precipitation of insoluble AgCl_2 from the samples which contained silver nanoparticles. The samples were filtered to remove any undigested material and diluted to 10 mL.

ICP-MS was performed at the Centre for Water Resource Studies at Dalhousie University. The detection limits were 0.100 ppb for gold and 0.200 ppb for silver. Figure 2.15 outlines a diagram of the ICP-MS instrumentation. The liquid sample entered the nebulizer and was aerosolized. The torch is composed of three nested tubes, and radio frequency coils at one end of the torch provide power. Argon gas flowed around the inner walls of the outer two torch tubes, and a radio frequency field heated the gas to form plasma composed of Ar^+ ions and electrons. As the sample entered the torch, it was first dried to form a gas, atomized, and then ionized by the plasma. The ionic plasma of atoms and electrons then moves to the mass spectrometer, where the elements were separated by mass and gold and silver were detected.

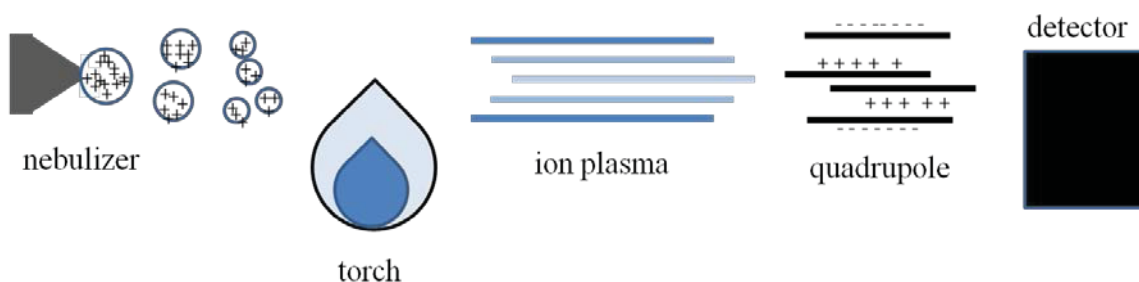


Figure 2.15 Inductively Coupled Plasma – mass spectrometer (ICP-MS) diagram.

The sample sprays into the ICP-MS through a nebulizer. Argon gas flows around the inner walls of the two outer torch layers. The radio frequency coils cause a field to heat the argon gas, to form a plasma of Ar^+ ions and electrons. The sample enters the inner torch tube and collides with the plasma, first reducing the sample to atoms, and then positively ionizing those atoms. The ion plasma then moves into a quadrupole to separate the ions by mass. The ions are detected, and we measure the elemental gold and silver.

We discussed how mice were injected with EGF containing gold and silver nanoparticles for analysis with Raman spectroscopy. We also introduced inductively coupled plasma – mass spectrometry for the quantification of atomic gold and silver present in the liver, kidneys, and spleen of the mice. The next section summarizes the entire Methods chapter.

2.11 SUMMARY OF METHODS

Many techniques were utilized to assess the formation and functionality of a new nanoprobe consisting of EGF protein bioconjugated to gold and silver nanoparticles via α -lipoic acid. They are: TOF-MS, In-Solution Tryptic Digestion, HPLC, LTQ-MS, TEM, UV-Vis, zeta potential, ELISA of the protein-linker or tagged nanoparticles, dark field microscopy of nanoparticle tagged A431 cells, Raman spectroscopy and SERS of nanoparticles or of cells, ICP-MS of tissue samples, and nanoparticle stability in saline solution. The next chapter presents the results of these tests, in addition to explaining the EGF-linker synthesis protocol.

CHAPTER 3: APPROACHES AND RESULTS

The new methods developed for preparation and creation of the EGF-linker and EGF-linker coated gold and silver nanoparticles, in addition to data collected from the characterization tests, will be presented in this chapter. It is the subject of a patent application and is being considered for inclusion in the catalogue of:

DVS Sciences Inc.
70 Esna Park Drive, Unit 12
Markham, ON, CANADA L3R 6E7
+1 (905) 513-1704

3.1 EGF-LINKER FORMATION THROUGH CARBODIIMIDE CHEMISTRY

Proteins are composed of amino acids, linked together in a chain by amide bonds. Amide bonds form between a primary amine on one amino acid and a carboxylic acid on another, where these reactive groups form the backbone of the amino acids and not the side chain groups. Protein production in cells uses enzymes to reduce the activation energy barrier and form amide bonds. One synthetic method of formation of these bonds involves the introduction of heat, which would cook the proteins. In the formation and amide bond between α -lipoic acid and EGF, we instead use reaction chemistry involving a carbodiimide. This carbodiimide first converts the carboxylic acid to an active ester, and then addition of the protein containing the amine allows the reaction to occur. We discuss these reactions in more detail later in this section.

EGF protein has three potential sites for the reaction of carboxylic acid with amine groups for carbodiimide mediated amide bond formation: one of two lysine (K) amino acids or the amino terminus (Figure 3.1). These amino acids contain a primary amine on their side chain, which can be modified through an amide bond formation reaction if the site is sterically accessible. For reference, see V. Besada et al. (1990) for the structure of EGF [82]. Overall, we wish to perform the following reaction to form the EGF-linker (Equation 8).

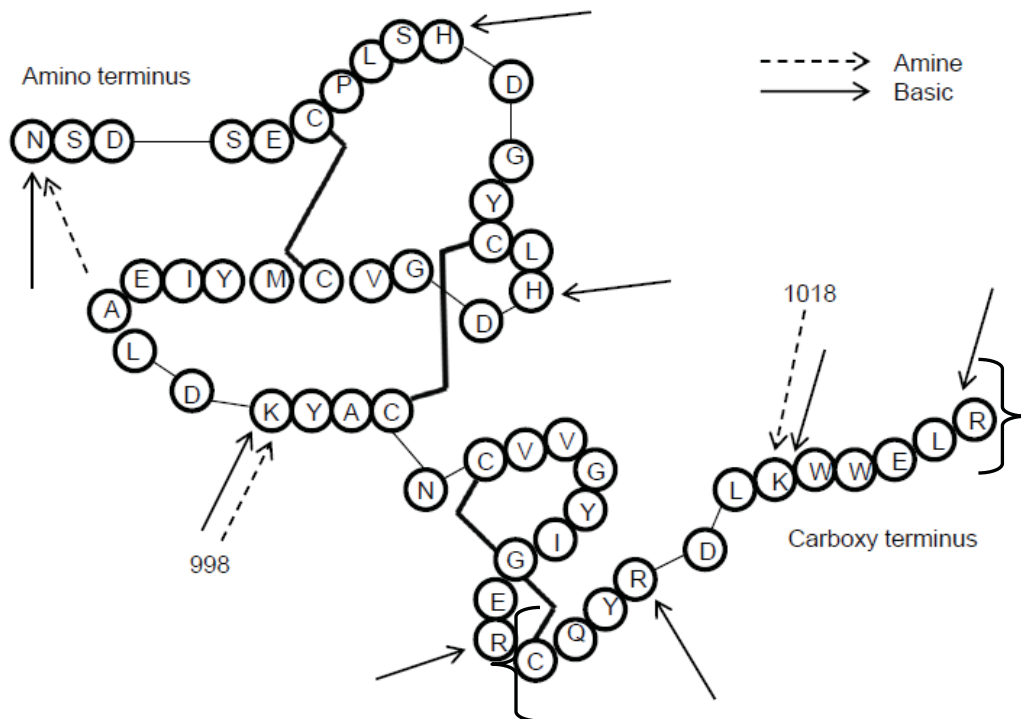
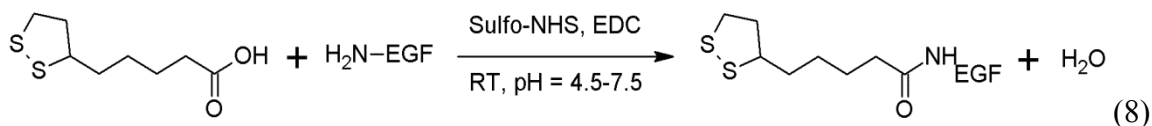


Figure 3.1 Amine groups (dashed arrows) on Human EGF protein.

Linker addition can occur at one of 2 lysine (K) sites or the amino terminus. Of the 8 basic amino acids (solid arrows), the ionizable proton sites are: the amino terminus, lysine (K), arginine (R), and histidine (H). The brackets at the carboxy terminus show the sequence matched to the Sequest program in Section 3.2.3 from the LTQ-MS data.



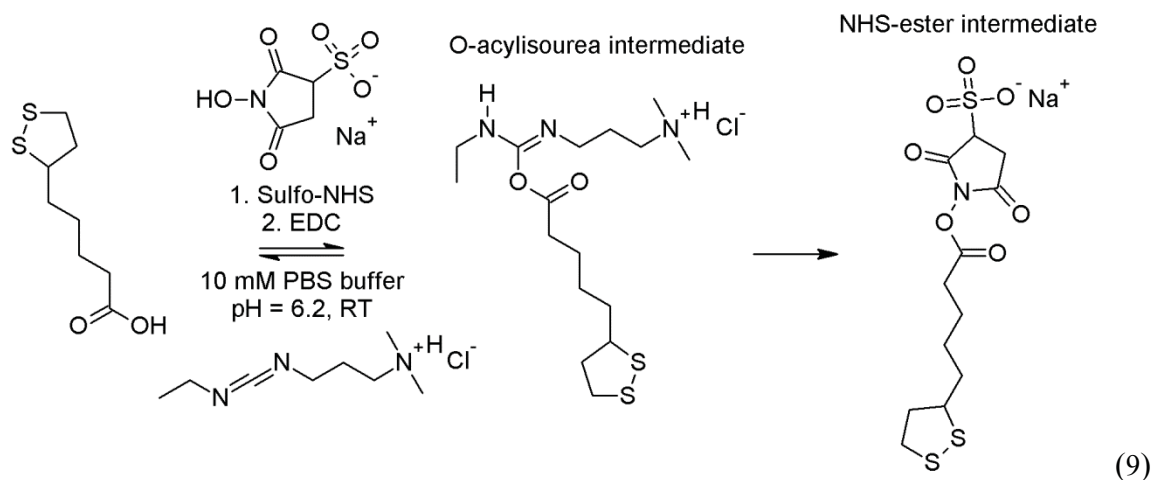
We activate α -lipoic acid (206 g/mol), add it to the protein, and lose water to form the new protein complex. EDC stands for 1-ethyl-3-[3-dimethylaminopropyl] carbodiimide which, in the presence of carboxylic acid ($\text{R-C}(=\text{O})\text{OH}$, R = alkyl chain) and primary amine (R-NH_2 , R = alkyl chain) groups, forms amide bonds at lower temperatures than usual (room temperature versus 100°C). Carbodiimides have the chemical structure $\text{R-N}=\text{C}=\text{N-R}$ (R = alkyl chain). This decreased reaction temperature is necessary to avoid deactivation and cooking the protein. Sulfo-NHS (N-hydroxysulfosuccinimide) increases

the rate and yield of reactions with carbodiimides by forming a more stable reactive ester (R-C(=O)O-R, R = alkyl chain) intermediate [83] [84].

The α -lipoic acid (T5625), EDC (03450), pH 7.4 10 mM PBS buffer (P3813), and HEPES salt (H3375), were obtained from Sigma-Aldrich (St. Louis, USA). Sulfo-NHS (24510) was purchased from Thermo Fisher Scientific (Waltham, USA), EGF (PHG0313) from Life Technologies/ Invitrogen (Grand Island, USA), methanol (A452-4) from Fisher Scientific (Ottawa, Canada), and sodium hydroxide (S-3700) and concentrated hydrochloric acid (H-6100) from ACP (Montreal, Canada). The Amicon filters (UFC500324) were obtained from Millipore (Billerica, USA). Sulfo-NHS and EDC were weighed in a glove box as they react with moisture. They were stored at the suggested temperatures, 4°C for Sulfo-NHS and -20°C for EDC, and later plastic containers partially filled with desiccant were added to reduce moisture exposure. The sodium hydroxide and hydrochloric acid were used to adjust the pH of the HEPES and PBS buffer solutions.

The reaction is a two-step process of linker activation followed by amide bond formation. The molar ratios of reactants are 120 α -lipoic acid : 3200 sulfo-NHS : 1300 EDC : 1 EGF. We obtain the appropriate molar ratios by using the following volumes and concentrations: 50 μ L of 1.6 mg/mL α -lipoic acid (0.08 mg) : 55 μ L of 40.7 mg/mL sulfo-NHS (2.24 mg) : 50 μ L of 16 mg/mL EDC (0.80 mg) : 200 μ L of 0.1 mg/mL EGF (0.02 mg). α -lipoic acid is not directly soluble in water. Consequently a stock solution of α -lipoic acid in equal volumes of methanol and 10 mM PBS (pH 6.2) ensures dissolution. The other two reactants in the first step, EDC and sulfo-NHS, were diluted in 10 mM PBS (pH 6.2). The EGF protein aliquots were made up and stored frozen until use in pH 7.4, 50 mM HEPES buffer.

We describe the linker activation step below (Equation 9).



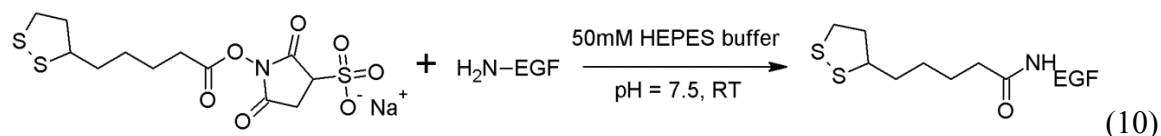
α -lipoic acid reacts with EDC to form the short lived O-acylisourea intermediate, which only lasts for a fraction of a second in solution. If the O-acylisourea intermediate is hydrolyzed, the α -lipoic acid reverts back to its original form, while EDC is used up, as the carbodiimide is converted to a urea group (C(=O)(NHR)₂, R=alkyl chain). The sulfo-NHS interacts with the intermediate and displaces the carbodiimide, giving a more stable ester intermediate. The NHS-ester has a half life of approximately 4 to 5 hours at pH 7, and 10 minutes at pH 8.6 [82] [83].

All of the reagents used in the first step were made up in the pH 6.2 PBS buffer to try and obtain better conversion of the carboxylic acid on α -lipoic acid to the activated NHS-ester. There are a range of pH values which are acceptable for the first step, from pH 4-6.5 or 7. The papers by V. Besada et al. (1990) and J. V. Staros et al. (1986), as well as the Pierce/Thermo Scientific product datasheets on EDC and sulfo-NHS, give more information [82] [83]. Lower pH is better for the first step (eg. 4-5), but PBS is limited in its buffering range down to about pH 6. We could not use a different buffer (eg. imidazole buffer) for this first step because it had an imidazole group which seemed to take part in the reaction with α -lipoic acid. Refer to Section 3.2.1 for a TOF-MS spectrum of the first α -lipoic acid to EGF addition attempt with imidazole buffer. If a different buffer with a lower pH was used for the first step, it could not contain any primary amine or carboxylic acid groups.

We experimented with a variety of reaction times (15, 30, 45, or 60 minutes) to maximize yield of the product. 30 minutes is optimum for the first step. The order of

addition of the reactants to the solution is important, as the EDC half-life is so short. α -lipoic acid and sulfo-NHS were mixed in the appropriate stoichiometric ratios, and then we add EDC in 10 mM PBS (pH 6.2) buffer. This order of reactant addition ensures that sulfo-NHS is present when the short-lived O-acylisourea intermediate forms.

In the amide bond formation step, where the EGF-linker forms, the following reaction occurs (Equation 10).



The nitrogen from the amine group on EGF attacks the carbonyl group of the NHS-ester intermediate to form the amide bond between α -lipoic acid and EGF, sulfo-NHS acts as a catalyst and regenerates. In particular, 155 μ L of NHS-ester intermediate from the first step adds to 200 μ L of 0.1 mg/mL of EGF protein, the 50 mM HEPES buffer (pH 7.4) raises the pH, and the reaction proceeds at room temperature. Occasional mixing of the solutions occurs at both steps to reduce diffusion limiting effects. After reacting for 2 hours, 7.5 μ L of 0.1 M NaOH raises the pH of the solution above pH 9, and the solution is left for 30 minutes. NaOH regenerates the carboxylic acid groups on α -lipoic acid from any NHS-ester intermediates that did not react with EGF. EGF self additions and multiple α -lipoic acid additions are limited through control of the reaction pH, time, and the order of reactant addition.

We purify the reaction mixture with Amicon 3 kDa MWCO centrifugal filters to remove reaction byproducts, unreacted α -lipoic acid, and buffers. The protein purity can be assessed with UV-Visible spectrophotometry or time-of-flight – mass spectrometry. 137.5 μ L deionized water increases the solution volume to 500 μ L. We centrifuge the solution 6 times at 14000 rcf for 30 minute intervals at a temperature of 21°C. Five washes of 18.2 M Ω cm deionized distilled water removes contaminants. The solution volume adjusts to give a final concentration identical to that at the start, 0.02 mg in 200 μ L or 0.1 mg/mL EGF-linker. The type of diluent depended on the intended use of the protein, characterization with TOF-MS or use with nanoparticles. The protein recovered

from the filter was split into equal volumes, one half was diluted with deionized water for use with TOF-MS, while the other half was diluted with 50 mM HEPES buffer (pH 7.4) prior to addition to nanoparticles. If splitting the recovered protein, the final volumes were halved to retain the same starting concentration, to give 0.01 mg in 100 μ L or 0.1 mg/mL EGF-linker. We submit the purified solution for ESI-TOF mass spectrometry analysis or dilute for use.

Any mouse EGF used in the experiments was from Invitrogen (PMG8041, Life Technologies/ Invitrogen, Grand Island, USA) [23]. Attempts to form α -lipoic acid conjugated mouse EGF were performed using the same techniques as above with the Human EGF. The molar ratios of reactants are 120 α -lipoic acid : 3200 sulfo-NHS : 1300 EDC : 1 EGF, and the reagent volumes are identical to those above. The reaction times used are 30 and 120 minutes at steps 1 and 2, respectively. As noted in Section 1.2, α -lipoic acid can only bind to the amino terminal amine, as both lysines are not present in mouse EGF. The synthesized α -lipoic acid bound to mouse EGF samples were characterized with TOF-MS in Section 3.2.1.

We modified Human EGF protein by a carbodiimide reaction, to form an amide bond between an amine side chain on EGF and the carboxylic acid group of the linking molecule, α -lipoic acid. In the next section, we characterize the α -lipoic acid conjugated Human and mouse EGF.

3.2 EGF-LINKER CHARACTERIZATION

We present the Time-of-Flight – mass spectrometry analysis of the intact EGF-linker protein in this section. We also present enzyme-linked immunosorbent assay (ELISA) data for the EGF-linker proteins. ELISA of EGF-linker proteins affixed to gold and silver nanoparticles are in a future section, Section 3.5.5. We display the Linear Ion Trap – mass spectrometry results from the EGF-linker sample cleaved into peptides by trypsin.

3.2.1 Time-of-Flight – Mass Spectrometry (TOF-MS)

Time-of-Flight – mass spectrometry was used to confirm whether α -lipoic acid had been successfully attached to EGF. TOF-MS was only able to identify whether attachment had occurred, not which site α -lipoic acid occupied. Identification of the α -lipoic acid attachment site was attempted with linear ion trap – mass spectrometry (LTQ-MS) in Section 3.2.3.

Figure 3.2 is a plot of the mass to charge ratio versus intensity following injection of pure EGF protein into the TOF-MS. A singly charged EGF protein should exhibit a peak at $m/z = 6200$. However, peaks appear at $m/z = 1245.0$ and $m/z = 1037.7$. These peak positions can be reconciled with EGF protein carrying charges of +5 and +6, respectively. More precisely, the expected peak positions are: $m/z = 1244.1$ (+5) and $m/z = 1036.9$ (+6). Charging is due to the abundance of ionizable protons which make up the protein, and there are several present on EGF. The eight amino acids present in EGF which could be ionized are: the amino terminus, two each of lysine (K) and histidine (H), and three arginines (R) (Figure 3.1). All our TOF-MS spectra show peaks due to +5 and +6 charges. The reason for the relative abundance of each is unknown at present. Lack of production of the protein at charge states which are not observed, like the +8 charge, could be due to the inaccessibility of internal amino acids from the way EGF folds; especially when forming gas phased ions with ESI. Note also, smaller intensity satellite peaks appear adjacent to the main peaks at larger values of m/z . These are due to heavier isotopes of the protein. The actual and predicted m/z peak values for EGF are within 1 m/z unit. Due to the high resolution of the TOF-MS, as discussed in Section 2.4.1, one would expect the values to be within 0.006 m/z units. As the actual values for EGF, and all subsequent EGF-linker values discussed later in the chapter, were lower than the predicted m/z values by about 1 m/z unit, the discrepancy must be some unknown or unrealized systematic uncertainty or calculation error.

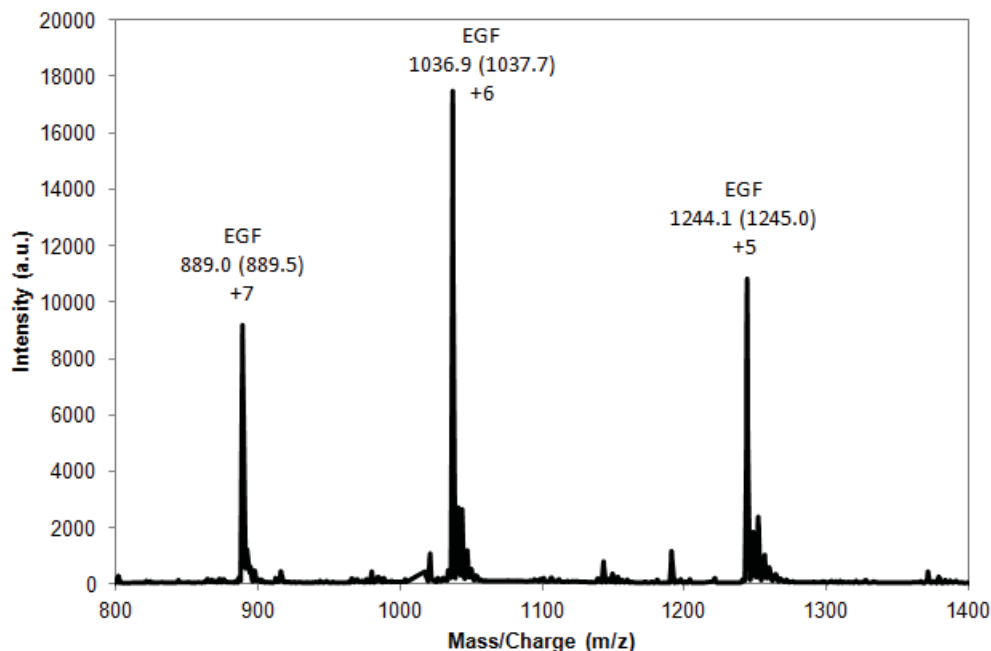


Figure 3.2 TOF-MS of Human EGF protein.

The EGF protein peaks for +5 and +6 charges appear at $m/z = 1244.1$ and $m/z = 1036.9$, respectively. These peaks are close to the predicted values of $m/z = 1245.0$ (+5) and $m/z = 1037.7$ (+6).

When imidazole buffer was used instead of 10 mM PBS buffer in early attempts, no addition of α -lipoic acid to EGF was observed in the TOF-MS characterization (Figure 3.3). We expect spectra that have at least some α -lipoic acid addition to look like the spectrum in Figure 3.4. The EDC had been recently purchased, as these were some of the first cross-linking experiments attempted. Sulfo-NHS was not used during the early reactions, it was purchased later to increase the experimental yields. Therefore, degradation of these reagents was not a concern. If the imidazole group took part in the reaction, as it was a buffer it was in abundance and would outnumber the α -lipoic acid molecules present. In this case, it would be unlikely that α -lipoic acid would be converted to the activated ester group.

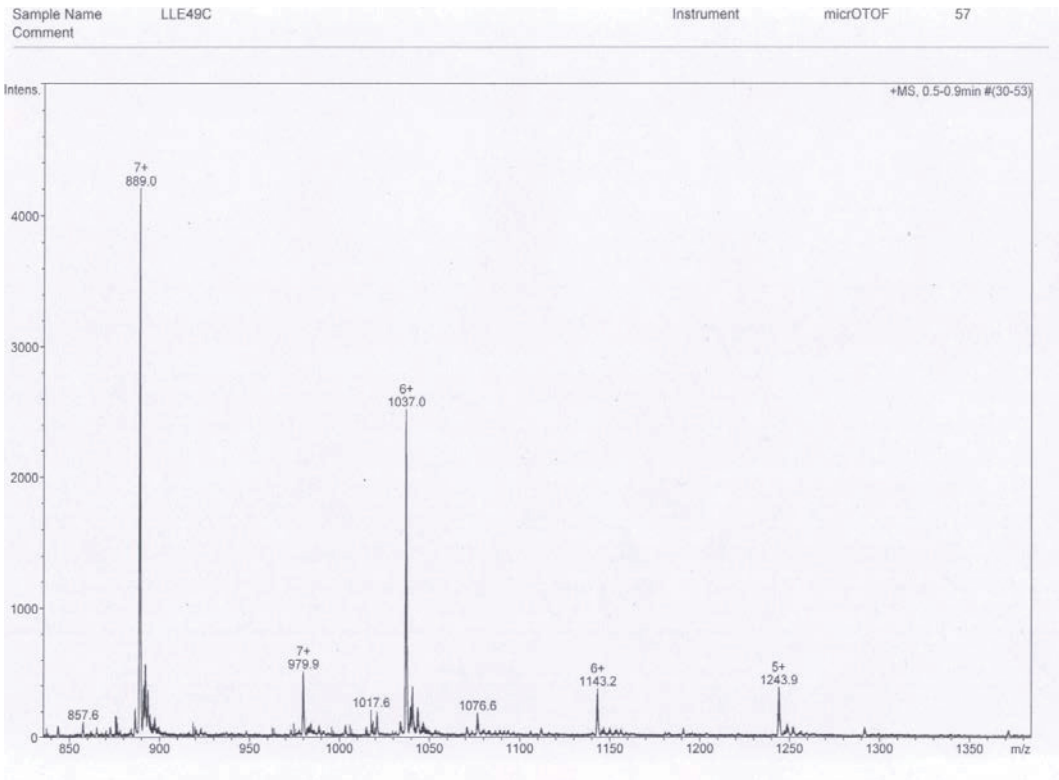


Figure 3.3 TOF-MS of Human EGF-linker protein sample LLE49C.

EGF-linker peaks were not observed during early attempts, indicating the α -lipoic acid attachment was unsuccessful. Imidazole buffer could have interfered with EDC, preventing transformation of α -lipoic acid to an ester.

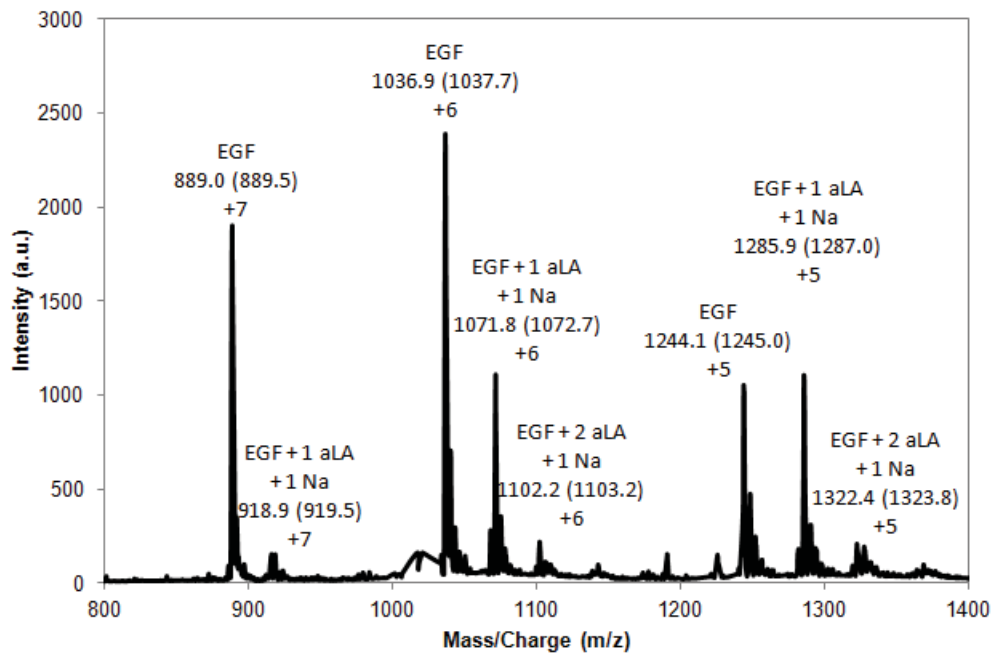


Figure 3.4 TOF-MS of Human EGF-linker sample LLE118A-3.

The purified reaction solution (Equation 8) contains both EGF-linker and EGF. The peaks for EGF with single linker attachment are at $m/z = 1285.9$ (+5) and $m/z = 1071.8$ (+6). Additional weak peaks correspond to EGF with two linkers at $m/z = 1322.4$ (+5) and $m/z = 1102.2$ (+6). All peak positions are similar to expected values. Not all EGF is converted to EGF-linker, the yield with one linker is $\leq 50\%$.

The molecular weight of α -lipoic acid is 206 Daltons. Its addition to EGF should produce peaks at $m/z = 1282.6$ (+5) and $m/z = 1069.0$ (+6), whereas the peaks are at slightly offset values of $m/z = 1285.9$ and $m/z = 1071.8$ (Figure 3.4). The replacement of a hydrogen atom by sodium accounts for this small discrepancy and is a consequence of the use of NaOH in the final quenching step of the EGF-linker formation reaction. The corresponding peak positions with sodium salts should appear at $m/z = 1287.0$ (+5) and $m/z = 1072.7$ (+6), which is close to those we observe, the values remain within 1 m/z unit. We also note very weak peaks near $m/z = 1320$ (+5) and $m/z = 1100$ (+6), from the addition of two α -lipoic acid linker molecules to EGF. Based on the +5 charge peaks we obtain a singly linked EGF yield of at most 50% with a very minor contribution from the doubly linked EGF. The data in Figure 3.4 is of sample LLE118A-3, but the m/z peak positions are representative of all EGF-linker samples.

Table 3.1 lists the relative ratio of linked vs. unlinked EGF peaks for all TOF-MS characterizations of Human EGF-linker. Two average (mean) ratios of the peak heights were calculated between the linked-EGF and unlinked-EGF m/z values, expressed in percentages. R1 was the ratio at peaks with m/z values of 1071.6 (1068.3-1072.0) m/z / 1036.9 (1036.8-1037.1) m/z and R2 was the ratio at 1285.7 (1281.7-1286.3) m/z / 1244.1 (1243.8-1244.3) m/z , while the numbers in brackets were the m/z range. The largest yield of linked-EGF was from LLE118A-3, while samples LLE118A-1 and LLE134A-1 were deemed sufficient for use with nanoparticles, and are denoted with an asterisk (*). Sample LLF23A-2 also gave great yields, but was not used as the spectral intensities did not seem consistent with other TOF-MS spectra, or other spectra collected from samples synthesized at the same time (Figure 3.5). Although, this reduced signal intensity could be due to the conversion of EGF to EGF-linker.

Table 3.1 Human EGF to Human EGF-linker peak ratios from TOF-MS.
R1 = 1071.6 (1068.3-1072.0) m/z / 1036.9 (1036.8-1037.1) m/z, R2 = 1285.7 (1281.7-1286.3) m/z / 1244.1 (1243.8-1244.3) m/z, where R is the ratio between the mean linked-EGF and unlinked-EGF m/z values, and the numbers in brackets are the range. The reaction time (RxnT) at the 2nd step was 120 minutes for all samples.

Sample ID	Date Made	Molar Ratios				RxnT at 1 st Step (min.)	R1 (%)	R2 (%)
		α -lipo :	Sulfo- NHS :	EDC :	EGF			
LLE107A-1 (EGF)	-	-	-	-	-	-	-	-
LLE49C	28/07/2010	4	0	2	1	5	-	-
LLE107A-2	18/05/2011	60	1600	650	1	15	19.2	32.5
LLE107A-3	18/05/2011	650	150	60	1	15	19.2	57.6
LLE118A-1*	27/05/2011	60	1600	650	1	30	34.5	88.2
LLE118A-2	27/05/2011	60	1600	650	1	60	15.6	42.0
LLE118A-3*	27/05/2011	120	3200	1300	1	30	46.7	105.1
LLE118A-4	27/05/2011	120	3200	1300	1	60	23.5	51.1
LLE134A-1*	21/06/2011	60	1600	650	1	45	33.7	61.8
LLE134A-2	21/06/2011	120	3200	1300	1	45	26.0	45.6
LLE134A-3	21/06/2011	180	4800	1950	1	45	9.8	16.5
LLE134A-4	21/06/2011	180	4800	1950	1	30	11.8	21.0
LLF6A-1	05/07/2011	120	3200	1300	1	30	5.4	11.8
LLF6A-2	07/07/2011	120	3200	1300	1	30	5.7	11.1
LLF6A-3	07/07/2011	120	3200	1300	1	30	12.3	20.9
LLF23A-1	04/08/2011	120	3200	1300	1	30	22.6	63.5
LLF23A-2	04/08/2011	120	3200	1300	1	30	120.9	216.7
LLF23A-3	07/08/2011	120	3200	1300	1	30	23.4	43.4
LLG28A-1	09/04/2012	120	3200	1300	1	30	2.7	8.1
LLG28A-2	09/04/2012	120	3200	1300	1	30	3.1	8.0
LLG28A-3	09/04/2012	120	3200	1300	1	30	7.2	17.3

* Samples used in subsequent experiments

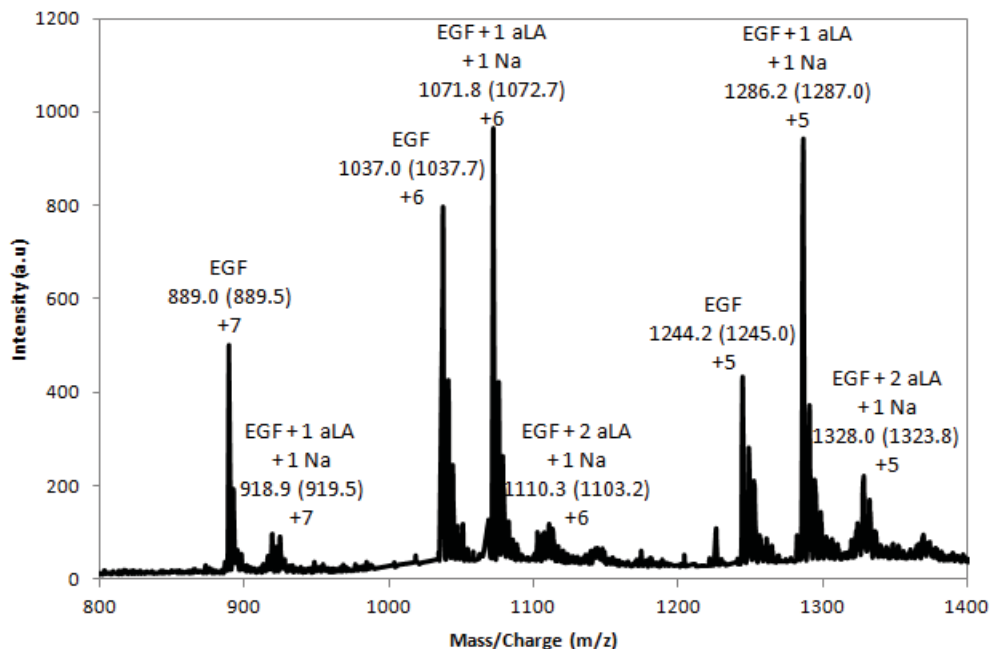


Figure 3.5 TOF-MS of Human EGF-linker protein sample LLF23A-2.

The conversion of EGF (1037.0 and 1244.2 m/z peaks) to EGF with one α -lipoic acid linker (1071.8 and 1286.2 m/z peaks) was higher for this sample than others observed in Table 3.1. The signal intensities seemed low when compared to Figure 3.2.

Figure 3.6 correlates the sample ID with synthesis date to better see the peak ratios, which correspond to the experimental yield. All samples presented in this figure were synthesized in an identical manner; some were prepared on different dates. The reaction time at each step for the samples shown was 30 minutes at the first step and 120 minutes for the second. The molar ratios of the reactants were constant at α -lipoic acid = 120, Sulfo-NHS = 3200, EDC = 1300, and EGF = 1. A reduced yield as the months progressed could be due to the degradation of EDC and sulfo-NHS over time. Similar yields were not obtained for the samples, as was the case with many samples which attempted to reproduce the yield of LLE118A-3. Even samples prepared on the same date with identical reagents, as was the case with samples LLF23A-1, and -2, have wildly differing yields. It is still unclear why so much variability in the yield was obtained when producing samples with identical procedures, or even within duplicate samples.

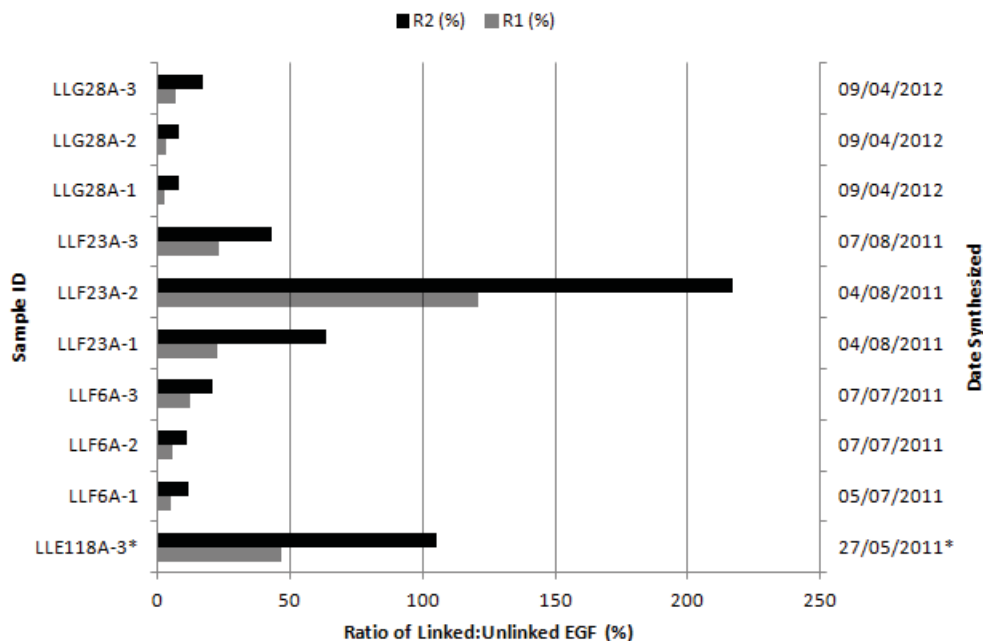


Figure 3.6 TOF-MS peak ratios of Human EGF-linker.

R1 = 1071.6 (1068.3-1072.0) m/z / 1036.9 (1036.8-1037.1) m/z, R2 = 1285.7 (1281.7-1286.3) m/z / 1244.1 (1243.8-1244.3) m/z, where R is the ratio between the linked-EGF and unlinked-EGF mean m/z values, and the numbers in brackets are the range. The reaction time at each step for the samples shown was 1st = 30 min., 2nd = 120 min. The molar ratios of the reactants were constant at α -lipoic acid = 120, Sulfo-NHS = 3200, EDC = 1300, and EGF = 1.

Mouse EGF does not have exactly the same sequence as Human EGF (Table 1.1), the substitution of amino acids means the predicted m/z values will be slightly different. Mouse EGF should produce peaks at m/z = 1200.0 (+5) and m/z = 1000.0 (+6), while the addition of a single sodium salt should give m/z = 1204.6 (+5) and m/z = 1003.8 (+6). We expect the m/z values of a single α -lipoic acid molecule attached to mouse EGF to produce peaks at m/z = 1237.6 (+5) and m/z = 1031.3 (+6), and peak positions with sodium salts should appear at m/z = 1242.2 (+5) and m/z = 1035.2 (+6). As mentioned previously, Human EGF has three potential attachment sites. Both of the lysine amino acids are not present in mouse EGF, only the amino terminus is available to attach α -lipoic acid. Mouse EGF has lysine substitutions for serine and arginine amino acids (Table 1.1). The amide bond formation reaction should still attach α -lipoic acid to the

amino terminus as long as it is accessible. An inaccessible amino terminus, or buried amino terminus, is from surrounding amino acids folding in conformations that envelop the amine terminal. Post translational modifications at the amino terminus can also impede reaction progression.

Table 3.2 lists the relative ratio of linked vs. unlinked mouse EGF peaks for all TOF-MS characterizations of mouse EGF-linker. Two mean ratios of the peak heights were calculated between the linked-EGF and unlinked-EGF m/z values, expressed in percentages. R1 was the ratio at peaks with m/z values of 1039.3 (1039.0-1040) m/z / 1009.0 (1009.0-1009.0) m/z and R2 was the ratio at 1212.5 (1211-1215) m/z / 1176.6 (1175-1177.2) m/z; the numbers in brackets were the range of the m/z. These values were not particularly close to the predicted values. The +5 peaks around 1000 m/z were slightly higher than expected, while the +6 peaks in the 1200 m/z range were much lower. The m/z shifts were not all in the same direction, indicating this may not be a systematic uncertainty. It is not clear why the 1200 m/z range peaks were so far from the expected values. All of the samples which tried to bind α -lipoic acid to mouse EGF seemed to have low intensity, and were not used for any further experiments.

Table 3.2 Mouse EGF to mouse EGF-linker peak ratios from TOF-MS. R1 = 1039.3 (1039.0-1040) m/z / 1009.0 (1009.0-1009.0) m/z, R2 = 1212.5 (1211-1215) m/z / 1176.6 (1175-1177.2) m/z, where R is the ratio between the mean linked-EGF and unlinked-EGF m/z values, and the numbers in brackets are the range. The reaction time (RxnT) at the 2nd step was 120 minutes for all samples.

Sample ID	Date Made	Molar Ratios				RxnT at 1 st Step (min.)	R1 (%)	R2 (%)
		α -lipo :	Sulfo- NHS :	EDC :	EGF			
LLG42A-1	17/05/2012	120	3200	1300	1	30	117.6	93.7
LLG42A-2	17/05/2012	120	3200	1300	1	30	95.8	76.9
LLG42A-3	17/05/2012	120	3200	1300	1	30	317.0	200.0
LLG42A-4 (EGF)	-	-	-	-	-	-	-	-
LLG56C	12/06/2012	120	3200	1300	1	30	242.6	153.3

Figure 3.7 and Figure 3.8 are typical TOF-MS spectra of mouse EGF and α -lipoic acid linked mouse EGF, respectively. The spectra represented by Figure 3.8 are poor, in the sense that the synthesis failed and α -lipoic acid linked mouse EGF was not formed.

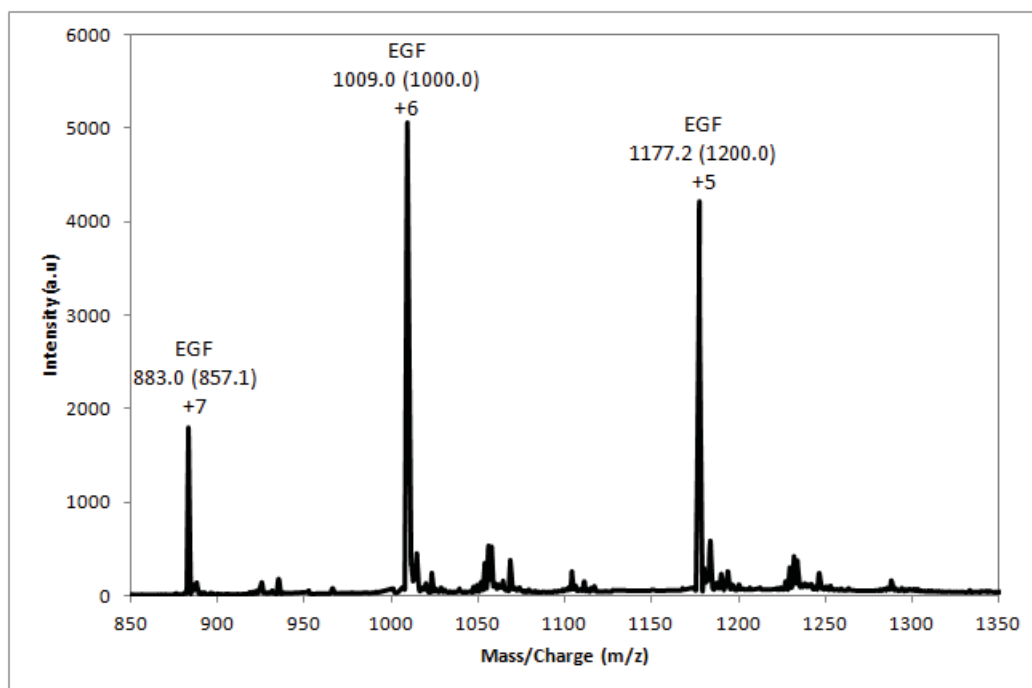


Figure 3.7 TOF-MS spectrum of mouse EGF.

The EGF peaks are present at 1009.0 and 1177.0 m/z. The reaction time at each step and the molar ratios are in Table 3.2.

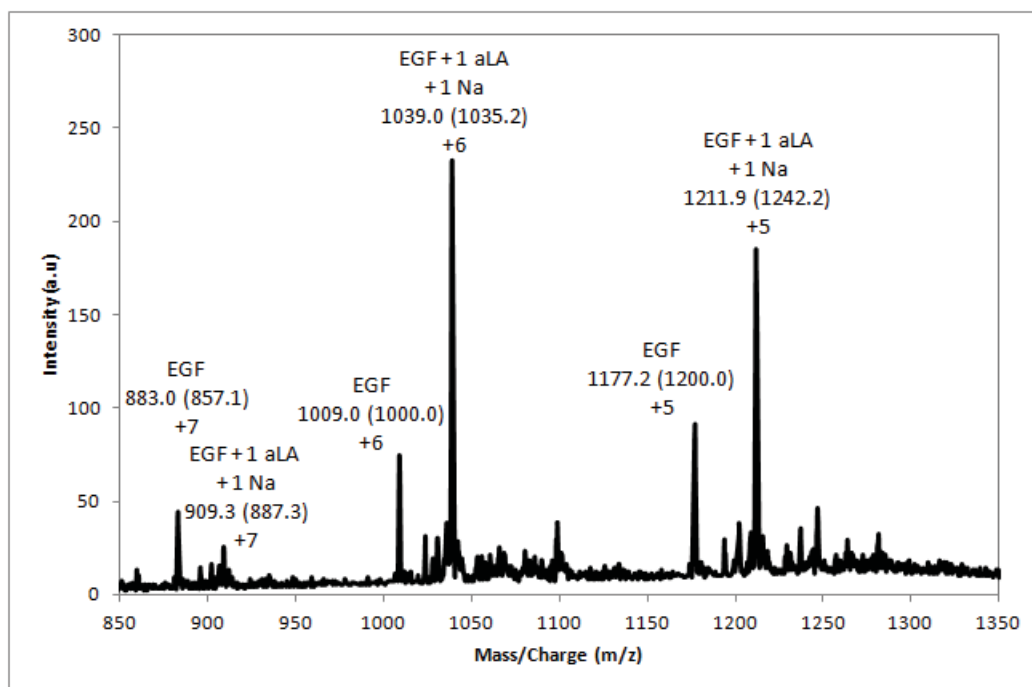


Figure 3.8 TOF-MS spectrum of mouse EGF-linker.

The conversion of EGF (1009.0 and 1177.0 m/z peaks) to EGF with one α -lipoic acid linker (1039.0 and 1212.0 m/z peaks) was higher for this sample than others observed in Table 3.2, however, overall the signal intensities were low when compared with the EGF only sample in Figure 3.7. The signal intensities of the 1176.6 m/z and 1212.5 m/z peaks were higher when compared to the LLG56C sample. The reaction time at each step and the molar ratios are gathered in Table 3.2.

Lack of indication of α -lipoic acid attachment to mouse EGF from TOF-MS spectra of means that the EDC and Sulfo-NHS were inactive from possible exposure to moisture over time, or α -lipoic acid cannot attach at the amino terminus of mouse EGF, or both those scenarios occurred. The folding should still be the same between the Human and mouse EGF variants, as the sequences are still similar. It is not clear whether post translational modifications, or surrounding amino acids hiding the amino terminus are blocking binding. We cannot compare the mouse EGF samples to the Human EGF as we do not know if α -lipoic acid ever was bound to the amino terminus (Section 3.2.3). The signal intensities of the α -lipoic acid linked mouse EGF samples generally were much lower than the mouse EGF only sample for some unknown reason, the mouse EGF

should not have just vanished from the sample tube. Low intensities of the mouse EGF-linker samples is not accounted for by inactivity of EDC and Sulfo-NHS.

TOF-MS spectra for Human and mouse EGF, as well as α -lipoic acid additions to these proteins were observed. Next, additional characterization of EGF, in the form of tests of activity, was performed with ELISA.

3.2.2 Enzyme-linked Immunosorbent Assay (ELISA) of Human EGF Protein

EGF-ELISA allows for assessment of the EGFR binding affinity of EGF, the EGF-linker, and the EGF-linker coated nanoparticles. We will discuss the activities of EGF and EGF-linker proteins now; the activities of EGF-linker coated nanoparticles will be addressed in a future section.

The activity of the EGF at various concentrations is shown in Figure 3.9. The unlinked and linked EGF used in the experiment (kit and EGF-linker, respectively) gave approximately the same response, indicating that the EGF-linker was still active for the EGFR. Previous tests of the reactant EGF from Invitrogen used to form the EGF-linker showed activity identical to the EGF-linker. The Invitrogen EGF and EGF-linker 3 samples were measured with the Nanodrop UV-Vis (path length = 1 mm), the data were multiplied by a factor of 10 to compensate for the difference in path length. All other EGF data was obtained by microplate reader (path length = 10 mm) and plotted as collected. The concentrations of EGF used during the test were within the recommended ranges, they were from 200 pg/mL down to 0.8 pg/mL. The protein samples were diluted to be as nearly identical as the standard protein concentrations as possible, for easier comparisons of the activities.

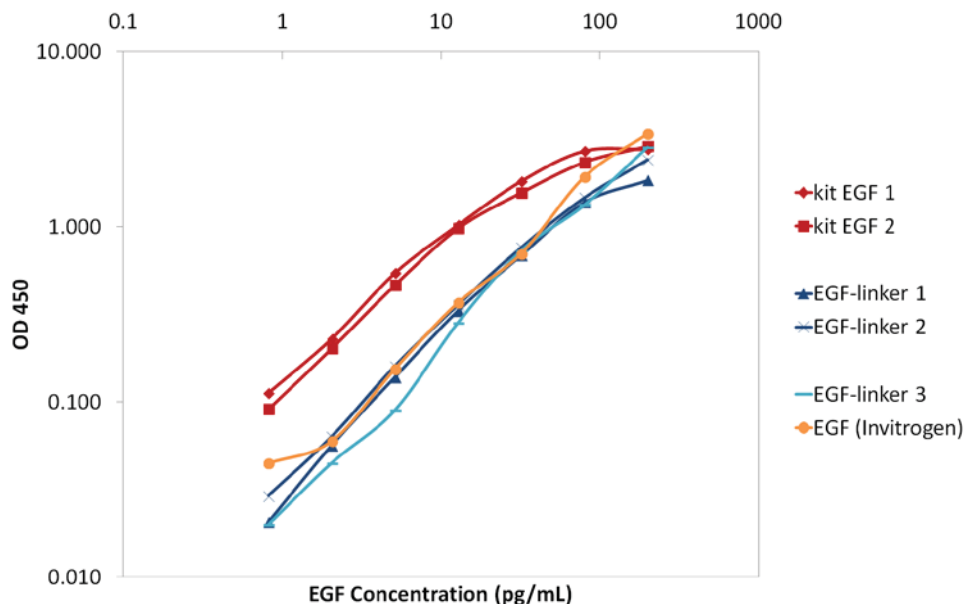


Figure 3.9 EGF-ELISA of EGF protein.

The total EGFR binding response was measured by the optical absorbance at 450 nm for various concentrations of EGF and EGF-linker. Both the stock (Invitrogen) EGF and the EGF-linker show activities near the standard (kit) EGF.

3.2.3 Confirmation of EGF-linker Attachment Site with LTQ-MS

Identification of which of the three likely sites to which α -lipoic acid linker binds involves cleaving the protein into peptides, cleaning these peptide fragments, and measuring their size (MW) using HPLC and ESI-LTQ-MS.

The In-Solution Trypsin Digestion reduces the protein into peptide fragments, measurement of changes in the fragment masses tells where α -lipoic acid attaches. During the digestion, it is possible that the addition of the α -lipoic acid molecule to EGF alters the charge on the amine group, as it converts to an amide, and would not allow trypsin to cleave after lysine. This would result in a missed cleavage and a larger peptide fragment than expected. In practice, the SpeedVac should have been used to concentrate the solution and remove organic solvents [71]. Although, the concentrations of methanol and acetonitrile were probably low enough that the tryptic digestion was mostly unaffected. At most, the digested sample contained 10 μ g of protein.

When cleaning the peptides with HPLC, the peptide elution time was confirmed from the insulin-linker peptide sample. The general elution time was known from previous runs with a protein standard, BSA (bovine serum albumin, 70 kDa). As stated in Section 2.4.3, of the 50 μL of each sample available for injection onto the column, two injections of 20 μL each were performed to clean the peptide samples, about half of the sample or at most 5 μg was cleaned. The precise amount of protein which was cleaned, to know how much to use for LTQ-MS, was determined from the UV-Vis detection of the protein response from HPLC. First, the linear equation of a standard curve of BSA was calculated ($y[\mu\text{g}] = 29866x[\text{absorption}] + 2300.4$). The UV-Vis absorption values of each of the two peptide injections were summed, and the blank absorption values were subtracted. The summed absorption values were then plugged into the linear BSA equation to find the weight of clean peptides. This gave 1.81 μg and 1.74 μg of peptides for each injection, for a total of 3.55 μg of clean peptides.

Issues with the throwaway insulin-linker HPLC cleaning run led to the decision not to use this insulin-linker with the LTQ-MS, to prevent LTQ-MS downtime or instrument damage. The UV-Vis peptide elution profile for the HPLC run was not clean, the peak was broader than the expected curve. This throwaway insulin-linker served its purpose by alerting to issues with the HPLC, and in the confirmation of the peptide retention time as predetermined by BSA. This is useful because the retention time varies slightly from column to column and with a newly packed column. This helped to ensure the EGF-linker peptides of interest were not wasted. An unlinked BSA protein sample was used as the standard or “throwaway” protein in this case.

Assuming complete digestion of the peptides with trypsin, the expected theoretical fragment m/z ratio following digestion and detection with LTQ-MS can be calculated using PeptideMass from ExPASy and the protein sequence from Section 1.2. Peptide fragment modifications from α -lipoic acid addition are not taken into account by this tool. Theoretical digestions of chymotrypsin can also be run with PeptideMass.

The Sequest software compares known protein sequences to experimental mass to charge ratios found with LTQ-MS by calculating and ranking the plausibility of a match. Using Sequest, we expect to see α -lipoic acid attached to certain peptides. Assuming

complete protein digestion by trypsin, 2 α -lipoic acid molecules could attach to the largest peptide containing the amino terminus and a lysine. 1 α -lipoic acid could attach to another peptide which contains the second lysine near the carboxy terminus. 3 other potential peptides do not change mass between the unlinked and linked EGF versions.

α -lipoic acid containing peptides were identified with the Sequest program, as demonstrated in Appendix B. The two hits from the program correspond to the amino terminus peptide with a missed cleavage. These samples are peptides 23 and 25, and bold font identifies the data in the appendix. Sequest notes that the missed cleavages give two potential binding sites, the amino terminus and the lysine. The peptide sequence corresponds to a portion of the carboxy terminus of the Human EGF protein from Figure 3.1, or cQyRDLkWWELR. The matches are actually the same MS spectrum, but α -lipoic acid could have attached only to the lysine site as the protein was still intact during the amide bond formation reaction and the amino terminus peptide was inaccessible. These matches by Sequest were not assured, some uncertainty exists as the peptides only rank as “medium” confidence. The mass spectrum for this sample appears in Figure 3.10. Sequest states that the identified fragment is 674.4000 m/z, has a +3 charge, and contains the carboxy terminus lysine groups, meaning its mass should be 2021.2 g/mol. We can see from the top, zoomed spectrum that the 674.4 m/z peak is not particularly prominent and may not be the peptide of interest. This 674.4 m/z peak is not present in the bottom, general spectrum which shows a larger m/z range. The two spectra were collected within a second of each other, and a peptide of interest should not disappear from the entire mass spectrum. The data presented in Figure 3.10 and Appendix B are of a single LTQ-MS run with the EGF-linker. Six experimental runs were performed, only the first showed any peptide matches to the EGF-linker by Sequest. When calculating the peptide sequence masses as a check, the mass of the carboxy terminus peptide of interest should be 2058.9 g/mol. The predicted peak position should then be 686.3 m/z with a +3 charge. It is unlikely this peptide matches Human EGF with a single conjugated α -lipoic acid molecule.

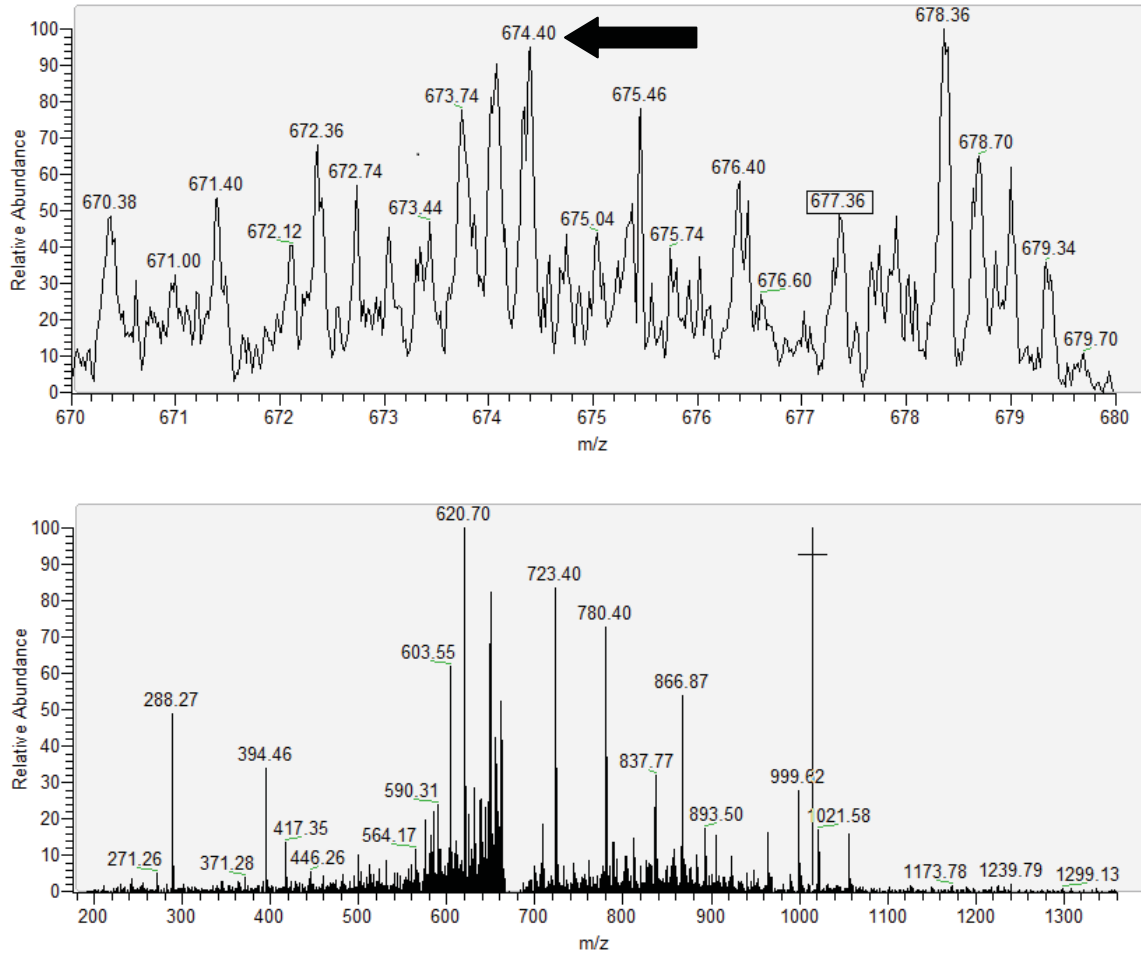


Figure 3.10 LTQ-MS spectra of trypsin digested, α -lipoic acid conjugated Human EGF.

The two mass spectra were recorded during the first of six runs at 60.84 minute elution time. The x-axis corresponds to the mass to charge ratio (m/z), while the y-axis shows the relative abundance of the ions. The spectra correspond to: the +3 charge peptide fragment identified at 674.4000 m/z by Sequest (top) and a broad m/z range for the same run (bottom).

The LTQ-MS instrument can see peptides in the range of 350 m/z to 2000 m/z, while it is most commonly used and calibrated to the range from 400 m/z to 1200 m/z [85]. The largest Human EGF peptide should have a +4 charge with no linkers attached (821.3 m/z), a +3 charge with one linker (1157.8 m/z), or a +2 charge with two linkers (1830.7 m/z), which should leave the peptide just within the detection range. The m/z values include the mass of one carbamidomethyl cysteine, which forms when the cysteine amino acids are capped during the protein trypsinization steps. As more α -lipoic acid

molecules add to Human EGF to form an amide bond, it is likely that the positive charge of the amine group on EGF disappears. Even assuming no missed cleavages of the peptide sequence occur, the large size of the amino terminus fragment (1157.8 m/z) and the possibility of the addition of two α -lipoic acid molecules (1830.7 m/z), causes difficulty in the detection of this peptide. If we choose chymotrypsin as our enzyme, some fragments may be too small or below the low end of the limit of detection, which would prevent measurement of the peptides. Note that missed cleavages of the peptide sequence occurred, resulting in larger fragments than expected. The factor that influenced the poor result most was probably that these large fragments approached and sometimes surpassed the maximum ideal mass to charge range of the LTQ-MS instrument. The use of an alternate MS instrument, like the TOF-MS with its 20-20000 m/z range, may help prevent detection issues caused by large peptides. Alternatives for the determination of the α -lipoic acid to EGF attachment site are in the Future Work Section 5.2.

3.2.4 EGF-linker Characterization Summary

The TOF-MS and ELISA measurements of the EGF-linker formed during the reaction procedure shows that the linked-EGF forms and remains active for EGFR with Human EGF proteins. TOF-MS of mouse proteins was not conclusive, as the EDC and sulfo-NHS amide bond formation reagents were likely degraded. LTQ-MS of α -lipoic acid conjugated to Human EGF protein and subsequently digested with a protease called trypsin did not definitively show addition to any amino acids.

3.3 CHARACTERIZATION OF SYNTHESIZED NANOPARTICLES

3.3.1 Transmission Electron Microscopy (TEM)

In transmission electron microscopy, metal nanoparticles appear dark as they absorb the electrons. Figure 3.11 shows the TEM images of these as synthesized

nanoparticles at magnifications ranging from 60,000X to 220,000X. The citrate stabilized AuNP mean diameter and standard deviation is 18.4 ± 5.1 nm. The size of the small AuNPs synthesized by sodium borohydride reduction are very reproducible, having a mean diameter and standard deviation of 3.8 ± 0.8 nm. The intermediate AgNPs diameter and standard deviation is 45.5 ± 25.0 nm. The citrate reduced silver nanoparticles have a poly-disperse size distribution when compared to gold. The small NaBH_4 reduced AgNP mean diameter and standard deviation is 5.2 ± 4.2 nm. For each sample, 100 particles were measured to obtain the averages. Histograms show the particle distributions in Figure 3.12.

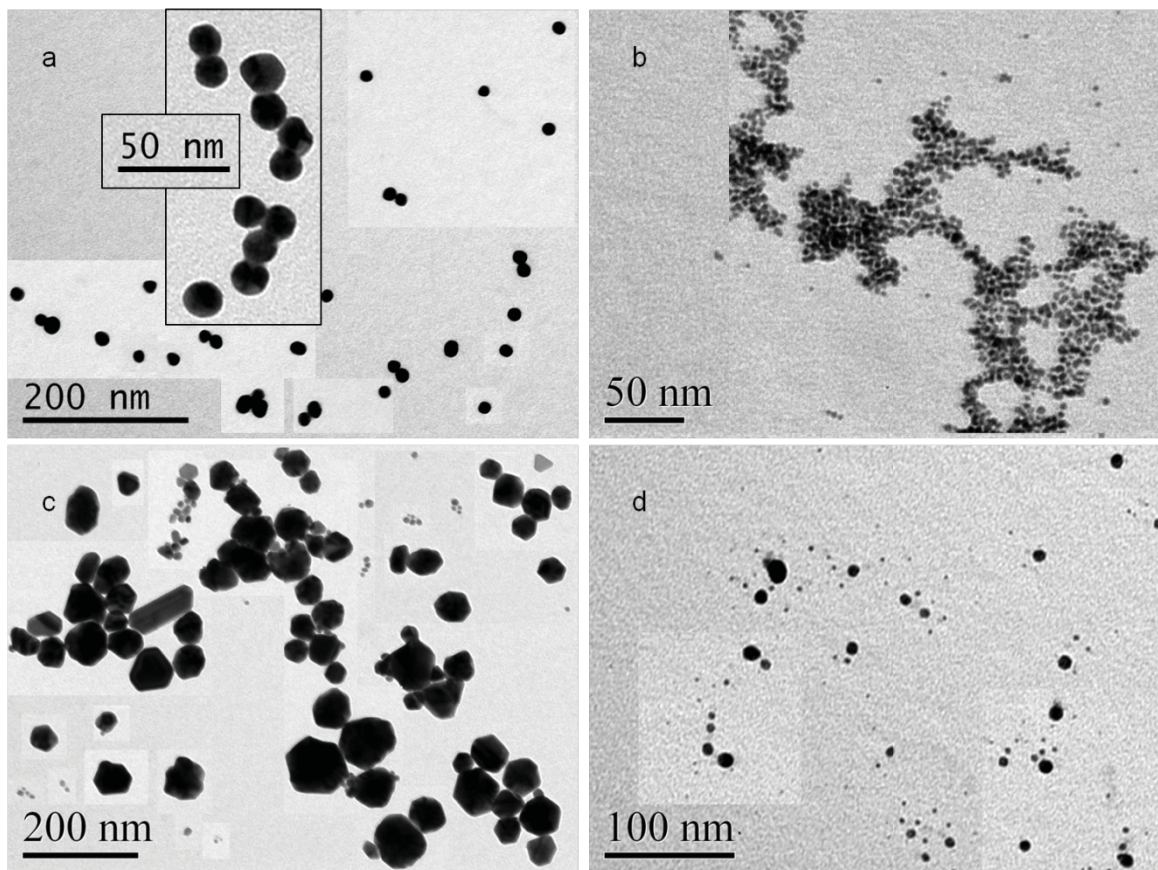
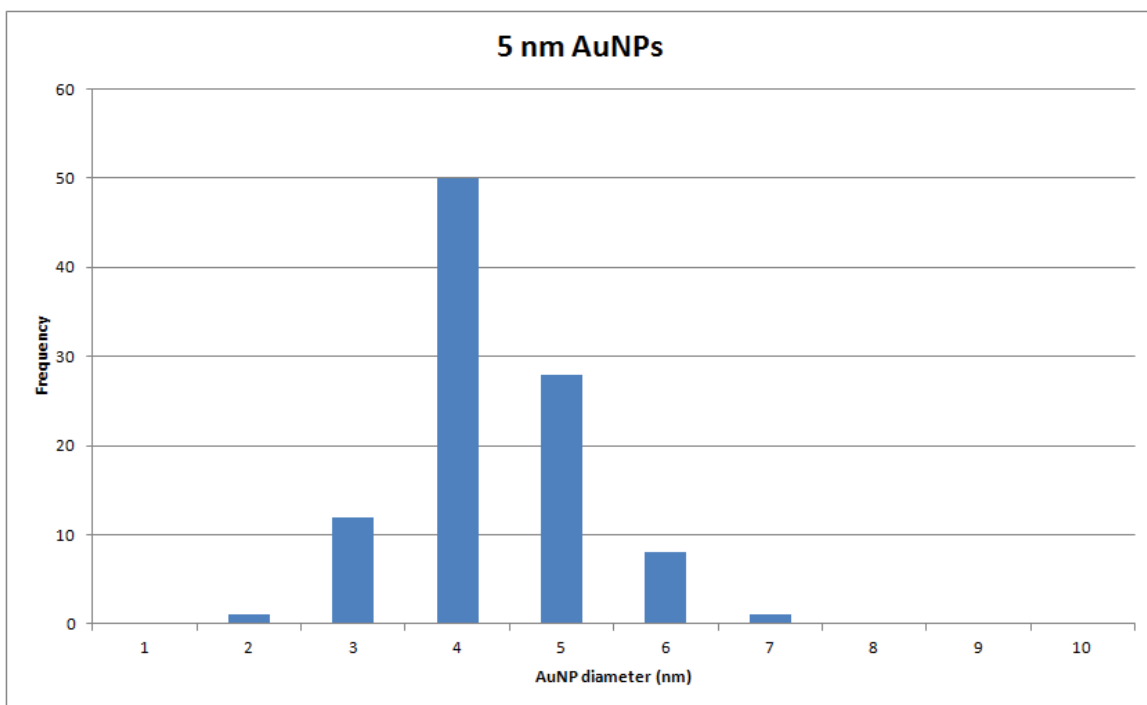
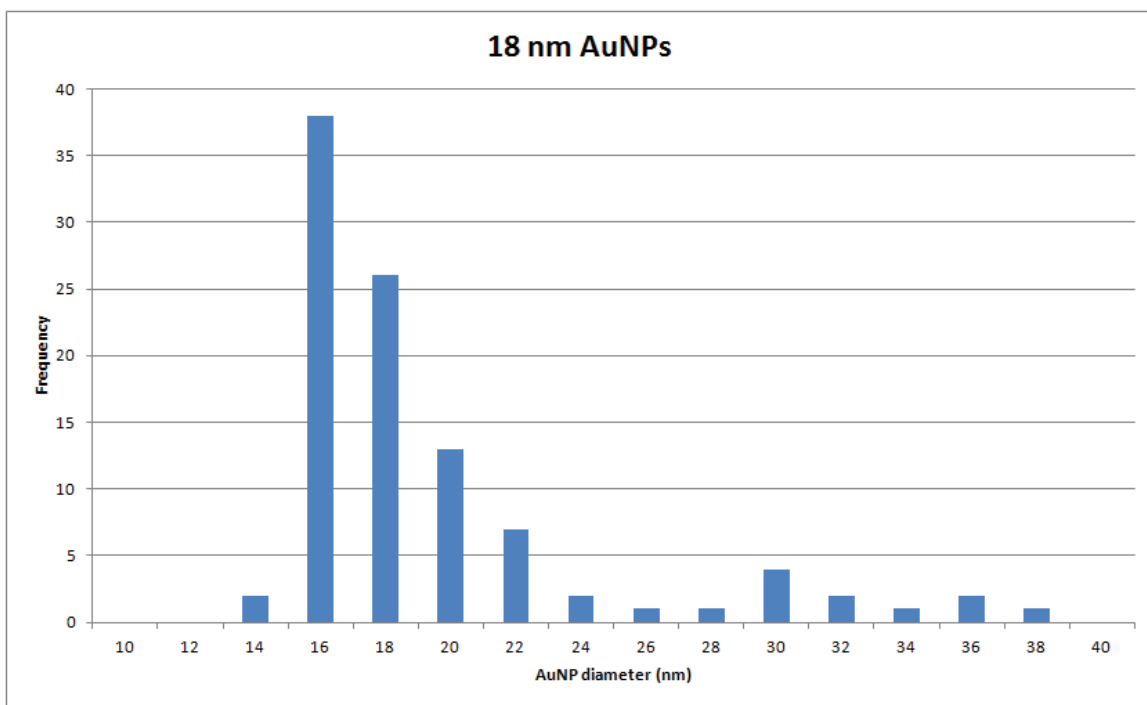


Figure 3.11 TEM of Au and AgNPs.

The nanoparticles in and image magnifications of each panel are: a) 18 nm AuNPs – 87,000 and 220,000X, b) 5 nm AuNPs – 160,000X, c) 45 nm AgNPs – 60,000X, and d) 5 nm AgNPs – 135,000X.



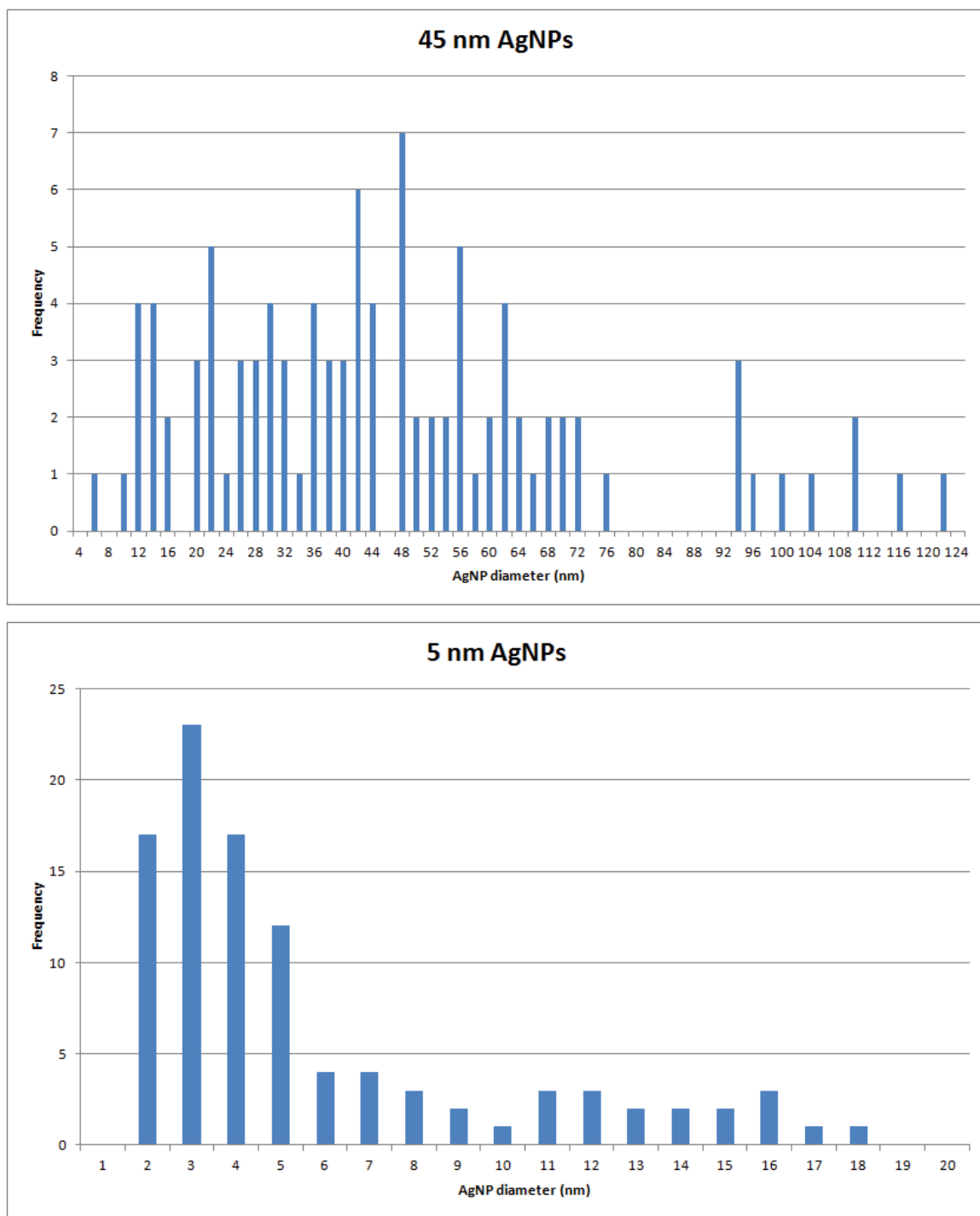


Figure 3.12 Au and Ag nanoparticle size distribution histograms from TEM. Histograms for all four nanoparticle types are above: 18 nm AuNPs, 5 nm AuNPs, 45 nm AgNPs, and 5 nm AgNPs.

3.3.2 Ultraviolet-Visible Spectrophotometry (UV-Vis)

UV-Vis spectra of 5 nm Au, 18 nm Au, 5 nm Ag, and 45 nm Ag are in Figure 3.13. Table 3.3 summarizes the maximum absorbance wavelengths and values, as well as the path length at which we measure the samples. The 5 nm AgNPs typically lasted two days prior to colour change, from bright yellow to brownish-black, and disintegration of the solution. One batch was anomalous and remained yellow for more than 2 months.

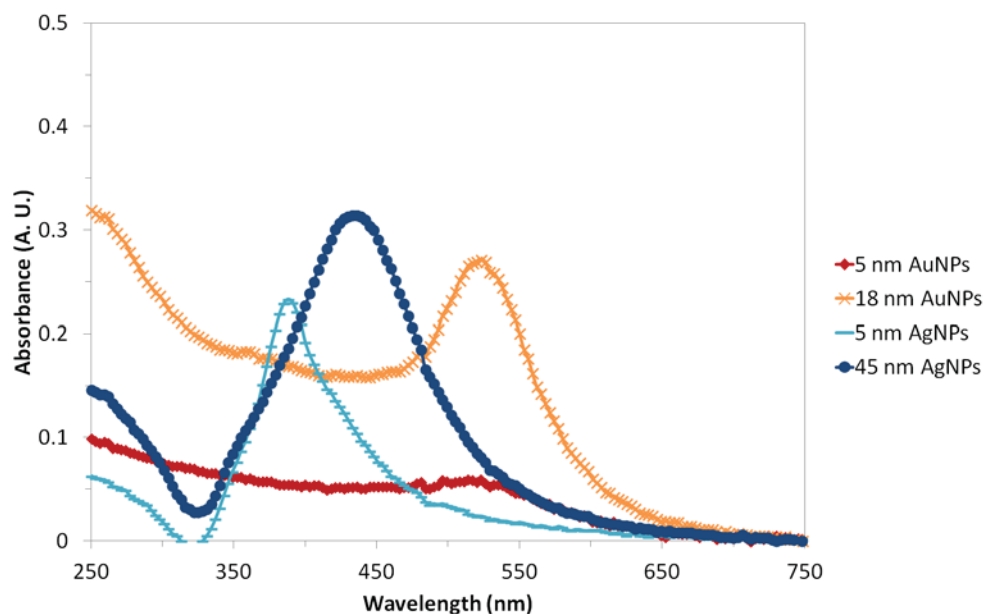


Figure 3.13 UV-Vis of Au and AgNPs.

The nanoparticle spectra are: a) 5 nm AuNPs, b) 18 nm AuNPs, c) 5 nm AgNPs, and d) 45 nm AgNPs. The spectra show the maximum absorbance wavelength, which is indicative of the optimal range of usefulness for SERS.

Table 3.3 UV-Vis properties of as synthesized nanoparticles.

Nanoparticle type	5 nm Au	18 nm Au	5 nm Ag	45 nm Ag
Maximum wavelength (nm)	514	521	384	432
Absorbance value (A. U.)	0.060	2.910	3.298	1.780
Path length (mm)	1	10	10	10
Extinction Coefficient (cm ²); Au: [86], Ag: [87]	3×10^{-11}	3×10^{-11}	2.91×10^{-11}	11.79×10^{-11}

3.3.3 Characterization of Synthesized Nanoparticles Summary

From the TEM and UV-Vis data for the as synthesized gold and silver nanoparticles we can obtain their size distribution and plasmon frequencies. The maximum absorbance wavelengths from UV-Vis red-shifted upon aggregation, meaning that one must tune the laser wavelength above this shifted value to obtain the greatest enhancement effect for SERS (Table 3.3).

3.4 ATTACHMENT AND STABILIZATION OF EGF-LINKER BOUND NANOPARTICLES

3.4.1 Attachment of EGF-linker to Nanoparticles

The modified EGF, or EGF-linker, was inherently activated towards the noble metals silver and gold because of the disulfide bridge on α -lipoic acid. We desire stable probes and obtain them by ensuring the protein was well affixed to the nanoparticles through the formation of the sulfur-metal bonds found in the attached α -lipoic acid linker molecule. Complete nanoparticle coverage was obtained through a combination of the EGF-linker formed above and excess α -lipoic acid to fill out any gaps in the nanoparticle coordination sphere.

α -lipoic acid was chosen for linkage to EGF and to ensure strong bonding to the nanoparticle based on research by J. A. Dougan et al (2007) [57]. They investigated disulfide (-S-S-), dithiol (-SH and -SH), and thiol (-SH) groups bound to gold and silver nanoparticles. The most stable bonds seemed to be the disulfides, which is one functional group α -lipoic acid contains. Disulfides with adjacent atoms forming a ring seemed to yield the most stable nanoparticle coatings. The disulfide end group of α -lipoic acid binds strongly to the nanoparticle while its carboxylic acid end group allows carbodiimide chemistry to link to EGF.

From the Protein Data Bank 1JL9 crystallographic structure we found the dimensions of an EGF monomer are: 3.071(5) nm x 3.071(5) nm x 4.352 nm [19]. We

assume EGF covers a planar area of 9.94 nm^2 . To ensure complete coverage, the number of EGF per nanoparticle is therefore,

$$\# EGF = \frac{1}{yield} \times \pi d^2 \div 9.94. \quad (11)$$

Here the *yield* is the fraction of EGF which converts into the EGF-linker and d is the nanoparticle diameter in nm. We use the as synthesized nanoparticle TEM diameter for the calculation. For complete coverage, we theoretically require 9.94 nm^2 of NP surface area per EGF. The shape of the protein may leave gaps between proteins in the nanoparticle coordination sphere, we use α -lipoic acid to help fill in any spaces.

3.4.2 Stabilization of Nanoparticles with α -lipoic Acid

A similar method as employed with the EGF-linker attachment determines the α -lipoic acid coverage. We assume α -lipoic acid occupies an area of 0.15 nm^2 , we require the number of α -lipoic acid Equation 12 gives. We calculate the surface area of occupancy (0.15 nm^2) from the theoretical covalent bond lengths: 0.15 nm by ~ 8 bonds $\times 0.15 \text{ nm}$. The procedure uses 50 times excess α -lipoic acid to ensure complete nanoparticle coverage.

$$\# \alpha - lipoic \ acid = 50 \times \pi d^2 \div 0.15 \quad (12)$$

For the 18 nm AuNPs (4.0×10^{10} AuNPs/mL), Equation 11 gives 107 EGF per nanoparticle ($1064 \text{ nm}^2 \text{ NPSA} / 9.94 \text{ nm}^2 \text{ NPSA per EGF} = 107 \text{ EGF}$). Therefore, to 1 mL of AuNPs, we add 9 μL of 0.01 mg/mL EGF-linker and 12 μL of 0.4 mg/mL α -lipoic acid.

For the poly-disperse 45 nm AgNPs (1.5×10^9 AgNPs/mL), one requires approximately 654 EGF per nanoparticle ($6504 \text{ nm}^2 \text{ NPSA} / 9.94 \text{ nm}^2 \text{ NPSA per EGF} = 654 \text{ EGF}$). Therefore, to 1 mL of AgNPs, we add 2 μL of 0.01 mg/mL EGF-linker and 12.2 μL of 0.4 mg/mL α -lipoic acid.

The 5 nm AuNPs (9.6×10^9 AuNP/mL) require 4.6 EGF per nanoparticle ($45.4 \text{ nm}^2 \text{ NPSA} / 9.94 \text{ nm}^2 \text{ NPSA per EGF} = 4.6 \text{ EGF}$). To 1 mL of AuNPs, we add 8.3 μL of 0.0001 mg/mL EGF-linker and 1.1 μL of 0.04 mg/mL α -lipoic acid.

For the 5 nm AgNPs (4.9×10^{10} AgNP/mL), 8.5 EGF per nanoparticle are needed ($84.9 \text{ nm}^2 \text{ NPSA} / 9.94 \text{ nm}^2 \text{ NPSA per EGF} = 8.5 \text{ EGF}$). To 1 mL of 5 nm AgNPs, we add 8.6 μL of 0.001 mg/mL EGF-linker and 1.2 μL of 0.4 mg/mL α -lipoic acid.

These quantities are summarized in Table 3.4. It is important to note that the quantity of EGF and α -lipoic acid required *per nanoparticle* increase by a factor of 6 when comparing the column for the 45 nm AgNPs to that of the 18 nm AuNPs, consistent with the increase in the area by R^2 . Similarly to Section 3.1, the α -lipoic acid solution is prepared by diluting the powder in equal volumes of methanol and deionized water. Dilutions ensure accuracy in pipetting the low α -lipoic acid and EGF volumes added to the 5 nm Au and AgNP samples in Table 3.4. We add EGF-linker and α -lipoic acid stepwise, and each attaches overnight. The nanoparticle concentrations were determined using the Beer-Lambert Law, or $A = \epsilon bc$. A is the maximum absorbance value from UV-Vis, ϵ is the molar absorptivity in cm^2 (Table 3.3), b is the path length in cm, and c is nanoparticle the concentration in NP/mL.

Table 3.4 Quantity of NPs, EGF, and α -lipoic acid for complete coverage of each NP type.

Type of NP	5 nm Au	18 nm Au	5 nm Ag	45 nm Ag
Concentration (NPs/mL)	0.96×10^{10}	4.0×10^{10}	4.9×10^{10}	$.15 \times 10^{10}$
# EGF per NP (from Eqn. 4)	4.6	107	8.5	654
Volume (mL) of NPs at the concentration stated above	1	1	1	1
Volume (μL) of 0.01 mg/mL EGF	.083	9	.86	2
Volume (μL) of 0.4 mg/mL α -lipoic acid	.11	12	1.2	12.2

We perform tests with nanoparticles coated solely with α -lipoic acid as control particles to the EGF-linker covered nanoparticles.

3.4.3 Nanoparticle Purification

We purify the nanoparticles using the method of S. Balasubramanian et al. (2010) to remove excess EGF-linker and α -lipoic acid [76]. We spin the 5 nm gold nanoparticles, 18 nm gold nanoparticles, 5 nm silver nanoparticles, and 45 nm silver nanoparticles at 14000 rcf, 7000 rcf, 10000 rcf, and 5000 rcf, respectively. We repeat the centrifugal steps three times for a total of four centrifuge steps, each for 30 minutes at 21°C, to maximize the nanoparticle recovery. Specifically, we spin the samples once to pellet, we then spin the supernatant to recover any additional nanoparticles, and finally we combine the pellets of both spins and dilute to 1 mL with deionized water. We repeat this process once.

3.4.4 Summary of Attachment and Stabilization of EGF-linker Bound Nanoparticles

A complex of α -lipoic acid bound Human EGF adds to nanoparticles to form a protein coating on the surface. We add α -lipoic acid in excess to the α -lipoic acid conjugated Human EGF coated nanoparticles to fill in any gaps remaining in this protein layer. Control nanoparticles contain only a layer of α -lipoic acid for comparisons to the α -lipoic acid conjugated Human EGF coated nanoparticles; results with these nanoparticles are in a future section. We complete purification of the nanoparticles to know that the excess α -lipoic acid bound EGF in the solution is no longer present, and to know interference with the characterization tests would not occur.

3.5 CHARACTERIZATION OF EGF-LINKER BOUND TO NANOPARTICLES

3.5.1 Stability in Saline Solution

Gold and silver nanoparticles are mixed in a 1:1 ratio with 10 mM PBS buffer at pH 7.4 to observe the stability of a variety of coatings (citrate, α -lipoic acid or EGF-linker) in a biological buffer over two days (Figure 3.14). The 10 mM PBS buffer sodium

chloride concentration is 0.8-0.9%, which is identical to that of mammalian physiological saline.

Unstable nanoparticle solutions at first turn dark as the nanoparticles aggregate. The solutions then become colorless as the aggregates settled out. Stable nanoparticles retain their colour (18 nm AuNPs - pink, 45 nm AgNPs - yellow). The EGF-linker and α -lipoic acid coated NPs are both stable at this higher salt content. Some of the stable nanoparticles look to be more concentrated at the bottoms of the tubes, especially the α -lipoic acid coated silver nanoparticles in Figure 3.14. The heavier nanoparticles naturally settle to the bottom of the vessel over time. Settling is reversible by shaking or mixing the tube of nanoparticles. The sample was prepared on August 16, 2011 and the photo captured on August 18. A repeat test showed that the coated nanoparticles were stable for more than three weeks.



Figure 3.14 Stability test of gold and silver nanoparticles in 10 mM PBS buffer.

18 nm gold (top row) and 45 nm silver (bottom row) nanoparticles. TOP ROW (Left-Right): as prepared (citrate) AuNPs with distilled water, AuNPs with 10 mM PBS, α -lipoic acid coated AuNPs with 10 mM PBS, EGF-linker coated AuNPs with 10 mM PBS, and α -lipoic acid/EGF-linker coated AuNPs with 10 mM PBS. BOTTOM ROW (Left-Right): same as top row except with

AgNPs. All fully coated nanoparticles (3 and 5 from left) were stable over more than two days at 0.45% salt content.

3.5.2 Transmission Electron Microscopy (TEM)

Figure 3.15 contains photos of 18 nm AuNPs, both as synthesized (citrate stabilized) and coated (EGF-linker with α -lipoic acid). The photos are at 87,000 and 220,000 times magnification. The functionalized nanoparticles seem to have a larger inter-particle spacing, indicating they are well coated.

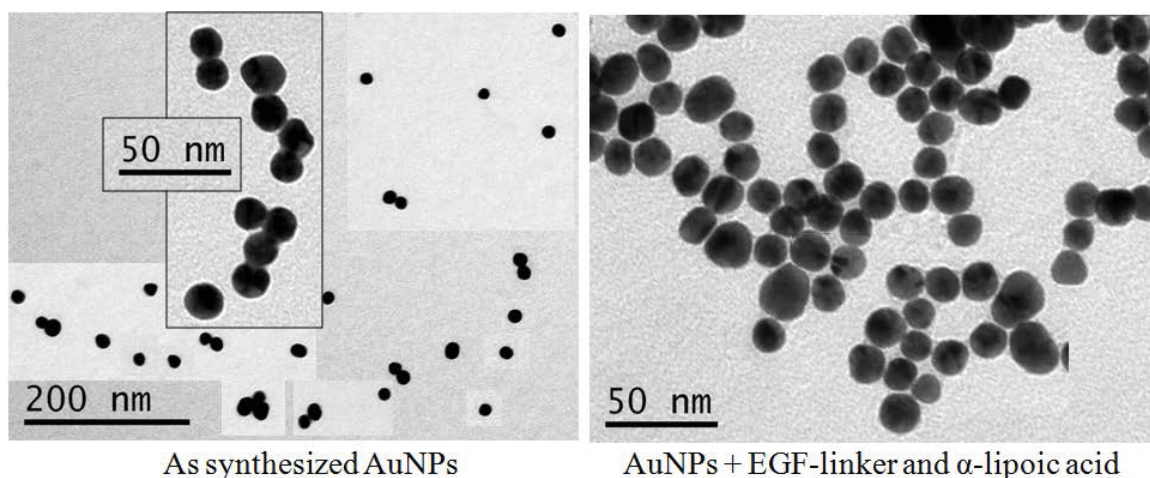


Figure 3.15 Transmission electron microscope images of 18 nm AuNPs as synthesized with citrate (left) and α -lipoic acid/EGF-linker (right) attached.

Inter-particle spacing of the as synthesized nanoparticles is smaller than of the α -lipoic acid/EGF-linker nanoparticles, suggesting the latter are well coated. Both images are taken at 87,000 and 220,000X magnification with an electron beam of 80 keV (15.5 pm).

3.5.3 Transmission Electron Microscopy (TEM) of EGF-NPs with Uranyl Acetate (UA)

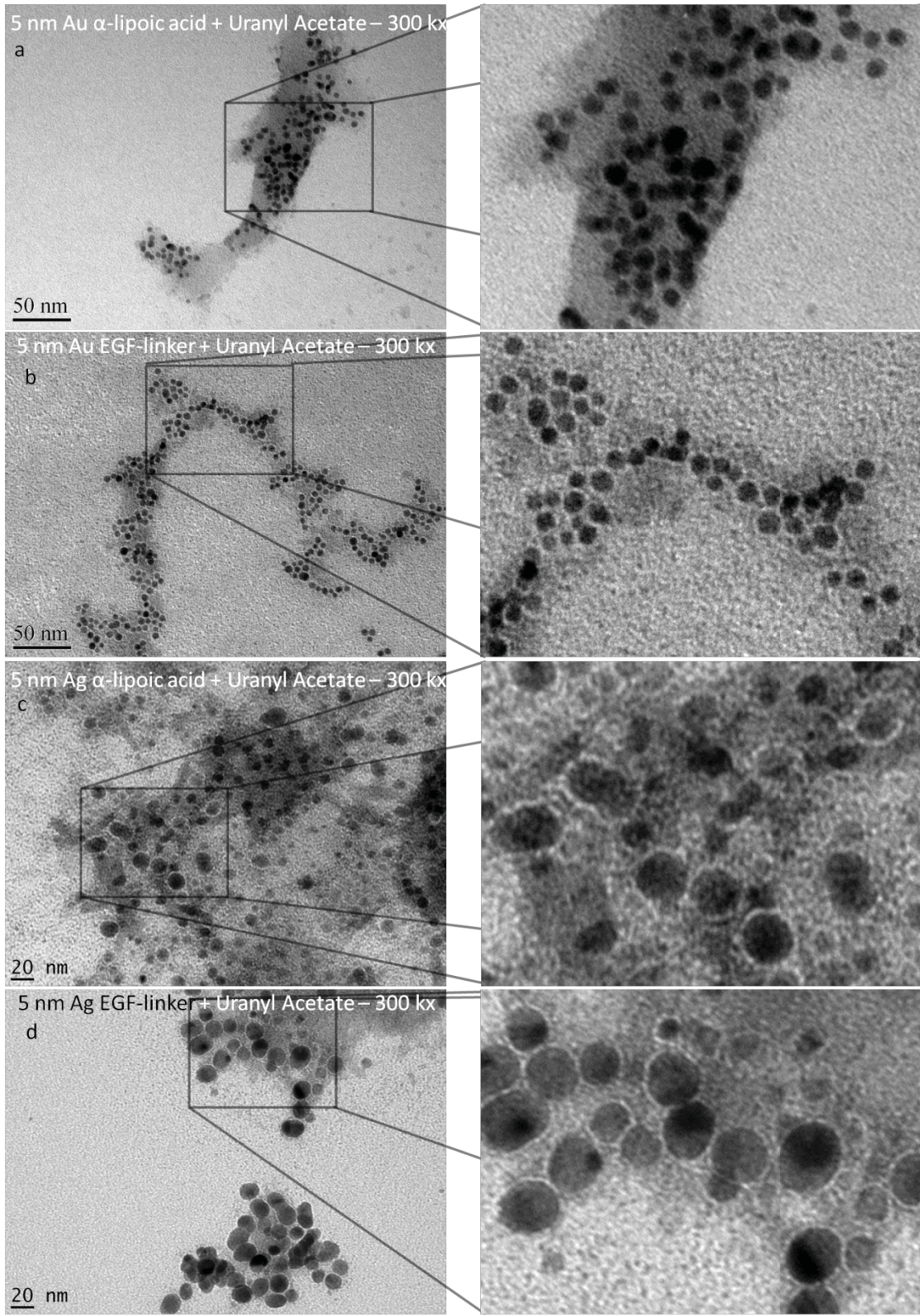
While metal nanoparticles appear dark, as they absorb the electrons from the beam, the uranyl acetate stain is visible as a lighter grey area around the nanoparticles that gradually fades into the still lighter grey of the background of the grid. The protein

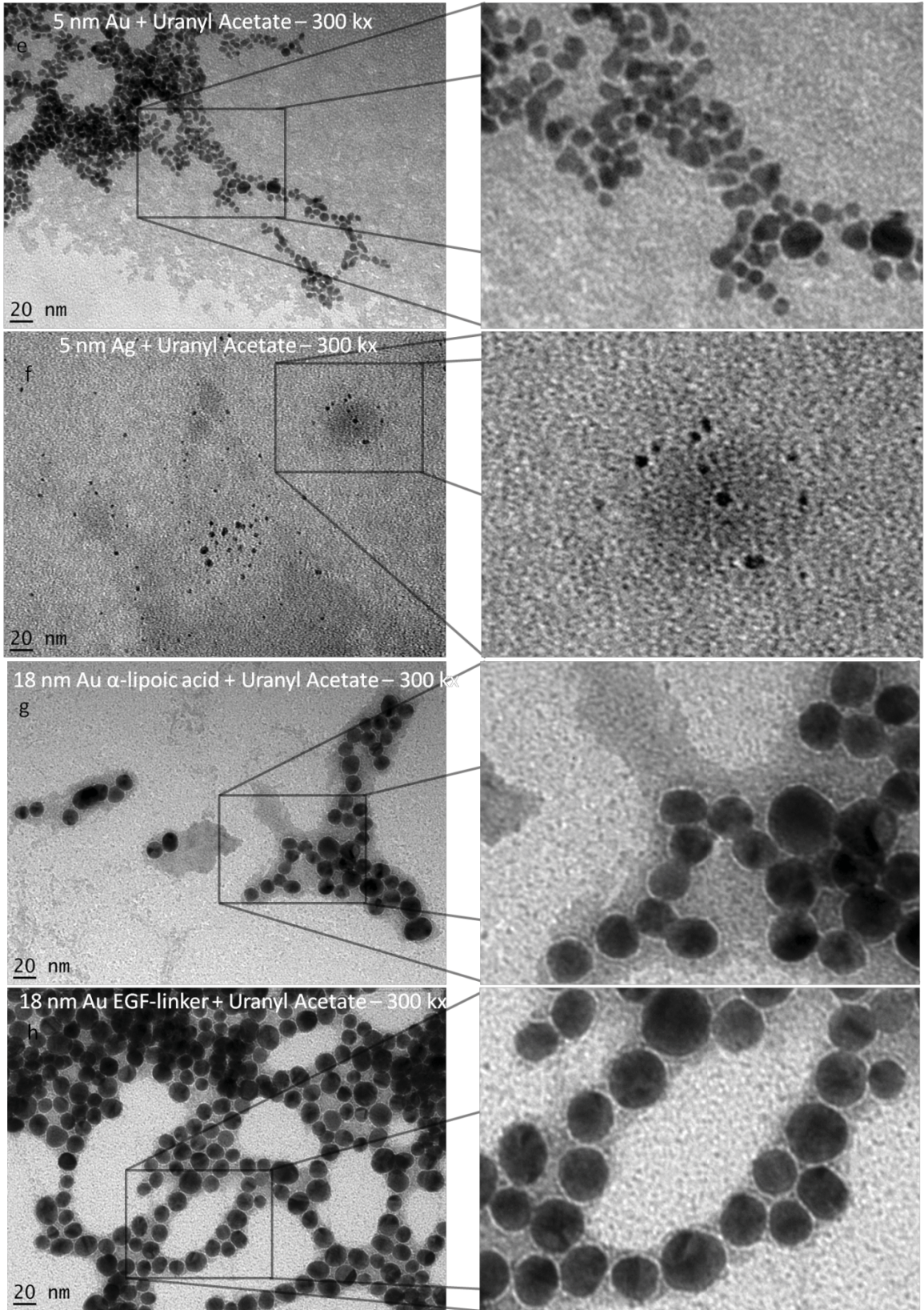
appears as a bright white-light ring directly around the nanoparticle from the transmission of electrons through this layer. We expect nanoparticles coated with the EGF-linker to have a ring of about 3-4.5 nm surrounding them [19] [48]. Those nanoparticles coated with α -lipoic acid will have a much thinner ring of around 0.9-1.2 nm, with this value derived from the average C-C bond length of 120-154 pm multiplied by 8 C-C bonds. It is important to note that these values represent hydrated protein and α -lipoic acid. Collapse of the tertiary protein structure upon drying could cause a reduction in the expected ring size. Visibility of the α -lipoic acid molecule surrounding the nanoparticles may be low due to the short length of the molecule. Uncoated nanoparticles will not have any bright ring interrupting the dark nanoparticle from the grey stain. This has been described previously by J. C. Trefry and D. P. Wooley (2012), with examples of coated nanoparticles from Morones and Frey (2007) and uncoated nanoparticles from Bradley (1962) [7] [88] [89].

During the first step in the staining procedure, the nanoparticles were spotted onto a carbon coated 300 mesh copper grid and air dried overnight, as was typical procedure for all TEM imaging. The staining protocol for the nanoparticles dried on the grids was developed using a few sources [7] [88] [89]. The procedure also referenced the departmental protocol for staining sections on TEM grids, and was obtained by personal communications with Ping Li, the director of the Scientific Imaging Suite in the Department of Biology at Dalhousie University. The staining procedure we used involved cleaning Petri dishes and tweezers with 70% solution of ethanol and water, and then placing the TEM grids to be stained on the Petri dishes. The TEM grids had been pre-spotted and dried with the nanoparticle solution of interest. Then 10 μ L of 2% weight by volume solution of uranyl acetate was added to each TEM grid for 20 seconds. The uranyl acetate solution was made up in ethanol and dispensed through a syringe to prevent air bubbles. Excess solution was removed from the TEM grids by dabbing the grid edge with a kimwipe. The grids were air dried overnight, and then were ready for imaging.

The images presented below in Figure 3.16 are a series of 5 nm Au, 5 nm Ag, 18 nm Au, and 45 nm AgNPs with either an α -lipoic acid, EGF-linker, or no coating. Uncoated nanoparticle samples were surrounded by borohydride (5 nm Au and AgNPs) or citrate

(18 nm Au and 45 nm AgNPs). All TEM with uranyl acetate stain of gold and silver nanoparticles tagged with α -lipoic acid linked EGF, except for sample f) 5 nm citrate AgNP, show a ring of 1-5 nm around some of the nanoparticles. This ring, which could be α -lipoic acid or EGF protein, was not always present, or of a uniform size. Collapse of the tertiary protein structure from lack of hydration does not seem to account for the discrepancies between the samples. Errors in staining the nanoparticles could have been caused by using the wrong TEM grids, the hydrophobic carbon coated grids would allow the hydrophilic uranyl acetate stain to aggregate in pockets solely around the nanoparticles. Large amounts of stain in one area may penetrate the proteins, as some are hydrophobic. This would leave a small ring around the nanoparticles due to the α -lipoic acid or other hydrophilic material at the nanoparticle surface. With an 80 kV beam of electrons from the TEM, we should only have 1-2 nm resolution of the sample. The electron beam can burn carbon in the sample at high magnification. Also, the carbon in the proteins is difficult to distinguish from that coating the grid substrate. The presence of EGF around the nanoparticles was not confirmed with the uranyl acetate staining TEM experiments.





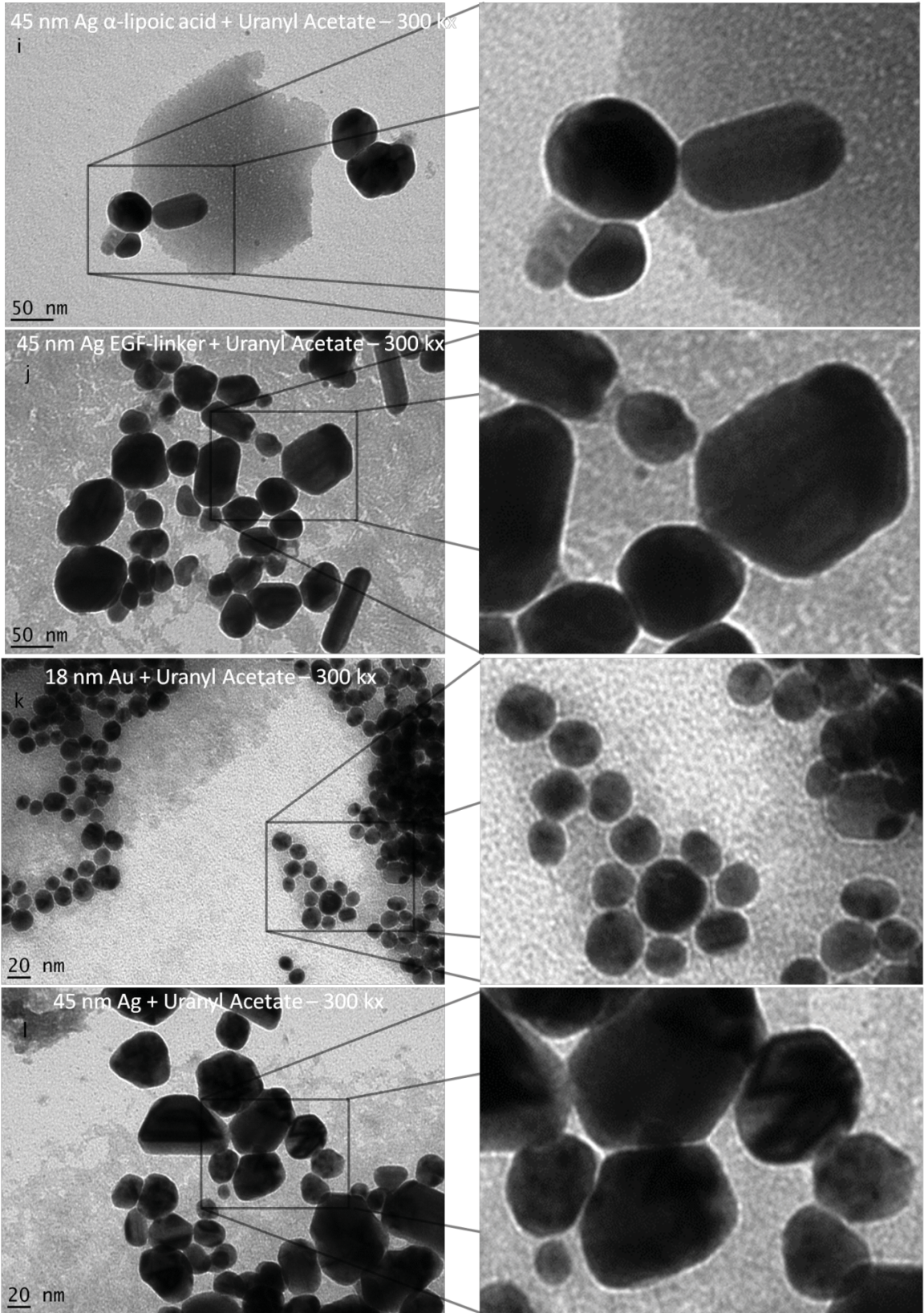


Figure 3.16 TEM images of 5 or 18 nm diameter Au or 5 or 45 nm AgNPs stained with uranyl acetate (UA).

Two magnifications of photos show each type of stained nanoparticle, the initial magnification is at 300 kx, while the zoomed area is 885 kx. As a scale reference for the zoomed panels on the right, the entire width is 355 nm. The samples are: a) 5 nm α -lipoic acid coated AuNPs, b) 5 nm EGF-linker coated AuNPs, c) 5 nm α -lipoic acid coated AgNPs, d) 5 nm EGF-linker coated AgNPs, e) 5 nm borohydride AuNPs, f) 5 nm borohydride AgNPs, g) 18 nm α -lipoic acid AuNPs, h) 18 nm EGF-linker AuNPs, i) 45 nm α -lipoic acid AgNPs, j) 45 nm EGF-linker AgNPs, k) 18 nm citrate AuNPs, l) 45 nm citrate AgNPs. Some samples show bright rings between the nanoparticle and the stain (all but f), however, the ring diameters do not conform to the predicted EGF and α -lipoic acid sizes (3-5 nm and 1 nm). Mistakes in the grid preparation, such as using hydrophobic carbon-only grids, probably caused the stain to pool in large amounts at one area. While the stain is normally repelled by the proteins, some hydrophobic portions could have taken up the stain, since it was in abundance. The bright spots could be any primarily hydrophilic material around the nanoparticles, like the portion of α -lipoic acid bound to the nanoparticles.

3.5.4 Ultraviolet-Visible Spectrophotometry (UV-Vis) Time Course Study

Displayed in Figure 3.17 are the time lapse UV-Vis absorption data for both gold and silver nanoparticles (18 nm and 45 nm, respectively). We add α -lipoic acid at time zero. Within experimental error, we observe no change in the maximum wavelength for the gold nanoparticles (Figure 3.17), whereas the absorbance profile of the silver nanoparticles shifts to longer wavelengths (Figure 3.17). This shift is approximately from 434 to 445 nm (Figure 3.18).

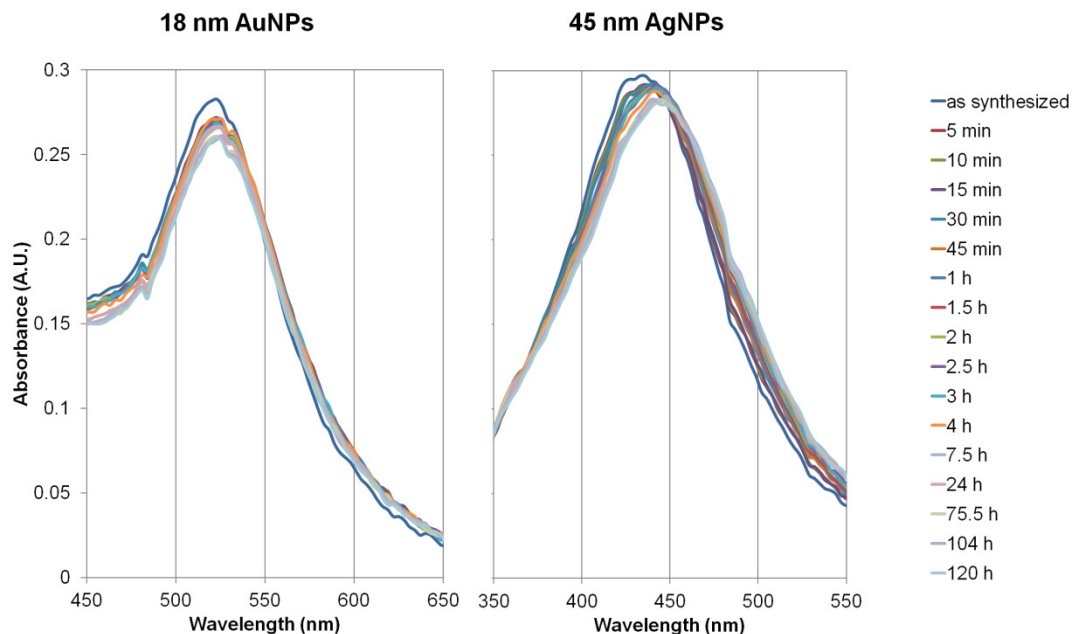


Figure 3.17 Time lapse UV-Vis absorption spectra of gold and silver nanoparticles with α -lipoic acid added at time zero.

Within experimental error, there is no change in the maximum wavelength of the absorption profile over time for the AuNPs. The maximum absorption peak of the AgNPs shifts to longer wavelengths over time.

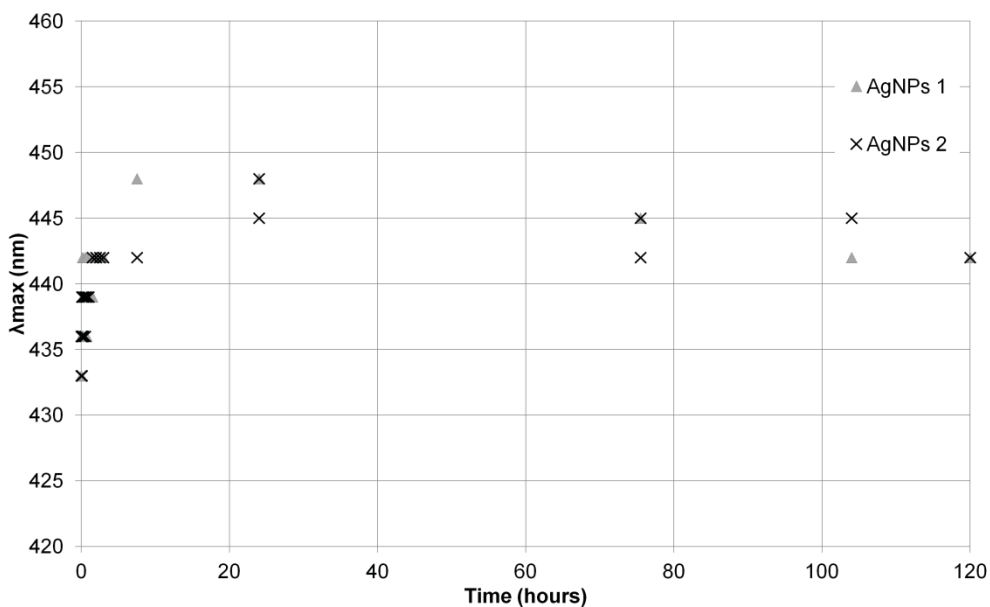


Figure 3.18 The maximum absorbance wavelength (λ_{max}) of silver nanoparticles following α -lipoic acid addition at $t = 0$.

The samples were tested in duplicate. The maximum absorption peak shifts to longer wavelengths upon addition of α -lipoic acid.

3.5.5 Enzyme-linked Immunosorbent Assay (ELISA) for EGF of Human EGF Tagged Nanoparticles

EGF-ELISA allows for assessment of the EGFR binding affinity of EGF, the EGF-linker, and the EGF-linker coated nanoparticles. The EMax microplate reader was used to collect this data. The activity of the EGF-linker bound to nanoparticles at various concentrations is shown in Figure 3.19, and is similar to the standard kit EGF. The 18 nm coated AuNPs did give significant activity (18 nm c EGF-Au 1 and 2, and 18 nm $\frac{1}{2}$ EGF-Au 1 and 2). “c” stands for complete EGF-linker coverage, while “ $\frac{1}{2}$ ” represents half EGF-linker coverage. Nanoparticles with only half the EGF-linker coverage have a slightly decreased response. The nanoparticle samples with the EGF-linker attached were centrifuged using the protocol outlined in Section 3.4.3 and diluted with the appropriate buffer prior to the test. Centrifuging should remove any of the α -lipoic acid conjugated Human EGF which did not attach to the nanoparticles. This seems to be the case. If there was an abundance of EGF remaining in the solution, the detected concentrations would be much higher than those seen with the 18 nm Au samples and we would not have a standard curve. Too much EGF would overload the well plate, the absorbance intensities would oscillate around the maximum observed values.

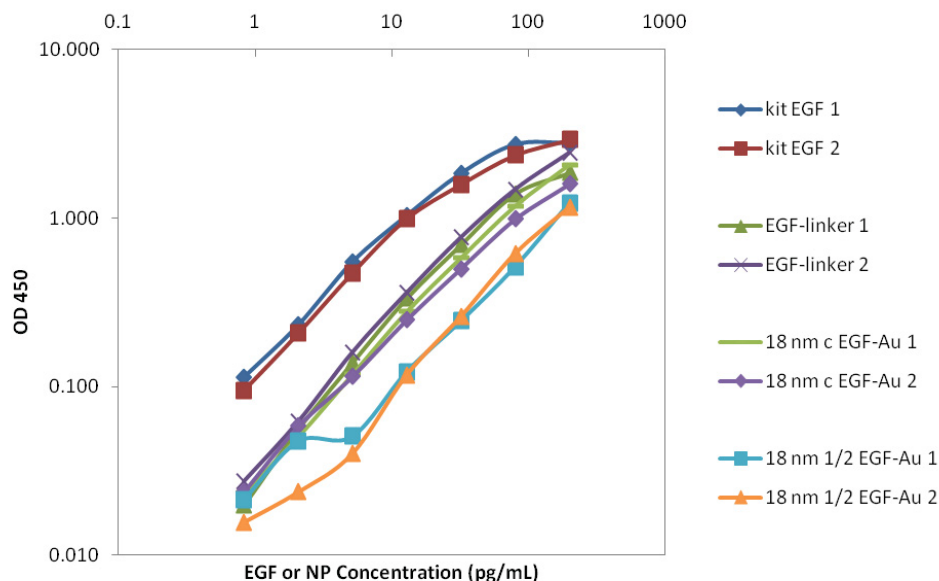


Figure 3.19 EGF-ELISA test of the total EGFR binding response for two concentrations of 18 nm Human EGF-linker and α -lipoic acid coated AuNPs.

The x-axis scale represents the nanoparticle, and not EGF, concentration for the samples containing nanoparticles. The EGF-linker samples are active as they follow the general trend of the kit EGF standard curve. “c” represents complete EGF-linker coverage and “1/2” is for half EGF-linker coverage of the nanoparticles. The nanoparticles with less EGF-linker show a slight decrease in binding affinity. Both EGF-linker coated nanoparticle sample types are active for EGFR.

The ELISA kit uses a sandwich assay detection method, where the EGF binds to a capture antibody on a well plate, and then a detection antibody binds to the plate bound EGF. The concentrations of EGF used in during the test were within the recommended ranges and were on the order of 200 pg/mL down to 0.8 pg/mL. The nanoparticle samples were not added based on the protein which should surround the nanoparticle. Instead, if we assume that only 1 EGF-linker per nanoparticle binds to the well plate, then all the other EGF-linkers coating the nanoparticle would not give a colorimetric response. We can then assume that 1 active EGF-linker per NP, so that the nanoparticle concentration is the limiting factor for the ELISA test. This seemed to be true, as the nanoparticle samples have similar responses as compared to the kit EGF and EGF-linker samples in Figure 3.19. Whereas in previous attempts to measure the EGF-linker concentration on nanoparticles, based on the amount of EGF-linker which should be bound to the

nanoparticles, we did not obtain the expected response with the kit as the high concentration of the EGF-linker did not give the expected standard curve response (Figure 3.20). This test was performed with the Signosis ELISA kit instead of the kit from RayBio. Also, the protein dilutions for the Signosis kit were slightly different and ranged from 2000 pg/mL to 31.3 pg/mL. The x-axis scale of the subsequent nanoparticle containing samples were adjusted as the response is not based on the EGF concentration, but on the nanoparticle concentration (Figure 3.19).

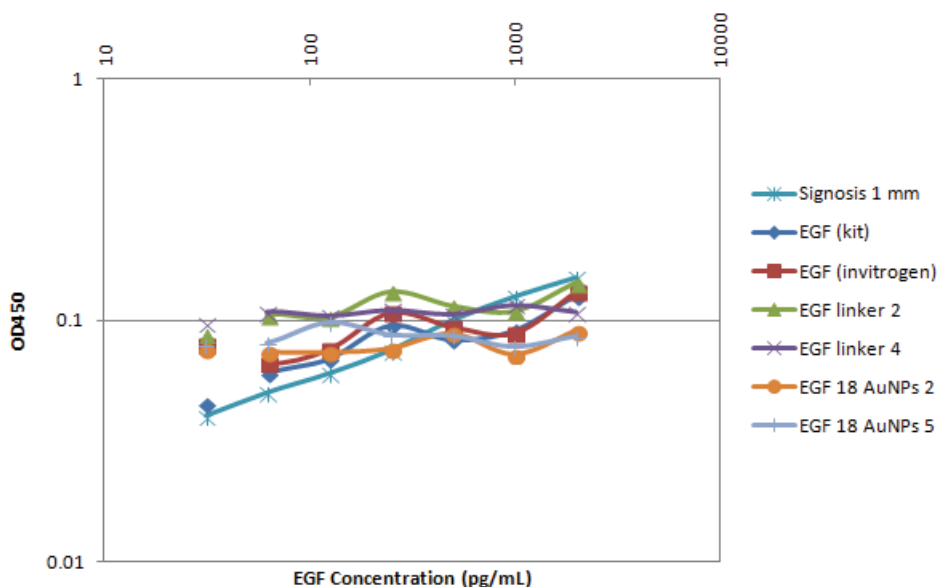


Figure 3.20 EGF-ELISA determination of the total EGFR binding response for 18 nm Human EGF-linker and α -lipoic acid coated AuNPs.

The Signosis ELISA kit was used for this test instead of RayBio the kit. One of the first ELISA tests performed, the concentration of EGF on the nanoparticles was used for the dilutions. The nanoparticle concentration was used to determine the dilution concentrations for the other tests in Figure 3.19 and Figure 3.21. The EGF concentration does not seem to decrease as would be expected in a standard curve for the 18 nm AuNP samples, while the EGF-linker samples decrease slightly.

The 45 nm EGF-linker AgNPs gave a slightly weaker response as compared to the 18 nm EGF-linker AuNPs, EGF-linker, and the kit EGF (Figure 3.21). We may be able to attribute the reduction in response to the large diameter of the 45 nm AgNPs blocking adjacent well plate binding sites, reducing the maximum response attainable

from the test. The small nanoparticles did not give repeatable results, and did not always seem to be active (Figure 3.21). There is a plausible reason for this observation. Larger proteins wrap around small nanoparticles, as they are not repelled by the surface, this can hide the active EGFR binding site. The 5 nm Ag EGF-linker 1 sample did not follow the expected standard curve trend. The 5 nm Ag EGF-linker 2 sample gave absorbance values near zero, which do not show up on the plot and indicate that the EGF-linker did not bind to the well plate.

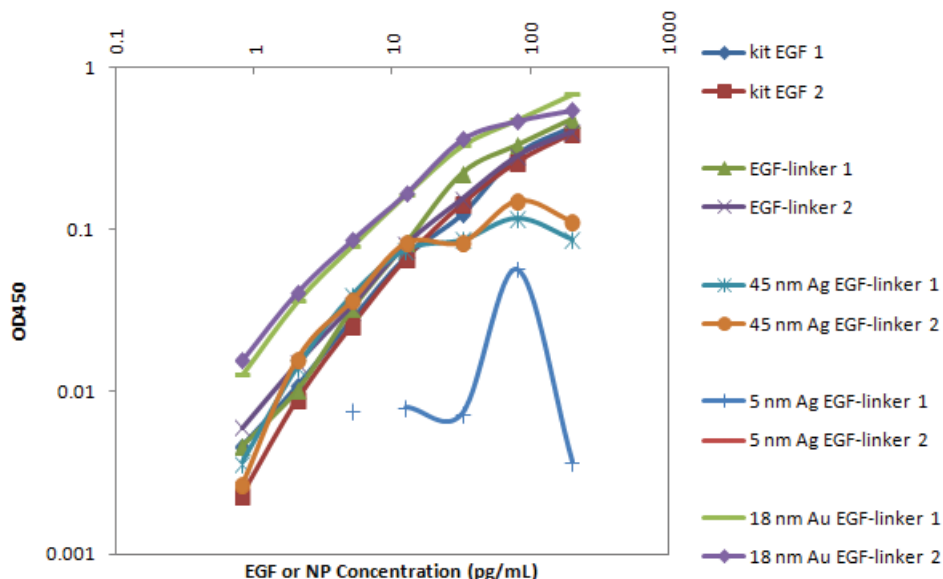


Figure 3.21 EGF-ELISA test of the total EGFR binding response EGF-linker and 18 nm Au, 5 nm Ag, and 45 nm Ag nanoparticle samples coated with Human EGF-linker and α -lipoic acid.

The EGF-linker and 18 nm Au and 45 nm AgNPs tagged with EGF-linker all gave similar responses to those seen from the kit EGF and were active for EGFR. The 5 nm AgNPs coated with EGF-linker did not give optical absorbance responses near the standard kit EGF and were not reproducible. The responses for the 5 nm AgNP EGF-linker 2 sample were near zero.

3.5.6 Zeta Potential

The zeta potential was tested for gold and silver nanoparticles to ensure their stability. Stability depends on the surface charge of the nanoparticles, stability at alkaline

pH means that the particles have negative surface charges, this also means these particles aggregate at low pH. Stability at acidic pH infers positive surface charge, and that the nanoparticles aggregate at high pH.

In addition to stability in salt solution, nanoparticle stability was assessed through the zeta potential for gold and silver nanoparticles with a variety of coatings. The coatings were α -lipoic acid, or EGF-linker with α -lipoic acid to fill in any gaps in the coordination sphere. As stated earlier, a zeta potential below -30 mV or above 30 mV implies particle stability. A summary of the zeta potential values is available in Table 3.5. Both the 5 and 45 nm AgNPs were not stable upon addition of the pH 7.4 10 mM PBS, while the 18 nm AuNPs were.

Table 3.5 Zeta potentials of a variety of nanoparticle types.

Type of NP	5 nm Ag	18 nm Au	18 nm Au	45 nm Ag	45 nm Ag
Coating (aLA = α -lipoic acid)	EGF + aLA, aLA	EGF + aLA, aLA	aLA	EGF + aLA, aLA	aLA
Zeta potential (mV)	-31.47	-38.71	-43.09	-36.45	-39.06
Zeta potential after 1:1 pH 7.4 10 mM PBS (mV)	-0.4299	-35.43	-31.90	0.1432	0.3630

3.5.7 Raman of EGF-linker or α -lipoic Acid Coated Nanoparticles

Raman data of nanoparticles were collected from the T64000 spectrometer at Dalhousie. The samples were not sterilized by filtration, but excess Human EGF was removed from the nanoparticles using the method outlined in Section 3.4.3.

20 μ L of 33 pM nanoparticle solution were mixed with 20 μ L MgSO₄ just prior to measurement, to replicate aggregation of nanoparticles on cells *in vivo*. The nanoparticles were imaged with the 150 grooves/mm grating and a 50X LWD lens at a 633 nm laser excitation. 2 scans were averaged over 5 s for each measurement. Figure 3.22 shows the nanoparticle samples. The SERS response from the α -lipoic acid conjugated EGF 45 nm AgNPs was greatest, followed by the α -lipoic acid conjugated EGF 5 nm AgNPs and then the α -lipoic acid coated 45 nm AgNPs. The 5 nm and 18 nm AuNPs, coated with either

the α -lipoic acid conjugated EGF or simply α -lipoic acid, gave little SERS response. It is possible that the 45 nm AgNPs aggregates which are responsible for the SERS signal could have simply been larger than the silver ones, since the nanoparticles are larger to begin with. Alternatively, more intense SERS signals could have been observed from the 45 nm AgNPs because these nanoparticles have more facets and corners, as observed from the TEM data in Sections 3.3.1 and 3.5.3.

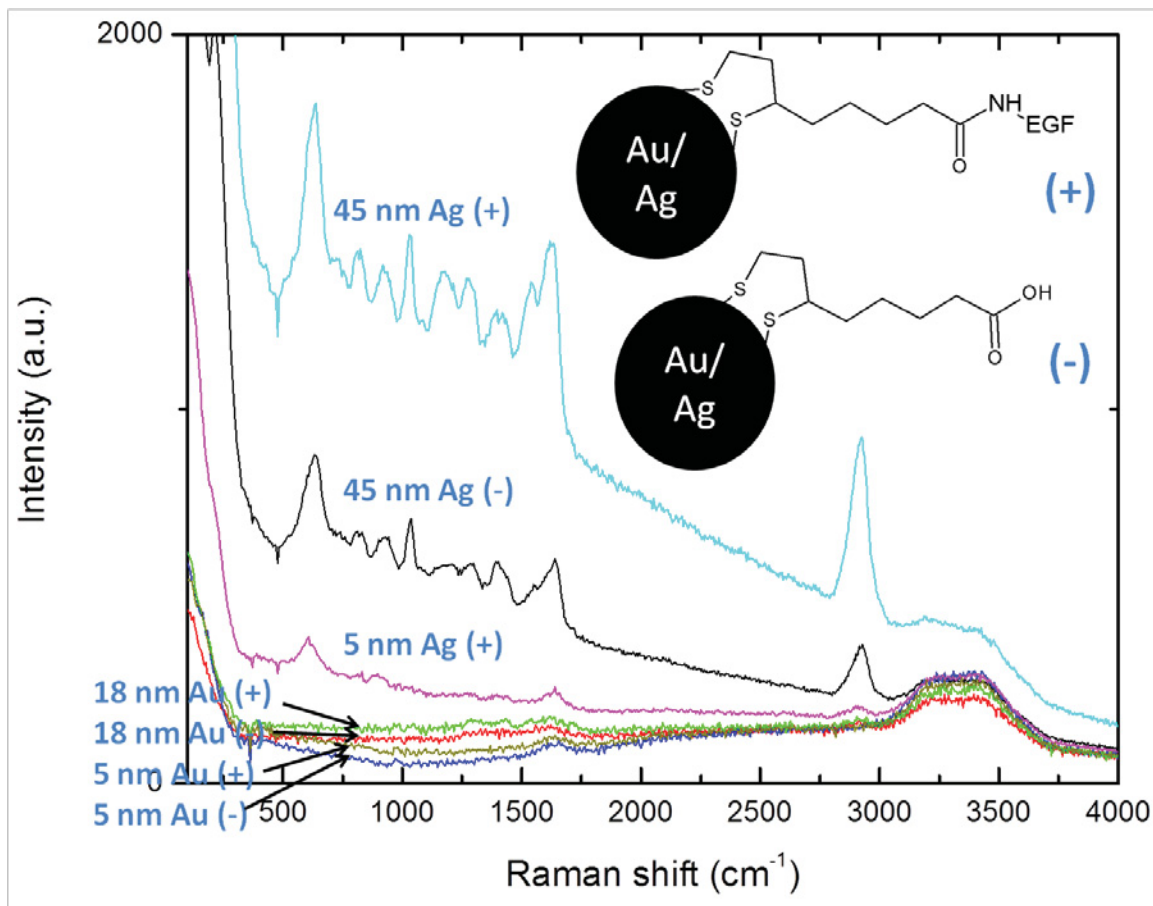


Figure 3.22 Raman spectroscopy of 5 nm Au, 18 nm Au, 5 nm Ag, and 45 nm Ag nanoparticle samples coated with α -lipoic acid conjugated Human EGF (+) or α -lipoic acid (-) and aggregated with 100 mM MgSO_4 (Dalhousie).

A 1:1 ratio of MgSO_4 aggregated the nanoparticle solutions just prior to measurement. Samples were imaged with a 50X LWD lens and a 633 nm laser. 5 scans were averaged over 10 s for each measurement. The 45 nm AgNPs gave the most SERS, followed by the 5 nm AgNPs. Regardless of the coating, the 5 nm and 18 nm AuNPs did not show much SERS.

Figure 3.23 shows repetition of the data collection of the Raman spectra of nanoparticles artificially agglomerated with MgSO_4 . The α -lipoic acid samples were measured in solution and as the dry powder, the α -lipoic acid in solution has fewer spectra features. Aggregated 45 nm AgNPs coated with either α -lipoic acid conjugated Human EGF or α -lipoic acid gave strong SERS signals. The 45 nm AgNPs tagged with EGF gave the most SERS of the nanoparticle samples. Raman shifts at 3000, 1500, and 1000 cm^{-1} from both SERS active 45 nm AgNP samples generally match peak positions of the in solution α -lipoic acid spectra, although nanoparticle spectra show broadening. The 45 nm AgNPs with a citrate coating did not show SERS. As well, the 18 nm AuNPs coated with citrate, α -lipoic acid conjugated Human EGF, or α -lipoic acid lacked SERS. We expect to see the α -lipoic acid features, present in the 45 nm AgNPs coated with α -lipoic acid conjugated Human EGF, when imaging nanoparticles in cells or tissues.

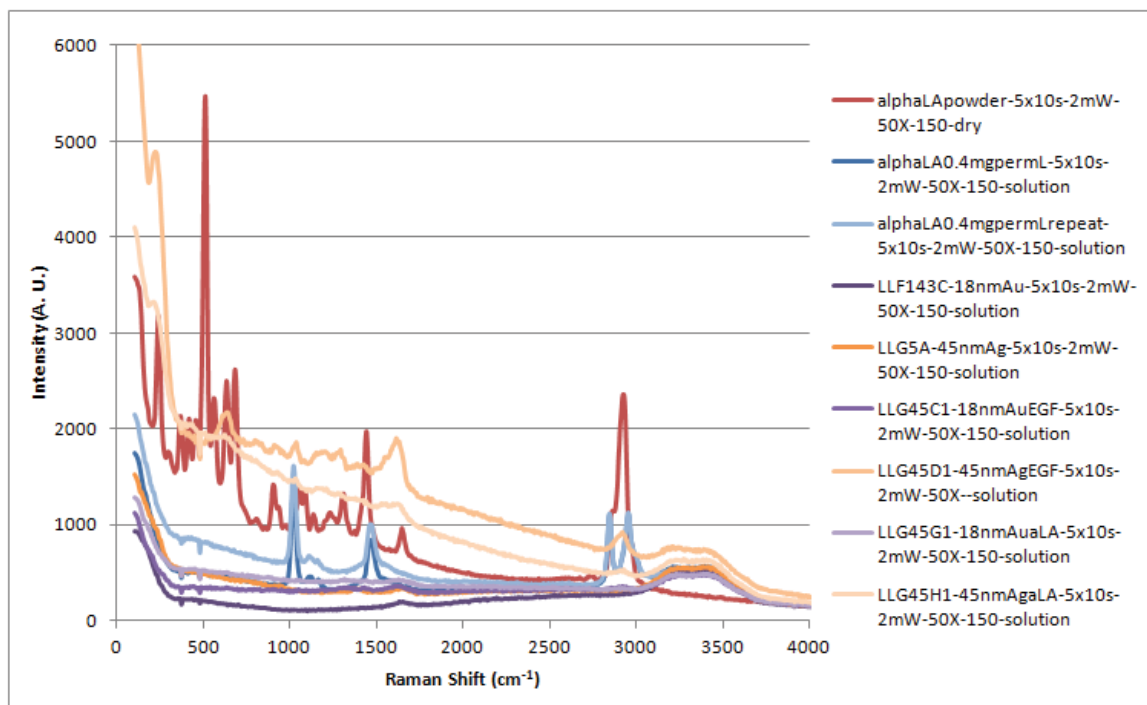


Figure 3.23 Raman spectroscopy of 18 nm Au and 45 nm Ag nanoparticle samples coated with citrate, α -lipoic acid conjugated Human EGF, or α -lipoic acid and then aggregated with 100 mM MgSO_4 (Dalhousie).

A 1:1 ratio of MgSO_4 aggregated the nanoparticle solutions just prior to measurement. Samples were imaged with a 50X LWD lens and a 633 nm laser. 5 scans were averaged over 10 s for each measurement. The α -lipoic acid samples were measured in solution and as a dry powder, the solution

spectra lose many features. Both the α -lipoic acid conjugated Human EGF and the α -lipoic acid coated 45 nm AgNPs aggregated samples gave SERS. The 45 nm AgNPs tagged with EGF gave the most SERS of the nanoparticle samples. The peaks near 3000, 1500, and 1000 cm^{-1} from the SERS positive 45 nm AgNP samples match the in solution α -lipoic acid spectra, although the peaks in the nanoparticle spectra are broader. The 18 nm AuNPs were coated with citrate, α -lipoic acid conjugated Human EGF, or α -lipoic acid. All three samples, and the 45 nm AgNPs with a citrate coating, did not show SERS.

The best spectral enhancement from SERS occurs by tuning the laser wavelength to the plasmon absorbance wavelength of the nanoparticles from UV-Vis. As the nanoparticles aggregate or form assemblies on cell surfaces, the plasmon red-shifts. For ~ 30 nm gold nanoparticles, the plasmon starts at 520 nm for nanoparticles in solution and shifts to 650 nm for nanoparticles on cells [41].

3.5.8 Summary of EGF-Nanoparticle Characterization Techniques

The EGF-nanoparticle characterization techniques show that the nanoparticles are stable at increased salt content. TEM with UA gives rings of similar diameter around both α -lipoic conjugated EGF and α -lipoic acid only coated nanoparticles, which does not confirm the presence of EGF. Upon α -lipoic acid addition, the plasmon absorbance wavelength is constant over time for the 18 nm gold nanoparticles, but shifts to higher wavelengths for 45 nm silver nanoparticles. The α -lipoic acid conjugated Human EGF bound to 18 nm and 45 nm nanoparticles is still active for the EGFR. Zeta potentials of the α -lipoic acid conjugated Human EGF 5 and 45 nm AgNPs were not stable after 10 mM PBS addition, while the α -lipoic acid conjugated Human EGF 18 nm AuNPs were. Raman measurements of nanoparticles showed the most intense SERS response for the α -lipoic acid conjugated EGF 45 nm AgNPs, followed by the α -lipoic acid conjugated EGF 5 nm AgNPs and the α -lipoic acid coated 45 nm AgNPs. The spectra features roughly matched those of the α -lipoic acid solution. Insignificant SERS response was seen from the 5 nm and 18 nm AuNPs, coated with either the α -lipoic acid conjugated EGF or α -lipoic acid. Next, we will look at *in vitro* imaging of A431 cancer cells with dark field microscopy and Raman spectroscopy.

3.6 *IN VITRO* CELL IMAGING

3.6.1 Dark Field Microscopy of A431 Cells with α -lipoic Acid Control of EGF-linker Active Nanoprobes

The four images in Figure 3.24 are of A431 cells incubated with 18 nm AuNPs, or 45 nm AgNPs coated with α -lipoic acid/EGF-linker. The nanoprobes and cell structures do not seem to be present in the nucleus, which is expected as the EGFR should be engulfed into endosomes and lysosomes [9]. Light scattering from silver α -lipoic acid/EGF-linker coated nanoprobes (Figure 3.24 a and c, Figure 3.25 b and e) seems less intense than the gold (Figure 3.24 b and d, Figure 3.25 c and f). If some scattering is from the nanoparticles, this could be explained by the halogen lamp used for illumination, as it lacks some wavelengths necessary to excite the silver particles. Additional images in Figure 3.25 represent A431 cells incubated with 50 mM HEPES buffer (negative control), 18 nm AuNPs, or 45 nm AgNPs coated with α -lipoic acid (positive controls). The control cells incubated with the buffer (Figure 3.25 a and d) do not look very different from the cells with the control or active nanoparticles. All contain bright spots at the surface and interior of the cells. Dark field does not confirm the activity or specificity of the EGF-linker/ α -lipoic acid coated NPs. These nanoparticle samples were not sterilized with any method prior to use with the A431 cancer cells, but excess α -lipoic acid conjugated Human EGF was removed using the protocol in Section 3.4.3.

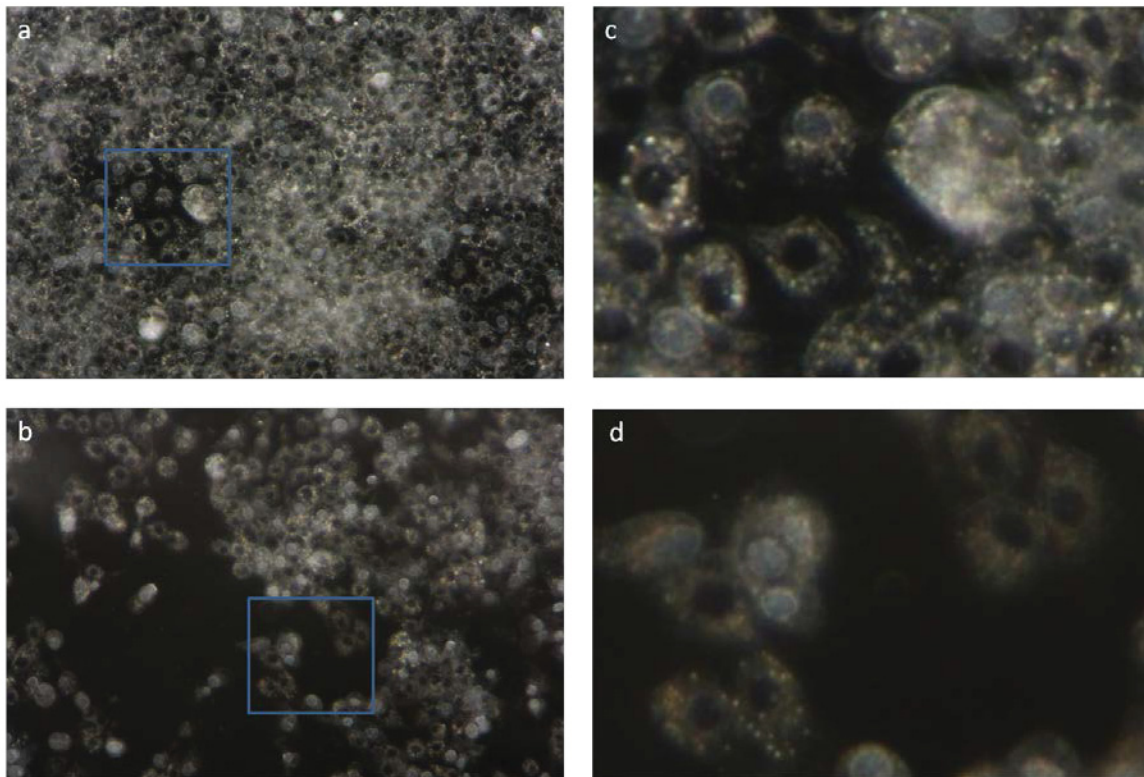


Figure 3.24 Dark field microscopy of A431 (cancer) cells following 30 minute incubation with α -lipoic acid/EGF-linker coated Au- or Ag-based nanoprobes. Images were obtained using a 20X objective lens and a 12.2 MP Canon XSi DSLR. The incubation medium contained: a. 12.5 nmol (75 X) of 18 nm AuNPs, or b. 16.2 nmol (96 X) of 45 nm AgNPs. Enlarged sections are from the blue boxes and are displayed as: c. magnification of 18 nm AuNPs from a, and d. magnification of 45 nm AgNPs from b.

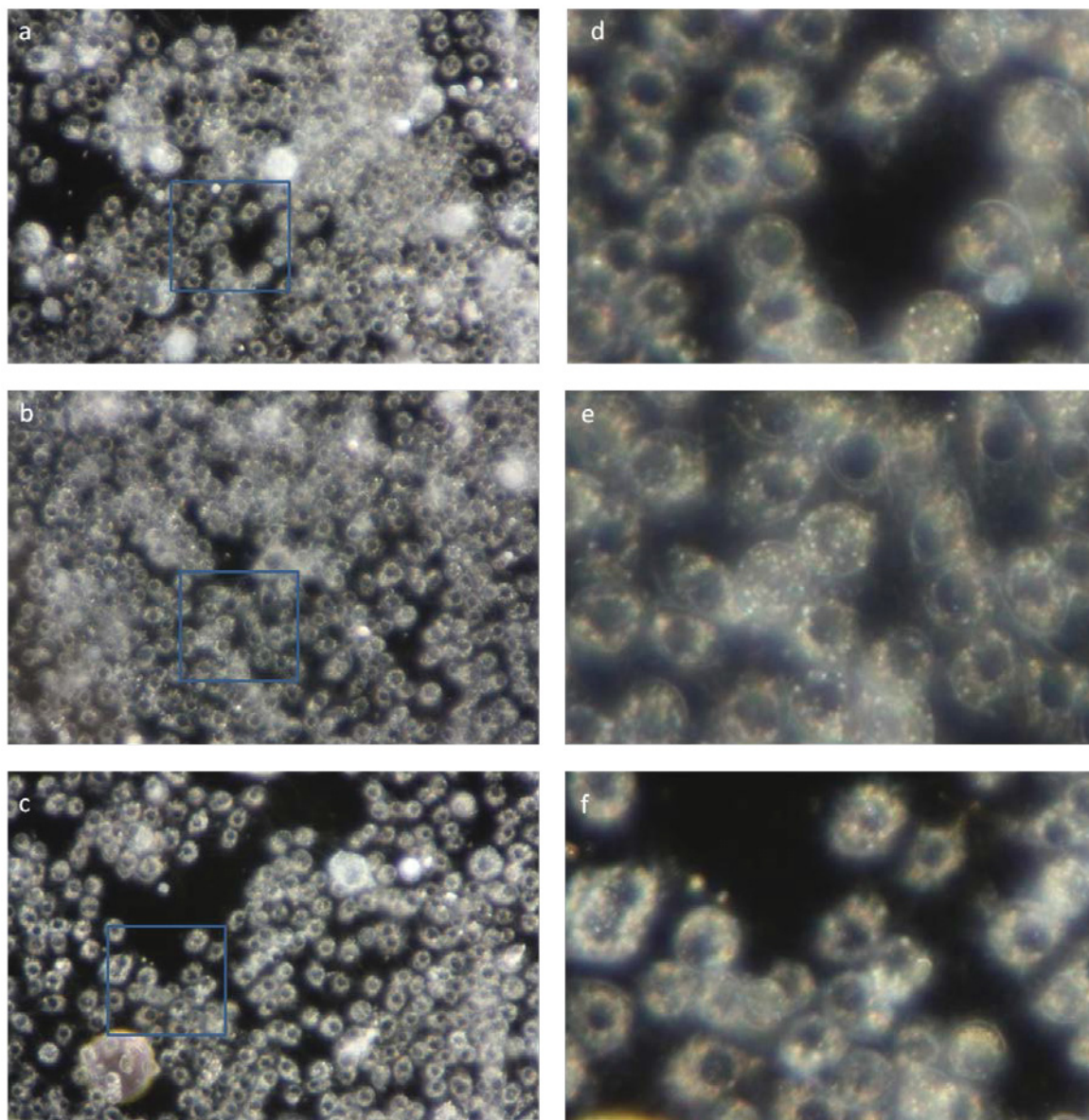


Figure 3.25 Dark field microscopy of A431 (cancer) cells following 30 minute incubation with 50 mM HEPES buffer or α -lipoic acid coated Au- or AgNP. Images were obtained using a 20X objective lens and a 12.2 MP Canon XSi DSLR. The incubation medium contained a. 50 mM HEPES buffer, b. 12.5 nmol (75 X) of 18 nm AuNPs, or c. 16.2 nmol (96 X) of 45 nm AgNPs. Enlarged sections from the blue boxes correspond to: d. magnification of control cells in buffer from a, e. magnification of 18 nm AuNPs from b, and f. magnification of 45 nm AgNPs from c.

Dark field microscopy *in vitro* studies of A431 cancer cells exhibited similar scattering from cytoplasmic structures following incubation with EGFR-active or EGFR-

inactive nanoprobe, as well as without nanoprobe, which implies the scattering is not nanoprobe dependent but rather-inherent to the cell. The bright spots seen with dark field microscopy could be due to lipid pockets. More conclusive identification of these bright spots on the cells may be determined by Raman spectroscopic lipid signatures (eg. CDFH-DA to measure the reactive oxygen species) or by fluorescence imaging with a lipid sensitive probe (eg. BODIPY or Nile Red). Bright spots on the A431 cells caused by lipids seems more likely than if they were the result of using 50 mM HEPES buffer instead of MEM alpha cell medium for incubation. It was thought that the lower salt content of the HEPES buffer could have promoted the cells to engulf more vesicles because the cells were not at optimal conditions, however, repeat dark field microscopy experiments with cells incubated with nanoparticles in MEM α cell medium very showed similar bright spots on the cells (data not shown). Negative results from the dark field microscopy are because the images need to be processed to extract scattering information from the nanoparticles [90]. Image processing involves taking the ratio of the intensities in the RGB channels to isolate the signals from gold and silver nanoparticles.

3.6.2 SERS of A431 cells with Active EGF-linker or Control α -lipoic Acid Nanoprobes

Raman spectroscopy tells about the molecules present in by measuring bond vibrations from laser light shining on a sample. Using metal nanoparticles, the signals should be enhanced to give SERS. The TEM with uranyl acetate staining in Figure 3.16, even though the staining was flawed, the images tell us about the quality of SERS we should expect from the different nanoparticle sizes. The nanoparticles, especially 45 nm AgNPs, are faceted which should give brighter SERS signals, as sharp corners and angles amplify the SERS signal.

Bulk Raman measurements of cells were attempted with a 5X low magnification objective and the 785 nm laser. These nanoparticles were not sterilized before tagging the cells for imaging. The A431 cancer cell pellets images were obtained with the Renishaw Raman spectrometer at Stanford (Figure 3.26). More SERS seemed visible from the 45 nm α -lipoic acid linked EGF nanoparticles than the control cells with no EGF-linker.

Experiments undertaken to replicate the signals seen involved imaging cells spread on the glass bottom Petri dish with a scan encompassing many cells using the Renishaw Raman spectrometer streamline scanning mode. Upon repetition of the imaging (data not shown) and inspection of the data, no SERS was observed. It appears that the signals from Figure 3.26 were not from the cells, or the nanoparticles, but were instead caused by the polymer cryovials used to freeze and ship the cells. Repeat attempts to image with fresh cells were undertaken at Dalhousie. It is possible that increased incubation times of the cells with the nanoparticles, from 30 minutes to 1 or more hours could cause more nanoparticles to be engulfed and allow the cells to be seen with Raman spectroscopy.

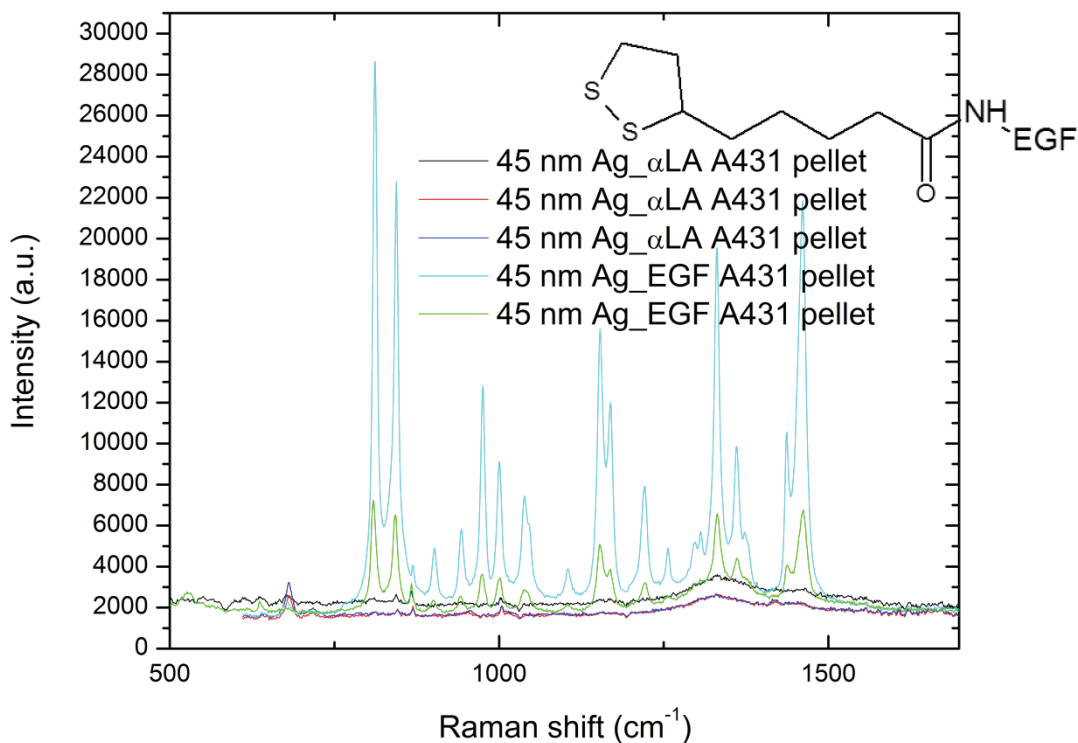


Figure 3.26 Raman of A431 cancer cell pellets following 30 minute incubation with α -lipoic acid/EGF-linker coated AgNPs (Stanford).

Samples were imaged with a 5X lens and a 785 nm laser for 10 s and averaged over 5 scans. What appeared to be SERS enhancement was seen from the 45 nm α -lipoic acid linked Human EGF nanoparticles attached to cells. These spectra looked different from those of positive control cells incubated with α -lipoic acid coated 45 nm AgNPs. Repeat experiments showed that SERS was not apparent. The signal from the cells tagged with 45 nm α -lipoic acid linked

Human EGF nanoparticles likely were caused by the polymer tubes used to freeze the cells.

Bulk Raman measurements were attempted at Dalhousie University with freshly tagged cells, reduce interfering Raman signals from the cryovials used to freeze and ship the cells. These nanoparticles were sterilized by filtration before use (Section 2.7). A 20X lens was to be used to see many cells for the bulk measurements. Upon calibration, it was discovered that the signal intensity of the Si standard was poor. The internal optics of the instrument were calibrated for the 50X LWD and the 100X lenses, recalibration was not possible in the short amount of imaging time available after the cells were tagged. A 633 nm laser at 3 mW power was used and the grating was 150 grooves/mm. A 50X LWD lens was used for imaging, each sample was measured for 20 s and averaged over 4 scans. Individual points on cells were manually imaged instead of the bulk measurement, about 20 spectra were collected per cell. Post-processing of the data included removing the fluorescence background with the Vancouver Raman Algorithm. No SERS was observed for A431 cancer cells tagged with or without the α -lipoic acid linked EGF 45 nm nanoparticles (Figure 3.27). It was unlikely that SERS would have been observed, as the cell maps were not collected and we know that only 1 in 10^6 photons are Stokes Raman scattered. These measurements were not bulk measurements, because of the high magnification used. It is not known if SERS would have been observed if a lower power objective could have been used. The Human EGF coated α -lipoic nanoparticles did not appear to have more SERS intensity than the α -lipoic acid coated ones. Both types of cells seemed to have some slight features from the MEM α medium, possibly because the medium was in abundance around the cell.

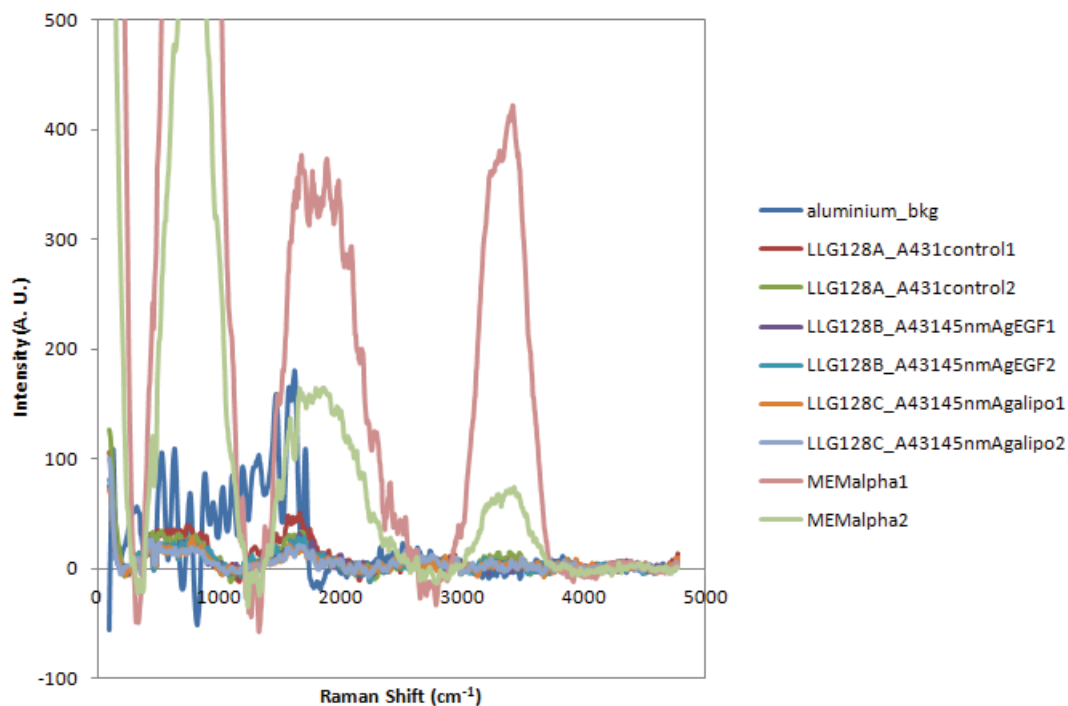


Figure 3.27 Raman of A431 cancer cell pellets following 30 minute incubation with α -lipoic acid/EGF-linker coated AgNPs (Dalhousie).

A 50X LWD lens was used at 20 s, each spectrum is an average of 4 scans. A 633 nm laser at 3 mW power was used and the grating was 150 grooves/mm. The fluorescence background was subtracted from the images with the Vancouver Raman Algorithm. No SERS enhancement was seen from the cells, the cells containing α -lipoic acid only and EGF-linker tagged nanoparticles look similar. Also, the all the cell spectra seem to contain some of the broad peaks from the medium, although it is less intense as the medium is near the cells and should not be at focus of the laser.

3.6.3 *In Vitro* Cell Imaging Summary

Dark field microscopy was not adequate for assessment of the specificity of the EGF-linker gold and silver nanoparticles by *in vitro* cell imaging as was performed above, post-processing of the photos is necessary to extract the nanoparticle signals. Inherent signal intensities, possibly due to lipid droplets, were present in all cells. Bulk Raman spectroscopy measurements performed at Stanford did not show signals from the nanoparticles within the cells, but of the plastic tubes used for their transport. Bulk measurements of cells could not be performed at Dalhousie, as the instrument was not

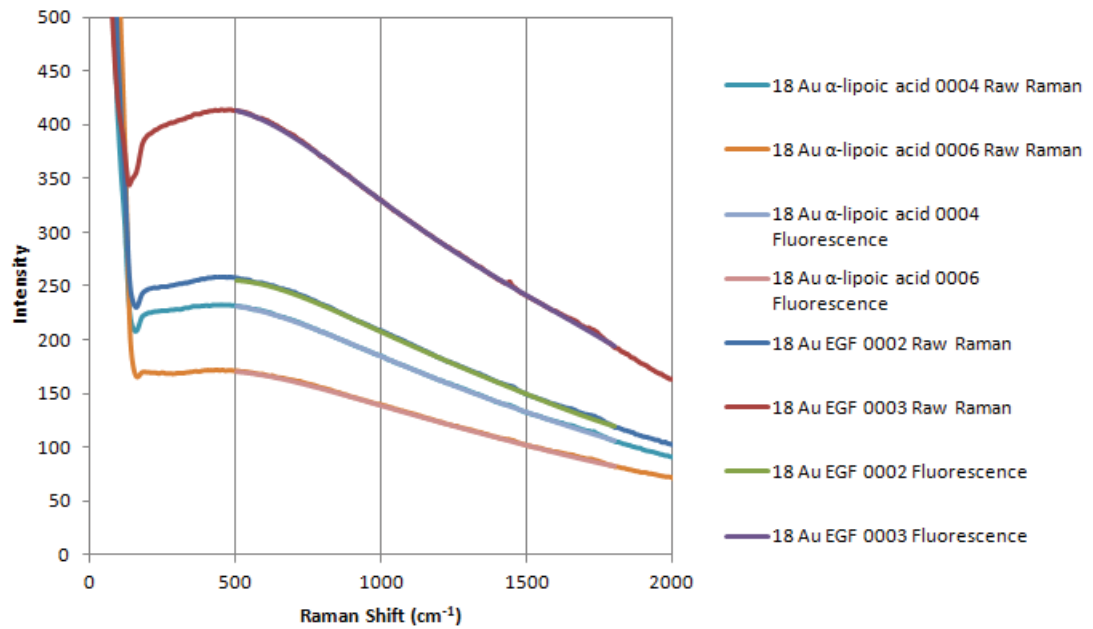
calibrated for a low powered objective. The Raman spectra collected were not different between the A431 cancer cells tagged with EGF-linker or α -lipoic acid, and did not show SERS.

3.7 *EX VIVO* BIODISTRIBUTION

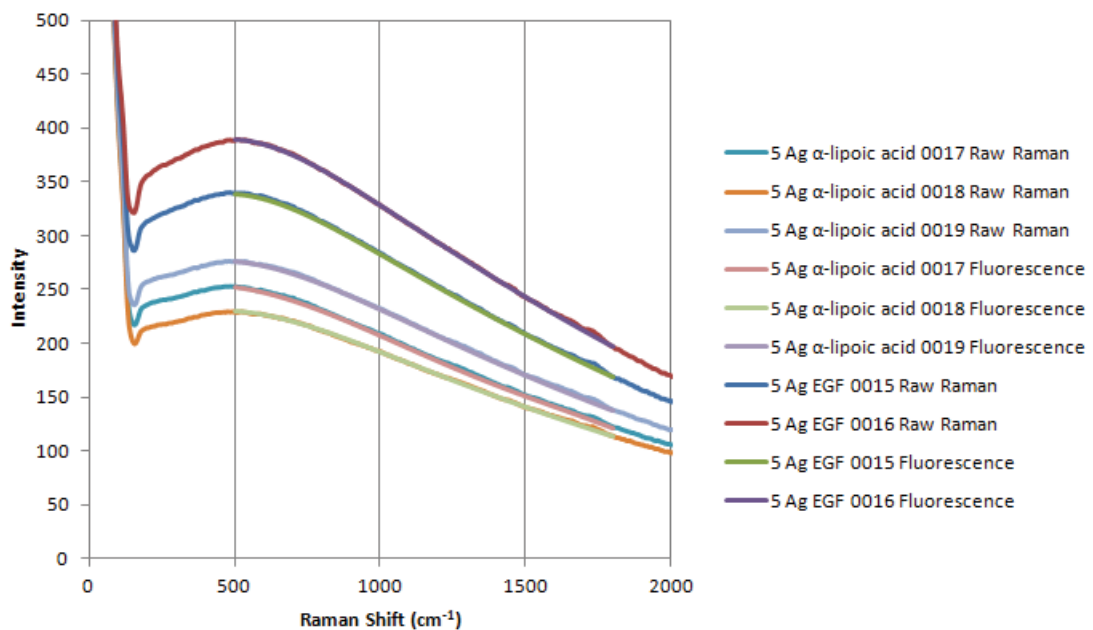
3.7.1. Raman of Mouse Tissues

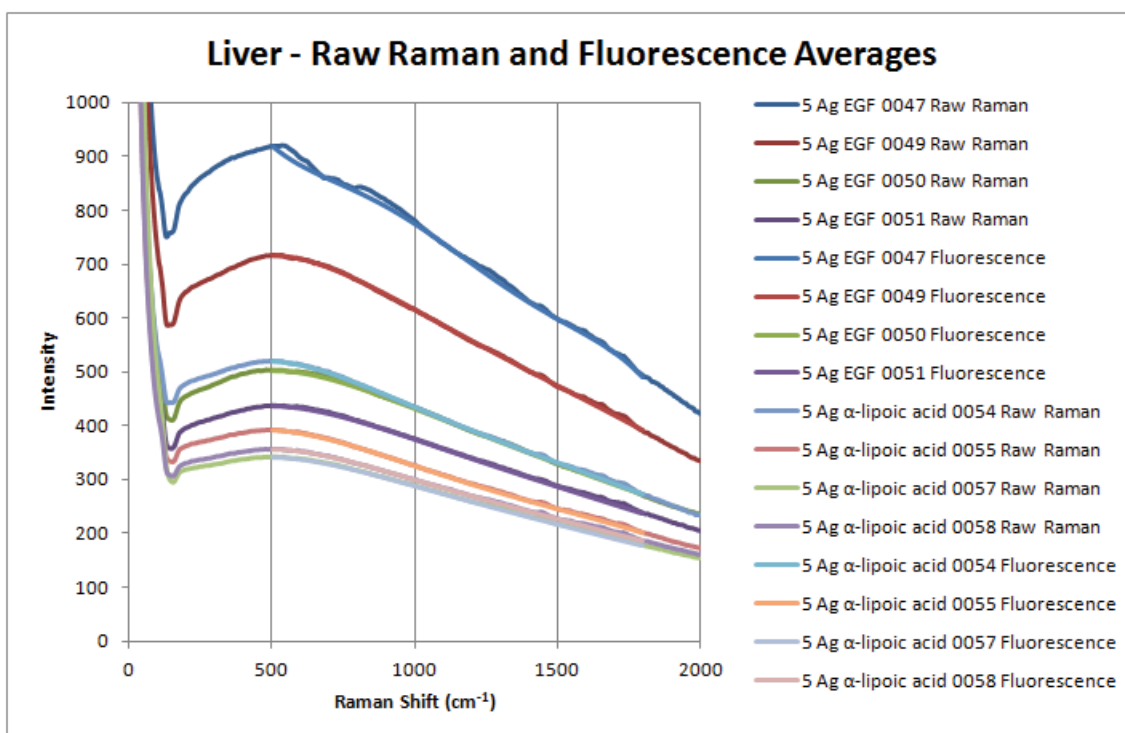
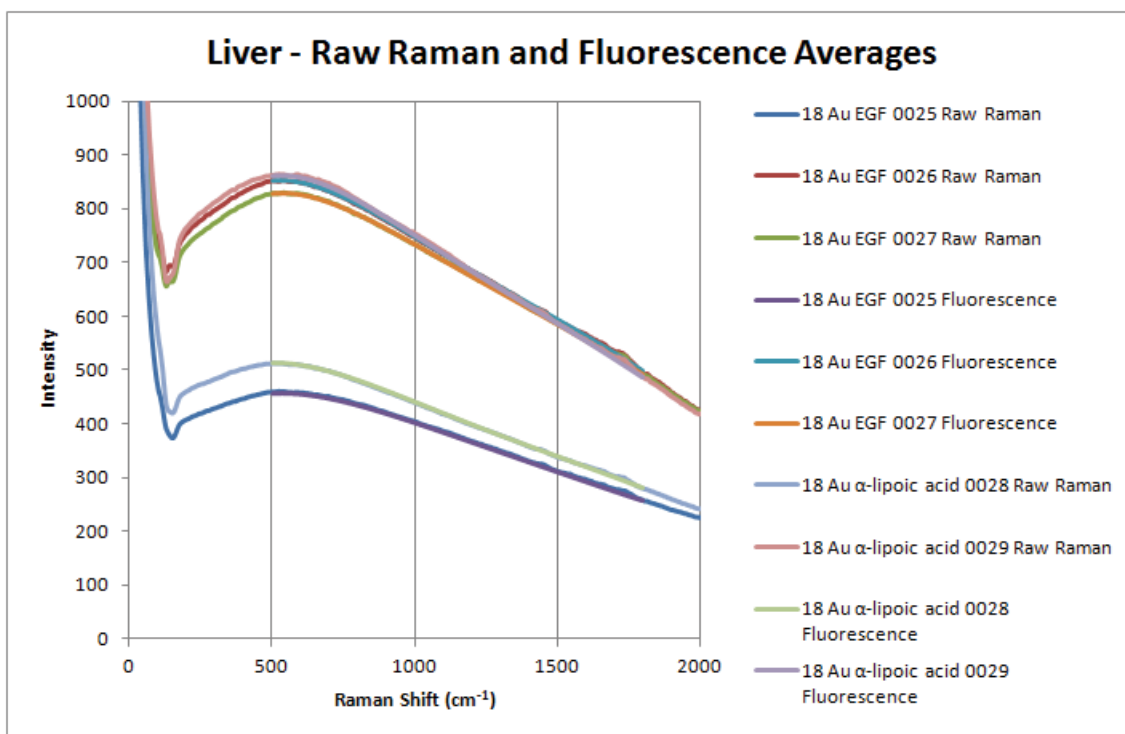
Figure 3.28 shows the initial Raman spectra, as well as the fluorescence background subtraction spectra from the Vancouver Raman Algorithm program. Raman spectra of mice kidneys, liver, and spleen, in Figure 3.29, did not show significant Raman signals and definitely did not exhibit SERS when imaged with a 785 nm laser using the Raman spectrometer outlined in Section 2.9.3 at the BCCA. The spectra were of two distinct injections, 18 nm AuNPs or 5 nm AgNPs, and these nanoparticles were coated with the α -lipoic acid conjugated Human EGF or simply α -lipoic acid. These spectra were compared to a control spectra obtained from mouse injected with a solution of 0.9% sterile saline. For all three tissue types, each spectrum is average of 3 scans. The kidney and liver data were collected with a 1 second exposure time. The intensity of the signals from the spleen required shorter exposure times of only 0.1 seconds. The mouse spleen spectra were generally 10 orders of magnitude more intense than those of the kidneys and 3 times more intense than the liver tissues. Some of the signals in Figure 3.29 may be artificial as a result of the background subtraction process.

Kidney - Raw Raman and Fluorescence Averages



Kidney - Raw Raman and Fluorescence Averages





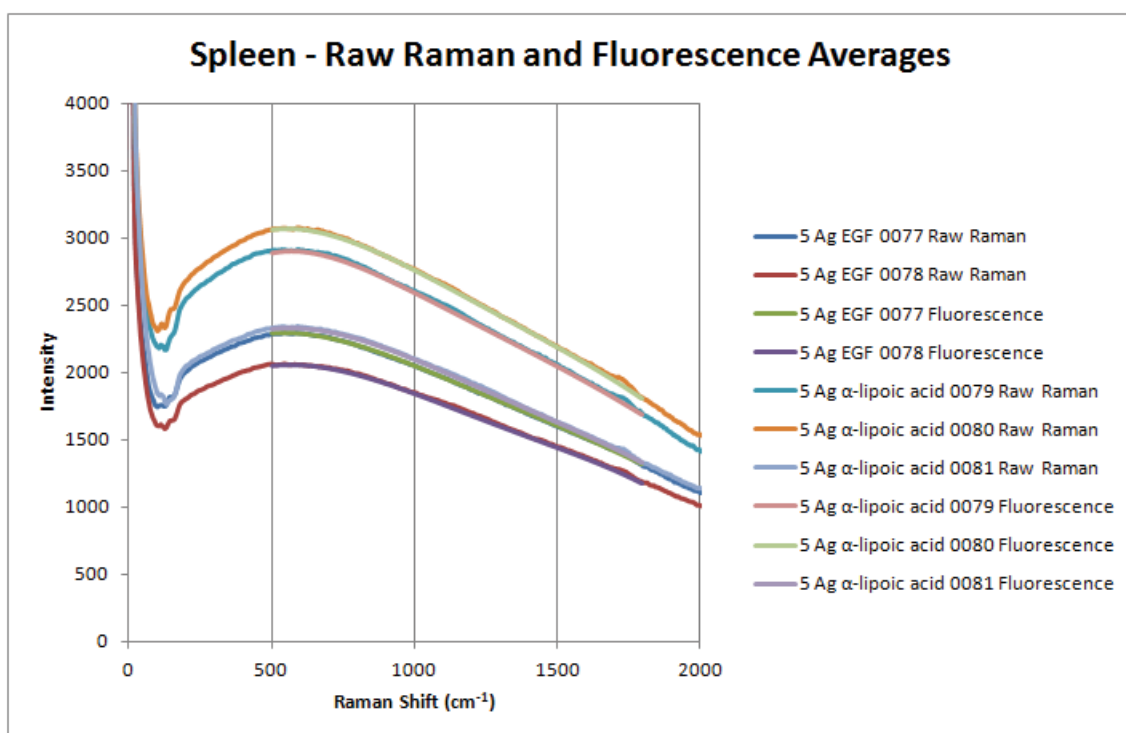
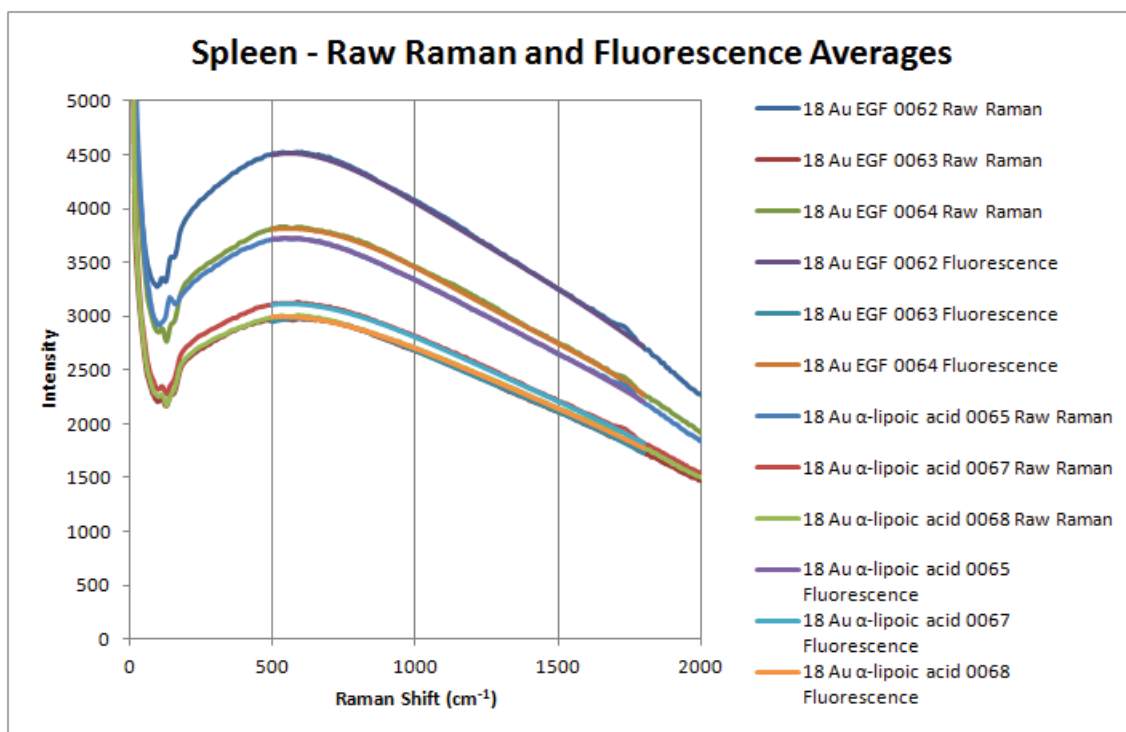
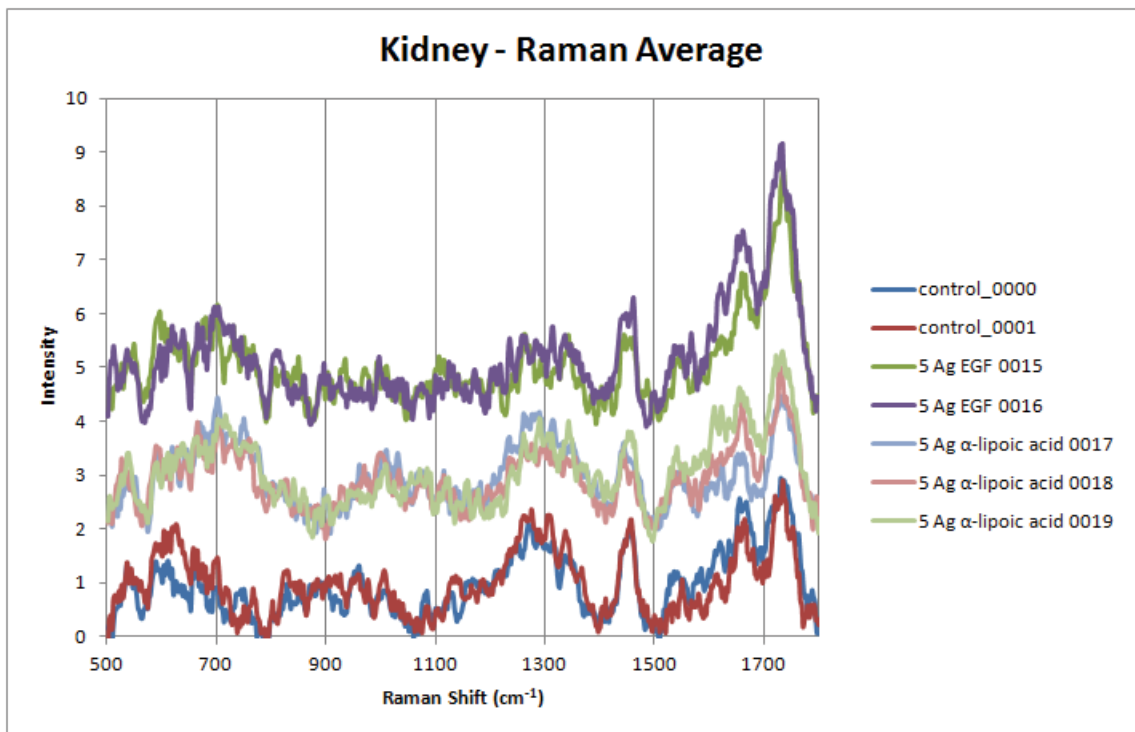
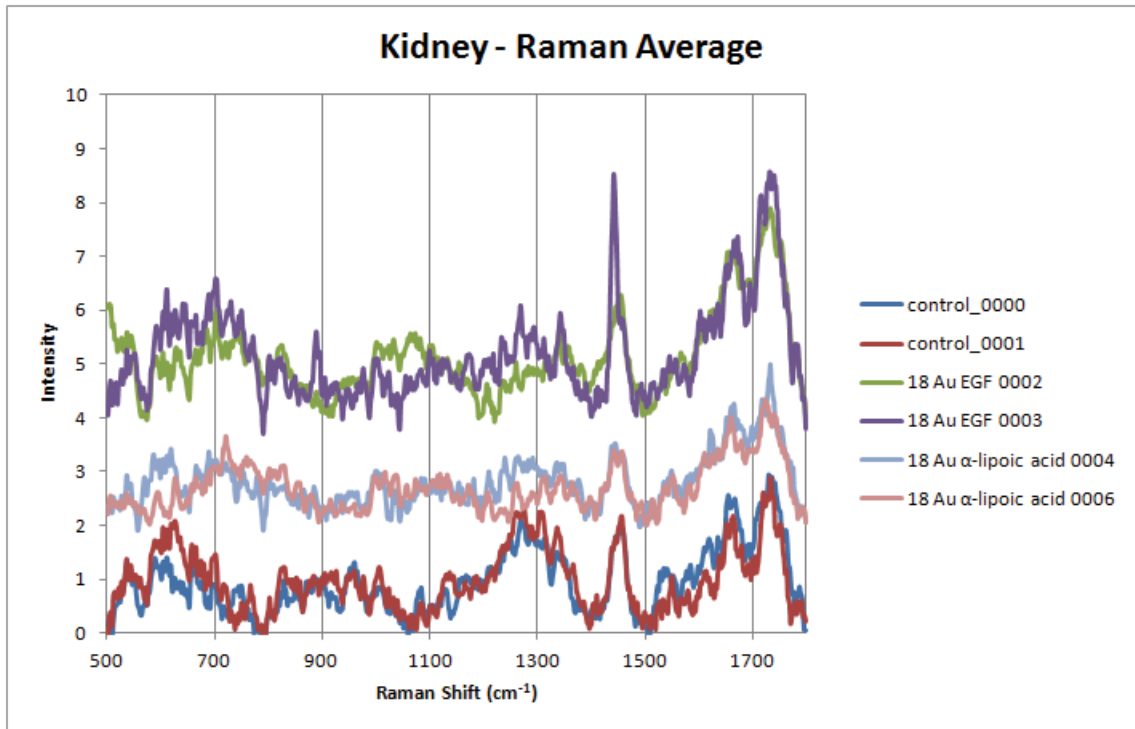
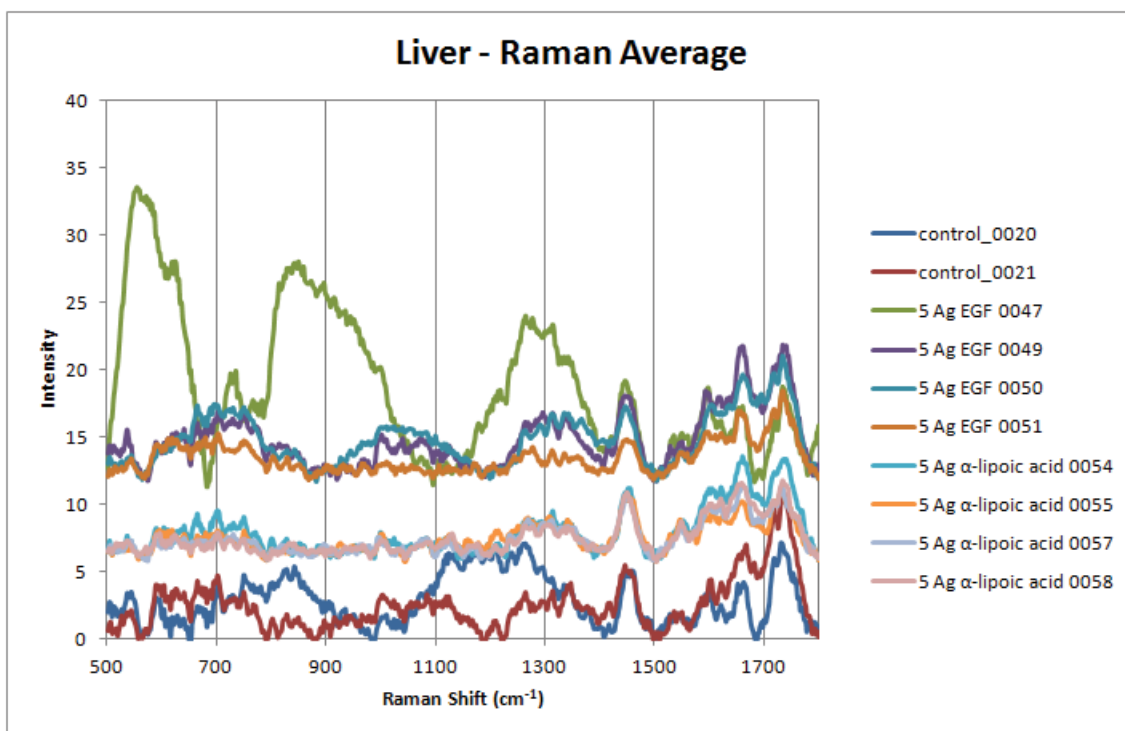
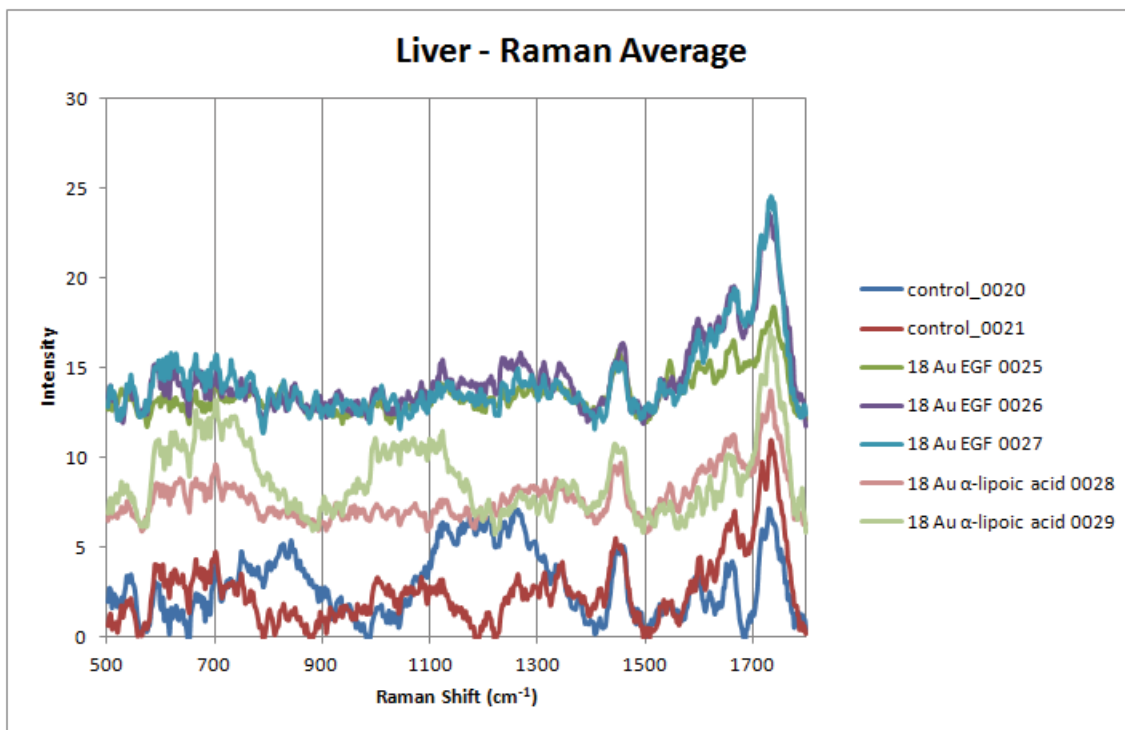


Figure 3.28 Raw Raman and fluorescence spectra of mouse kidneys, liver, and spleen.

The initial Raman spectra of each organ contain a broad fluorescence signal due to the tissue. These background fluorescence signals were subtracted using the Vancouver Raman Algorithm. Slight SERS signals are present between 500-2000 cm^{-1} , however, they are weak and difficult to distinguish.

The exposure times for each tissue type was 1 second, 1 second, and 0.1 seconds for the kidneys, liver, and spleen. The data were normalized to 1 second exposure time. The tissue response from the spleen is 3-4 and 8-10 times more intense than the liver and kidney data, respectively.





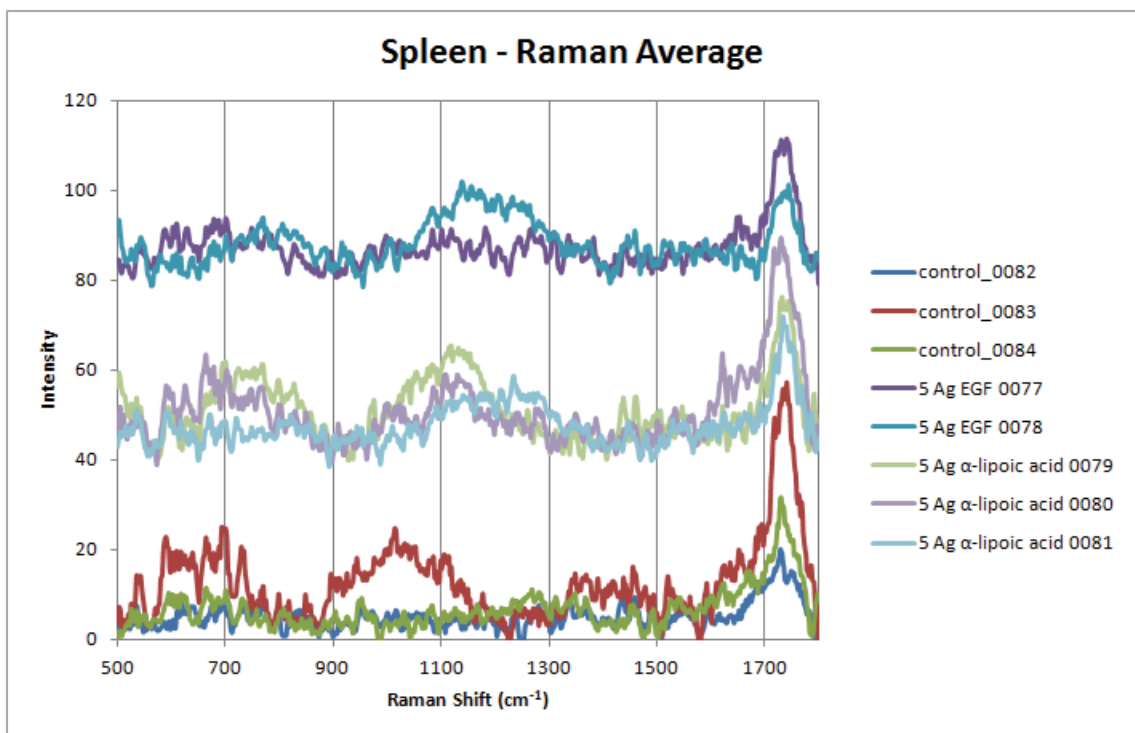
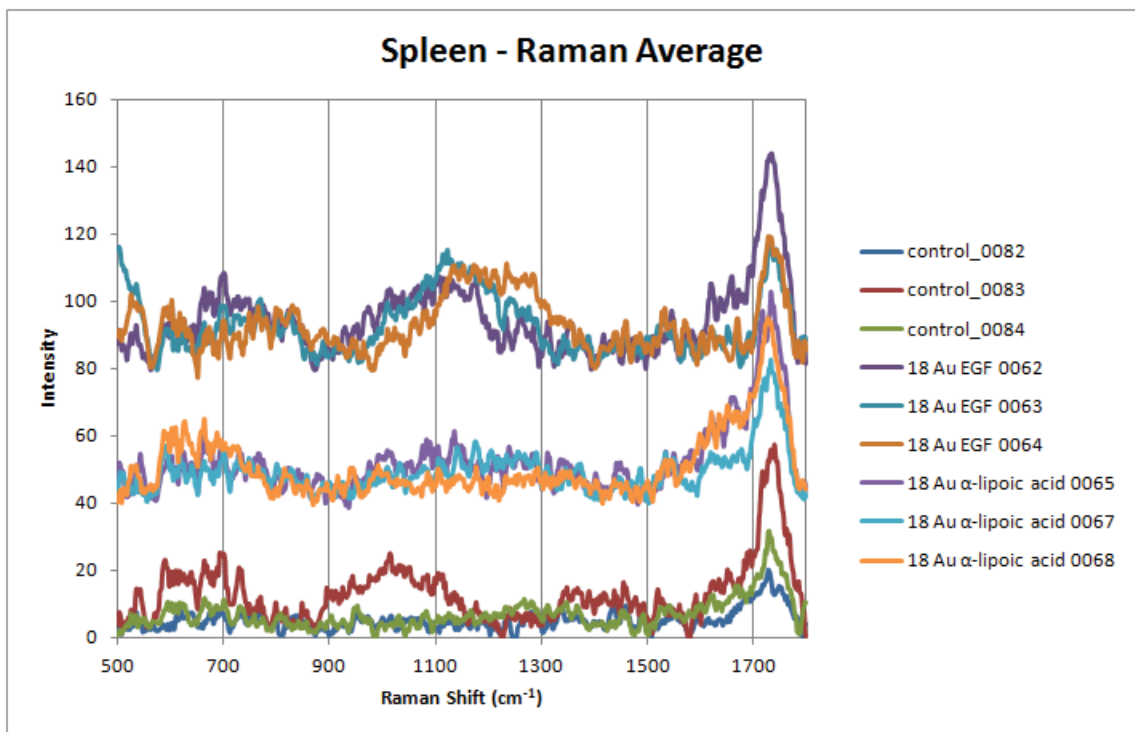


Figure 3.29 Average Raman spectra of mouse kidneys, liver, and spleen.

The Raman spectra of each organ were measured and later background subtracted with the Vancouver Raman Algorithm. No distinct SERS signals are visible when once compares the spectra for the α-lipoic acid conjugated EGF coated NPs, α-lipoic acid coated NPs, and 0.9% saline control tissues.

The kidney and liver samples were collected with 1 second exposure times, the spleen data used 0.1 seconds. The data are normalized to 1 second exposure times. The spleen tissue response is 3 and 10 times more intense than the liver and kidney data, respectively.

A few issues could have caused the poor SERS response of the tissues. The lack of SERS from the samples could be due to too few particles within the tissues to create SERS. Alternatively, the Raman signals in the tissues could have been too weak to compete with the overall fluorescence signal from the darker, fattier tissues like the kidneys, liver, and especially the spleen [91]. It is possible the nanoprobe were not effective at producing a SERS signal at the 785 nm laser excitation used, or that the laser power was too low. The nanoprobe likely did not have active protein attached, due to the 70% ethanol used to sterilize the nanoparticles, and were not specific for EGFR, so they could not accumulate in the tissues.

3.7.2. Inductively Coupled Plasma – Mass Spectrometry (ICP-MS) of Mouse Tissues

We wish to assess the biodistribution and toxicity of the α -lipoic acid or α -lipoic acid/EGF-linker coated 5 and 18 nm gold and 5 and 45 nm silver nanoparticles in mouse models. Specifically, we analyze specific mouse organs to study where the nanoparticles travel, whether the particles seem to get stuck or cause an immune response, and if the mice seem to become ill.

The injected metal concentrations are 2.19 ppm for gold and 1.20 ppm for silver. This is below the rates of silver nanoparticles which could be toxic from Section 1.1, where 250 $\mu\text{g}/\text{mL}$ is simply 250 ppm. The circulating metal concentrations are 0.164 ppm for gold and 0.090 ppm for silver, assuming that the injected concentrations distribute evenly throughout the mice. Even distribution probably does not occur. The nanoparticles should ideally be filtered out by the kidneys and we hope that the nanoparticles with the Human EGF attached would be taken up by cells with EGFRs. Figure 3.30 and Figure 3.31 display the ICP-MS results by tissue type (liver, kidney, and spleen) for 18 nm gold and 5 nm silver nanoparticles, respectively. The rudimentary functions of the kidneys, liver, and spleen are: excretion of waste, toxicity and immune response, and immune

response, respectively. The metal content of the tissues are all above the detection limit (gold – 0.100 ppb, silver – 0.200 ppb), except for the lack of gold in the 0.9% sterile saline control mouse in Figure 3.30, as expected. Only the values for silver in the control mouse in Figure 3.31 were unexpected, the values should be below the detection limit. The presence of silver in the control mice could indicate cross contamination (unlikely), interference of another metal or component in the sample matrix with the silver signal, or the inherent presence of silver in the mice through food, their cage material or medicines. Very little EGF-linker/ α -lipoic acid coated gold nanoparticles seemed to be taken up by the spleen, liver and kidneys.

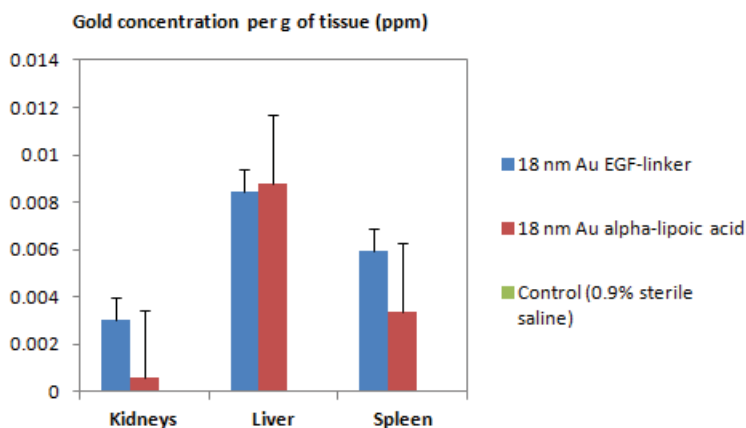


Figure 3.30 ICP-MS of mouse organs containing 18 nm gold nanoparticles coated with α -lipoic acid or α -lipoic acid/EGF-linker.

90 μ L of nanoparticles or sterile 0.9% saline solution were injected through the tail vein. The concentration used was 1000 pmoles of atomic gold or silver metal. The 0.9% saline control mouse contained no gold. The data are normalized to the concentration of circulating gold per g of mouse tissue (0.164 ppm). The EGF-linker gold nanoparticles seemed to be taken up more by the kidneys and spleen than the α -lipoic acid control particles, indicating that these EGF-linker particles were excreted and caused an immune response, respectively. Note that Human EGF was used, Human and mouse EGF have about 70% sequence match. The nanoparticle sterilization protocol with 70% ethanol could have denatured EGF and caused it to be inactive for EGFR.

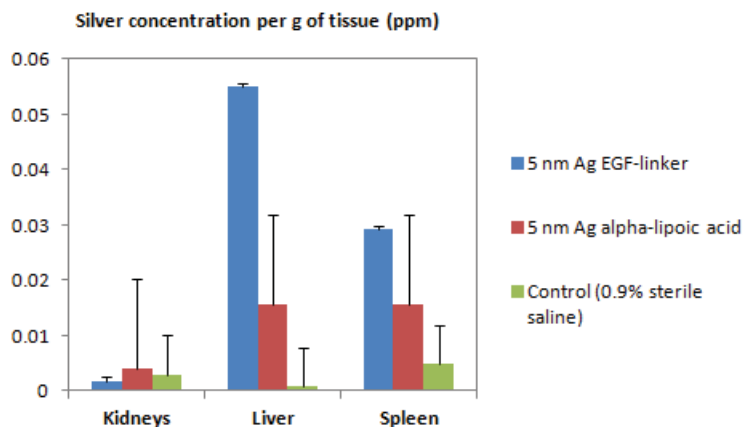


Figure 3.31 ICP-MS of mouse organs containing 5 nm silver nanoparticles coated with α -lipoic acid or α -lipoic acid/EGF-linker.

The samples were processed in an identical manner as the 18 nm gold nanoparticle containing tissues in Figure 3.30. The data are normalized to the concentration of circulating silver per g of mouse tissue (0.090 ppm). The 0.9% saline control mouse contained some silver, possibly from interferences from another metal or component in the matrix. The EGF-linker silver nanoparticles seemed to be taken up more by the liver and spleen than the α -lipoic acid control particles, indicating that these EGF-linker particles either were toxic or caused an immune response.

Very little of the 18 nm EGF-linker gold nanoparticles seem to be taken up by the organs, so some of the particles could still have been circulating, which would make them more likely to be taken up by tumors in vitro through the EPR effect.

We found the EGF-linker and α -lipoic acid 5 nm silver nanoparticles more in the liver and spleen, leading to the possibility that the particles were toxic or caused an immune response. The mice injected with the silver nanoparticles did not die or show distress, the next day they looked well and were running, hiding, eating, and drinking. Therefore, the silver nanoparticles are either not toxic at the experimental concentration or the mice did not yet show signs of toxicity.

Human EGF was used to form the EGF-linker that coated the injected nanoparticles. Human and mouse EGF share a 70% sequence match, which could be the cause the observed immune response, as compared to the nanoparticles coated solely with α -lipoic acid. Further testing with mouse EGF may show reduced immune response. The nanoparticle sterilization protocol with 70% ethanol could have skewed the observed

responses. The ethanol may have denatured the EGF protein, either reversibly or irreversibly, causing it to be inactive for EGFR. If the process is reversible, it is also unclear whether the protein would refold properly to its native conformation and retain activity [92].

3.7.3. *Ex Vivo* Biodistribution Summary

Raman of mouse kidney, liver, and spleen tissues was completed. The tissues did not exhibit SERS from the 18 nm Au or 5 nm AgNPs, coated with α -lipoic acid conjugated Human EGF or only α -lipoic acid, as compared to mouse injected solely with the 0.9% sterile saline. Some background fluorescence was observed from the kidney and liver tissues, and particularly from the spleen tissue.

ICP-MS showed EGF-NPs in tissues, the EGF-NPs were excreted and cause an immune response (18 nm Au), while they were toxic or caused an immune response (5 nm Ag). The mice appear to be unaffected 24 hours following injection of the 5 nm AgNPs, as they were running, eating, drinking, and playing, which leads us to believe that these nanoparticles were not toxic in the concentrations injected. The use of Human EGF instead of mouse EGF could have caused some difficulty in conjugation of the EGF-linker nanoparticles by the cellular EGFR. Additionally, the nanoparticle sterilization protocol with 70% ethanol could have denatured the EGF-linker.

3.8 SILVER-GOLD CORE-SHELL NANOPARTICLES

Scattering from silver nanoparticles at the plasmon frequency is much more intense than from gold, mainly because an interband transition in gold “steals” electrons from the gold plasmon band [47]. However, silver nanoparticles have been shown to exhibit antimicrobial properties [8]. As such, while the strong plasmon resonance of silver maximizes the SERS effect, bare silver nanoparticles could have a deleterious effect *in vivo*. For these reasons it is desirable to synthesize a silver nanoparticle

protected by a gold coating to ensure biocompatibility. Silver-gold core-shell nanoparticles (AgAuNPs) were synthesized in early 2013 by first year DISP students, Joe Loung and Stefan Jukes, under my direction. They built on the research presented in Sections 3.1 to 3.5 to test the AgAuNPs, which should retain the excellent SERS capabilities of silver nanoparticles while the gold coating reduces any apprehensions with regards to silver toxicity.

3.8.1 Synthesis of Ag-Au core-shell nanoparticles (AgAuNPs)

Nanoparticles were synthesized according to the method outlined by Zhang et al. (2007) [93]. The sources of the majority of chemical, gold chlorate trihydrate, silver nitrate, sodium borohydride, and deionized distilled water, were outlined in Section 2.1. Polyvinylpyrrolidone (PVP, Molecular weight 10 000 g/mol, PVP10) was purchased from Sigma-Aldrich (St. Louis, USA), and potassium hydroxide (KOH, P-4250, min. 85%) was obtained from ACP Chemicals (Montreal, Canada). Stock solutions were prepared at the beginning of the experiment using volumetric flasks, with the exception of the sodium borohydride of which a fresh solution was made just prior to use. Ultra high purity dry nitrogen gas was also used during the experiment (purity level 5.0, Praxair, Mississauga, Canada).

The first synthesis of silver seed nanoparticles closely followed the paper by Zhang et al. (2007) to replicate their results [93]. The general procedure for the silver seed nanoparticles required a 3 neck + thermometer/bubbler port flask cleaned in warm water and Sparkleen initially and then was cleaned using aqua regia followed by three rinses with deionised water. See the procedure for using aqua regia to clean glassware in Appendix C. Teflon coated stirring bars were also cleaned in aqua regia, and then stored in water prior to use. All other glassware was cleaned using warm water and Sparkleen followed by three rinses with distilled water. During the reaction, solutions were stirred and sometimes heated using a hotplate with stirring capabilities and Teflon coated stirring bars.

To synthesise the 8.1 nm silver seed nanoparticles, the silver nitrate reduction method described in the paper was used [93]. 41.5 mL deionized water, 2.5 mL 20 mM silver nitrate, 1 mL 20 mM KOH and 2.5 mL 0.2 M PVP (concentration based on the monomer, molecular weight: 111.14 g/mol) were mixed in a sealed three neck flask under bubbling nitrogen gas for 30 minutes at room temperature. 2.5 mL of 0.1 M freshly prepared NaBH₄ was then added to the solution. The solution was then stirred for 30 minutes, and aged for 48 hours at room temperature to remove excess NaBH₄. These nanoparticles are referred to as 8.1 nm silver seed nanoparticles as that was the target diameter from the paper, however, this does not mean the actual nanoparticles were 8.1 nm in diameter. After aging, nanoparticles were stored at 4°C to prevent decay, with the exception of the 8.1 nm Ag seed nanoparticles which were left on the lab bench for a week.

In the synthesis of the second batch of seed nanoparticles, 12 nm AgNPs, a much higher concentration of sodium borohydride was used than outlined in the paper. 0.315 mL of 15 mg/mL NaBH₄, or 0.8 M, instead of the 2.5 mL of 3.78 mg/mL NaBH₄, or 0.1 M, was added. The overall number of moles of NaBH₄ added was the same. Two silver seed hydrosols of 8.1 and 12 nm diameters were synthesized.

The second synthesis protocol, that of the Ag-Au core-shell nanoparticles, used the formula given in the paper (Equation 13) as well as another determined from supplemental data received in an email from the authors (Equation 14), in order to determine the ratio of reactants required for the desired nanoparticle size [93]. In the equations below, d is the nanoparticle diameter, m is the moles of Ag, while n is the moles of Au used in the synthesis, and V is the solution volume.

$$\frac{d_{alloy}}{d_{Ag}} = \sqrt[3]{\frac{m-2n}{m}} \quad (13)$$

$$\frac{V \text{ 20mM AgNO}_3}{V \text{ 20 mM KOH}} = \frac{\text{Diameter AgNP} - 3.548}{1.5826} \quad (14)$$

The gold coating was formed on the silver seed nanoparticles using the following protocol to produce the AgAuNPs. 20 mL of the AgNP seed hydrosol was refluxed with vigorous stirring and heated to boiling, as the three neck flask sat in a silicon oil bath for even heating. The setup was very similar to Figure 2.1. 2.86 mL 20 mM gold chlorate trihydrate solution was then added to the hydrosol and allowed to react for 10 more minutes with continued stirring. The solution was then cooled and aged for 24 hours at 4°C. After 24 hours the nanoparticles were centrifuged at 2000 rpm for 3 minutes, to remove the silver chloride reaction by-product. An additional spin or two in the centrifuge was used if the nanoparticle solutions still seemed cloudy with the chalky-white silver chloride precipitate. The nanoparticles, as well as their supernatant, were then collected and characterized. These AgAuNPs were also stored at 4°C. Three AgAuNP hydrosols were synthesized, two were from the 8.1 nm diameter AgNPs and one was from the 12 nm AgNPs.

In Section 2.1, the trisodium citrate (Figure 3.32) acts as both a reducing agent and a capping agent. The -OH group on the citrate oxidises to a =O when the ionic Au^{3+} or Ag^+ reduce to metallic Au^0 or Ag^0 . To cap the nanoparticles, excess citrate groups are attracted to the nanoparticle by weak London dispersion forces and sit around the nanoparticle. The overall negative charge on the citrate groups causes adjacent nanoparticles to repel each other, which prevents nanoparticle agglomeration. Amines form bonds with metals like gold and silver. The PVP polymer (Figure 3.32) contains a tertiary amine, which has an electron pair available for bonding to the reduced Ag^0 seed nanoparticles or Au^0 coating. As noted in Section 1.5, the disulfide (-S-S-) group α -lipoic acid in displaces the citrate or the PVP groups surrounding the gold, silver, or core-shell silver-gold nanoparticles.

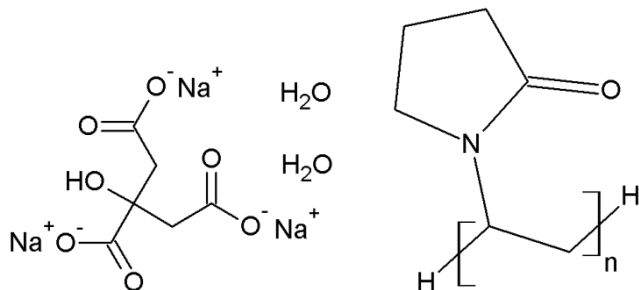


Figure 3.32 Trisodium citrate dihydrate (left) and Polyvinyl pyrrolidone (PVP, right) nanoparticle reducing and capping agents.

3.8.2 Characterization of Gold Coated Silver Nanoparticles

Ultraviolet-visible spectrophotometry measurements were obtained with the Nanodrop ND-1000, as described in Section 2.3. The absorption profiles can be observed in Figure 3.33. Silver nanoparticles usually absorb around 400 nm, while gold nanoparticles absorb near 520 nm. We expect the absorption profile of the gold coated silver nanoparticles to be somewhere between these two values. The nanoparticle concentration, as determined from the absorbance and the extinction coefficient, are tabulated in Table 3.6. As noted from the absorbance and nanoparticle concentrations, there were about 10 times more of the silver seed nanoparticles than the gold coated silver nanoparticles. It is not known why this occurred. When making the gold coated particles, the solution is primarily made up of the silver seed nanoparticles and is contained with a reflux condenser, which should prevent any nanoparticle losses. The colloid absorbance did not decrease significantly between the silver and gold coated silver nanoparticles for Zhang et al. (2007) [93].

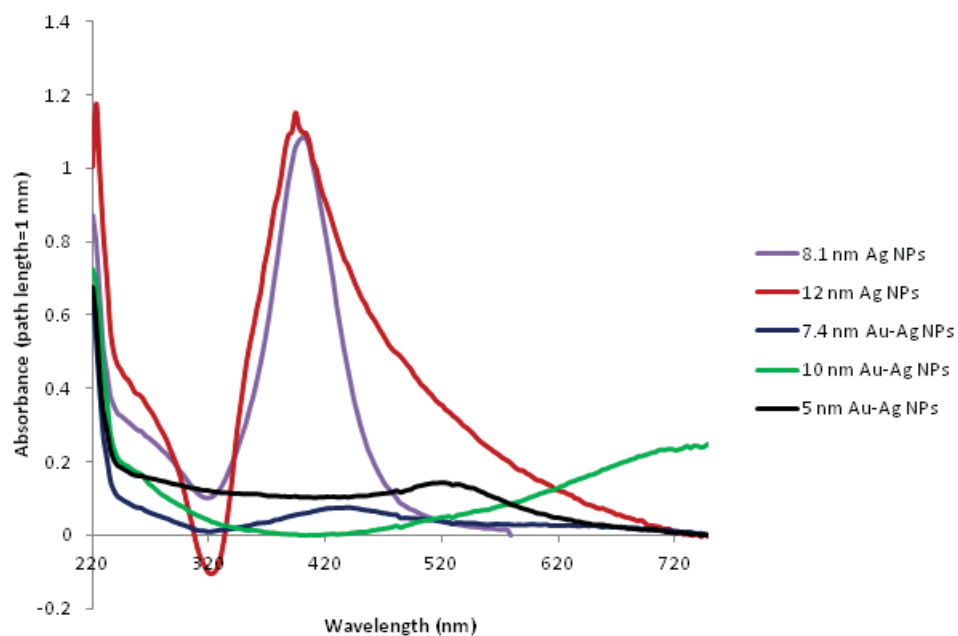


Figure 3.33 UV-Vis of Ag and AgAuNPs.

The nanoparticle spectra are: 12 nm AgNPs, 10 nm AgAuNPs, 8.1 nm AgNPs, 7.4 nm AgAuNPs, and 5 nm AgAuNPs.

Table 3.6 UV-Vis and TEM properties of synthesized Ag and AgAuNPs.

Nanoparticle type	12 nm Ag	10 nm AgAu	8.1 nm Ag	7.4 nm AgAu	5 nm AgAu
Maximum wavelength (nm)	394	~750	400	439	519
Absorbance value (A. U.)	1.150	Maximum not clear	1.082	0.075	0.142
Path length (mm)	10	10	10	10	10
Extinction Coefficient (cm ²); Au: [86], Ag: [87]	2.91 x 10 ⁻¹¹	3 x 10 ⁻¹¹	2.91 x 10 ⁻¹¹	3 x 10 ⁻¹¹	3 x 10 ⁻¹¹
Concentration (NP/mL)	38.3 x 10 ¹⁰	-	36.1 x 10 ¹⁰	2.5 x 10 ¹⁰	4.7 x 10 ¹⁰
Mean Diameter ± Standard Deviation (nm)	-	28.5 ± 13.4 (rings) N = 54	-	9.4 ± 3.4 N > 100	7.5 ± 2.0 N > 100

Table 3.6 shows the average nanoparticle diameters and standard deviations from TEM. The smaller AgAuNPs, 7.4 nm and 5 nm, were within the standard deviation of the predicted size. The 10 nm AgAuNPs were not close to the predicted size, they seemed 3 times larger. The data for the 12 nm and 8.1 nm AgNPs is not available, the grids were imaged but were not clear enough to use ImageJ. An average could be determined by hand, this was not completed due to lack of time. Figure 3.34 shows the nanoparticle TEM images. A hollow shell was observed from the 10 nm AgAuNPs and a small number of the 7.4 nm AgAuNP was observed which could have been composed entirely of gold. As electrons move more efficiently through the non-existent core of the nanoparticles, the nanoparticle centre appears transparent [94]. A test of the nanoparticle composition could be performed with ICP-MS or atomic absorption spectroscopy. This ring also alters the optical properties of the nanoparticles, which is why the 10 nm AgAuNP absorbance was red-shifted to the near-Infrared region. Wu et al. (2009) found that a variety of heterogeneous AgAuNP samples had absorbance shifted to 700-1000 nm [94]. This effect was not seen with the 5 nm AgAuNPs, possibly because the silver core remained intact, that the nanoparticles behaved analogously to small gold nanoparticles. Zhang et al. (2007), whose protocol our AgAu nanoparticle synthesis was based, did not observe this effect. They seemed to have a homogeneous alloy formed between the gold deposited onto the silver core, which prevented the appearance of any rings in their TEM images.

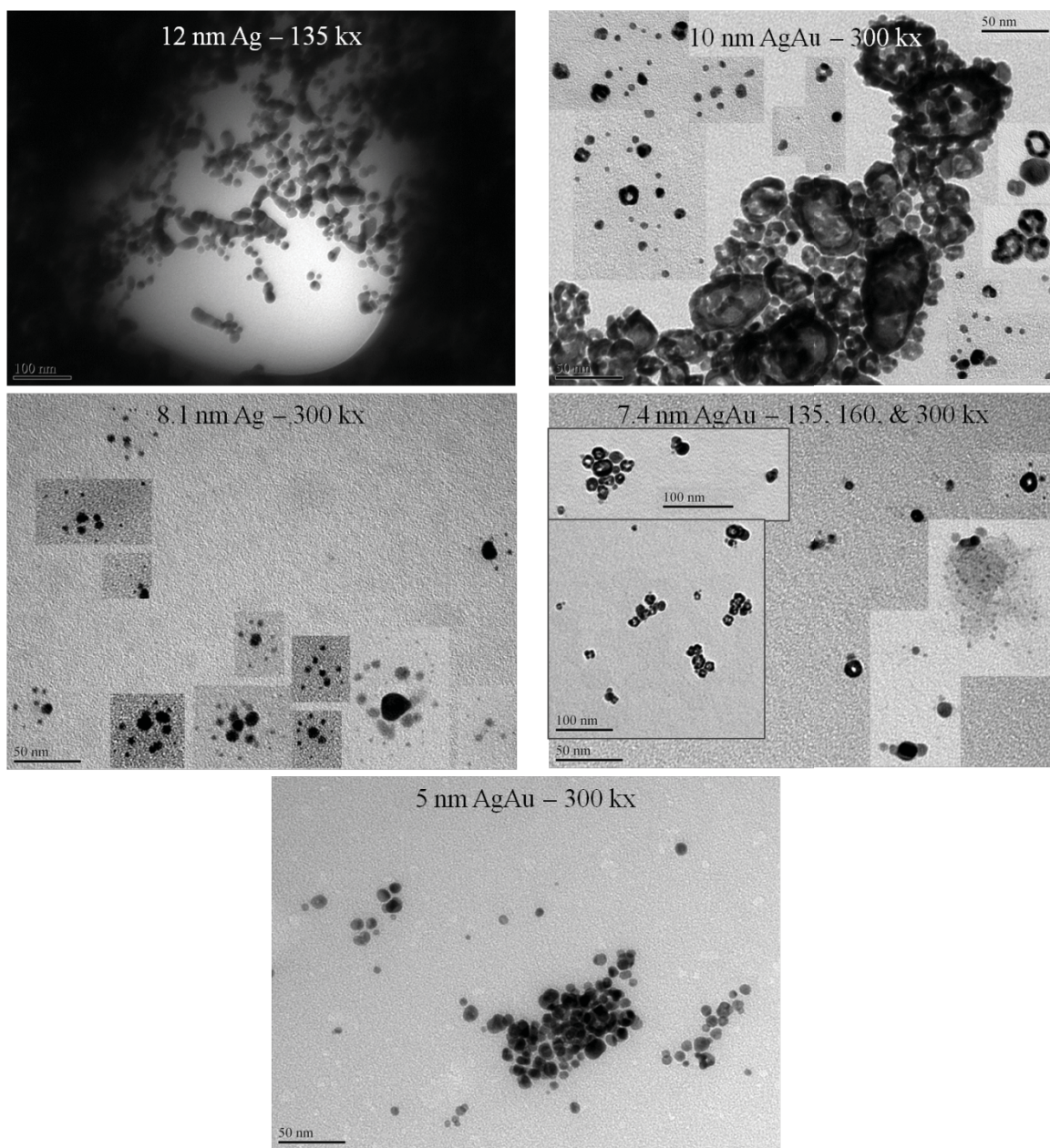


Figure 3.34 TEM images of Ag and AgAu nanoparticles.

From top left, the images are: 12 nm AgNPs, 10 nm AgAuNPs, 8.1 nm AgNPs, 7.4 nm AgAuNPs, and 5 nm AgAuNPs. The image magnifications range from 135-300 kx. Many of the 10 nm AgAuNPs and a few of the 7.4 nm AgAuNPs formed appeared as rings. These rings were actually caused by the silver core transmitting more electrons than the gold shell, caused by a longer path length through the outer gold shell.

When PVP coated nanoparticles were mixed in a 1:1 ratio with 10 mM PBS buffer, the nanoparticles did not change colour or agglomerate irreversibly Figure 3.35. The PVP coated nanoparticles had increased stability as compared to citrate, borohydride, and the α -lipoic acid coated nanoparticles described in Sections 2.1 and 3.5.1.



Figure 3.35 Stability test of core-shell silver-gold nanoparticles in 10 mM PBS buffer.

As-prepared nanoparticles mixed in a 1:1 ratio with PBS buffer (top row) or mixed in a 1:1 ratio with deionized water as a control (bottom row). Left-Right: 12 nm AgNPs, 10 nm AgAuNPs, 5 nm AgAuNPs, 7.4 nm AgAuNPs, and 8.1 nm AgNPs. PVP stabilizes all five nanoparticle samples. All nanoparticles were stable over 2 months at 0.45% salt content.

The PVP coating seems to preclude necessity of storing the nanoparticles at 4°C (Figure 3.36). All five types of the silver seed as well as the core-shell gold-silver nanoparticles were diluted with an equal volume of deionized water and left on the lab bench for 3 consecutive months. No visual change in the appearance, or colour, of the nanoparticle solutions is apparent, as well the nanoparticles do not seem to have suffered any agglomeration.

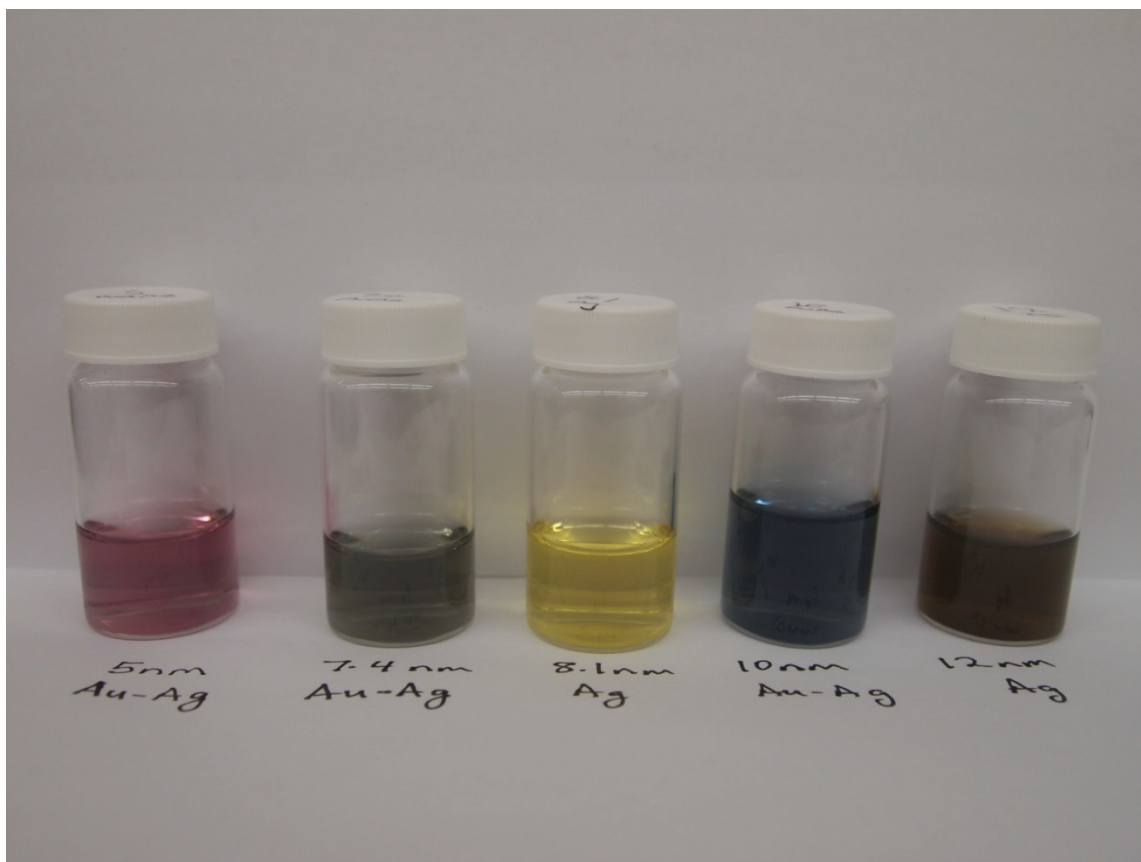


Figure 3.36 Stability test of core-shell silver-gold nanoparticles at room temperature.

As-prepared nanoparticles were mixed in a 1:1 ratio with deionized water. Left-Right: 5 nm AgAuNPs, 7.4 nm AgAuNPs, 8.1 nm AgNPs, 10 nm AgAuNPs, and 12 nm AgNPs. PVP stabilizes all five nanoparticle samples. All nanoparticles were stable for more than 3 months at room temperature.

The ELISA measurements were obtained in the same manner as that described in Section 2.6. An EGF-ELISA kit from RayBiotech was used for the measurements, although the Nanodrop ND-1000 was not used for the spectrophotometric measurements, due to issues with the computer. Instead, a SpectraMax Plus 384 microplate reader was used to make the measurements. The data is presented in Figure 3.37. Each sample present is an average of duplicate measurements. Four nanoparticle samples were tested, the 8.1 nm AgNPs, 7.4 nm AgAuNPs, 12 nm AgNPs, and 10 nm AgAuNPs. The 5 nm AgAuNPs were not tested as there were not enough space in the testing kit, and because the nanoparticles looked like they were starting to clump together after centrifuging. None of the other nanoparticles taken through the centrifugal steps seemed to have issues

with agglomeration. The nanoparticle concentrations from UV-Vis were used to determine the 1 EGF per nanoparticle ratio, to know the amounts to be added to the well plate. The EGF response for nanoparticle samples was near that of the kit and α -lipoic acid conjugated EGF samples. The overall shape of the curve of the 8.1 nm AgNPs and 7.4 nm AgAuNPs was very similar to the standards. Slight offset of the values could be due to miscalculation of the concentration amounts, from the estimate of extinction ratios of the AgAuNPs. The 12 nm AgNP and part of the 10 nm AgAuNP curve shapes were abnormal, especially for the 12 nm AgNP sample. The EGF, or nanoparticle, concentration seems to increase instead of decrease. It appears that at least for the 8.1 nm AgNPs and the 7.4 nm AgAuNPs samples, the ELISA test was positive and these samples contain active EGF bound to the nanoparticle surface.

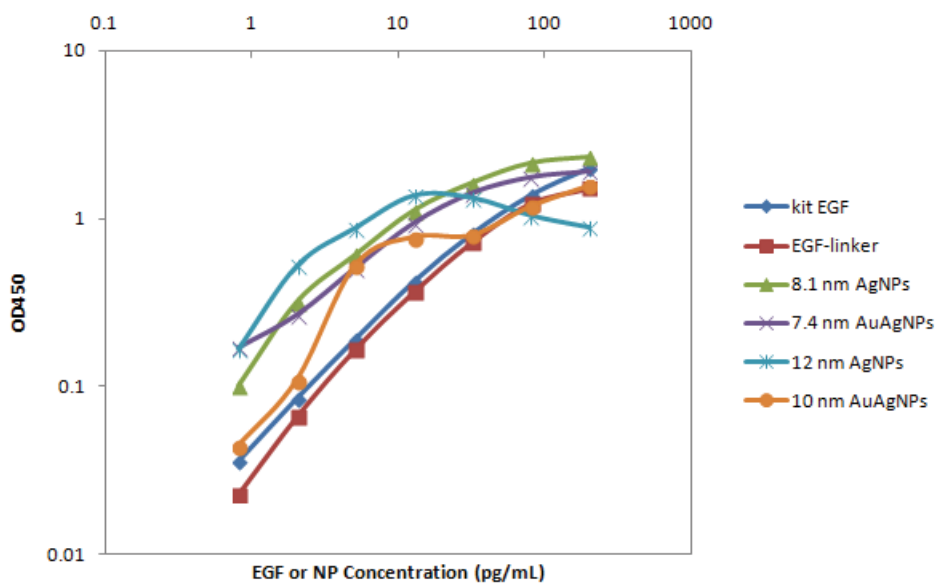


Figure 3.37 EGF-ELISA test of silver-gold core-shell nanoparticles coated with EGF-linker.

The ELISA samples were as follows: 8.1 nm AgNPs, 7.4 nm AgAuNPs, 12 nm AgNPs, and 10 nm AgAuNPs. The 5 nm AgAuNPs were not tested. The nanoparticles were coated with α -lipoic acid conjugated Human EGF and an excess of α -lipoic acid. Odd trends were observed from the 12 nm AgNPs and 10 nm AgAuNPs, as the nanoparticle concentration increases or remains constant where it should decrease. Generally, the test seems to indicate that EGF is bound to the nanoparticles.

3.8.3 Silver-Gold Core-Shell Nanoparticle Summary

Core-shell silver-gold nanoparticles of 10 nm, 7.4 nm, and 5 nm diameter were synthesized from 12 nm and 8.1 nm diameter silver nanoparticles. The UV-Vis maxima of the 7.4 nm and 5 nm AgAuNPs appeared near the expected maximum of pure gold nanoparticles (520 nm), which suggest they are homogeneous alloys. The 10 nm AgAuNPs were not as expected, they seemed to have a shell formed only of gold which caused the maximum wavelength to red-shift greatly to 750 nm. The actual nanoparticle diameters from TEM for the 7.4 nm and 5 nm AgAuNPs were close, they were within the standard deviation. The predicted diameter from TEM for the 10 nm AgAuNPs were almost 3 times larger in reality. This size increase matches the ring-like appearance of the 10 nm AgAuNPs, which corresponds to a nanoparticle composition of a heterogeneous gold shell over the silver core. The stability of the PVP silver and gold coated silver nanoparticles, either when mixed in a 1:1 ratio with water at room temperature or with a 1:1 ratio of 10 mM PBS buffer, was greater than previously tested citrate or borohydride synthesized gold or silver nanoparticles. Even after weeks had passed, the nanoparticles still had not agglomerated. Four types of nanoparticle samples were tested with ELISA, the 8.1 nm Ag, 7.4 nm AgAu, 12 nm Ag, and 10 nm AgAu. The 12 nm AgNP and part of the 10 nm AgAuNP curves did not linearly decrease as was expected. Pipetting errors during the sample dilutions, or mixing up of the sample tubes would not entirely account for the observed trends, and may be due to estimates of the AgAu absorption coefficients. The EGF-ELISA response of the 8.1 nm Ag and 7.4 nm AgAuNP samples was near that of the standards, which suggests the presence of active EGF on the nanoparticle surface.

3.9 SUMMARY OF APPROACHES AND RESULTS

The protocol to create a functional attachment between α -lipoic acid and Human EGF protein, to attach EGF protein to gold, silver, and core-shell silver-gold

nanoparticles through the disulfide bonds on α -lipoic acid, was presented. Successful synthesis of this new protein complex and its attachment to the nanoparticles was validated and monitored with TOF-MS, LTQ-MS, TEM, UV-Vis, 10 mM PBS buffer, ELISA, zeta potential, Raman spectroscopy, dark field microscopy, and ICP-MS.

The TOF-MS and ELISA measurements of the reaction product, α -lipoic acid conjugated EGF, shows that the amide bond forms and the Human EGF remains active for EGFR. However, TOF-MS of α -lipoic acid attached to mouse EGF did not show the amide bond formation, as the EDC and sulfo-NHS reagents were likely degraded. The α -lipoic acid bound Human EGF protein was digested with a protease called trypsin, cleaned with HPLC, and tested with LTQ-MS. The LTQ-MS analysis did not definitively confirm the addition of α -lipoic acid to any amino acids on Human EGF.

The TEM and UV-Vis data tell the size distribution and plasmon frequencies. The mean and standard deviation of the nanoparticles were 18.4 ± 5.1 nm and 3.8 ± 0.8 nm gold and 45.5 ± 25.0 nm and 5.2 ± 4.2 nm silver. The 45 nm AgNPs were poly-disperse. The maximum absorbance wavelengths from UV-Vis were near expected values.

A protein coating forms on the nanoparticle surface when α -lipoic acid attached to Human EGF adds to nanoparticles. Subsequent addition of excess α -lipoic acid to the EGF-nanoparticles fills any gaps remaining in the protein layer. Control nanoparticles simply contain α -lipoic acid. Nanoparticle purification by centrifugation removes excess α -lipoic acid conjugated EGF from the solution to prevent interference with tests.

The α -lipoic acid conjugated Human EGF nanoparticles are stable at 0.45% salt content when mixed with 10 mM PBS buffer. Uranyl acetate stained TEM grids demonstrate bright rings of similar diameters around α -lipoic conjugated Human EGF and α -lipoic acid only coated nanoparticles. The uniform ring size, which should match the EGF protein or α -lipoic acid radius, does not confirm the presence of EGF attached to the nanoparticles. Upon α -lipoic acid addition, the plasmon absorbance wavelength from UV-Vis is constant over time for the 18 nm gold nanoparticles, but shifts to higher wavelengths for 45 nm silver nanoparticles. ELISA shows the α -lipoic acid conjugated Human EGF bound to 18 nm Au and 45 nm AgNPs remain active for EGFR. Activities from ELISA for α -lipoic acid conjugated Human EGF on the 5 nm Au and 5 nm AgNPs could not be determined. Zeta potentials of the α -lipoic acid conjugated Human EGF 18

nm AuNPs were stable after 10 mM PBS addition, while the α -lipoic acid conjugated Human EGF 5 nm and 45 nm AgNPs were not. Raman spectra of nanoparticles artificially aggregated with MgSO_4 showed the greatest SERS intensity for the α -lipoic acid conjugated EGF 45 nm AgNPs, followed by the α -lipoic acid conjugated EGF 5 nm AgNPs and then α -lipoic acid coated 45 nm AgNPs. The spectra features looked similar to those observed from the α -lipoic acid solution. The 5 nm and 18 nm AuNPs, coated with either the α -lipoic acid conjugated EGF or α -lipoic acid, gave no SERS response.

The specificity of the α -lipoic acid conjugated Human EGF attached to gold and silver nanoparticles on cancer cells could not be assessed by dark field microscopy. Signals inherent to the cells, possibly from lipid droplets, were present in all cell samples. Bulk Raman spectroscopy measurements of many cancer cells, performed at Stanford, did not show signals for the α -lipoic acid conjugated Human EGF-NPs, but of the plastic tubes used for transport. Bulk cells measurements could not be performed at Dalhousie, as the instrument was not calibrated to use a low powered objective. Raman spectra of the EGF-NPs on cancer cells were similar to control cancer cells and did not show SERS.

Raman measurements of mouse kidney, liver, and spleen tissues containing 18 nm Au or 5 nm AgNPs, coated with α -lipoic acid conjugated Human EGF or only α -lipoic acid, did not exhibit SERS. Kidney, liver, and spleen spectra were compared to tissues from a mouse injected solely with 0.9% sterile saline. Strong fluorescence was observed from all three tissue types, especially from the spleen. ICP-MS showed α -lipoic acid conjugated Human EGF coated 18 nm Au and 5 nm AgNPs in tissues, the 18 nm EGF-AuNPs were excreted and cause an immune response, while the 5 nm EGF-AgNPs were toxic or caused an immune response. We believe that the 5 nm AgNPs were not toxic in the concentrations injected, as the mice appeared unaffected 24 hours after injection – they were running, eating, drinking, and playing. Nanoprobes using Human EGF instead of mouse EGF could have caused issues with attachment to cellular EGFR, as the two proteins share 70% of their amino acid sequence. The nanoparticle sterilization protocol with 70% ethanol could have denatured the α -lipoic acid conjugated Human EGF.

12 nm and 8.1 nm diameter silver nanoparticles synthesized core-shell silver-gold nanoparticles of 10 nm, 7.4 nm, and 5 nm diameters. The UV-Vis maxima for most nanoparticles were typical, the 7.4 nm and 5 nm AgAuNPs absorbance was near the

expected maximum of pure gold nanoparticles (520 nm) which suggest they are core-shell nanoparticles. The 10 nm AgAuNPs were not as expected, they seemed to have a heterogeneous shell which caused a large red-shift of the maximum wavelength to 750 nm. The actual nanoparticle diameters from TEM for the 7.4 nm and 5 nm AgAuNPs were within the standard deviation. The predicted diameter for the 10 nm AgAuNPs was not near the actual value, the nanoparticles were almost 3 times larger. This increase in size corresponds to the ring-like appearance of the 10 nm AgAuNPs, which suggests that the nanoparticles are composed of a heterogeneous gold shell over the silver core. The stability of the PVP coated Ag and AgAuNPs, either when mixed in a 1:1 ratio with water at room temperature or with a 1:1 ratio of 10 mM PBS buffer, was greater than previously tested citrate or borohydride synthesized Au or AgNPs. Even after weeks had passed, the nanoparticles still had not agglomerated. The activity of the α -lipoic acid conjugated Human EGF on 8.1 nm Ag, 7.4 nm AgAu, 12 nm Ag, and 10 nm AgAu was assessed with ELISA. The 12 nm AgNP and part of the 10 nm AgAuNP curves did not linearly decrease as expected. The EGF-ELISA response of the 8.1 nm Ag and 7.4 nm AgAu nanoparticle samples was near that of the standards, which suggests active EGF was present on the nanoparticle surface.

α -lipoic acid conjugated Human EGF was attached to a variety of gold, silver, and core-shell silver-gold nanoparticles. Data from the TOF-MS, TEM, UV-Vis, time-lapse UV-Vis, 10 mM PBS buffer, ELISA, and Raman spectroscopy of nanoparticles, techniques support the successful synthesis of the modified nanoparticles. LTQ-MS, TEM with uranyl acetate stain, zeta potential, Raman spectroscopy of cells and of tissues, dark field microscopy of cells, and ICP-MS of tissue techniques are less conclusive or do not corroborate the attachment of α -lipoic acid conjugated Human EGF to nanoparticles. Assessment of these results will be addressed next in the Discussion chapter.

CHAPTER 4: DISCUSSION

Cancer was the leading cause of death in Canada in 2009, surpassing heart disease [95]. More cost effective imaging and treatment options will save lives, help to reduce the costs associated with and stress on the health care system, and improve health care resource access in developing countries. We targeted the transmembrane protein EGFR, over-produced on the surface of some cancers, in the development of a new nanoprobe. Through carbodiimide chemistry, gold or silver nanoparticles were successfully attached to EGF protein through a short ligand, α -lipoic acid. These nanoprobes allow the occurrence of an effect called SERS, or surface enhanced Raman spectroscopy, which should make cancer cells more visible than normal cells. These particles were validated by various techniques for use as SERS optical imaging probes. Silver nanoparticles have not previously been attached to EGF.

We discuss more about the α -lipoic acid bound EGF nanoprobe synthesis and characterization (Section 4.1), *in vitro* cell imaging (Section 4.2), and *ex vivo* tissue imaging (Section 4.3).

4.1 AU, AG, & AG-AU- α -LIPOIC ACID-EGF SYNTHESIS AND CHARACTERIZATION

Human EGF protein was modified by a carbodiimide reaction, to form an amide bond between an amine group on EGF and the carboxylic acid group of α -lipoic acid. α -lipoic acid cross-links EGF to nanoparticles, to form a signal enhancing nanoprobe for Raman spectroscopy.

Time-of-Flight – mass spectrometry demonstrated the carbodiimide based coupling of the carboxylic acid group on α -lipoic acid to one or more of the three (amino terminal, or one of two lysine) amine groups on Human EGF. TOF-MS of mouse EGF did not show the α -lipoic acid protein complex. The EDC and sulfo-NHS amide bond formation reagents were stored at 4°C and -20°C, respectively. These chemicals were not

initially stored with desiccant, which could have allowed exposure to moisture and gradual degradation through inadequate vial seals. The amino acid sequences of Human and mouse EGF are 70% identical. Both lysine amino acids in Human EGF, which contain a side chain amine group, are replaced in mouse EGF with other amino acids which lack an amine. It is also possible that the way in which mouse EGF folds causes inaccessibility of the amino terminus, and α -lipoic acid could never bind to mouse EGF. LTQ-MS of α -lipoic acid conjugated to Human EGF protein and subsequently digested with a protease, trypsin, did not show α -lipoic acid addition to any amino acids. EGF-ELISA measurements confirmed the activity of α -lipoic acid conjugated to Human EGF.

Citrate or borohydride capped nanoparticles were synthesized according to established methods, and were characterized with TEM and UV-Vis. The α -lipoic acid conjugated Human EGF forms a layer of protein on the nanoparticle surface. The EGF protein is not uniform in size and likely leaves spaces between molecules on the surface. Excess α -lipoic acid adds to the nanoparticles already coated with α -lipoic acid bound EGF, to fill in any gaps remaining in the protein layer. In order to compare any data collected using α -lipoic acid bound EGF, we use nanoparticles coated with a layer of α -lipoic acid as positive controls. Nanoparticle purification ensures removal of any excess α -lipoic acid conjugated EGF in the solution. This helps prevent interference effects in other characterization tests, such as ELISA, cell imaging, and tissue imaging.

The modified EGF protein attached to gold and silver nanoparticles was assessed with a variety of techniques. Compared with bare nanoparticles, UV-Vis spectra of Ag nanoprobe exhibit significant plasmon red-shift, while there was no discernible shift for 18 nm Au nanoprobe. A UV-Vis time course study of 45 nm AgNPs exposed to α -lipoic acid exhibited a significant 10-15 nm red-shift in the maximum absorption wavelength. This could be indicative of attachment of the molecule to the silver nanoparticles.

α -lipoic acid conjugated Human EGF-nanoparticles on TEM grids stained with uranyl acetate showed a ring of protein around the nanoparticles. The bright rings were smaller than the hydration diameter of EGF. The rings are probably not from EGF staining, but of artifacts surrounding the nanoparticles. Accidental use of hydrophobic carbon only TEM grids likely allowed the hydrophobic uranyl acetate stain to accumulate around the nanoparticles. While some stain would be repelled by the polar amino acids in

EGF, some would be attracted to the non-polar amino acids. The large, localized pocket of uranyl acetate stain would hinder the view of polar amino acids in EGF. Issues with detection of the protein around the nanoparticles could also be caused by the 80 kV lower resolution electron beam. The beam can burn carbon in the sample, and it can be difficult to distinguish the carbon in the protein from that which coats the TEM grid. The presence of EGF around nanoparticles stained with uranyl acetate was not confirmed with TEM.

Stability of the α -lipoic acid bound EGF attached to nanoparticles was qualitatively demonstrated with photos of samples mixed with an equal volume of 10 mM PBS, to raise the salt content to 0.45%. The physiological salt content is 0.9%. The photos show that the nanoparticles are stable at 0.45% salt content, which corroborates the UV-Vis results and suggested the EGF-linker successfully attached to the Au and AgNPs. As a complement to the 10 mM PBS, the zeta potential gives quantitative information about nanoparticle stability. Zeta potential measurements of the α -lipoic acid conjugated Human EGF protein on 5 nm and 45 nm AgNPs show instability after the 10 mM PBS addition. The α -lipoic acid conjugated Human EGF 18 nm AuNPs were intact and should remain dispersed while in the acidic pH range.

ELISA confirmed the excellent binding affinity of linked-EGF, as it is active alone and following conjugation to 18 nm Au and 45 nm AgNPs. The EGF-ELISA test showed similar activities of the protein and protein-NP samples as compared to the standard kit EGF. The activity of the small 5 nm EGF-linker coated Au and AgNPs could not be measured by the test. Smaller EGFR specific peptides must be engineered for use with small nanoparticles, because the EGF will occasionally wrap around the small nanoparticles. This is consistent with a negative results from 5 nm AuNP or AgNPs coated with α -lipoic acid conjugated EGF and α -lipoic acid.

Raman imaging of nanoparticles, which were artificially aggregated with MgSO_4 to mimic the predicted SERS response of cells, was successful. Using a 632.8 nm laser, SERS was observed with 33 pM nanoparticles. The most intense SERS response was from the α -lipoic acid conjugated EGF 45 nm Ag, followed by the α -lipoic acid conjugated EGF 5 nm Ag, while the α -lipoic acid coated 45 nm Ag gave the third most intense response. The spectra features from the nanoparticles roughly matched those of the α -lipoic acid solution, although the peaks from the nanoparticles showed broadening.

Insignificant SERS response was seen from the 5 nm and 18 nm AuNPs, coated with either the α -lipoic acid conjugated EGF or α -lipoic acid. The large silver nanoprobe response is only one order of magnitude lower than the best SERS particles available on the market, Oxonica particles [60].

There are four different bimetallic nanoparticle structures, a homogeneous alloy, a heterogeneous alloy, a core-shell shape, and an interface of two metal nanoparticle types. PVP stabilized, core-shell silver-gold nanoparticles of 10 nm, 7.4 nm, and 5 nm diameter were synthesized from 12 nm and 8.1 nm diameter silver nanoparticles. The UV-Vis maxima for most of the nanoparticles were typical, those of the 7.4 nm and 5 nm AgAuNPs appeared near the expected value for pure AuNPs (520 nm) which suggests they are core-shell structures with a very small silver core. The 10 nm AgAuNPs were atypical and seemed to have a shell which could have been entirely composed of gold. The shell caused a great red-shift in the maximum wavelength to 750 nm. The actual nanoparticle diameters from TEM for the 7.4 nm and 5 nm AgAuNPs were close, they were within the standard deviation. The 10 nm AgAuNP predicted diameter was not close to the actual value, the synthesized nanoparticles were almost 3 times larger. The size increase corresponds to TEM images in which the AgAuNPs appear as rings, suggesting a heterogeneous gold shell over the silver core. The core-shell method is difficult to control and can destroy the internal silver core structure. Since the gold and silver salt solutions both react alone with the reducing agent, it is likely that the silver core was entirely etched away to form a gold ring as seen with the 10 nm AgAuNPs. The use of a milder reducing agent which is active only in the presence of silver would ensure that the gold can only be reduced onto the silver surface. This reducing agent could be ascorbic acid or vitamin C, which is the L enantiomer only. The silver seed nanoparticle acts as a catalyst for the ascorbic acid to reduce Au^{3+} to Au^0 onto the metallic silver surface. C. J. Murphy et al. at the University of South Carolina made core-shell silver-gold nanoparticles and nanorods with ascorbic acid as the reducing agent [96]. Another group at Northwestern University may have a protocol which uses ascorbic acid makes Ag-Au core-shell nanoparticles only, but the paper could not be found. The stability of the PVP coated Ag and AgAuNPs, either when mixed in a 1:1 ratio with water at room temperature or with a 1:1 ratio of 10 mM PBS buffer, was greater than the citrate or

borohydride capped gold or silver nanoparticles. The nanoparticles were stable for weeks, at least, without agglomeration. The 8.1 nm Ag, 7.4 nm AgAu, 12 nm Ag, and 10 nm AgAu nanoprobe were tested with ELISA, the 5 nm AgAuNPs were not tested because the well plate lacked space. The 12 nm AgNP and 10 nm AgAu nanoprobe curves did not linearly decrease as expected. The EGF-ELISA response of the 8.1 nm Ag and 7.4 nm AgAu nanoprobe was near that of the standards. While the small, borohydride capped Ag and Au nanoparticles did not show activity with ELISA, the positive results with Ag-Au core-shell nanoparticles is likely due to the influence of PVP. A positively charged surface causes EGF to wrap around the nanoparticle while steric repulsion by PVP prevents wrapping.

4.2 *IN VITRO* CELL IMAGING

Dark field microscopy was also used to assess the nanoprobe activity. Images of probes incubated *in vitro*, with EGFR over-expressing A431 cancer cells, showed bright objects in the cells but excluded from the nucleus. It seems that the bright spots are cell structures. These bright spots could be due to vesicles within the cytoplasm of the cells, or lipid droplets. Photos of the α -lipoic acid coated control nanoparticles on A431 cells looks identical to the EGF-linker coated active nanoparticles incubated with A431 cells, as well as to control cells incubated without nanoparticles. Dark field microscopy may still be adequate for assessment of the specificity of the α -lipoic acid conjugated Human EGF gold and silver nanoparticles *in vitro*, analysis of the RGB signals may provide more information as to the distribution of nanoparticles.

EGFR over-expressing A431 cancer cells are targeted through the biocompatible nanoprobe. The surface plasmon of aggregated metal nanoparticles is excited by using 632.8 nm or 785 nm laser wavelengths which leads to enhanced Raman spectra – referred to as surface enhanced Raman spectroscopy (SERS). As EGFR is engulfed through endocytosis, we expect to see the aggregated nanoprobe in endosomes and lysosomes when using a confocal microscope for white light and Raman imaging. Previously, with a

632.8 nm laser, we demonstrated signal to noise ratios of 850:1 at 1583 cm^{-1} and 7 orders of magnitude enhancement with 30 nm AuNPs tagged with anti-EGFR antibody and incubated with A431 cells [43]. At Stanford, bulk Raman spectra of cell pellets did not show nanoparticle signals within the cells. Intense signals were from the plastic tubes used to freeze and ship the cells. Bulk cell pellets measurements were not obtained at Dalhousie, as the spectrometer was not calibrated for a low powered objective. High magnification Raman spectra were nearly identical between the A431 cancer cells tagged with α -lipoic acid or EGF-NPs; the nanoprobe was not SERS active. It was statistically unlikely for SERS to be observed from the high magnification Raman data because SERS occurs only in 1 in 10^6 scattered photons and too few spectra were obtained.

4.3 *EX VIVO* BIODISTRIBUTION

Small EGF-coated nanoparticles should avoid an immune response. Select mouse organs were harvested 24 hours following tail vein injection of control α -lipoic acid coated gold and silver nanoparticles or active EGF-linker versions to determine the nanoprobe biodistribution with Raman and ICP-MS. Raman spectra from mouse kidney, liver, and spleen tissues containing the 18 nm Au or 5 nm AgNPs, coated with α -lipoic acid conjugated Human EGF or only α -lipoic acid, looked similar to tissues from a mouse injected with 0.9% sterile saline. High background fluorescence observed from the kidney, liver, and spleen tissue could mask the SERS signals.

ICP-MS showed EGF-NPs in tissues, the EGF-NPs were excreted and cause an immune response (18 nm Au), while they were toxic or caused an immune response (5 nm Ag). The mice were unaffected 24 hours following injection of the 5 nm AgNPs, as they were running, eating, drinking, and playing, which implies that these nanoparticle concentrations injected were not toxic. The use of Human EGF instead of mouse EGF could have caused difficulty in binding the EGF-NPs to the cellular EGFR. Reduced stability of the AgNPs, noted from the zeta potential measurements, could have caused separation of the coating from the nanoparticles and left bare nanoparticles sequestered in the spleen and liver.

The use of 70% ethanol to sterilize the both the α -lipoic acid conjugated Human EGF and α -lipoic acid coated nanoparticles samples before injection into the mice likely denatured the protein. It is unclear whether the denaturation of the α -lipoic acid conjugated Human EGF, or of proteins in general, by alcohols is reversible or irreversible. If the process is reversible, it is also unclear whether the protein would refold properly to retain activity once the ethanol was removed. G. McDonnell and A. D. Russell state that the particular reaction chemistry of alcohols, like methanol and ethanol, on proteins is not well understood, but that the enhanced efficacy of alcohols in the presence of water may lead the alcohol to cause cell membrane damage and fast protein denaturation. Which interferes with cell metabolism and causes cells to lyse [92].

Due to the protein denaturation by alcohols, ethanol should not be used for sterilization of nanoparticles. Alternative sterilization methods include sterile filtration, which is sufficient if large scaffolds or groups of proteins which stick together are not present; gamma or e-beam irradiation, which are non-thermal processes and are acceptable so long as it is agreeable that the irradiated protein solution will contain particulate matter and bacterial remnants which could cause an immune response; natural light (UV) irradiation, which is also a non-thermal process; or microwave, which is a thermal process and would cause some heating of the sample [97] [98]. The last four alternatives, especially gamma and e-beam irradiation, seem to be more practical for high throughput manufacture of commercialized drugs or proteins. One of these sterilization methods would be employed as a final step before the EGF coated nanoparticles were imaged with cells, tissues, or animal models. A method for sterile filtration of EGF coated nanoparticles was outlined in Section 2.7.

In addition, aseptic techniques could be employed to reduce the risk of the introduction of impurities to the EGF-NPs by bacteria, viruses, fungi, or other unwanted contaminants. Aseptic techniques include the use of mechanical and barrier engineering controls, such as an autoclave, a biosafety cabinet, and 70% ethanol sterilization of general use surfaces and the packages of supplies. Techniques similar to those used for cell culture would be adequate (Section 2.7 and Appendix A).

CHAPTER 5: CONCLUSIONS AND FUTURE WORK

α -lipoic acid used as a cross linking molecule between EGF protein, both Human and mouse forms, and nanoparticles were synthesized. The α -lipoic acid was first bound to the EGF through an amide bond formation reaction using carbodiimide chemistry. This modified EGF could then be attached to gold, silver, or core-shell silver-gold nanoparticles through disulfide bonds on the α -lipoic acid molecule. These nanoparticles should then allow targeted detection of cancers over-expressing the EGFR, while the metal nanoparticles simultaneously act as signal enhancers during Raman imaging to give SERS. In the future, these EGF linked nanoparticles could also act as a treatment through thermal heating of cancerous tissues when struck by laser light, as small nanoparticles vibrate more and release those vibrations as heat to surrounding tissues.

5.1 CONCLUSIONS

Novel EGFR-specific gold and silver nanoprobe were synthesized and validated by various techniques as SERS optical imaging probes. The α -lipoic acid was conjugated to through an amide bond EGF using a carbodiimide reaction. Nanoprobes were formed from the α -lipoic acid conjugated EGF attached to 5 nm and 18 nm AuNPs and 5 and 45 nm AgNPs. The nanoprobes were stable at 0.45% salt content from 10 mM PBS, while zeta potential showed stability of the 18 nm gold nanoprobes only. TEM showed the particle spacing increased between EGF-NPs as compared to α -lipoic acid-NPs. ELISA confirms the 18 nm Au and 45 nm Ag nanoprobes effectively bind to EGFR. TOF-MS shows that the α -lipoic acid does add to Human EGF, but not mouse EGF. Identification of which amino acids the α -lipoic acid linker binds was not possible with LTQ-MS. Nanoparticles artificially aggregated with $MgSO_4$ had the greatest SERS intensity for 45 nm Ag EGF-NPs, followed by 5 nm Ag EGF-NPs and then 45 nm Ag α -lipoic acid-NPs. 5 nm and 18 nm Au EGF-NPs or α -lipoic acid-NPs were not SERS active.

Dark field microscopy of the A431 cells with or without the EGF-linker coated nanoprobe showed bright spots in the cytoplasm. Further testing is necessary to understand if these bright spots are due to lipids, and if dark field microscopy is acceptable for testing the uptake of nanoparticles in cells. Bulk Raman spectroscopy measurements, performed at Stanford, of many cancer cells tagged with α -lipoic acid conjugated Human EGF nanoparticles showed signals for the plastic tubes used for transport. Bulk measurements of cells could not be performed at Dalhousie; however, at high magnification Raman spectra of the EGF-NPs on cancer cells were not different from the control cancer cells, and did not show SERS.

Raman spectroscopy measurements of mouse kidney, liver, and spleen tissues containing 18 nm Au or 5 nm AgNPs, coated with α -lipoic acid conjugated Human EGF or only α -lipoic acid, did not exhibit SERS when compared to tissues from a mouse injected with the 0.9% sterile saline. Analysis of the immune response of the EGF-linker coated nanoparticle uptake in mice with ICP-MS showed increased uptake by 18 nm Au and 5 nm Ag EGF-NPs compared to α -lipoic acid coated nanoparticles. The uptake suggested immune response and excretion, from particles in the liver and kidneys. The nanoparticles did not appear to be toxic to the mice in the concentration used. The use of Human EGF instead of mouse EGF could have caused the immune response. The probable denaturation of EGF by the sterilization procedure with 70% ethanol could also have skewed the results.

12 nm and 8.1 nm diameter silver nanoparticles were used to synthesize core-shell silver-gold nanoparticles of 10 nm, 7.4 nm, and 5 nm diameters. The typical UV-Vis maximum for the 7.4 nm or 5 nm AgAuNPs absorbance suggests the particles are core-shell structures. The 10 nm AgAuNPs seemed to be made of a gold shell without any silver core, which caused a large red-shift of the maximum wavelength to 750 nm. The actual nanoparticle diameters from TEM for the 7.4 nm and 5 nm AgAuNPs were within the standard deviations, while the 10 nm AgAuNPs were almost 3 times larger. Larger AgAuNPs than expected corresponds to a ring structure in the TEM images, which corresponds to a heterogeneous gold shell over the silver core. The stability of the PVP coated Ag and AgAu nanoparticles, either when mixed in a 1:1 ratio with water at room temperature or with a 1:1 ratio of 10 mM PBS buffer, was greater than previously tested

citrate or borohydride synthesized gold or silver nanoparticles. The nanoparticles did not aggregate and settle, even after weeks had passed. Activity of the 8.1 nm AgNP, 7.4 nm AgAuNP samples showed trends similar to the standard EGF with ELISA. The 12 nm AgNP and part of the 10 nm AgAuNP curves did not linearly decrease as was expected.

5.2 FUTURE WORK

5.2.1 SERS Imaging and Photothermal Therapy Treatment

Many avenues are available for continued development of a surface enhanced Raman spectroscopy based imaging system using EGF protein coated nanoparticles as the signal enhancers for cancer detection. The Ag- and Au-based EGF nanoprobe will allow researchers to target tissues which contain EGFR over-expressing cells. The nanoprobe would be useful for imaging via SERS and as a treatment with photothermal therapy. Photothermal therapy involves the heat transfer from vibrating nanoparticles to tissues. This is greater in small nanoparticles as they are less SERS active and convert laser energy to heat. Many small nanoparticles targeted to a particular area, by the density of an over-expressed receptor, would heat the cancer cells upon illumination with laser light. Normal cells surrounding the cancerous tissue would be largely unaffected, as they contain fewer surface receptors and would not undergo substantial thermal heating.

5.2.2 Core-Shell Silver-Gold Nanoparticles

Silver nanoparticles have a high SERS activity but may be toxic in high concentrations. Gold nanoparticles are less bright, but are biocompatible above 3 nm diameter. Core-shell silver-gold nanoparticles (AgAuNPs) retain the desired aspects of the individual nanoparticle compositions. The use of these nanoparticles could allow observation of SERS active molecules, while reducing the worry of silver toxicity.

Dalhousie Integrated Science Program (DISP) students Joe Loung and Stefan Juckes worked on the synthesis and EGF conjugation to and characterization of the core-shell silver-gold nanoparticles in early 2013. The PVP coating surrounding these nanoparticles should aid with nanoparticle stability. Measurements of the stability at higher temperature (37°C), to mimic conditions the human body, are necessary to compare to physiological conditions. Amine-PEG (polyethylene glycol) attached to nanoparticles with carbodiimide chemistry would produce a PEG coated nanoparticle. A PEG coating confers great stability and avoids an immune response.

The composition of the core-shell silver gold nanoparticles, and the ratio of gold to silver, should be confirmed with ICP-MS or atomic absorption spectroscopy. The number of surface atoms available for binding to a ligand such as α -lipoic acid, EGF-linker, PVP, or thiol-PEG could be determined through the known nanoparticle size. The use of a weaker reducing agent, like ascorbic acid, is necessary to allow gold (III) to reduce only on the silver seed nanoparticle surface and to definitively form core-shell silver gold nanoparticles like the method by C. J. Murphy et al. at the University of South Carolina or another group at Northwestern University.

Quantification of the EGF per nanoparticle is necessary. Measuring the amount of EGF left in the supernatant, and on EGF by using a reducing agent to detach EGF the on nanoparticles. The sum of these quantities should equal that added to the initial solution.

TEM with uranyl acetate staining to confirm the presence of the α -lipoic acid conjugated EGF surrounding the nanoparticles must occur for the 12 nm Ag, 10 nm AgAu, 8.1 nm Ag, 7.4 nm AgAu, and 5 nm AgAu nanoprob. Repeat staining is necessary for the 5 nm and 18 nm Au and 5 nm and 45 nm AgNPs. Both nanoparticle sets must be stained on TEM grids which are less hydrophobic than the carbon only grids. Alternatively, dynamic light scattering could be used to ensure protein attachment. This could occur by measuring the hydrodynamic radius of the citrate, borohydride, and PVP coated nanoparticles, for comparison to those nanoparticles with α -lipoic acid or EGF conjugated α -lipoic acid coatings. Fluorescence staining of the nanoparticles with fluorescence dyes specific for EGF would confirm the presence of the EGF-linker.

Scanning tunneling electron microscopy or atomic force microscopy could also detect changes on the nanoparticle surfaces.

Next steps will address characterization of the EGF-linker coated core-shell silver-gold nanoparticles, especially ELISA and with cells. For all ELISA tests, even those experiments with gold or silver nanoparticle samples, whether non-specific nanoparticles (coated solely with α -lipoic acid) give a response was not tested. A positive ELISA response should not occur for the α -lipoic acid coated nanoparticles; however, this control experiment must be completed for all ELISA tests. Repeat ELISA tests are also necessary for the following nanoprobe: 5 nm Au, 5 nm Ag, 12 nm Ag, and 10 nm AgAuNPs, as they did not follow the standard EGF curve and have not definitively been shown to be active for EGFR. As well, thermogravimetric analysis will be used to determine presence and fraction of lipoic acid on nanoparticles.

Studies of the PVP coated AgAu nanoparticles in mice are necessary. Injected nanoparticles, as well as PEG-AgAuNPs, should avoid uptake and remain in circulation. These core-shell silver-gold nanoparticles are the best choice for SERS imaging.

5.2.3 LTQ-MS for Identification of α -lipoic acid to EGF Attachment Site

Instrument limitations can lead to detection issues with the creation of too large or too small peptides from the theoretical fragmentation of Human EGF protein digested with trypsin. Instead of trypsin, the use of the enzyme chymotrypsin could create smaller fragments, although chymotrypsin is less specific and can be more prone to missed sequence cleavages. Also, as an alternative to the sole use of LC-MS separation with the LTQ-MS, described in the Method Sections 2.4.2, 2.4.3, and 2.4.4, alternative MS methodology can allow further separation of the peptides, as well as a large detection limit range for confirmation of which site α -lipoic acid attaches on EGF protein. Dr. Alejandro Cohen (alejandro.cohen@dal.ca) at the Proteomics Core Facility, located in the Life Sciences Research Institute (LSRI) at Dalhousie University, discussed a more direct method for the α -lipoic acid attachment site determination [99]. Greater separation of the

peptides is possible if sodium dodecyl sulfate polyacrylamide gel electrophoresis (SDS-PAGE) occurs prior to LC-MS. SDS-PAGE separates proteins by their electrophoretic mobility, or their amino acid sequence length and charge [73]. A SDS, or surfactant, coating unfolds the peptides and gives a net negative charge. Wells at one end of an acrylamide gel hold the peptides in place near the negative electrode. The gel has a built in gradient made up of subsequently smaller acrylamide pore size spacing to allow the peptide separation. The gradient, or pore spacing, can be customized for use with larger or smaller peptides and proteins, to give greater separation at the ideal molecular weight range. Current is run through the gel, and the peptides move towards the positive electrode. This gives the preliminary size separation, as the larger peptides or proteins can only move a certain distance through the gel before the acrylamide pores become too small to allow progression towards the positive electrode. Post processing with Coomassie Blue or silver stain then allows visualization of the peptide bands and a rough determination of the molecular weight, as compared to a ladder, or a set of standard peptide mass bands. The peptides bands of interest can then be cut out of the gel and run with MS to get another two degrees of separation of the peptides through both retention time and then mass to charge or, simply, the mass of a peptide. The high resolution liquid chromatography-tandem mass spectrometer at the Proteomics Core Facility should have high enough resolution and m/z range to detect whether α -lipoic acid molecule has attached to EGF protein. Hopefully this MS also has a large enough m/z detection range to detect the missed cleavage amino terminus α -lipoic acid conjugated EGF peptide produced by the trypsin digest, which is on the order of 5033 Da with a +3 or +4 charge. The LTQ-MS detection range is 300-2000 m/z, while the TOF-MS is 20-20000 m/z.

An alternate method for the determination of the α -lipoic acid attachment site uses the technique nuclear magnetic resonance (NMR) spectroscopy. NMR detects particular features of atomic isotopes containing odd numbers of protons or neutrons. The features include the detection of ring patterns and functional groups of molecular structures through a particular chemical shift, or a measure of how close electrons are to the nucleus of an atom to *shield* the atom from the magnetic field. As well, the resonant coupling patterns of isotopes tell the quantity and location of similar isotopes within a structure.

NMR of protein solutions would use the ^{13}C and ^1H isotopes to determine whether α -lipoic acid had attached to EGF, by comparing to a NMR spectrum containing only EGF.

5.2.4 *In Vitro* and *Ex Vivo* Imaging

In addition to the A431 cancer cells, normal cells must be tested with the EGF-NPs to assess their effectiveness. Normal Human bronchial epithelial cells (NHBE, CC-2540, Lonza, Basel, Switzerland) are grown in bronchial epithelial growth medium (BEGM) supplemented with nutrients (CC-3170, Lonza, Basel, Switzerland). These cells are not an immortal line, they are guaranteed by the supplier to grow for 15 passages before they cease to divide.

Dark field microscopy was used to attempt to assess the nanoprobe activity. Images of probes incubated with A431 cancer cells showed objects present in the cells and excluded from the nucleus; however, it is unclear if the bright spots are nanoparticles, cell structures, or lipid droplets. A negative dark field result conflicts with ELISA data that suggests the probes were active and specific for EGFR and that the probes should be ingested by the cells into endosomes and lysosomes. RGB analysis of the dark field photos would separate the nanoparticle scattering signals. Conclusive identification of the bright spots on the cells, with an additional imaging technique such as Raman spectroscopic lipid signatures (eg. CDFH-DA to measure the reactive oxygen species) or fluorescence imaging with a lipid sensitive probe (eg. BODIPY or Nile Red), is required to understand the dark field microscopy data.

With the SERS hyperspectral images, it is possible to use co-expression of the EGF-linker coated nanoprobe attached to a fluorescent dye in addition to fluorescent endosome probes with fluorescence microscopy to check that the SERS and cellular endosome locations match *in vitro*. This would help confirm the SERS data. Additional work with regards to *in vitro* cell imaging could determine whether larger (20 or 60 nm) Ag EGF-NPs yield increased SERS as compared to the small, 5 nm Au and AgNPs.

The *ex vivo* ICP-MS data requires that the mouse EGF, and not Human EGF, is used to eliminate the possibility of miss assigned immune responses. Also, sterile filtration instead of 70% ethanol as the sterilization protocol for the nanoparticles would prevent the likely inactivation of the EGF-NPs, which reduces the nanoprobe specificity. These *ex vivo* studies with mice could assess the long-term toxicity of the nanoprobes, as well as continue to test the nanoprobe effectiveness with a larger sample size.

5.2.5 Raman Post-processing with Principle Components Analysis (PCA)

Post-processing of the data collected from Raman imaging is necessary to quickly distinguish patterns between samples. Post-processing is especially crucial when imaging cells or tissues, as the data collected forms a data cube – Raman shift vs. intensity data collected at each point maps across a predetermined area – or hyperspectral image. These hyperspectral images are generally referred to as cell maps.

PCA, principle components analysis, separates out the major signatures in a set of data to leave the last component or last few components as placeholders. These placeholders encompass less common or less pronounced signatures within the data. The code was written in MATLAB to read in the LabSpec 4 and 5 hyperspectral image data files. PCA is useful for separating and grouping the common signatures in a data set, so there are fewer signatures to analyze. Further interpretation of the PCA components is necessary to understand any output and see whether there are common signatures between datasets, as these signatures could be markers indicative of cancer. Either multivariate curve resolution (MCR), which looks for pure spectra of individual components within the data, or linear discriminant analysis (LDA), which determines the signals that are common and intense to identify markers for cancer vs. normal cells or tissue, could give meaningful information about the trends in the data. MCR and LDA can be used to look for Raman shifts characteristic of cancers.

The PCA and MCR code was developed using hyperspectral Raman data of A431 cancer and NHBE cells obtained before the start of the MSc. program. PCA code was

written during a class, CHEM 5205: Chemometrics, with Dr. Peter Wentzell. Code containing MCR equations, to analyze the components from PCA, are also included with the PCA code. These MATLAB code files are located in the lab. During PCA, the code can output how much of the data each component encompasses. The primary components are made up of general or the most common Raman signal in a dataset. The last component is made up on the signals which are 'left over', and is not encompassed by the principle components. The unique 'left over' component is available for use with LDA or MCR. The data was normalized before PCA with another program, Vancouver Raman Algorithm [80] [81]. More coding is necessary to write a program to use LDA in the search for common signatures between cancerous and normal cell datasets.

BIBLIOGRAPHY

- [1] R. Weissleder, "Molecular Imaging in Cancer," *Science*, vol. 312, no. 5777, pp. 1168-1171, 2006.
- [2] J. H. Grossman and S. E. McNeil, "Nanotechnology in Cancer Medicine," *Phys. Today*, vol. 65, no. 8, pp. 38-42, 2012.
- [3] K. Kneipp, "Surface-enhanced Raman scattering," *Phys. Today*, vol. 60, no. 11, pp. 40-46, 2007.
- [4] M. J. Abrams and B. A. Murrer, "Metal compounds in therapy and diagnosis," *Science*, vol. 261, no. 5122, pp. 725-730, 1993.
- [5] C.-Y. Tsai, A.-L. Shiau, S.-Y. Chen, Y.-H. Chen, P.-C. Cheng, M.-Y. Chang, D.-H. Chen, C.-H. Chou, C.-R. Wang and C.-L. Wu, "Amelioration of Collagen-Induced Arthritis in Rats by Nanogold," *Arthritis Rheum.*, vol. 56, no. 2, pp. 544-554, 2007.
- [6] Y. Pan, S. Neuss, A. Leifert, M. Fischler, F. Wen, U. Simon, G. Schmid, W. Brandau and W. Jahnen-Dechent, "Size-Dependent Cytotoxicity of Gold Nanoparticles," *Small*, vol. 3, no. 11, pp. 1941-1949, 2007.
- [7] J. C. Trefry and D. P. Wooley, "Rapid assessment of antiviral activity and cytotoxicity of silver nanoparticles using a novel application of the tetrazolium-based colorimetric assay," *J. Virol. Methods*, vol. 183, no. 1, pp. 19-24, 2012.
- [8] M. E. Samberg, S. J. Oldenburg and N. A. Monteiro-Riviere, "Evaluation of Silver Nanoparticle Toxicity in Skin in Vivo and Keratinocytes in Vitro," *Environ. Health Perspect.*, vol. 118, no. 3, pp. 407-413, 2010.
- [9] X. Qian, X.-H. Peng, D. O. Ansari, Q. Yin-Goen, G. Z. Chen, D. M. Shin, L. Yang, A. N. Young, M. D. Wang and S. Nie, "In vivo tumor targeting and spectroscopic detection with surface-enhanced Raman nanoparticle tags - supplementary figures," *Nat. Biotechnol.*, vol. 26, no. 1, pp. 83-90, 2008.
- [10] R. L. Jones and I. E. Smith, "Efficacy and safety of trastuzumab," *Expert Opin. Drug Saf.*, vol. 3, no. 4, pp. 317-327, 2004.
- [11] T. W. J. Gadella and T. M. Jovin, "Oligomerization of Epidermal Growth Factor Receptors on A431 Cells Studied by Time-resolved Fluorescence Imaging Microscopy. A Stereochemical Model for Tyrosine Kinase Receptor Activation," *J. Cell Biol.*, vol. 129, no. 6, pp. 1543-1558, 1995.
- [12] Y. Abe, M. Odaka, F. Inagaki, I. Lax, J. Schlessinger and D. Kohda, "Disulfide Bond Structure of Human Epidermal Growth Factor Receptor," *J. Biol. Chem.*, vol. 273, no. 18, pp. 11150-11157, 1998.

- [13] K. M. Ferguson, M. B. Berger, J. M. Mendrola, H. Cho, D. J. Leahy and M. A. Lemmon, "Structure of the extracellular domain of human epidermal growth factor (EGF) receptor in an inactive (low pH) complex with EGF (1NQL)," RCSB PDB (Protein Data Bank), 2003. [Online]. Available: <http://www.rcsb.org/pdb/explore/explore.do?structureId=1NQL>. [Accessed 29 April 2013].
- [14] S. Choi, Y. Choi, N. T. Dat, C. Hwangbo, J. J. Lee and J.-H. Lee, "Tephrosin induces internalization and degradation of EGFR and ErbB2 in HT-29 human colon cancer cells," *Cancer Lett.*, vol. 293, pp. 23-30, 2010.
- [15] D. S. Krause and R. A. VanEtten, "Tyrosine kinases as targets for cancer therapy," *N. Engl. J. Med.*, vol. 353, pp. 172-187, 2005.
- [16] P. P. DiFiore and G. N. Gill, "Endocytosis and mitogenic signaling," *Opin. Cell Biol.*, vol. 11, pp. 483-488, 1999.
- [17] W. J. Wu, S. Tu and R. A. Cerione, "Activated Cdc42 sequesters c-Cbl and prevents EGF receptor degradation," *Cell*, vol. 114, pp. 715-725, 2003.
- [18] K. B. Runkle, C. L. Meyerkord, N. V. Desai, Y. Takahashi and H.-G. Wang, "Bif-1 suppresses breast cancer cell migration by promoting EGFR endocytic degradation," *Cancer Biol. Ther.*, vol. 12, no. 10, pp. 956-966, 2012.
- [19] H. S. Lu, J. J. Chai, B. R. Huang, C. H. He and R. C. Bi, "Crystal structure of human epidermal growth factor (1JL9)," RCSB PDB (Protein Data Bank), 2001. [Online]. Available: <http://www.rcsb.org/pdb/explore/explore.do?structureId=1JL9>. [Accessed 10 August 2011].
- [20] Invitrogen, *Recombinant Human Epidermal Growth Factor (Hu EGF) Product Analysis Sheet*, Camarillo: DCC-08-1232 Rev 0.03, 2008.
- [21] ExpASy, "Compute pI/Mw," 2005. [Online]. Available: http://web.expasy.org/compute_pi/. [Accessed 28 04 2013].
- [22] UniProtKB/Swiss-Prot, "P01133 EGF_Human," 21 07 1986. [Online]. Available: <http://www.uniprot.org/uniprot/P01133>. [Accessed 07 05 2013].
- [23] Invitrogen, *Recombinant Mouse Epidermal Growth Factor (EGF) Product Analysis Sheet*, Camarillo: DCC-10-0208 Rev 1.0, 2010.
- [24] N. C. I. B. (National Centre for Biotechnology Information), "BLAST (Basic Local Alignment Search Tool)," [Online]. Available: http://blast.ncbi.nlm.nih.gov/Blast.cgi?CMD=Web&PAGE_TYPE=BlastHome. [Accessed 29 02 2012].
- [25] B. Ozanne, C. S. Richards, F. Hendler, D. Burns and B. Gusterson, "Over-expression of the EGF receptor is a hallmark of squamous cell carcinomas," *J. Pathology*, vol. 149, no. 1, pp. 9-14, 1986.

- [26] R. E. Sobol, R. W. Astarita, C. Hofeditz, H. Masui, R. Fairshter, I. Royston and J. Mendelsohn, "Epidermal growth factor receptor expression in human lung carcinomas defined by a monoclonal antibody," *J. Natl. Cancer Inst.*, vol. 79, no. 3, pp. 403-407, 1987.
- [27] D. Veale, N. Kerr, G. J. Gibson and A. L. Harris, "Characterization of epidermal growth factor receptor in primary human non-small cell lung cancer," *Cancer Res.*, vol. 49, no. 5, pp. 1313-1317, 1989.
- [28] T. A. Lieberman, N. Razon, A. D. Bartal, Y. Yarden, J. Schlessinger and H. Soreq, "Expression of epidermal growth factor receptors in brain tumors," *Cancer Res.*, vol. 44, no. 2, pp. 753-760, 1984.
- [29] A. L. Harris, S. Nicholson, J. R. C. Sainsbury, D. Neal, K. Smith, J. R. Farndon and C. Wright, "Epidermal growth factor receptors: a marker of early relapse in breast cancer and tumor state progression in bladder cancer; interactions with neu," *Cancer Cells*, vol. 7, pp. 353-357, 1989.
- [30] J. R. C. Sainsbury, A. J. Malcolm, D. R. Appleton, J. R. Farndon and A. L. Harris, "Presence of epidermal growth factor receptor as an indicator of poor prognosis in patients with breast cancer," *J. Clin. Pathol.*, vol. 38, no. 11, pp. 1225-1228, 1985.
- [31] A. Eisbruch, M. Blick, J. S. Lee, P. G. Sacks and J. Gutterman, "Analysis of the epidermal growth factor receptor gene in fresh human head and neck tumors," *Cancer Res.*, vol. 47, no. 13, pp. 3603-3605, 1987.
- [32] D. E. Neal, C. Marsh, M. K. Bennett, P. D. Abel, R. R. Hall, J. R. Sainsbury and A. L. Harris, "Epidermal growth factor receptor in human bladder cancer: Comparison of invasive and superficial tumors," *Lancet*, vol. 1, no. 8425, pp. 366-368, 1985.
- [33] F. Hendler, A. Shum-Siu, L. Nanu, D. Yuan and B. Ozanne, "Increased EGF receptors and the absence of an alveolar differentiation marker predict a poor survival in lung cancer," *Proc. Am. Soc. Clin. Oncol.*, vol. 8, p. 223, 1989.
- [34] D. Veale, T. Ashcroft, C. Marsh, G. J. Gibson and A. L. Harris, "Epidermal growth factor receptor in non-small lung cell cancer," *Br. J. Cancer*, vol. 55, no. 5, pp. 513-516, 1987.
- [35] P. Hollinger and H. Bohlen, "Engineering antibodies for the clinic," *Cancer Metastasis Rev.*, vol. 18, no. 4, pp. 411-419, 1999.
- [36] L. M. Weiner, "Monoclonal antibody therapy of cancer," *Semin. Oncol.*, vol. 26, no. 5 S14, pp. 43-51, 1999.
- [37] K. Towns, P. L. Bedard and S. Verma, "Matters of the heart: Cardiac toxicity of adjuvant systemic therapy for early stage breast cancer," *Curr. Oncol.*, vol. 15, no. S1, pp. S16-29, 2008.

- [38] E. R. Hsu, E. V. Anslyn, S. Dharmawardhane, R. Alizadeh-Naderi, J. S. Aaron, K. V. Sokolov, A. K. El-Naggar, A. M. Gillenwater and R. R. Richards-Kortum, "A far-red fluorescent contrast agent to image epidermal growth factor receptor expression," *Photochem. Photobiol.*, vol. 79, no. 3, pp. 272-279, 2004.
- [39] E. R. Hsu, A. M. Gillenwater and R. R. Richards-Kortum, "Detection of molecular changes associated with oral cancer using a molecular-specific fluorescent contrast agent and single-wavelength spectroscopy," *Appl. Spectros.*, vol. 59, no. 9, pp. 1166-1173, 2005.
- [40] K. Sokolov, M. Follen, J. Aaron, I. Pavlova, A. Malpica, R. Lotan and R. Richards-Kortum, "Real time vital optical imaging of precancer using anti-epidermal growth factor receptor antibodies conjugated to gold nanoparticles," *Cancer Res.*, vol. 63, no. 9, pp. 1999-2004, 2003.
- [41] J. Aaron, N. Nitin, K. Travis, S. Kumar, T. Collier, S. Y. Park, M. Jose-Yacamán, L. Coghlan, M. Follen, R. Richards-Kortum and K. Sokolov, "Plasmon resonance coupling of metal nanoparticles for molecular imaging of carcinogenesis in vivo," *J. Biomed. Optics*, vol. 12, no. 3, pp. 034007-1-034007-11, 2007.
- [42] K. K. Maiti, U. S. Dinish, C. Y. Fu, J.-J. Lee, K.-S. Soh, S.-W. Yun, R. Bhuvaneswari, M. Olivo and Y.-T. Chang, "Development of biocompatible SERS nanotag with increased stability by chemisorption of reporter molecule for in vivo cancer detection," *Biosens. Bioelectron.*, vol. 26, no. 2, pp. 398-403, 2010.
- [43] L. Lucas, X. K. Chen, A. Smith, M. Korbelik, H. Zeng, P. W. K. Lee and K. C. Hewitt, "Imaging EGFR distribution using surface-enhanced Raman spectroscopy," in *Proc. SPIE 7192*, San Jose, 2009.
- [44] D. J. Giard, S. A. Aaronson, G. J. Todaro, P. Arnstein, J. H. Kersey, H. Dosik and W. P. Parks, "In Vitro Cultivation of Human Tumors: Establishment of Cell Lines Derived From a Series of Solid Tumors," *J. Natl. Cancer Inst.*, vol. 51, pp. 1417-1423, 1973.
- [45] H. Haigler, J. F. Ash, S. J. Singer and S. Cohen, "Visualization by fluorescence of the binding and internalization of epidermal growth factor in human carcinoma cells A-431," *Proc. Natl. Acad. Sci. USA*, vol. 75, no. 7, pp. 3317-3321, 1978.
- [46] F. Friedl, I. Kimura, T. Osato and Y. Ito, "Studies on a New Human Cell Line (SiHa) Derived from Carcinoma of Uterus. I. Its Establishment and Morphology," *Proc. Soc. Exp. Biol. Med.*, vol. 135, no. 2, pp. 543-545, 1970.
- [47] K. Kneipp, M. Moskovitz and H. Kneipp, *Surface Enhanced Raman Scattering: Physics and Applications*, vol. 103, Heidelberg: Springer, 2006, pp. 1-464.

- [48] P. Diagaradjane, J. M. Orenstein-Cardona, N. E. Colon-Casasnovas, A. Deorukhkar, S. Shentu, N. Kuno, D. L. Schwartz, J. G. Gelovani and S. Krishnan, "Imaging epidermal growth factor receptor expression in vivo: Pharmacokinetic and biodistribution characterization of a bioconjugated quantum dot nanoprobe," *Clin. Cancer Res.*, vol. 14, no. 3, pp. 731-741, 2008.
- [49] N. Ibaraki, L.-R. Lin and V. N. Reddy, "A study of growth factor receptors in human lens epithelial cells and their relationship to fiber differentiation," *Exp. Eye Res.*, vol. 63, no. 6, pp. 683-692, 1996.
- [50] C.-L. Tseng, T.-W. Wang, G.-C. Dong, S. Y.-H. Wu, Y. T.-H. M.-J. Shieh, P.-J. Lou and F.-H. Lin, "Development of gelatin nanoparticles with biotinylated EGF conjugation for lung cancer targeting," *Biomaterials*, vol. 28, no. 27, pp. 3396-4005, 2007.
- [51] N. de Jonge, D. B. Peckys, G. J. Kremers and D. W. Piston, "Electron microscopy of whole cells in liquid with nanometer resolution," *Proc. Natl. Acad. Sci. USA*, vol. 106, no. 7, pp. 2159-2164, 2009.
- [52] M. Creixell, A. P. Herrera, V. Ayala, M. Latorre-Esteves, M. Perez-Torres, M. Torres-Lugo and C. Rinaldi, "Preparation of epidermal growth factor (EGF) conjugated iron oxide nanoparticles and their internalization into colon cancer cells," *J. Magn. Magn. Mater.*, vol. 322, no. 15, pp. 2244-2250, 2010.
- [53] L. J. Lucas and K. C. Hewitt, "Nanobiophotonics for molecular imaging of cancer: Au- and Ag-based Epidermal Growth Factor Receptor (EGFR) specific nanoprobe," in *Proc. SPIE 8234*, San Francisco, (2012)..
- [54] H. Moini, L. Packer and N.-E. L. Saris, "Antioxidant and Prooxidant Activities of α -Lipoic Acid and Dihydrolipoic Acid," *Toxicol. Appl. Pharmacol.*, vol. 182, no. 1, pp. 84-90, 2002.
- [55] R. Winter, "Alpha Lipoic Acid: What You Need To Know," [Online]. Available: <http://health.howstuffworks.com/wellness/natural-medicine/alternative/alpha-lipoic-acid.htm>. [Accessed 27 06 2013].
- [56] U. o. M. Medical Centre, "Alpha-lipoic acid," [Online]. Available: <http://umm.edu/health/medical/altmed/supplement/alphalipoic-acid>. [Accessed 27 06 2013].
- [57] J. A. Dougan, C. Karlsson, W. E. Smith and D. Graham, "Enhanced oligonucleotide-nanoparticle conjugate stability using thioctic acid modified oligonucleotides," *Nucl. Acids Res.*, vol. 35, no. 11, pp. 3668-3675, 2007.
- [58] O. Horovitz, M. Tomoaia-Cotisel, C. Racz, G. Tomoaia, L.-D. Bobos and A. Mocanu, "The Interaction of Silver Nanoparticles with Lipoic Acid," *Studia Universitatis Babeş-Bolyai, Chemia*, vol. 54, no. 3, pp. 89-96, 2009.

- [59] M. K. Kahn, L. D. Minc, S. S. Nigavekar, M. S. T. Kariapper, B. M. Nair, M. Schipper, A. C. Cook, W. G. Lesniak and L. P. Balogh, "Fabrication of $\{^{198}\text{Au}^0\}$ radioactive composite nanodevices and their use for nanobrachytherapy," *Nanomedicine: NBM*, vol. 4, no. 1, pp. 57-69, 2008.
- [60] S. Keren, C. Zavaleta, Z. Cheng, A. de la Zerda, O. Gheysens and S. S. Gambhir, "Noninvasive molecular imaging of small living subjects using Raman spectroscopy," *Proc. Natl. Acad. Sci. USA*, vol. 105, no. 15, pp. 5844-5849, 2008.
- [61] G. Frens, "Controlled nucleation for the regulation of the particle size in monodisperse gold suspensions," *Nature Phys. Sci.*, vol. 241, no. 105, pp. 20-22, 1973.
- [62] J. Turkevich, P. C. Stevenson and J. Hillier, "A study of the nucleation and growth processes in the synthesis of colloidal gold," *Discuss. Faraday Soc.*, vol. 11, pp. 55-75, 1951.
- [63] K. C. Grabar, R. G. Freeman, M. B. Hommer and M. J. Natan, "Preparation and characterization of Au colloid monolayers," *Anal. Chem.*, vol. 67, no. 4, pp. 735-743, 1995.
- [64] P. C. Lee and D. Meisel, "Adsorption and surface-enhanced Raman of dyes on silver and gold sols," *J. Phys. Chem.*, vol. 86, no. 17, pp. 3391-3395, 1982.
- [65] M. Noyong, K. Gloddek, J. Mayer, T. Weirich and U. Simon, "cis-Pt mediated assembly of gold nanoparticles on DNA," *J. Cluster Sci.*, vol. 18, no. 1, pp. 193-204, 2007.
- [66] K. C. Song, M. S. Lee, T. S. Park and B. S. Lee, "Preparation of colloidal silver nanoparticles by chemical reduction method," *Korean J. Chem. Eng.*, vol. 26, no. 1, pp. 153-155, 2009.
- [67] I. Jalal, Private Communication, 2009.
- [68] D. o. C. Dalhousie University, "Instrumentation: Bruker microTOF Focus Mass Spectrometer," [Online]. Available: <http://www.dal.ca/faculty/science/chemistry/research/maritime-mass-spectrometry-laboratory/instrumentation.html>. [Accessed 03 07 2013].
- [69] UniProtKB/Swiss-Prot, "P01308 INS_HUMAN," 21 07 1986. [Online]. Available: <http://www.uniprot.org/uniprot/P01308>. [Accessed 06 06 2013].
- [70] M. J. Wall, A. M. J. Crowell, G. A. Simms, G. H. Carey, F. Liu and A. A. Doucette, "Implications of partial tryptic digestion in organic-aqueous solvent systems for bottom-up proteome analysis," *Anal. Chim. Acta*, vol. 703, pp. 194-203, 2011.
- [71] A. M. J. Crowell, E. J. Stewart, Z. S. Take and A. A. Doucette, "Critical assessment of the spectroscopic activity assay for monitoring trypsin activity in organic-aqueous solvent," *Anal. Biochem.*, vol. 435, no. 2, pp. 131-136, 2013.

- [72] S. Tatur, M. Maccarini, R. Barker, A. Nelson and G. Fragneto, "Effect of Functionalized Gold Nanoparticles on Floating Lipid Bilayers," *Langmuir*, vol. 29, no. 22, pp. 6606-6014, 2013.
- [73] Malvern, "Zeta Potential - An Introduction on 10 Minutes," Zetasizer Nano series technical note MRK654-01, Worcestershire.
- [74] J. V. Jokerst, Z. Miao, C. Zavaleta, Z. Cheng and S. S. Gambhir, "Affibody-Functionalized Gold-Silica Nanoparticles for Raman Molecular Imaging of the Epidermal Growth Factor Receptor," *Small*, vol. 7, no. 5, pp. 625-633, 2011.
- [75] nanoComposix, "Zeta Potential Analysis of Nanoparticles," San Diego, 2012.
- [76] S. K. Balasubramanian, L. Yang, L.-Y. L. Yung, C.-N. Ong, W.-Y. Ong and L. E. Yu, "Characterization, purification, and stability of gold nanoparticles," *Biomaterials*, vol. 31, no. 34, pp. 9023-9030, 2010.
- [77] D. Hula, Private Communication, 2011.
- [78] P. Hughes, D. Marshall, Y. Reid, H. Parkes and C. Gelber, "The cost of using unauthenticated, over-passaged cell lines: How much more data do we need?," *Biotechniques*, vol. 43, no. 5, pp. 575-586, 2007.
- [79] ATCC, "Passage number effects in cell lines: Why they happen and what you can do about it," *Technical Bulletin no. 7*, pp. 1-3, 2007.
- [80] J. Zhao, H. Lui, D. I. McLean and H. Zeng, "Automated Autofluorescence Background Subtraction Algorithm for Biomedical Raman Spectroscopy," *Appl. Spectrosc.*, vol. 61, no. 11, pp. 1225-1232, 2007.
- [81] J. Zhao, H. Lui, D. I. McLean and H. Zeng, "Vancouver Raman Algorithm," 24 July 2008. [Online]. Available: <http://www.flintbox.com/public/project/1956>.
- [82] V. Besada, W. Antuch, A. Cinza, I. Rojas, M. Quintana, T. Takao, Y. Shimonishi and G. Padron, "Chemical characterization of recombinant human epidermal growth factor," *Anal. Chim. Acta*, 239(2), 301-305 (1990)., vol. 239, no. 2, pp. 301-305, 1990.
- [83] J. V. Staros, R. W. Wright and D. M. Swingle, "Enhancement by N-hydroxysulfosuccinimide of water soluble carbodiimide-mediated coupling reactions," *Anal. Bioc.*, vol. 156, no. 1, pp. 220-222, 1986.
- [84] Z. Grabarek and J. Gergely, "Zero-length crosslinking procedure with the use of active esters," *Anal. Bioc.*, vol. 185, no. 1, pp. 131-135, 1990.
- [85] A. Doucette, Private Communication, 2012.
- [86] P. K. Jain, K. S. Lee, I. H. El-Sayed and M. A. El-Sayed, "Calculated Absorption and Scattering Properties of Gold Nanoparticles of Different Size, Shape, and Composition: Applications in Biological Imaging and Biomedicine," *J. Phys. Chem. B*, vol. 110, no. 14, pp. 7238-7248, 2006.

- [87] D. D. Evanoff and G. Chumanov, "Size-Controlled Synthesis of Nanoparticles. 2. Measurement of Extinction, Scattering, and Absorption Cross Sections," *J. Phys. Chem. B*, vol. 108, no. 37, pp. 13957-13962, 2004.
- [88] J. R. Morones and W. Frey, "Environmentally Sensitive Silver Nanoparticles of Controlled Size Synthesized with PNIPAM as a Nucleating and Capping Agent," *Langmuir*, vol. 23, pp. 8180-8186, 2007.
- [89] D. E. Bradley, "A Study of the Negative Staining Process," *J. Gen. Microbiol.*, vol. 23, pp. 503-516, 1962.
- [90] C. M. MacLaughlin, E. P. K. Parker, G. C. Walker and C. Wang, "Evaluation of SERS labeling of CD20 on CLL cells using optical microscopy and fluorescence flow cytometry," *Nanomed. Nanotechnol. Biol. Med.*, vol. 9, no. 1, pp. 55-64, 2013.
- [91] N. Huang, M. Short, J. Zhao, H. Wang, H. Lui, M. Korbelik and H. Zeng, "Full range characterization of the Raman spectra of organs in a murine model," *Opt. Express*, vol. 19, no. 23, pp. 22892-22909, 2011.
- [92] G. McDonnell and A. D. Russell, "Antiseptics and Disinfectants: Activity, Action, and Resistance," *Clin. Microbiol. Rev.*, vol. 12, no. 1, pp. 147-179, 1999.
- [93] Q. Zhang, J. Y. Lee, J. Yang, C. Boothroyd and J. Zhang, "Size and composition tunable Ag-Au alloy nanoparticles by replacement reaction," *Nanotechnology*, vol. 18, no. 24, pp. 1-8, 2007.
- [94] G. Wu, A. Mikhailovsky, H. A. Khant and J. A. Zasadzinski, "Synthesis, Characterization, and Optical Response of Gold Nanoshells Used to Trigger Release from Liposomes," *Method Enzymol.*, vol. 464, pp. 279-304, 2009.
- [95] C. C. S. A. C. o. C. Statistics, "Canadian Cancer Statistics 2013," Canadian Cancer Society, Toronto, ON, 2013.
- [96] C. J. Murphy, T. K. Sau, A. M. Gole, C. J. Orendorff, J. Gao, L. Gou, S. E. Hunyadi and T. Li, "Anisotropic Metal Nanoparticles: Synthesis, Assembly, and Optical Applications," *J. Phys. Chem. B*, vol. 29, no. 13857-13870, p. 109, 2005.
- [97] S. Ruhl, P. Berlenbach, S. Langenfelder, D. Horl, N. Lehn, K.-A. Hiller, G. Schmalz and H. Durchschlag, "Integrity of Proteins in Human Saliva after Sterilization by Gamma Irradiation," *Appl. Environ. Microb.*, vol. 77, no. 3, pp. 749-755, 2011.
- [98] A. Yaman, "Alternative methods of terminal sterilization for biologically active macromolecules," *Curr. Opin. Drug Discov. Devel.*, vol. 4, no. 6, pp. 760-763, 2001.
- [99] A. Cohen and K. Hewitt, Private Communication, 2013.

APPENDIX A Cell Culture

Leanne Lucas

August 2008

Caring for Cells

The following procedures describe methods for the maintenance of adherent cells, specifically A431 cancer cells. Basic instructions for the Normal Human Bronchial Epithelial (NHBE) cells are noted when procedures or reagent amounts differ. Proper training in the use of biohazards and any unfamiliar instrumentation is recommended.

Always remember to wear the appropriate personal protective equipment (gloves, safety glasses, lab coat, etc.) and/or to use appropriate engineering controls (biosafety cabinet, fume hood, glove box, etc.).

Apparatus

flasks (75 cm²) (Sigma-Aldrich, CLS430641)
Petri dishes (25 cm²)
Petri dishes (13 cm²)
glass bottomed Petri dishes (MatTek Cultureware, P35G-1.5-10-C) (13 cm²)
coverslips
10 mL disposable pipettes
5 mL disposable pipettes
autopipette
10% bleach solution
70% ethanol solution
15 mL centrifuge tubes
cell scrapers (Sigma-Aldrich, CLS3010)
water and ethanol proof marker
tape
MEM α medium (Invitrogen, 12571-063)
fetal bovine serum (FBS) (Sigma-Aldrich, F2442)
sterile dimethyl sulfoxide (DMSO) (Sigma-Aldrich, D2650-5X5ML)
penicillin streptomycin solution (PenStrep) (Invitrogen, 15140-122)
laminar air flow hood or biosafety cabinet
hemocytometer
1-10 μ L pipette tips (sterile)
1-10 μ L micropipette
centrifuge
5% CO₂ 37°C incubator
10X PBS or 0.01 M PBS solution (Invitrogen, Cat No. 70013-032 or Sigma, P3813)
37°C waterbath
cell dissociation buffer (Invitrogen, Cat No. 13150-016)
trypsin EDTA 0.25% (Invitrogen, Cat No. 25200-072)
bronchial epithelial growth medium (BEGM) and supplements (Lonza, CC-3170)
waste beaker

Solutions

The PBS solution should be sterile, if mixing up the PBS (like from Sigma) it should be autoclaved and the pH adjusted before use. To preserve sterility, solutions should never be opened in the air, they should only be opened in the laminar air flow hood. PBS solution should be refrigerated.

Alternatively, one could make their own PBS solution. The BCCA-CRC uses 1 g of Potassium Phosphate (monobasic), 5.75 g Sodium Phosphate (dibasic), 1 g Potassium Chloride, and 40 g Sodium Chloride diluted in 5 L of deionized water. Adjust the pH to 7.4 before diluting completely. Again, the solution should be autoclaved before use with the cells.

The A431 cell medium consists of the MEM α medium supplemented with 10% FBS by volume and 1% PenStrep by volume. The FBS contains growth factors while the PenStrep ensures contamination resistance from bacteria. Per 100mL of cell medium: there would be 10 mL of FBS, 1 mL PenStrep, and 89 mL of MEM α . Also, the cell medium is light sensitive and should be stored it in the dark. It also must also be refrigerated.

The Normal Human Bronchial Epithelial (NHBE) cells use the bronchial epithelial growth medium (BEGM), it is a serum free medium which was supplemented with extra nutrients.

Solutions which are to come in contact with the cells, like the cell medium and PBS, should be warmed for about 20-30 minutes in a 37°C water bath before use. The exception to this is trypsin and cell dissociation buffer.

FBS is a biological solution, it has particular storage considerations. It must be stored frozen (-20°C). When needed, FBS should be thawed in the fridge overnight and then allowed to thaw completely at room temperature. During the room temperature thaw, it is appropriate to agitate the container occasionally to break up any precipitates. Repeated freeze-thaw cycles are discouraged, it is appropriate to aliquot the FBS for future use.

PenStrep has many of the same considerations as FBS. It must be stored frozen (-5°C – -20°C). To use it the solution, thaw it at room temperature. Repeated freeze-thaw cycles are also detrimental to the integrity to the solution and should be avoided.

General Procedure

Starting A New Culture

This procedure gives general instructions for starting cell lines from cryovials, as cells are usually received frozen.

First, wear appropriate gloves and spray them with 70% ethanol to remove any bacteria. Allow the blower of the laminar air flow hood to run for 20 to 30 minutes if it has been shut off, this sterilizes the environment. Spray the hood sprayed down with 70% ethanol to remove any remaining contaminants. Spray down any supplies needed for the procedure (pipettes, flasks, automatic pipette, medium, etc.) with 70% ethanol and place them in the hood.

In the biosafety hood, pipette the cell medium into the flask that the cells are to be grown. If the medium was not already warm, the flask could be placed in the incubator for approximately 30 minutes. The amount of medium depends on the flask or dish size. For the glass bottomed dishes, 2 mL is sufficient while 10 -15 mL is appropriate for flasks. When starting a culture, the larger flasks should be used to allow space for the cell culture to establish. A general rule is that cells should be frozen slowly and thawed quickly. Once the medium is ready, carefully obtain the cells from the liquid nitrogen storage dewars. Thaw the cells briefly in a lukewarm water bath, thawing probably should not take more than 3 to 5 minutes. Once the cells are suspended in a liquid, the container should be sprayed with 70% ethanol and placed in the hood. Pipette the cell solution into the prepared flask. Pipette the medium up and down to ensure dispersion of the cells in the flask. Place the cells in the incubator. Discard the used pipettes in the biohazard waste bag (level 1, clear) and spray down the hood with some more 70% ethanol. Sterilize any waste solutions which have come in contact with the cells with 10% bleach solution. 10% bleach solutions should be kept away from the metal of the laminar hood as it will dissolve them. The frozen cells were in a special freezing medium. If it were desired, the cells could be spun and the supernatant removed, but this is not necessary as the solution is diluted with a lot of cell medium. The cells are more sensitive once they have been unfrozen and need about a day or so before transport.

To ensure healthy, uncontaminated cell cultures, never move hands, arms, or instruments over open cells flasks or dishes as bacteria could fall into them. Also, pipettes that touch the outsides of containers should not be placed in solutions that are going to touch the cells. Covers of solution containers and flasks should never be set down in the hood, as residual bacteria may cause contamination.

Changing The Medium

This is a quick and simple procedure which is necessary to keep the cells from starving. As such, medium changes should be completed every two to three days, or once the medium changes from red to orange, if the cells are not being passed. This is more applicable to slower growing, normal cells.

Wear gloves sterilized with 70% ethanol. Warm the cell medium in the 37°C water bath. Sterilize the laminar air flow hood with 70% ethanol. Sterilize and move the appropriate solutions and materials into the hood. Sterilize the cell flask or Petri dish before placing it in the hood. Pipette out the old cell medium. Add fresh medium. Return the cells to the incubator. Discard the used pipettes in the biohazard waste bag (level 1, clear) and spray down the hood with 70% ethanol. Sterilize any waste solutions which have come in contact with the cells with a 10% bleach solution. 10% bleach solutions should be kept away from the metal of the biosafety hood as it will dissolve them.

Passing Cells

This procedure is slightly more involved than simply changing the cell medium. It is employed to aliquot the cells so they do not get too crowded, or confluent, in their container and die. In general, quickly growing cells should be passed every three to four days. Two variations of passing the cells are possible: one using trypsin to detach the

cells and the other using the cell dissociation buffer. Trypsin, an enzyme, degrades the proteins on the cell surface causing it to detach. It is fast acting as it detaches the cells in 5 to 10 minutes when placed in the 37°C incubator. The cell dissociation buffer does not work as well and must be used in conjunction with cell scrapers to completely remove the cells. We did not use the cell dissociation buffer for the thesis experiments.

Wear gloves sterilized with 70% ethanol solution. Warm the cell medium and PBS solution in a 37°C water bath. Sterilize the laminar hood. Sterilize and move the appropriate solutions and materials into the hood. Sterilize the cell flask or Petri dish before placing it in the hood. Pipette out the old cell medium. Rinse the cells at least twice with some PBS buffer. Pipette in the cell detacher. With trypsin, use 2-3 mL for the cancer cells. For NHBE cells, use 2 mL of 1/8th of 0.25% trypsin diluted with PBS. Place the cells in the incubator for 5-10 minutes to detach. With the cell dissociation buffer, 4-5 mL is sufficient. Since the dissociation buffer is not enzymatic, the 37°C incubator will have no effect on the cells. Allow these cells to detach for 5-10 minutes and then scrape gently with a cell scraper. The normal cells do not respond well to the cell dissociation buffer. In either case, confirm visually with a white light microscope that the cells detached. Pipette the detached cell solution into a centrifuge tube. Use more PBS solution to rinse the flask, to ensure the majority of cells were collected. Spin the tube at 600 rcf for 3 minutes to pellet the A431 cells, or at 200 rcf for 8 minutes for NHBE cells. Remove the supernatant and resuspend the cells in 5-10 mL of medium. Pipette the cells into a new flask or Petri dishes, and make these dishes up to of cell medium. Generally, one flask of confluent cells will yield 3 or 4 flasks of cells. Use of a hemocytometer, to precisely measure number of cells in solution, is ideal. Then appropriate amounts of cells can be used. For our experiments, we used half a million to one million cells per mL of solution or dish. For more instructions on hemocytometers, see the next section.

Check to confirm the presence of cells in the new flasks or Petri dishes. Label the new flasks with the initials of the technician, the cell line name, the date, and the passage number. Return the passed cells to the incubator. Clean up the hood area.

For the Raman and dark field microscopy experiments, place a removable glass cover slip in an ordinary small Petri dish and allow the cells to attach. Clean and dry the cover slips with 70% ethanol in the biosafety cabinet before use.

The passage number tells the amount of times a cell line has been transferred from one flask to another. Although cells theoretically have an unlimited passage number, it is important to keep track as long term subculturing and contamination can introduce variations into the cells. This could lead to the differentiation of the cells into a group which is no longer representative of the cell stock. To reduce experimental errors introduced from long term subculturing, discard the cells after 50 passages [78] [79]. Earlier replacement of the cells is acceptable. Checks exist to ensure the cells are still representative of the original tissue. The tests include visual inspections, phenotypic tests, and tests on cellular protein levels.

Using a Hemocytometer

A hemocytometer allows one to count cells, and determine the number of cells contained in a volume of solution. To use the hemocytometer, first confirm that it is free

from cellular debris. Take an aliquot of the medium containing resuspended cells and remove it from the hood. Use a micropipettor to measure 10 μ L of the cell suspension onto the arrow of the hemocytometer. Place the coverslip over the hemocytometer to spread the solution into the hemocytometer grids. There are four grids, and each of these grids has 16 squares. Use a microscope to count the cells in the grids. Once the cells have been counted, use the following equation to calculate the number of cells in solution or per mL,

$$\frac{X \text{ \# cells counted} \times 10^4}{\text{mL}} = \frac{X \text{ cells}}{\text{mL}}$$

and

$$\frac{X \text{ cells}}{\text{mL}} \times Y \text{ mL of medium} = X \text{ \# cells in total of } Y \text{ \# grids}$$

Eg.

$$\frac{58 \times 10^4}{\text{mL}} = \frac{1.45 \text{ million cells}}{\text{mL}}$$

and

$$\frac{1.45 \text{ million cells}}{\text{mL}} \times 10 \text{ mL of medium} = 14.5 \text{ \# cells in a total of 4 grids}$$

Add the amount of medium which yields the desired number of cells per mL to the appropriate Petri dish type. The type of dish depends on the experiment. Usually cells were grown on ordinary Petri dishes or flasks, and the glass bottomed Petri dishes were used for Raman imaging. In the example, about 0.7 mL of solution would yield approximately 1 million cells. More cell medium can be used to dilute the cells further if the concentration of cells is too high for accurate pipetting.

It is important to properly clean the hemocytometer to prevent counting erroneously high numbers of cells. Flush the hemocytometer and the coverslip with a copious amount of water and then with some 95% ethanol. Use a microscope to perform a visual inspection of the cell counting area to see if the cellular debris has been removed. If not, then again flush the hemocytometer with water and then a small amount of micro-90 cleaning solution to complete the process. Flush the hemocytometer with water, air dry, inspect with a microscope, and then return to its case.

Freezing Down Cells

This process is convenient if the cells are not needed in experiments for some time or to ensure that a backup supply of cells is readily available.

Prepare the freezing medium ahead of time. Freezing medium consists of 10% DMSO by volume and MEM α medium supplemented with 10% FBS by volume. A volume of 15 mL of freezing medium would contain 1.5 mL each of DMSO and FBS and 12 mL of the MEM α medium. Wear gloves sterilized with 70% ethanol. Warm the freezing medium and PBS solution in the 37°C water bath. Sterilize the laminar hood. Sterilize and move the appropriate solutions and materials into the hood. Sterilize the cell flask or Petri dish before placing it in the hood. Pipette out the old cell medium. Rinse the

cells at least twice with the PBS solution. Add 2 to 3 mL of the appropriate concentration of trypsin and incubate at 37°C for 5 to 10 minutes. Spin at 600 rcf for 3 minutes, or 200 rcf for 8 minutes for normal cells, to remove the trypsin and add the appropriate amount of freezing medium. Although the general principle is that one flask of cells can yield about 3-5 cryovials, count the cells to determine the number of cryovials needed. 3 to 5 million cells are usually frozen per vial. Each vial can easily contain approximately 1.5 mL of cell solution. Label the cryovial with the cell culture name, the passage number, the date, the approximate number of cells, and the initials of the technician. Conserve the current passage number when freezing down or thawing a line. There are two options for freezing cells slowly. If many freezing down procedures are going to be performed, it might be useful to invest in a Mr. Frosty. A Mr. Frosty is a container with an isopropanol lining which provides a cooling rate of -1°C per minute. The cells can be placed inside and the container placed in a -80°C freezer. After adequate time (2+ hours), the vials can be transferred to the liquid nitrogen storage tanks. Alternatively, the vials could be placed at -4°C for a few hours, and transferred to successively colder freezers (-20°C, -80°C) for some time until they are cold enough to be transferred into the liquid nitrogen tanks.

A website with general info about cell care and cell lines is www.atcc.org.

APPENDIX B LTQ-MS Data Output by Sequest

	Confidence Level	Sequence	Modifications	Search Engine Rank	Peptides Matched	XCorr	# Missed Cleavages	Ion Inject Time [ms]
149	High	YAcNcVVG YIGER	C3(Carbamidomethyl); C5(Carbamidomethyl)	1	1	4.31	0	120
152	High	YAcNcVVG YIGER	C3(Carbamidomethyl); C5(Carbamidomethyl)	1	1	4.12	0	96
35	High	cQYRDLKWWELR	C1(Carbamidomethyl)	1	1	4.10	2	182
57	High	cQYRDLKWWELR	C1(Carbamidomethyl)	1	1	3.98	2	12
49	High	cQYRDLKWWELR	C1(Carbamidomethyl)	1	1	3.96	2	36
65	High	cQYRDLKWWELR	C1(Carbamidomethyl)	1	1	3.91	2	8
37	High	cQYRDLKWWELR	C1(Carbamidomethyl)	1	1	3.90	2	6
47	High	cQYRDLKWWELR	C1(Carbamidomethyl)	1	1	3.89	2	17
34	High	cQYRDLKWWELR	C1(Carbamidomethyl)	1	1	3.81	2	200
150	High	YAcNcVVG YIGER	C3(Carbamidomethyl); C5(Carbamidomethyl)	1	1	3.76	0	193
43	High	cQYRDLKWWELR	C1(Carbamidomethyl)	1	1	3.61	2	113
62	High	cQYRDLKWWELR	C1(Carbamidomethyl)	1	1	3.37	2	23
58	High	cQYRDLKWWELR	C1(Carbamidomethyl)	1	1	3.31	2	15
40	High	cQYRDLKWWELR	C1(Carbamidomethyl)	1	1	3.27	2	184
42	High	cQYRDLKWWELR	C1(Carbamidomethyl)	1	1	3.20	2	96
63	High	cQYRDLKWWELR	C1(Carbamidomethyl)	1	1	3.19	2	19
153	High	YAcNcVVG YIGER	C3(Carbamidomethyl); C5(Carbamidomethyl)	1	1	3.10	0	189
54	High	cQYRDLKWWELR	C1(Carbamidomethyl)	1	1	3.03	2	200
94	High	DLKWWELR		1	1	2.95	1	0
41	High	cQYRDLKWWELR	C1(Carbamidomethyl)	1	1	2.83	2	200
64	High	cQYRDLKWWELR	C1(Carbamidomethyl)	1	1	2.83	2	11
96	High	DLKWWELR		1	1	2.81	1	16
76	High	DLKWWELR		1	1	2.78	1	1
77	High	DLKWWELR		1	1	2.74	1	0
92	High	DLKWWELR		1	1	2.74	1	0
84	High	DLKWWELR		1	1	2.74	1	0
82	High	DLKWWELR		1	1	2.74	1	200
148	High	YAcNcVVG YIGER	C3(Carbamidomethyl); C5(Carbamidomethyl)	1	1	2.73	0	200
79	High	DLKWWELR		1	1	2.73	1	4
81	High	DLKWWELR		1	1	2.69	1	173
151	High	YAcNcVVG YIGER	C3(Carbamidomethyl); C5(Carbamidomethyl)	1	1	2.68	0	200
164	High	YAcNcVVG YIGER cQYR	C3(Carbamidomethyl); C5(Carbamidomethyl); C14(Carbamidomethyl)	1	1	2.66	1	122
75	High	DLKWWELR		1	1	2.66	1	200
88	High	DLKWWELR		1	1	2.65	1	22
44	High	cQYRDLKWWELR	C1(Carbamidomethyl)	1	1	2.63	2	146
83	High	DLKWWELR		1	1	2.61	1	0
91	High	DLKWWELR		1	1	2.59	1	1

93	High	DLKWWELR		1	1	2.58	1	2
95	High	DLKWWELR		1	1	2.57	1	0
36	High	cQYRDLKWWELR	C1(Carbamidomethyl)	1	1	2.54	2	200
147	High	YAcNcVVGyIGER	C3(Carbamidomethyl); C5(Carbamidomethyl)	1	1	2.53	0	200
161	High	YAcNcVVGyIGER cQYR	C3(Carbamidomethyl); C5(Carbamidomethyl); C14(Carbamidomethyl)	1	1	2.51	1	169
165	High	YAcNcVVGyIGER cQYR	C3(Carbamidomethyl); C5(Carbamidomethyl); C14(Carbamidomethyl)	1	1	2.51	1	143
48	High	cQYRDLKWWELR	C1(Carbamidomethyl)	1	1	2.50	2	3
78	High	DLKWWELR		1	1	2.49	1	9
80	High	DLKWWELR		1	1	2.49	1	54
87	High	DLKWWELR		1	1	2.49	1	10
56	High	cQYRDLKWWELR	C1(Carbamidomethyl)	1	1	2.46	2	6
163	High	YAcNcVVGyIGER cQYR	C3(Carbamidomethyl); C5(Carbamidomethyl); C14(Carbamidomethyl)	1	1	2.45	1	162
85	High	DLKWWELR		1	1	2.45	1	10
86	High	DLKWWELR		1	1	2.37	1	18
90	High	DLKWWELR		1	1	2.36	1	0
61	High	cQYRDLKWWELR	C1(Carbamidomethyl)	1	1	2.34	2	14
46	High	cQYRDLKWWELR	C1(Carbamidomethyl)	1	1	2.30	2	166
60	High	cQYRDLKWWELR	C1(Carbamidomethyl)	1	1	2.29	2	200
89	High	DLKWWELR		1	1	2.17	1	75
53	High	cQYRDLKWWELR	C1(Carbamidomethyl)	1	1	2.05	2	40
139	High	yAcNcVVGyIGER	Y1(Phospho); C3(Carbamidomethyl); C5(Carbamidomethyl)	1	2	1.80	0	144
141	High	yAcNcVVGyIGER	Y1(Phospho); C3(Carbamidomethyl); C5(Carbamidomethyl)	1	2	1.80	0	200
33	High	cQYRDLKWWELR	C1(Carbamidomethyl)	1	1	1.79	2	99
154	High	YAcNcVVGyIGER	C3(Carbamidomethyl); C5(Carbamidomethyl)	1	1	1.71	0	200
140	High	yAcNcVVGyIGER	Y1(Phospho); C3(Carbamidomethyl); C5(Carbamidomethyl)	1	2	1.63	0	200
100	High	NsDSEcPLSHDGY cLHDGvcMYIEAL DK	S2(Phospho); C6(Carbamidomethyl); C14(Carbamidomethyl); C20(Carbamidomethyl)	1	5	1.61	0	200
105	High	NSDsEcPLSHDGY cLHDGvcMYIEAL DK	S4(Phospho); C6(Carbamidomethyl); C14(Carbamidomethyl); C20(Carbamidomethyl)	2	5	1.59	0	200
129	High	WWELR		1	1	1.57	0	3
126	High	WWELR		1	1	1.56	0	21
128	High	WWELR		1	1	1.53	0	9
122	High	WWELR		1	1	1.52	0	25
136	Medium	yAcNcVVGyIGER	Y1(Phospho); C3(Carbamidomethyl); C5(Carbamidomethyl)	1	2	1.51	0	179
131	High	WWELR		1	1	1.48	0	8
121	High	WWELR		1	1	1.47	0	109

120	High	WWELR		1	1	1.47	0	104
132	High	WWELR		1	1	1.44	0	5
45	Medium	cQYRDLKWWELR	C1(Carbamidomethyl)	1	1	1.44	2	96
25	Medium	cQyRDLKWWELR	N-Term(Lipo); C1(Carbamidomethyl); Y3(Phospho)	1	2	1.41	2	193
52	Medium	cQYRDLKWWELR	C1(Carbamidomethyl)	1	1	1.41	2	200
125	High	WWELR		1	1	1.39	0	47
109	Medium	NSDSEcPLSHDGY cLHDGvcMYIEAL DK	C6(Carbamidomethyl); S9(Phospho); C14(Carbamidomethyl); C20(Carbamidomethyl)	3	5	1.38	0	200
16	High	cQYRDLK	C1(Carbamidomethyl)	1	1	1.37	1	144
23	Medium	cQyRDLkWWELR	C1(Carbamidomethyl); Y3(Phospho); K7(Lipoyl)	2	2	1.36	2	193
127	High	WWELR		1	1	1.36	0	146
20	High	cQYRDLK	C1(Carbamidomethyl)	1	1	1.34	1	200
123	High	WWELR		1	1	1.34	0	32
124	High	WWELR		1	1	1.33	0	200
104	Medium	NSDsEcPLSHDGY cLHDGvcMYIEAL DK	S4(Phospho); C6(Carbamidomethyl); C14(Carbamidomethyl); C20(Carbamidomethyl)	1	5	1.31	0	200
130	High	WWELR		1	1	1.29	0	26
162	High	YAcNcVVGyIGER cQYR	C3(Carbamidomethyl); C5(Carbamidomethyl); C14(Carbamidomethyl)	1	1	1.26	1	200
157	Medium	yAcNcVVGyIGER cQYR	Y1(Phospho); C3(Carbamidomethyl); C5(Carbamidomethyl); Y9(Phospho); C14(Carbamidomethyl)	1	3	1.25	1	200
99	Medium	NsDSEcPLSHDGY cLHDGvcMYIEAL DK	S2(Phospho); C6(Carbamidomethyl); C14(Carbamidomethyl); C20(Carbamidomethyl)	2	5	1.22	0	200
108	Low	NSDSEcPLSHDGY cLHDGvcMYIEAL DK	C6(Carbamidomethyl); S9(Phospho); C14(Carbamidomethyl); C20(Carbamidomethyl)	3	5	1.16	0	200

	Sequence	Charge	m/z [Da]	MH+ [Da]	ΔM [ppm]	RT [min]	Ions Matched	Spectrum File
149	YAcNcVVGyIGER	2	780.96271	1560.91814	143.97	53.17	20/24	EGF_C2_02.RAW
152	YAcNcVVGyIGER	2	780.84875	1560.69023	-2.04	52.63	21/24	EGF_C2_04.RAW
35	cQYRDLKWWELR	2	877.07361	1753.13994	157.43	55.07	18/22	EGF_C1_01.RAW
57	cQYRDLKWWELR	2	877.07550	1753.14372	159.59	63.31	19/22	EGF_C2_02.RAW
49	cQYRDLKWWELR	2	877.00098	1752.99468	74.58	61.15	18/22	EGF_C1_03.RAW
65	cQYRDLKWWELR	2	877.42000	1753.83272	552.38	62.90	18/22	EGF_C2_04.RAW
37	cQYRDLKWWELR	2	877.05237	1753.09746	133.21	61.09	18/22	EGF_C1_01.RAW
47	cQYRDLKWWELR	3	585.32000	1753.94545	616.62	60.81	23/44	EGF_C1_03.RAW
34	cQYRDLKWWELR	3	585.38000	1754.12545	719.17	51.29	23/44	EGF_C1_01.RAW
150	YAcNcVVGyIGER	3	520.93866	1560.80143	69.21	53.39	24/48	EGF_C2_02.RAW
43	cQYRDLKWWELR	2	877.01917	1753.03105	95.33	54.78	18/22	EGF_C1_03.RAW

62	cQYRDLKWWELR	2	876.99158	1752.97588	63.86	61.90	17/22	EGF_C2_04.RAW
58	cQYRDLKWWELR	3	585.05206	1753.14164	158.40	63.86	24/44	EGF_C2_02.RAW
40	cQYRDLKWWELR	3	584.36566	1751.08243	-1017.37	50.82	24/44	EGF_C1_03.RAW
42	cQYRDLKWWELR	3	585.04462	1753.11930	145.66	54.68	24/44	EGF_C1_03.RAW
63	cQYRDLKWWELR	3	584.66000	1751.96545	-512.85	62.70	24/44	EGF_C2_04.RAW
153	YAcNcVVGyIGER	3	521.18000	1561.52545	532.84	52.92	23/48	EGF_C2_04.RAW
54	cQYRDLKWWELR	2	877.07843	1753.14958	162.93	62.03	17/22	EGF_C2_02.RAW
94	DLKWWELR	2	573.34753	1145.68779	67.67	62.52	13/14	EGF_C2_04.RAW
41	cQYRDLKWWELR	3	584.76000	1752.26545	-341.55	52.22	19/44	EGF_C1_03.RAW
64	cQYRDLKWWELR	4	439.24000	1753.93817	612.47	62.73	25/66	EGF_C2_04.RAW
96	DLKWWELR	3	382.55185	1145.64099	26.83	62.78	14/28	EGF_C2_04.RAW
76	DLKWWELR	3	382.55963	1145.66434	47.20	59.82	15/28	EGF_C1_01.RAW
77	DLKWWELR	2	573.39081	1145.77434	143.20	59.83	12/14	EGF_C1_01.RAW
92	DLKWWELR	2	573.34955	1145.69182	71.19	63.28	13/14	EGF_C2_02.RAW
84	DLKWWELR	2	573.31915	1145.63103	18.13	59.90	13/14	EGF_C1_03.RAW
82	DLKWWELR	2	572.91022	1144.81316	-696.27	58.59	12/14	EGF_C1_03.RAW
148	YAcNcVVGyIGER	2	781.37396	1561.74065	670.56	47.24	18/24	EGF_C1_03.RAW
79	DLKWWELR	2	573.37299	1145.73870	112.10	61.20	12/14	EGF_C1_01.RAW
81	DLKWWELR	2	573.38000	1145.75272	124.34	56.58	12/14	EGF_C1_03.RAW
151	YAcNcVVGyIGER	2	781.37811	1561.74895	675.87	56.71	18/24	EGF_C2_02.RAW
164	YAcNcVVGyIGERc QYR	3	723.70000	2169.08545	524.81	53.81	24/64	EGF_C2_02.RAW
75	DLKWWELR	2	573.38000	1145.75272	124.34	58.36	12/14	EGF_C1_01.RAW
88	DLKWWELR	1	1145.69165	1145.69165	71.04	61.57	9/14	EGF_C1_03.RAW
44	cQYRDLKWWELR	3	585.30000	1753.88545	582.43	56.20	23/44	EGF_C1_03.RAW
83	DLKWWELR	3	382.54718	1145.62699	14.60	59.89	16/28	EGF_C1_03.RAW
91	DLKWWELR	1	1145.78223	1145.78223	150.09	62.50	10/14	EGF_C2_02.RAW
93	DLKWWELR	3	382.57724	1145.71717	93.31	63.52	15/28	EGF_C2_02.RAW
95	DLKWWELR	1	1145.63062	1145.63062	17.77	62.53	9/14	EGF_C2_04.RAW
36	cQYRDLKWWELR	3	585.42000	1754.24545	787.52	57.62	21/44	EGF_C1_01.RAW
147	YAcNcVVGyIGER	2	781.82000	1562.63272	1241.06	42.73	18/24	EGF_C1_03.RAW
161	YAcNcVVGyIGERc QYR	3	723.44067	2168.30747	166.21	42.54	22/64	EGF_C1_01.RAW
165	YAcNcVVGyIGERc QYR	3	723.68000	2169.02545	497.16	52.94	24/64	EGF_C2_04.RAW
48	cQYRDLKWWELR	4	439.04611	1753.16262	170.37	60.99	28/66	EGF_C1_03.RAW
78	DLKWWELR	1	1145.77319	1145.77319	142.20	59.87	9/14	EGF_C1_01.RAW
80	DLKWWELR	1	1145.76477	1145.76477	134.85	61.33	10/14	EGF_C1_01.RAW
87	DLKWWELR	3	382.53336	1145.58551	-21.60	61.14	16/28	EGF_C1_03.RAW
56	cQYRDLKWWELR	4	439.32000	1754.25817	794.77	63.22	29/66	EGF_C2_02.RAW
163	YAcNcVVGyIGERc QYR	3	723.40302	2168.19449	114.11	42.33	22/64	EGF_C1_03.RAW
85	DLKWWELR	1	1145.69983	1145.69983	78.18	59.94	9/14	EGF_C1_03.RAW
86	DLKWWELR	2	573.37634	1145.74541	117.96	61.07	12/14	EGF_C1_03.RAW
90	DLKWWELR	3	382.57516	1145.71094	87.88	62.47	15/28	EGF_C2_02.RAW
61	cQYRDLKWWELR	4	438.54398	1751.15407	-976.42	61.41	30/66	EGF_C2_04.RAW
46	cQYRDLKWWELR	3	585.36000	1754.06545	684.99	57.67	20/44	EGF_C1_03.RAW
60	cQYRDLKWWELR	3	584.66000	1751.96545	-512.85	61.20	20/44	EGF_C2_04.RAW
89	DLKWWELR	2	573.34000	1145.67272	54.52	62.24	13/14	EGF_C2_02.RAW

53	cQYRDLKWWELR	4	439.00000	1752.97817	65.17	61.51	25/66	EGF_C2_02.RAW
139	yAcNcVVGyIGER	3	547.31696	1639.93631	-441.13	40.54	22/96	EGF_C1_03.RAW
141	yAcNcVVGyIGER	3	547.29749	1639.87790	-476.77	50.84	22/96	EGF_C2_04.RAW
33	cQYRDLKWWELR	4	438.58000	1751.29817	-894.06	51.24	25/66	EGF_C1_01.RAW
154	YAcNcVVGyIGER	2	780.86000	1560.71272	12.38	55.92	14/24	EGF_C2_04.RAW
140	yAcNcVVGyIGER	3	547.30261	1639.89328	-467.38	51.20	19/96	EGF_C2_02.RAW
100	NsDSEcPLSHDGYcL HDGvcMYIEALDK	4	841.86000	3364.41817	-269.72	23.92	37/240	EGF_C2_02.RAW
105	NSDsEcPLSHDGYcL HDGvcMYIEALDK	4	841.86000	3364.41817	-269.72	23.92	37/240	EGF_C2_02.RAW
129	WWELR	2	395.26968	789.53209	161.89	62.39	7/8	EGF_C2_02.RAW
126	WWELR	1	789.45233	789.45233	60.88	59.96	6/8	EGF_C1_03.RAW
128	WWELR	1	789.50293	789.50293	124.96	62.28	6/8	EGF_C2_02.RAW
122	WWELR	1	789.52997	789.52997	159.20	59.89	6/8	EGF_C1_01.RAW
136	yAcNcVVGyIGER	3	547.32080	1639.94785	-434.09	40.25	23/96	EGF_C1_01.RAW
131	WWELR	2	395.24719	789.48711	104.92	62.23	7/8	EGF_C2_04.RAW
121	WWELR	1	789.50848	789.50848	132.00	55.62	6/8	EGF_C1_01.RAW
120	WWELR	2	395.29099	789.57469	215.84	55.50	6/8	EGF_C1_01.RAW
132	WWELR	1	789.48102	789.48102	97.21	62.29	6/8	EGF_C2_04.RAW
45	cQYRDLKWWELR	4	439.32098	1754.26211	797.01	56.25	22/66	EGF_C1_03.RAW
25	cQyRDLKWWEL R	3	674.4000 0	2021.185 45	159.42	60.8 4	17/64	EGF_C1_01.R AW
52	cQYRDLKWWELR	3	584.96000	1752.86545	0.86	61.22	18/44	EGF_C2_02.RAW
125	WWELR	2	395.27240	789.53752	168.77	55.52	6/8	EGF_C1_03.RAW
109	NSDSEcPLSHDGYcL HDGvcMYIEALDK	4	841.86000	3364.41817	-269.72	23.92	33/240	EGF_C2_02.RAW
16	cQYRDLK	2	491.50000	981.99272	-493.67	51.06	5/12	EGF_C1_03.RAW
23	cQyRDLkWWELR	3	674.4000 0	2021.185 45	159.42	60.8 4	17/64	EGF_C1_01.R AW
127	WWELR	1	789.44818	789.44818	55.62	61.27	6/8	EGF_C1_03.RAW
20	cQYRDLK	2	491.84000	982.67272	198.66	50.11	7/12	EGF_C2_04.RAW
123	WWELR	1	789.51733	789.51733	143.20	61.23	6/8	EGF_C1_01.RAW
124	WWELR	1	789.38000	789.38000	-30.75	55.03	6/8	EGF_C1_03.RAW
104	NSDsEcPLSHDGYcL HDGvcMYIEALDK	4	841.86000	3364.41817	-269.72	16.94	36/240	EGF_C1_03.RAW
130	WWELR	1	789.51624	789.51624	141.81	63.36	6/8	EGF_C2_02.RAW
162	YAcNcVVGyIGERc QYR	2	1085.06000	2169.11272	537.38	52.14	7/32	EGF_C1_01.RAW
157	yAcNcVVGyIGERcQ YR	3	776.78000	2328.32545	191.43	61.25	25/158	EGF_C2_02.RAW
99	NsDSEcPLSHDGYcL HDGvcMYIEALDK	4	841.86000	3364.41817	-269.72	16.94	35/240	EGF_C1_03.RAW
108	NSDSEcPLSHDGYcL HDGvcMYIEALDK	4	841.86000	3364.41817	-269.72	16.94	38/240	EGF_C1_03.RAW

APPENDIX C Cleaning Glassware with Aqua Regia

Leanne Lucas
January 22, 2013

Scope

This method is applicable to glassware and Teflon coated containers or magnetic stir bars for the removal of noble metals (like gold and platinum). The addition of concentrated nitric acid (HNO_3) and then concentrated hydrochloric acid (HCl) to produce the aqua regia solution will also remove any silver metal deposited on the glassware.

Method Summary

Clean the glassware in the fume hood with aqua regia solution. Rinse the clean glassware with deionized water and dry in an oven. Dispose of used aqua regia appropriately by diluting in water and neutralizing.

Safety Notes

Material Safety Data Sheets (MSDS) should be reviewed and understood prior to starting any procedure.

Safety glasses and appropriate safety attire (double gloves – nitrile – not latex gloves, safety glasses or goggles, face shield, lab coat, appropriate footwear) should be worn when handling chemicals. Take care when working with concentrated acids. Use the acids and aqua regia solution only in a fume hood.

Only use the Aqua Regia solution in glass or Teflon containers when heating. Other types of plastic are also ok if they are to be used at room temperature, but will be degraded over time and at higher temperatures by the concentrated acid mixture.

Ongoing chemical decomposition reactions cause the used aqua regia solutions produce fumes, DO NOT store in a closed container. Dilute copiously by slowly adding it to water to prepare for disposal through the Dalhousie Hazardous Waste Disposal. Clean up any spills with sodium bicarbonate (baking soda), or the chemical spill kit acid neutralizer. See also, attached below, the University of Manitoba, Environmental Health and Safety Office's Hazard Alert (03-002) entitled "Using Mixtures of Highly Corrosive Concentrated Acids, Ex: Aqua Regia and Piranha Solution" for important notes about safety and proper disposal of Aqua Regia solutions.

Protocol

Clean the glassware in the fume hood with aqua regia solution. Prepare the solution by adding the concentrated nitric and hydrochloric acids in a 3:1 ratio (eg. 30 mL HNO_3 to 10 mL HCl). Order of addition of the acids is important, adding the concentrated nitric

acid and then the concentrated hydrochloric acid will allow the concentrated nitric acid to first dissolve any residual silver on the glassware. Addition of the hydrochloric acid first will cause the silver to form insoluble AgCl_2 , which may or may not be removed from the glassware (Private communication, Dan Chevalier, Minerals Engineering Centre, research notebook p. LLF88).

Rinse the clean glassware with deionized water and dry in an oven.

NEVER STORE AQUA REGIA IN A CLOSED CONTAINER, the acid mixture is unstable and undergoes decomposition reactions. Closed containers of aqua regia will build up pressure and cause the container to explode, spilling the acidic contents, spreading fumes, and potentially create significant damage and personal injury. Dispose of the used aqua regia appropriately by diluting copiously by slowly adding it to water to prepare for disposal as chemical laboratory waste through the Hazardous Waste Disposal program. The slow addition of the acid to the water is to be careful of the heat generated. 50 mL of the used aqua regia solution can be slowly added to 1 L of water, and then add to the aqua regia dilute waste in the chemical room acid cabinet (Private communication, Kevin Borgal and Andy George, Department of Physics and Atmospheric Science at Dalhousie University).



UNIVERSITY
OF MANITOBA

Environmental Health and Safety Office

Hazard Alert (03-002)

USING MIXTURES OF HIGHLY CORROSIVE CONCENTRATED ACIDS Ex: AQUA REGIA and Piranha Solution

There have been accidents involving the use of aqua regia and Piranha Solution. In one incident, a graduate student at the University of Manitoba used an etching solution of aqua regia and glycerol for electro-polishing a nickel superalloy. Only a portion of the solution was used after preparation, the remainder was stored in a capped plastic bottle inside a fume hood. Within 45 minutes, the bottle burst, spewing the contents everywhere, damaging computer equipment nearby and filling the room with acid fumes. Fortunately there were no injuries. (No one was in the room when the container failed.) In another similar incident, this one occurring in September 1998 in an Ontario University (<http://www.uwo.ca/ohs/hazalerts/aquareg.htm>), a graduate student was using aqua regia for the cleaning of NMR tubes. After finishing with the material, he placed the waste aqua regia, about 50-80 ml, in a 4L Winchester bottle, capping it tightly and storing it in a flammable solvent storage cabinet prior to disposal. About an hour later it exploded, filling the lab with acid fumes. A nearby bottle of pyridine broke and leaked onto the floor. It dissolved floor tiles and created a lingering bad smell.

Aqua regia is a mixture of concentrated hydrochloric acid and concentrated nitric acid. It has been used for centuries for dissolving noble metals (gold, platinum). Piranha Solution is a mixture of concentrated sulfuric acid and hydrogen peroxide. Aqua regia and Piranha solution are highly corrosive and very powerful oxidizing agents. Even without other materials present, a slow chemical reaction occurs in aqua regia and brown fumes of nitrogen peroxide are produced. The activity of Aqua Regia as a dissolving agent decreases slowly and thus, by definition, the solution is unstable. **Aqua Regia should be freshly prepared, never stored in a closed vessel. Render it safe by dilution and neutralization.**

The following are proper procedures for handling and using highly corrosive concentrated acids such as Aqua Regia and Piranha Solution.

1. These acids should only be prepared and used when absolutely necessary. If a milder reagent will work, try to avoid using aqua regia and like. Aqua regia and Piranha solution are not recommended for routine cleaning of glassware.
2. When using highly corrosive acids, wear appropriate personal protective equipment (safety splash goggles, gloves and laboratory coat) and **work in a clean, properly working chemical fume hood**. Keep the fume hood's sash down at working height (usually 11 inches) when reactions are in progress. Leave the sash closed if the hood is unattended. It is essential that any one working with such corrosives has unimpeded access to an emergency eye wash and safety shower. These must be within 100 feet of the work area.
3. Prepare only the amount needed for immediate use. Label container as per WHMIS procedures. **Never store** mixtures of highly corrosive acids and never put it in a sealed container, since pressure from evolving gases accumulates and possibly cause an explosion. Never take these acids out of the fume hood in which they are prepared and do not store them there either. Use them immediately after preparation and destroy any excess in the fume hood in which they were prepared. Aqua regia can be destroyed safely by cautiously adding it to water to dilute, and then neutralize the diluted solution with sodium bicarbonate (baking soda). The resulting contents can be disposed as chemical laboratory waste through EHSO Hazardous Waste Program (474-8633). A box or two of ordinary sodium bicarbonate (baking soda) or other commercial spill kits should be nearby to effectively neutralize acid spills.
4. For any solutions containing aqua regia such as the etching solution mentioned in the beginning, follow the same principles as outlined above. You can avoid accidents by adhering to the principles and getting specific instructions from your supervisor before handling aqua regia or other potentially hazardous reagents.
5. The aqua regia container must be glass or plastic. Although cold aqua regia does not rapidly attack plastics, Teflon is the only plastic truly resistant to oxidizing action of hot aqua regia. The container must be open or vented to allow the escape of chlorine, which is produced slowly.



<p>Main Office 191 Frank Kennedy Building Winnipeg MB R3T 2N2 Tel: (204) 474-6633 Fax: (204) 474-7829</p>	<p>Bannatyne Office T248 - 249 Basic Science Building Winnipeg MB R3E 0W3 Tel: (204) 789-3613 Fax: (204) 789-3906</p>
--	--

APPENDIX D Copyright Permission Letters

Copyright Permission Letter – TechConnect Nanotech 2012

Wednesday, February 20, 2013

Technical Proceedings of the 2012 Nanotechnology Conference and Trade Show, Nanotech 2012
Manager; TechConnect Copyrights Office; 696 San Ramon Valley Blvd., Ste. 423; Danville, CA 94526,
U.S.A.

I am preparing my Masters of Science thesis for submission to the Faculty of Graduate Studies at Dalhousie University, Halifax, Nova Scotia, Canada. I am seeking your permission to include a manuscript version of the following paper(s) as a chapter in the thesis:

EGF conjugated gold and silver nanoparticles for imaging EGFR over-expressing cells, L. J. Lucas and K. C. Hewitt, Nanotech 2012 Conference Proceedings Vol. 3, 202-205, 2012.

Canadian graduate theses are reproduced by the Library and Archives of Canada (formerly National Library of Canada) through a non-exclusive, world-wide license to reproduce, loan, distribute, or sell theses. I am also seeking your permission for the material described above to be reproduced and distributed by the LAC (NLC). Further details about the LAC (NLC) thesis program are available on the LAC (NLC) website (www.nlc-bnc.ca).

Full publication details and a copy of this permission letter will be included in the thesis.

Yours sincerely,

Leanne Lucas
MSc Candidate
Physics and Atmospheric Science, Dalhousie University

Permission is granted for:

- a) the inclusion of the material described above in your thesis.
- b) for the material described above to be included in the copy of your thesis that is sent to the Library and Archives of Canada (formerly National Library of Canada) for reproduction and distribution.

Name: Sarah J Wenning Title: VP, Operations
Signature: _____ Date: March 14, 2013

Copyright Permission Letter – SPIE Photonics West 2012

Wednesday, February 20, 2013

Proceedings of SPIE
Director of Publications, SPIE, P.O. Box 10, Bellingham, WA 98227-0010 U.S.A.

I am preparing my Masters of Science thesis for submission to the Faculty of Graduate Studies at Dalhousie University, Halifax, Nova Scotia, Canada. I am seeking your permission to include a manuscript version of the following paper as a chapter in the thesis:

Nanobiophotonics for molecular imaging of cancer: Au- and Ag-based Epidermal Growth Factor receptor (EGFR) specific nanoprobe, Leanne J. Lucas and Kevin C. Hewitt, Proceedings of SPIE, Vol. 8234, 82340C-1 – 82340C-15, 2012.

Canadian graduate theses are reproduced by the Library and Archives of Canada (formerly National Library of Canada) through a non-exclusive, world-wide license to reproduce, loan, distribute, or sell theses. I am also seeking your permission for the material described above to be reproduced and distributed by the LAC (NLC). Further details about the LAC (NLC) thesis program are available on the LAC (NLC) website (www.nlc-bnc.ca).


Full publication details and a copy of this permission letter will be included in the thesis.

Yours sincerely,

Leanne Lucas
MSc Candidate
Physics and Atmospheric Science, Dalhousie University

Permission is granted for:

- a) the inclusion of the material described above in your thesis.
- b) for the material described above to be included in the copy of your thesis that is sent to the Library and Archives of Canada (formerly National Library of Canada) for reproduction and distribution.

Name:  SPIE Publisher's permission is hereby granted under the following conditions: ~~(1) you obtain permission of the author(s)~~; (2) the material to be used has appeared in our publication without credit or acknowledgment to another source; and (3) you credit the original SPIE publication. Include the authors' names, title of paper, volume title, SPIE volume number, and year of publication in your credit statement.

Signature: _____

Director of Publications
SPIE
PO Box 10, Bellingham, WA 98227-0010 USA
360/676-3290 (Pacific Time) eric@spie.org

Eric Pepper, Director of Publications

Date 3/15/2013